nagra.

Arbeitsbericht NAB 16-13

Gas and water sampling from the FEBEX in situ test

May 2019

Ana María Fernández

National Cooperative
for the Disposal of
Radioactive Waste

Hardstrasse 73
P.O. Box 280
5430 Wettingen
Switzerland
Tel. +41 56 437 11 11

www.nagra.ch

nagra.

Arbeitsbericht NAB 16-13

Gas and water sampling from the FEBEX in situ test

May 2019

Ana María Fernández

KEYWORDS

Gas generation, porewater, in situ sampling, redox, hydrogen, methane, acetate, bentonite, engineered barrier

National Cooperative
for the Disposal of
Radioactive Waste

Hardstrasse 73
P.O. Box 280
5430 Wettingen
Switzerland
Tel. +41 56 437 11 11

www.nagra.ch

Nagra Arbeitsberichte ("Working Reports") present the results of work in progress that have not necessarily been subject to a comprehensive review. They are intended to provide rapid dissemination of current information.
This report was prepared on behalf of Nagra. The viewpoints presented and conclusions reached are those of the author(s) and do not necessarily represent those of Nagra.

Abstract

The FEBEX (Full-scale Engineered Barrier EXperiment in Crystalline Host Rock) full-scale heating *in situ* test was performed at the Grimsel Underground Laboratory in Switzerland with the general aim of studying the behaviour of near-field components in a repository for high-level radioactive waste.

One of the objectives of the FEBEX *in situ* experiment was to analyse the gases generated and transported through the bentonite barrier because the accumulation, consumption and release of gases from a HLW repository system may affect a number of processes that influence the long-term safety (e.g., gas pressure build-up, changes in bentonite properties, influence of groundwater transport, radiological hazard, ….).

In different phases of the FEBEX *in situ* test (First Operational Phase: 1996 – 2002, and Second Operational Phase: 2002 – 2015), various pipes were introduced inside the bentonite buffer for analysing the evolution of the gases and the chemical composition of the porewater. For this purpose, different gas/water sampling campaigns were performed since 1996 until 2011, before and after dismantling of Heater #1. Two additional campaigns were carried out in 2014 and 2015 during the FEBEX-DP Project for understanding the gas generation/consumption processes in the buffer and to establish the chemical conditions and redox state inside the bentonite barrier.

The main gases detected in the FEBEX *in situ* during the 18 years of experiment were O_2, N_2, CO_2, CO, H_2, CH_4 and other saturated and unsaturated aliphatic hydrocarbons (alkanes up to C5 and alkenes). Fluid pressures remained close to atmospheric pressure because the FEBEX *in situ* test cannot be considered as a gas-tight system, and any excess of gas pressure generated could be dissipated. The highest fluid pressures measured (between 2 and 4.5 bar) at the beginning of the experiment were related to water pressures because of the water inflow during the saturation process of the bentonite. Furthermore, part of the gases identified were consumed in different (bio)-geochemical processes. Although the concentration of oxygen decreased over time, oxygen was never depleted completely, showing minimum values between 3 and 0.2 vol.-%. However, the presence of hydrogen, methane and other hydrocarbons indicate the presence of spatial microenvironments where anoxic/anaerobic conditions were established, as confirmed by the reducing redox potentials calculated from hydrogen contents and measured in some pore waters collected from the different pipes.

Table of Contents

List of Tables

List of Figures

1 Introduction

1.1 The FEBEX Project

FEBEX (Full-scale Engineered Barrier EXperiment in Crystalline Host Rock) is a research and demonstration project that was initiated by Enresa (Spain) in 1994.

The aim of the project was to study the behaviour of near-field components in a repository for high-level radioactive waste in granite formations. The main objectives of the project can be grouped in two areas:

- demonstration of the feasibility of constructing the engineered barrier system in a horizontal configuration according to the Spanish concept for deep geological storage (AGP), and analysis of the technical problems to be solved for this type of disposal method
- better understanding of the thermo-hydro-mechanical (THM) and thermo-hydro-geochemical (THG or THC) processes in the near field, and development and validation of the modelling tools required for interpretation and prediction of the evolution of such processes

The project consisted of two large-scale tests (Fig. 1) – *in situ* and *mock-up* (the latter is managed by CIEMAT in Spain) – a series of laboratory tests, and THM and THG modelling tasks (ENRESA 2000).

The full-scale heating *in situ* test was performed at the Grimsel underground laboratory in Switzerland, also known as Grimsel Test Site (GTS), located 420 – 520 m below the surface. A complete description of the FEBEX Project objectives and test program can be found in Fuentes-Cantillana et al. (1998): "FEBEX Full-scale Engineered Barriers EXperiment in Crystalline Host Rock. Pre-operational stage summary report".

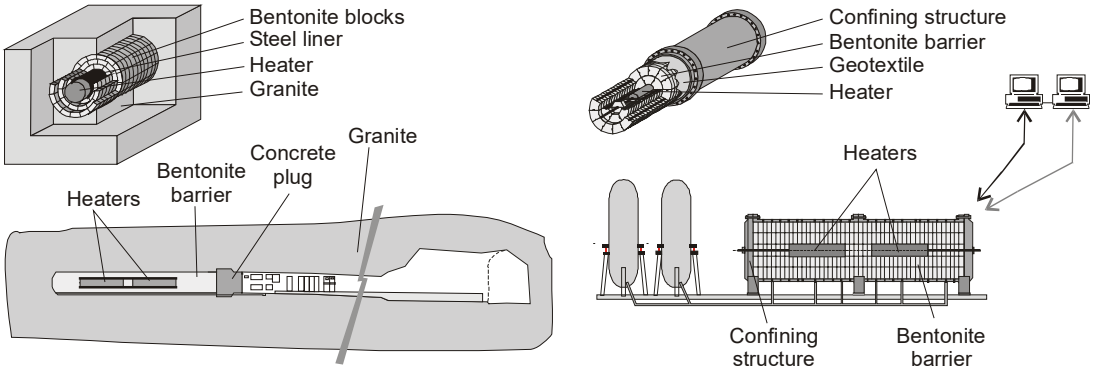

Fig. 1: Overall layout of FEBEX *in situ* test (left) and *mock-up* test (right)

Fuentes-Cantillana et al. (1998)

The project started in 1994 and has been supported by the European Commission through consecutive contracts, identified as FEBEX-I (contract nº FI4W-CT-95-0006) for the period January 1996 to June 1999, and FEBEX-II (contract nº FIKW-CT-2000-00016), from September 2000 to December 2004. Afterwards, near-field processes (NF-PRO) took place from January 2005 to December 2007. Finally, in January 2008 the *in situ* test was transferred from Enresa to a consortium composed by SKB (Sweden), POSIVA (Finland), CIEMAT (Spain), Nagra (Switzerland) with the more recent addition of KAERI (South Korea), together forming the FEBEX Consortium, which currently supports the project.

The final dismantling of FEBEX *in situ* experiment was carried out in 2015 and new partners, interested in taking part in the planned sampling and analysis operations, have been incorporated to the Consortium (now called FEBEX-DP) for that purpose, namely US DOE (USA), Obayashi (Japan), RWM (UK), Andra (France), BGR (Germany) and SURAO (Czech Republic).

1.2 Test configuration during FEBEX-I

The installation of the FEBEX *in situ* test was carried out in the GTS. A horizontal drift with a diameter of 2.28 m was excavated in the Grimsel granodiorite especially for this experiment using a TBM (a tunnel boring machine). Two electrical heaters, of the same size and of a similar weight as the reference canisters, were placed in the axis of the drift (Fig. 2). The gap between the heaters and the rock was backfilled with compacted bentonite blocks, up to a length of 17.40 m, this requiring a total 115'716 kg of FEBEX bentonite (Tab. 1). The backfilled area was sealed with a plain concrete plug placed into a recess excavated in the rock and having a length of 2.70 m and a volume of 17.8 m^3. Fig. 3 shows schematically the dimensions and layout of the test components.

The concrete plug (made of plane concrete without anchors or any reinforcement), was constructed with the only function of supporting the mechanical thrust of the barrier when it was hydrated (swelling pressure up to 50 bar); i.e., it was not specifically required to be completely sealed against hydraulic or gas flow. The formulation of the concrete used (Tab. 2) corresponds to a concrete with a relatively low amount of clinker, compensating for this with the addition of silica fume. In addition, the type of cement used, by its composition, releases less heat when hydrated and has a greater resistance to sulphates than the normal Portland cements. 17 m^3 of material was pumped from outside the drift to construct the concrete plug by vibration in three phases (Fuentes-Cantillana & García-Siñeriz 1998).

A total of 632 sensors were placed in the system along a number of instrumented sections, both in the bentonite buffer and in the host rock, to monitor relevant parameters such as temperature, humidity, total and pore pressure, displacement, etc. Prior to the bentonite barrier emplacement, nineteen radial boreholes were drilled in 1996 in the test zone from the interior of the drift for the placement of the foreseen instrumentation in the surrounding rock mass (Fig. 4). The instruments were of many different kinds and their characteristics and positions are fully described in Fuentes-Cantillana and García-Siñeriz (1998): "FEBEX Full-scale Engineered Barriers Experiment in Crystalline Host Rock. Final design and installation of the *in situ* test at Grimsel".

A Data Acquisition and Control System (DACS) located in the service area of the FEBEX drift collected the data provided by the instruments. This system recorded and stored information from the sensors and also controlled the power applied to the electrical heaters, in order to maintain a constant temperature at the heaters/bentonite interface. The DACS allowed the experiment to be run in an automated mode, with remote supervision from Madrid. Data stored at the local DACS were periodically downloaded in Madrid and used to build the experimental Master Data Base. A complete description of the FEBEX *in situ* test that includes both the installation of the test and

the results gathered after two years of operation is given in Fuentes-Cantillana et al. (2000): "FEBEX Full-Scale Engineered Barriers Experiment for a deep geological repository for high level radioactive waste in crystalline host rock. Final Report".

The construction of the concrete plug was completed in October 1996, and the heating operation started on 27 February 1997 (taken as Day 0 in this report). A constant temperature of 100 °C was maintained at the heaters/bentonite interface, while the bentonite buffer was slowly hydrated with the water naturally seeping from a granitic rock formation. The total water inflow for the entire test zone (17.3 m) varied from 6.5 to 12.2 L/day, the most frequently encountered hydraulic conductivity being 1×10^{-11} m/s; and the hydraulic pressure along a horizontal plane through the axis of the gallery at a distance of 50 m being 7.2 bar (Huertas et al. 2006). The characteristics of the infiltrating granitic water are: diluted and reducing water (E.C. < 100 µm/cm, Eh -200 mV), pH close to 9 and of sodic-calcic-bicarbonate-fluoride water-type (Huertas et al. 2006). The main gases dissolved in the groundwater are N_2 (~ 97 vol.-%) and Ar (~ 3 vol.-%), the content of O_2 and other gases being very low or below detection limits (see Appendix A).

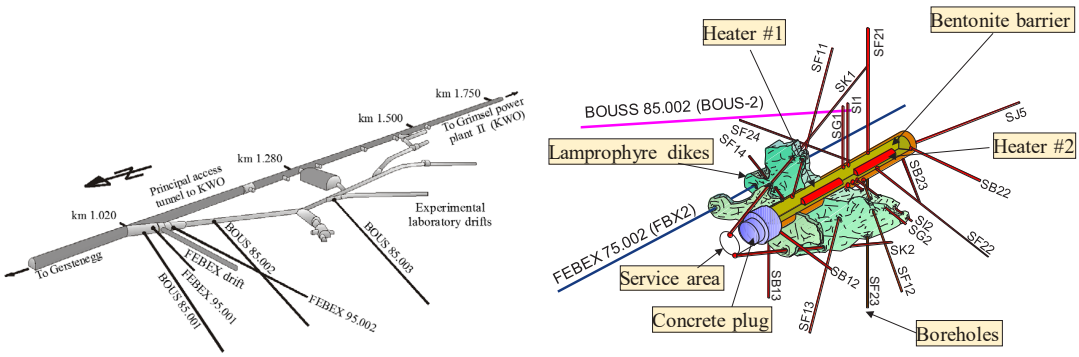

Fig. 2: a) Tunnel layout of the Grimsel Test Site (GTS). b) Scheme of the FEBEX *in situ* test during the First Operational Phase (1996 – 2002)

Huertas et al. (2006)

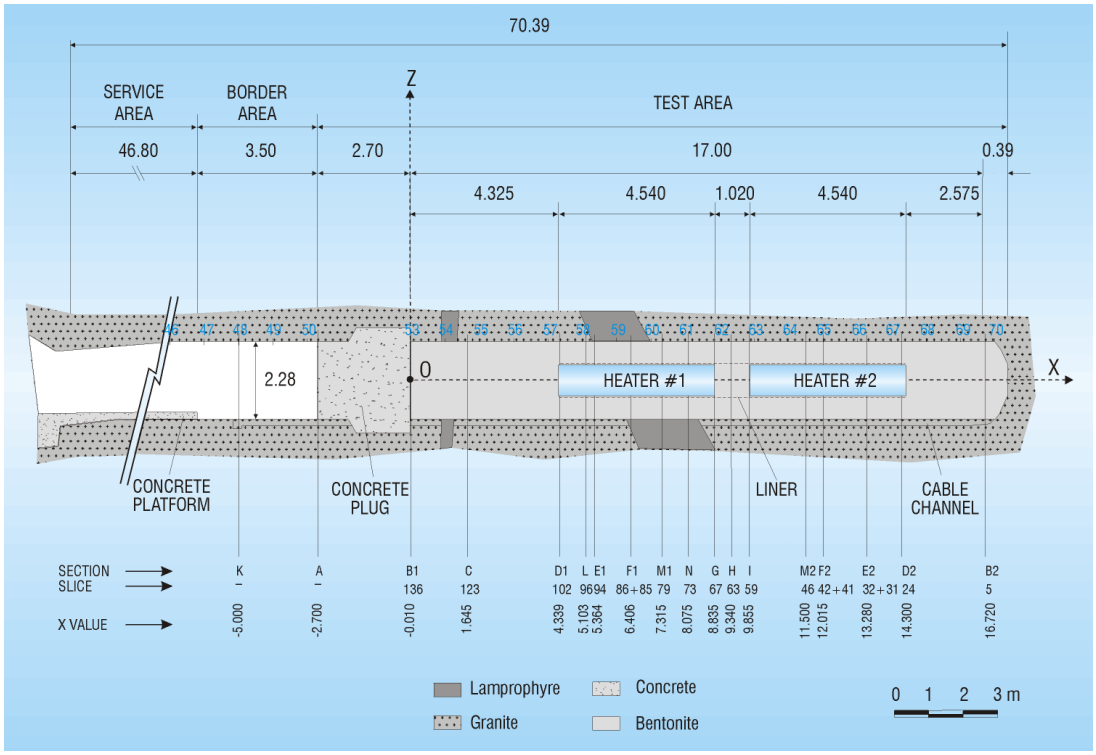

Fig. 3: General layout of the FEBEX *in situ* test: FEBEX-I configuration during the First Operational Phase 1996 – 2002

Huertas et al. (2006)

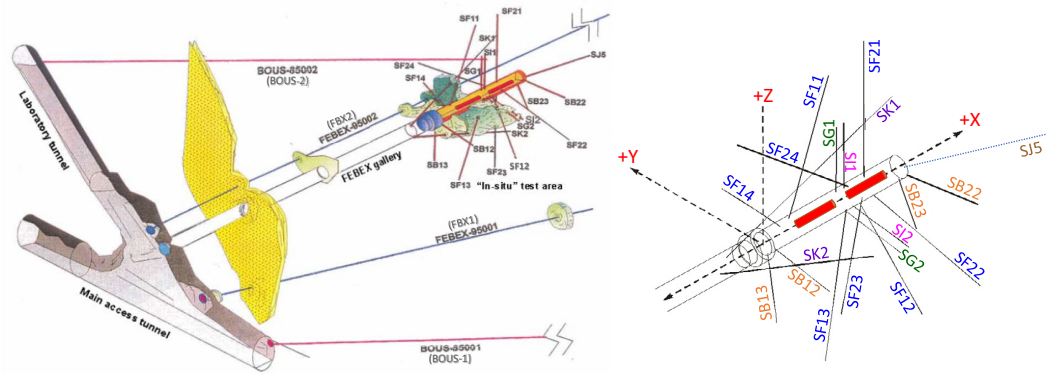

Fig. 4: Location of the sub-parallel and radial boreholes drilled for the instrumentation of the surrounding rock mass

Huertas et al. (2006) and Pardillo et al. (1997)

Tab. 1: Main characteristics of the FEBEX bentonite

Fernández et al. (2018, 2004)

Type of bentonite		Ca-Mg dioctahedral cis-vacant montmorillonite					
Structural formulae		$(Si_{3.94}Al_{0.06})^{IV}\ (Al_{1.35}Fe^{3+}_{0.21}Mg_{0.49}Ti_{0.01})^{VI}\ O_{10}(OH)_2\ X_{0.29}$					
S_{BET} (m^2/g)	59.5	S_{TOT} (m^2/g)	668 ± 21	CEC (meq/100g)	98 ± 2	ζ-potential (mV)	-33.4 ± 1.6
Cation exchange population (meq/100 g)				Na: 28; K: 2.85; Mg: 33.1; Ca: 33.2; Sr: 0.37; Ba: 0.01			
Main minerals (wt.-%)		Accessory minerals (wt.-%)				Poorly ordered minerals (wt.-%)	
Smectite	92 ± 3	Organic Matter (as CO_2)		0.35 ± 0.05		SiO_2	0.038 ± 0.005
Quartz	2 ± 1	Carbonates (calcite, dolomite)		0.60 ± 0.13			
Plagioclase	2 ± 1	Soluble sulfates (gypsum)		0.14 ± 0.01		Al_2O_3	0.035 ± 0.005
Cristobalite	2 ± 1	Low soluble sulfates (barite, celestite)		0.02 ± 0.00			
K-feldspars	Traces	Sulfurs		< d.l.		Fe_2O_3	0.105 ± 0.009
Tridymite	Traces	Chlorides (halite)		0.13 ± 0.02			
Calcite	Traces						

Tab. 2: Concrete characteristics of the two plugs constructed in the FEBEX *in situ* test

1st Concrete plug (1996)		**2nd Concrete plug (2002 – 2003)**		
Concrete characteristics (2.7 m length)		**Concrete characteristics** (Gunite)	**1st plug section** (1 m in 07/2002)	**2nd plug section** (2 m in 06/2003)*
Cement CEM I 32,5 HS (PCO Sulfacem)	160 kg/m³	Cement CEM II A-L 32,5 R	430 kg/m³	475 kg/m³
Silica fume (Sikafume HR)	60 kg/m³	Nanosilica MEYCO MS 660	30 kg/m³	60 kg/m³
Fine aggregate (Grimsel granite 4 – 8 mm)	660 kg/m³	Aggregate 0 – 8 mm	1'700 kg/m³	1700 kg/m³
Coarse aggregate (Grimsel granite 8 – 16 mm)	430 kg/m³	Steel fibres Dramix ZP 306	50 kg/m³	-
Sand (quartz 0.1 – 5.6 mm)	0.8 kg/m³	Polypropylene fibres	0.8 kg/m³	-
Filler limestone)	170 kg/m³	Accelerant MEYCO SA 160 E	6 %	6 %
Water	155 kg/m³	Curing compound MEYCO TCC 735	1 %	1 %
Superplasticizer (Sikament-12+)	13 kg/m³	Superplasticizer Glenium T803	1.5 %	1.5 %
w/c	0.72	w/c	0.40	0.46
Density (g/cm³) Air content	2.394 0.4 %	Density (g/cm³)	2.18 ± 0.01	2.24 ± 0.03
Compressive Strength (MPa)	47.1 (28 days)	Compressive Strength (MPa)	32 ± 4	40 ± 8
Hydraulic conductivity (m/s)	$< 1 \times 10^{-11}$	Hydraulic conductivity (m/s)	4.3×10^{-11}	9.4×10^{-11}

* A layer of approximately 3 – 4 cm of a sprayable polymer product (MASTERSEAL X345) was first applied on top of the existing temporary 1st plug section for the impermeabilisation of shotcrete (as a waterproof membrane) and for improving the water and gas tightness of the test. Data from Huertas et al. (2006) and Fuentes-Cantillana & García-Siñeriz (1998).

1.3 Dismantling of Heater #1 and test configuration afterwards (FEBEX-II)

A partial dismantling of the FEBEX *in situ* test was carried out during the spring of 2002 (from 2 April 2002 to 19 June 2002), after 5 years of continuous heating (Heater #1 was switched off on 28 February 2002). The operation included the demolition of the concrete plug, the removal of the section of the test corresponding to the Heater #1, and the sealing with a new shotcrete plug. A large number of samples from all types of materials were taken for analysis (Fig. 5). A number of instruments were subsequently dismantled, as well as a few new ones were installed. Accordingly, the system design was adapted, and the physical layout was changed in order to ease the partial dismantling operation.

The description of the partial dismantling operation is given in Bárcena et al. (2003): "Dismantling of the Heater 1 at the FEBEX *in situ* test. Description of operations". The configuration of the test, after completing the partial dismantling operation and construction of the full plug length, is shown in Fig. 6. A more complete report that describes the test from the conception up to two years of operation after the partial dismantling is given in Huertas et al. (2006): "FEBEX Full-scale Engineered Barriers Experiment. Updated Final Report 1994 – 2004".

The buffer and all components were removed up to a distance of 2 metres from Heater #2 to minimize disturbance of the non-dismantled area. A dummy steel cylinder with a length of 1 m was inserted in the void left by Heater #1 in the centre of the buffer. Some new sensors were installed in that one additional metre of bentonite buffer.

Additional sensors were introduced in boreholes drilled in the buffer parallel to the drift. To simplify this operation, the new concrete plug was constructed in two phases: an initial temporary plug measuring just 1 m in length, which was built immediately after dismantling (23 – 24 July 2002), and a second section to complete the plug length to the 3 m planned in the design of the experiment (built from 23 to 27 June 2003). Unlike FEBEX-I, the new plug was a parallel plug, without a recess excavated in the rock, constructed by shotcreting. The characteristics of the concrete used for the new plug were different to that used in the First Operational Phase (Tab. 2), being of a Gunite type (Bárcena et al. 2003).

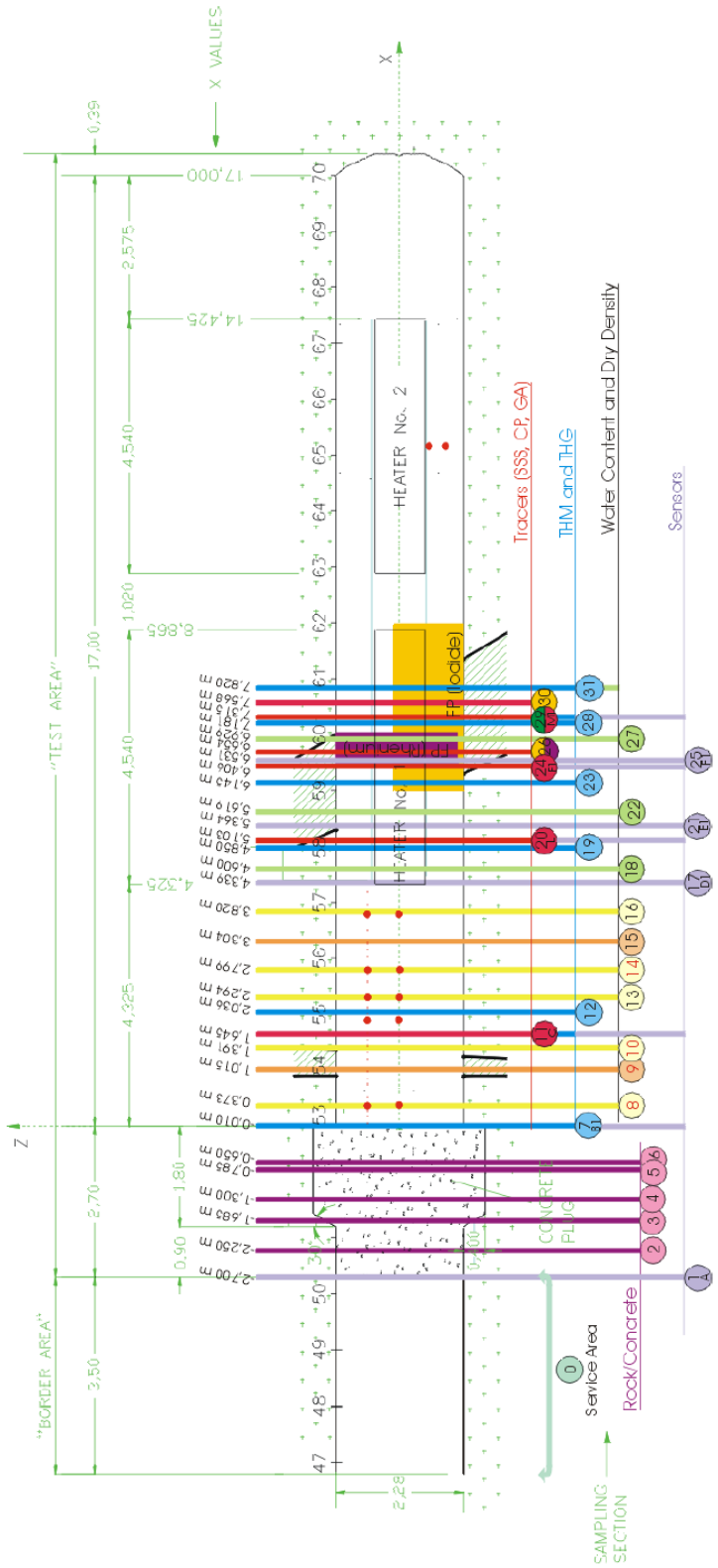

Fig. 5: Sampling layout during the dismantling of Heater #1
AITEMIN (2002)

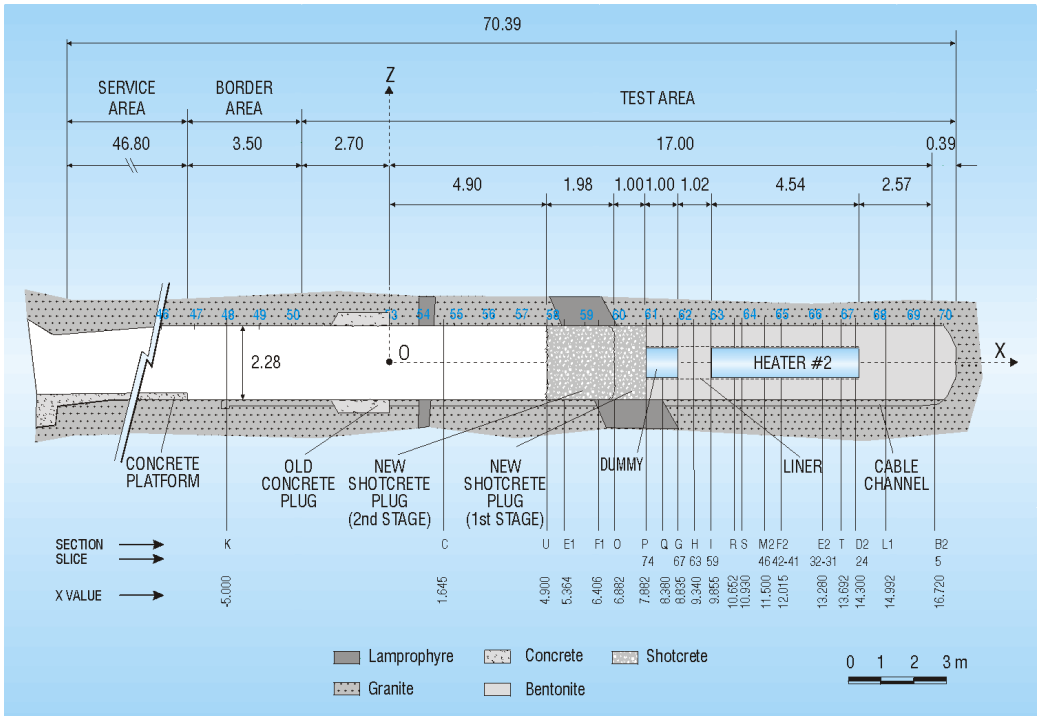

Fig. 6: Status of the FEBEX *in situ* test after the partial dismantling: FEBEX-II configuration in the Second Operational Phase 2002 – 2015

Huertas et al. (2006)

1.4 Concept of Heater #2 dismantling

Heater #2 was switched off on 24 April 2015. The objective of the second dismantling operation, carried out throughout 2015, was to dismantle all the remaining parts of the *in situ* test, including Heater #2 (Fig. 7). This operation includes carrying out a complete sampling of the bentonite, rock, relevant interfaces, sensors, metallic components and tracers to allow the analysis of the barrier condition after 18 years of heating and natural hydration (Fig. 8).

Analytical results will be compared with data obtained from the partial dismantling of Heater #1 (Huertas et al. 2006); the monitoring data (AITEMIN, 2014), as well as with the results derived from modelling efforts (Lanyon and Gaus, 2016). The results are expected to increase the current knowledge and confidence for the FEBEX-DP partners in bentonite performance with a focus on thermo-hydro-mechanical (THM) and thermo-hydro-chemical (THC) processes, as well as on corrosion and microbial activity (Bengtsson et al. 2017: NAB 16-15, Wersin & Kober 2017: NAB 16-16, Villar et al. 2017: NAB 16-17, Villar et al. 2017b: NAB 16-24; Fernández et al. 2018: NAB 16-25).

Indeed, the primary objectives of FEBEX-DP are a further understanding of the processes affecting the components of the *in situ* test through integration of the results of the dismantling with earlier monitoring and dismantling results with a focus on:

- characterisation of the key physical properties (density, water content) of the bentonite and their distribution
- characterisation of mineralogical interactions at buffer and material interfaces and potential impacts on porosity
- characterisation of corrosion processes on instruments and coupons under evolving redox conditions and saturation states
- characterisation of microbiological processes
- comparison with existing models (blind predictions prior to dismantling Heater #2)

All details about the planned dismantling operation of Heater #2 and sampling program are given in the reference documents: "FEBEX-DP (GTS) Full Dismantling Test Plan" (Bárcena & García-Siñeriz 2015a), "FEBEX-DP (GTS) Full Dismantling Sampling Plan" (Bárcena & García-Siñeriz 2015b) and its update (Rey et al. 2015).

All dismantling operations and sample logs are documented in NAB 16-11: Dismantling of Heater 2 at the FEBEX *in situ* test. Description of operations (García-Siñeriz et al. 2016: NAB 16-11), FEBEX-DP – Dismantling related supplementary documents (Kober & van Meir 2017: NAB 16-68), AN-618: Summary of Daily Reports (Kober 2015) and AN 15-578: Sample Log Book 34 to 62 FEBEX-DP (Abós & Martínez 2015).

The final physical conditions of the bentonite along the x-axis of the gallery after dismantling of the Heater #1 and Heater #2 (distribution of temperatures, water contents, dry densities and saturation degrees), are shown in Tab. 3 and Fig. 9, Fig. 10 and Fig. 11 (Daucausse & Lloret 2003, Martinez et al. 2016: NAB 16-19, Villar et al. 2016: NAB 16-12).

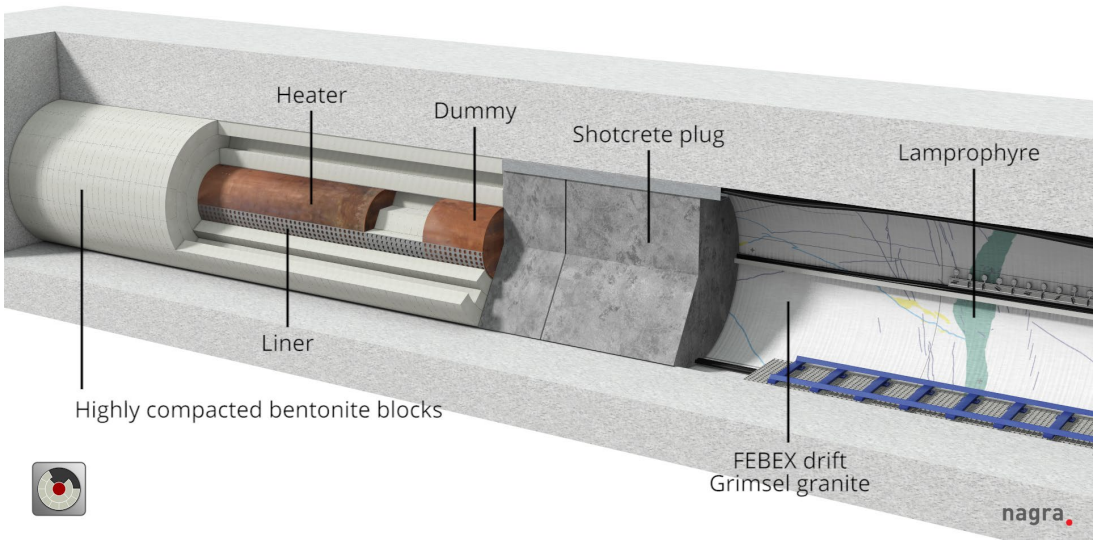

Fig. 7: 3D view of the FEBEX repository with Heater #2 situated horizontally in the centre of three rings of saturated bentonite buffer

Nagra

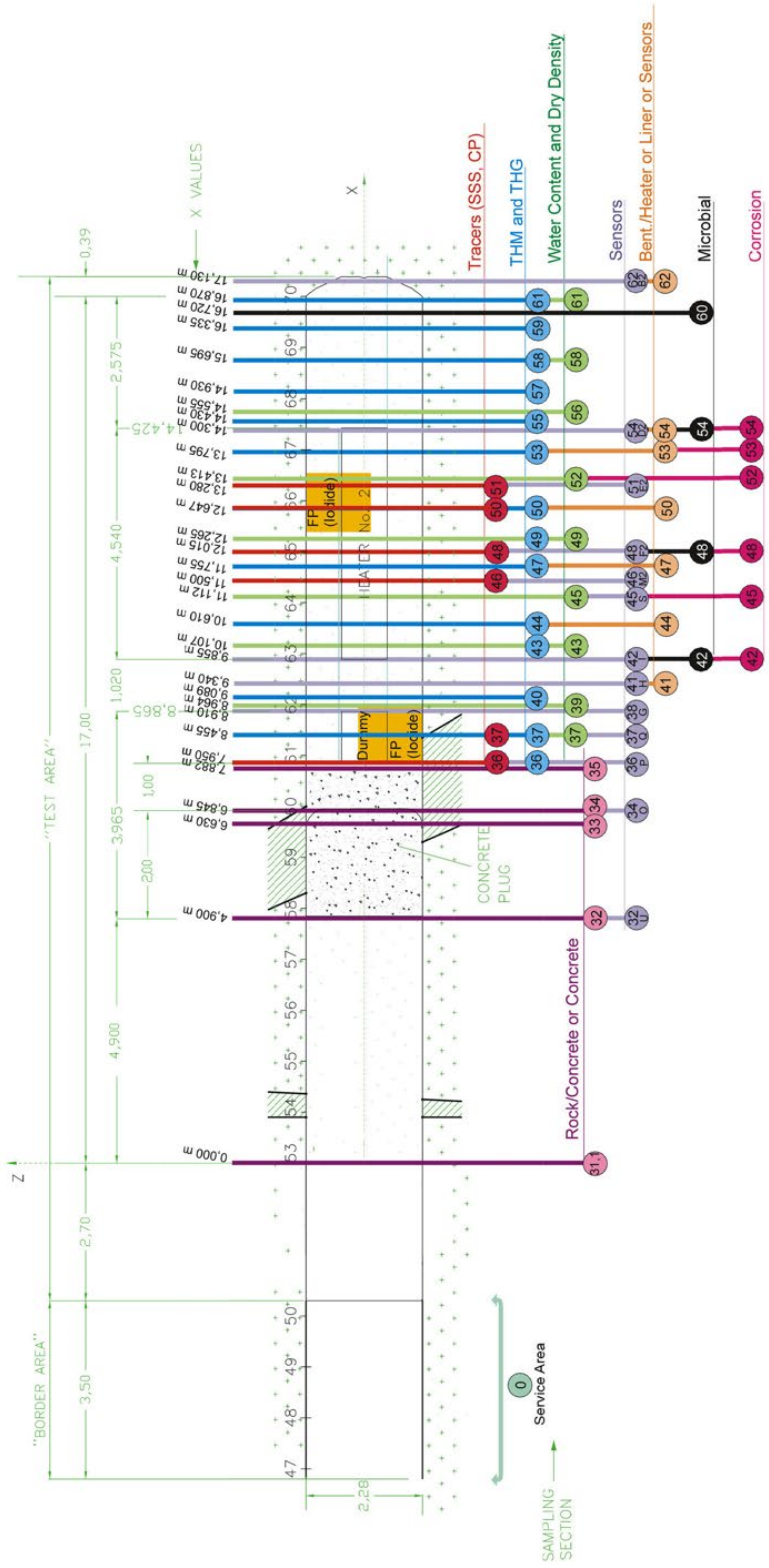

Fig. 8: Sampling layout during dismantling of Heater #2
Garcia-Siñeriz et al. (2016)

Tab. 3: Temperatures in different sections along x-coordinate

Martínez et al. (2016)

Operational Phase	**First Operational Phase: 1996 – 2002**				**Second Operational Phase: 2002 – 2015**					
GTS Gallery	**15 ± 2 °C**				**15 ± 2 °C**					
Bentonite ring	**Section B2** (gallery end)	**Section D1** (Heater #1 front)	**Section G** (Heater #1 rear end)	**Section I** (Heater #2 front)	**Section G (1 m from** Heater #2)*	**Section I** (Heater #2 front)	**Section S** (1 m into Heater #2)	**Section F2** (middle of Heater #2)	**Section D2** (Heater #2 rear end)	**Section B2** (gallery end)
Outer T (°C)	19 – 20	36 – 40	36 – 40	44	30 – 34	37 – 39	-	-	36 – 37	22
Intermediate T (°C)	20	48 – 52	56 – 58	60 – 62	34 – 39	54 – 63	72	75	54 – 56	20 – 22
Inner T (°C)	20	80 – 84	78 – 82	84 – 88	36 – 41	84 – 87	93	94 – 99	83 – 88	22

* After dismantling of Heater #1. Temperature at the Heater #1 surface in Section F1: 95 – 100 °C. Temperature at the Heater #2 surface in Section F2: 96 – 100 °C

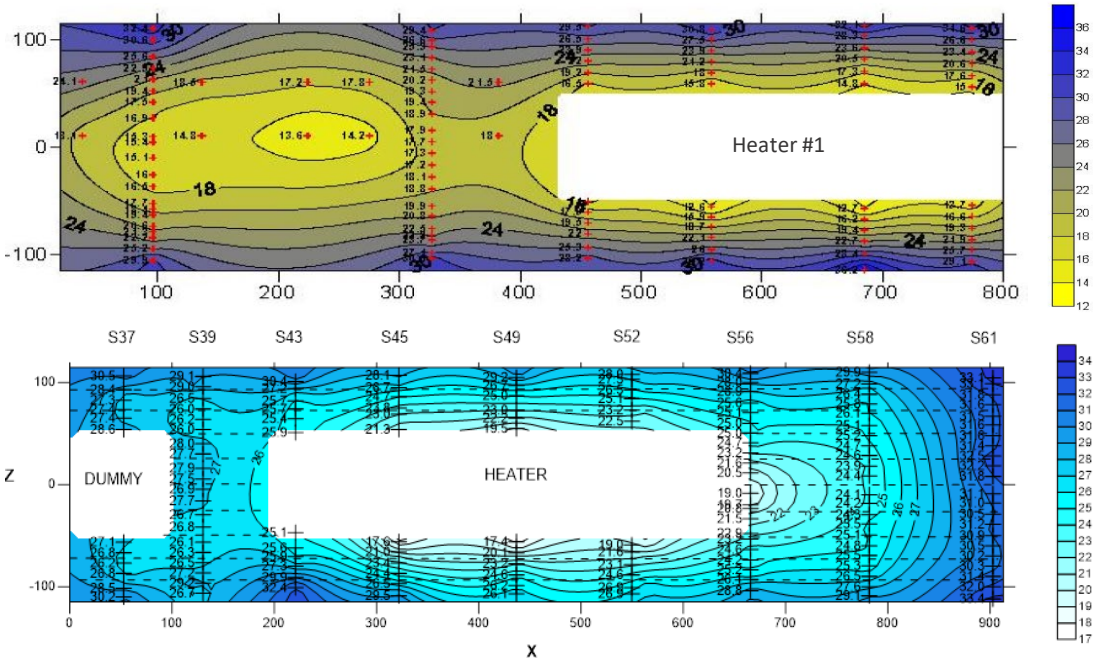

Fig. 9: Water content distribution in a vertical longitudinal section: a) data from dismantling of Heater #1 (Daucausse & Lloret 2003b) data from dismantling of Heater #2 (from Villar et al. 2016: NAB 16-12)

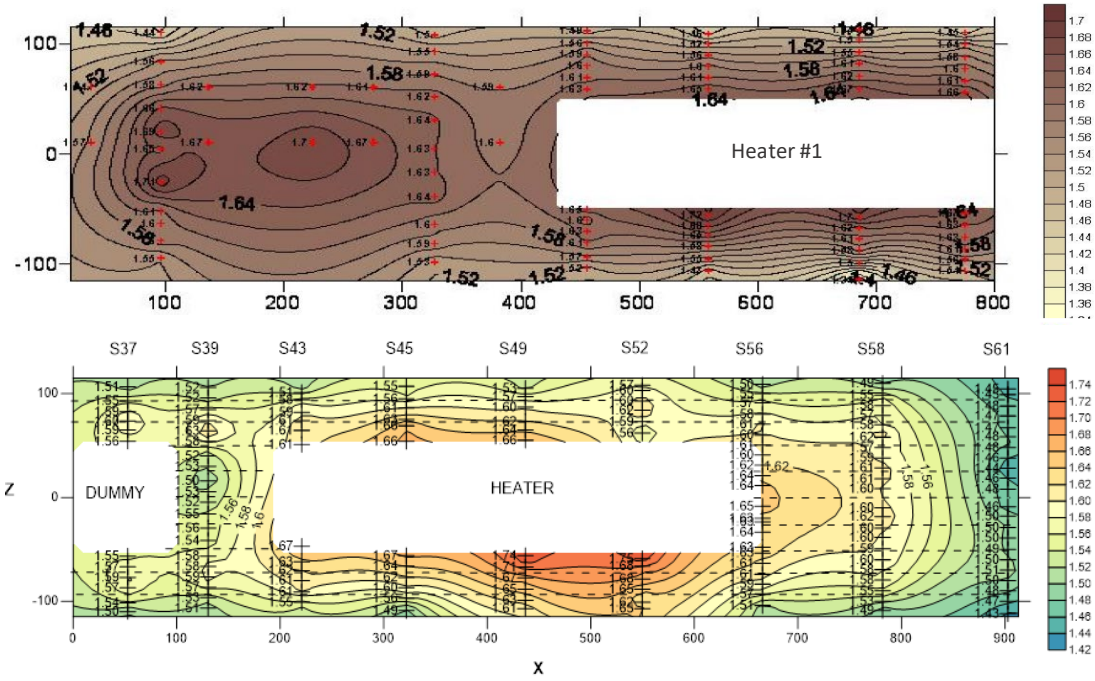

Fig. 10: Dry density distribution in a vertical longitudinal section: a) data from dismantling of Heater #1 (Daucausse & Lloret 2003, b) data from dismantling of Heater #2 (from Villar et al. 2016: NAB 16-12)

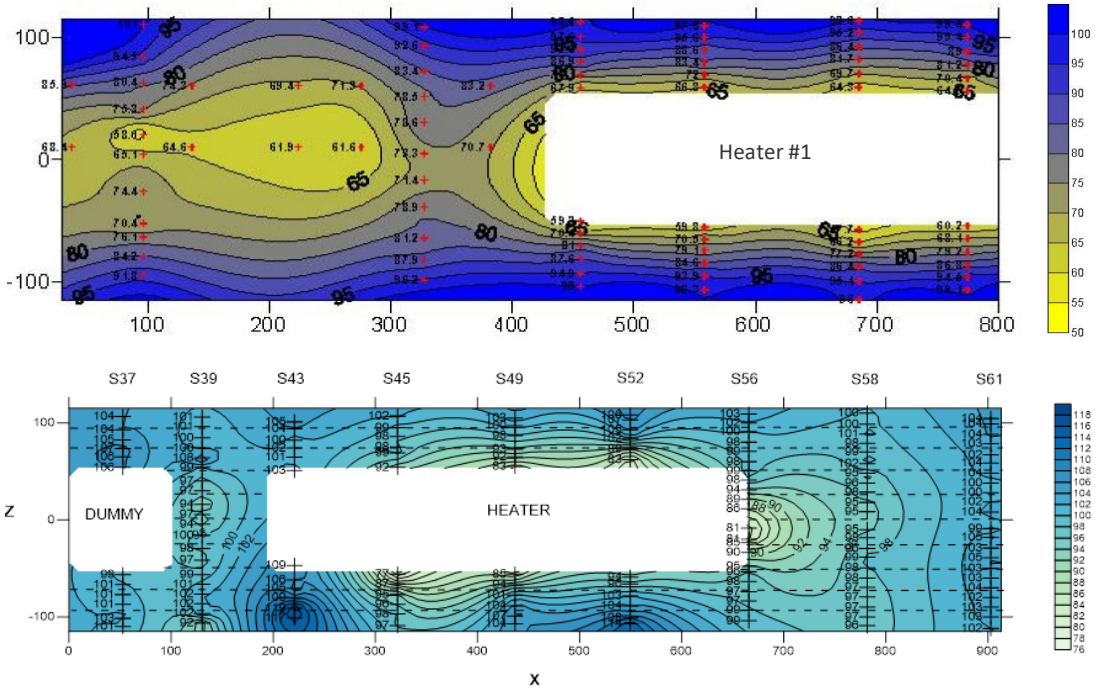

Fig. 11: Degree of saturation distribution in a vertical longitudinal section: a) data from dismantling of Heater #1 (Daucausse & Lloret 2003, b) data from dismantling of Heater #2 (from Villar et al. 2016: NAB 16-12)

1.5 Objectives of the gas and water sampling during FEBEX-I, FEBEX-II and dismantling phases

The accumulation, consumption and release of gases from a high-level radioactive waste (HLW) repository may affect a number of processes that influence long-term safety. Gas accumulation may eventually result in unacceptable build-up of gas pressures high enough to degrade the properties of the engineered barrier system or the host rock, or influence porewater movement. Furthermore, some of the gases produced may be radioactive (e.g. ^{14}C), so their release from the repository to the biosphere may represent a radiological hazard. Gas generation in the engineered barrier system (EBS) can be the consequence of different mechanisms (Horseman et al. 1999, Rodwell et al. 1999, NEA 2001, Rodwell et al. 2003, Marschall et al. 2005, Prítrský et al. 2006, Nagra 2008, Yu & Weetjens 2009, Wolfaardt & Korber 2012, Amman-Hidenbrand 2015, Leupin et al. 2016):

the corrosion of metals: iron, copper and aluminum, producing iron and/or copper sulfides and hydrogen gas. Furthermore, solid solutions (interstitial C, N) and ionic and intermediate carbides and nitrides present in the steel, as well as dissolved species in iron phases of the steel could release nitrogen and carbon (source term) compounds during corrosion; and may be hydrolysed by water and form hydrocarbons (e.g., methane, aldehydes, acetate, formate, oxalate, etc.), CO_2, CO and H_2 (see Wieland & Hummel 2015 and references therein, Swanton et al. 2015, Neeft 2018)

the abiotic and/or biotic (microbial) degradation of organic materials present in the backfill and buffer (e.g., cellulose, wood, cloths, rubber, etc.), releasing CO_2, hydrogen sulphide or methane

the radiolysis of water by α-, β- and γ-radiation, generating mainly hydrogen but also oxygen and short-lived radical species

the steam generation due to the high temperature at the surface of the high-level radioactive waste (HLW) canister

physical transport and interaction with the bentonite buffer and the host rock, which affect the gas composition in the pore space

activation and fission reactions: a) radioactive decay, mainly helium production due to alpha decay, and b) release of radioactive gases: radioisotopes such as ^{3}H, ^{14}C, ^{85}Kr and ^{129}I as fission or activation products, and radon (^{222}Rn and ^{220}Rn) as a daughter product of uranium and thorium decay

Of all these mechanisms the first two, metal corrosion and abiotic and/or microbial degradation of organic materials, are the main processes possible in the FEBEX context (see e.g., Johnson 2006, Norris 2010, Rodwell et al. 2003, Shaw 2015, Suckling et al. 2011). Microbial degradation (and specifically anaerobic degradation) could take place because there are several carbon sources present in the FEBEX set-up, such as organic matter and the presence of bacteria in the bentonite itself (Fig. 12 and Fig. 13). Although little – about 0.1 wt.-% organic matter – the presence of a large mass of bentonite (116 tons) may make this phenomenon important (ENRESA 2000, Fernández 2004, Fernández et al. 2004). This carbon source may support germination of bacterial spores and microbial activity (Fig. 13). Furthermore, the experimental layout contains a lot of organic materials which may be degraded, such as plastics, resins and mainly cellulose from the filter papers (FP, 1.371 kg total, 6.786 g each), which were used for introducing dissolved tracers (152 FP with NaI and 50 FP with Na_2ReO_4, Fig. E-13, García-Gutierrez 2001). The anoxic corrosion of various metal parts (steel, aluminum or iron alloys) from screws, bolts or sensors may give rise to gas formation (Fig. 12). The most important gases expected are hydrogen, methane and carbon dioxide. However, the extent to which corrosion occurs within any time interval will depend upon the availability of water, different parameters of the porewater (composition, pH, Eh, etc.) and the possible activity of microorganisms.

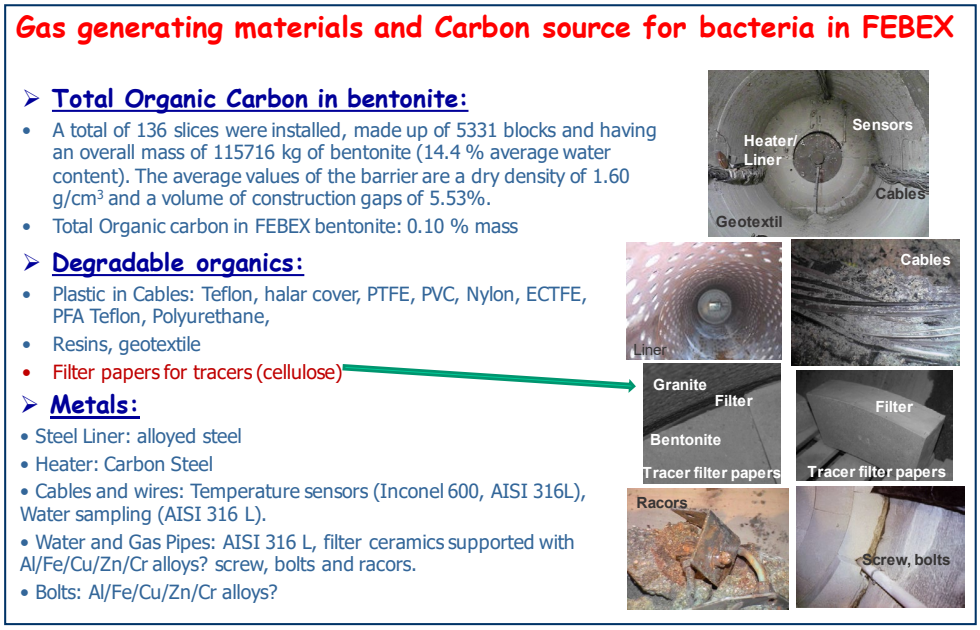

Fig. 12: Potential gas generating materials and carbon source for bacteria in the FEBEX *in situ* test

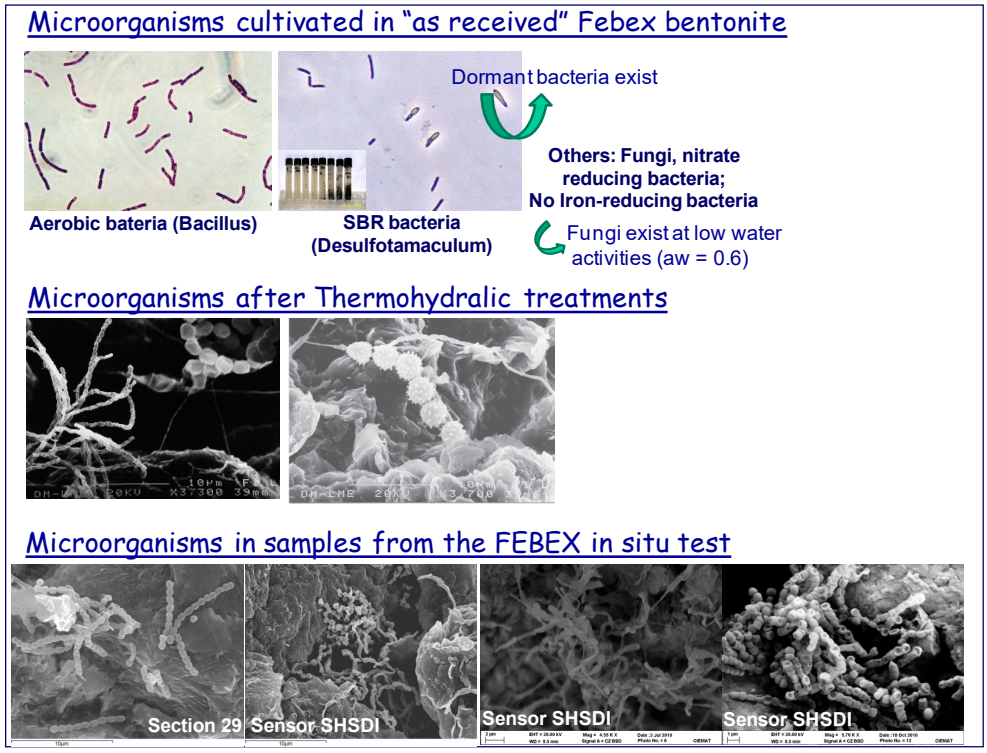

Fig. 13: Microorganisms observed in the FEBEX bentonite: a) cultivated in *as received* bentonite (Mingarro et al. 2004, Mingarro & Rodríguez 1999), b) observed after thermohydraulic treatments (Fernández & Villar 2010), and c) observed in samples from the first dismantling of the FEBEX *in situ* test (Huertas et al. 2006)

Gas generation rates depend not only on the waste components, but also on the detailed repository design (NEA 2001). The possible resultant gas transport can be either pressure-driven or take place dissolved in pore solution (through diffusion or advection) (Amman-Hidenbrand 2015).

One of the objectives of the FEBEX *in situ* test was to analyse the gases generated and transported through the bentonite barrier. However, knowledge and insights changed during the 18 years that the experiment lasted. Consequently, the focus and objectives of the sampling changed over time as well (see Section 1.5.1 below). As gas may be transported dissolved, porewater sampling was a necessary part of the gas sampling campaigns. To this end, sintered stainless steel filters were inserted to sample gas and porewater from the bentonite in situ in 2003. The results of this sampling are reported here and can show the evolution of the gas content and the porewater composition of compacted bentonite subjected to simultaneous heating and hydration. It is compared to all other porewater information obtained during the 18 years of the experiment (Fernández et al. 2018).

This report aims at reporting mainly the most complete gas and porewater sampling campaigns of August 2014 and January 2015 (i.e. during FEBEX-DP), but draws on the knowledge that was gathered before during FEBEX-I, FEBEX-II and after the first dismantling phase, which may help to explain the observed changes in concentration.

The data allow to characterize the *in situ* chemical conditions of the bentonite buffer before the dismantling operations. Furthermore, the data may be used for the interpretation of the buffer behaviour, as well as for the interpretation of the results of the post-mortem analysis, especially those related to corrosion and microbiology (see Wersin & Kober 2017: NAB 16-16, Bengtsson et al. 2017: NAB 16-15).

1.5.1 Gas and water sampling during the FEBEX *in situ* test

In the different phases of the FEBEX *in situ* test (First Operational Phase: 1996 – 2002, and Second Operational Phase: 2002 – 2015), various pipes were introduced inside the bentonite buffer with the aim of characterising the evolution of the gases and the chemical composition of the porewater (Fig. 14, Fig. 15). For this purpose, different gas/water sampling campaigns were performed since 1996, before and after dismantling of Heater #1 (Jockwer & Wieczorek 2008, Fernández et al. 2007).

During the FEBEX-I (1996 – 1999) and FEBEX-II (2000 – 2004) Projects (Fig. 3, Fig. 6), which finished with the dismantling of the first heater (Heater #1), the main objective of the gas/water analysis was to demonstrate the feasibility of *in situ* sampling for deriving the main gas and porewater composition and gas generation processes inside the buffer. However, prior to the dismantling of the second heater (Heater #2) in 2015, the collection of gas and porewater was carried out with the aim to establish the current redox state of the FEBEX *in situ* experiment.

For this purpose, during the FEBEX-DP Project (2013 – 2016) two additional gas/water sampling campaigns were performed for obtaining and characterizing the unaltered gas and porewater composition from the bentonite buffer. The first sampling campaign was performed in August 2014 (three years after the last campaign performed in August 2011), and a second one in January 2015. During these campaigns special precautions regarding the preservation of strict anoxic conditions during sampling were taken, for example, by checking the tightness of the sampling system and analysing both gas and water samples by the same laboratory, avoiding further manipulation of the sampling bags.

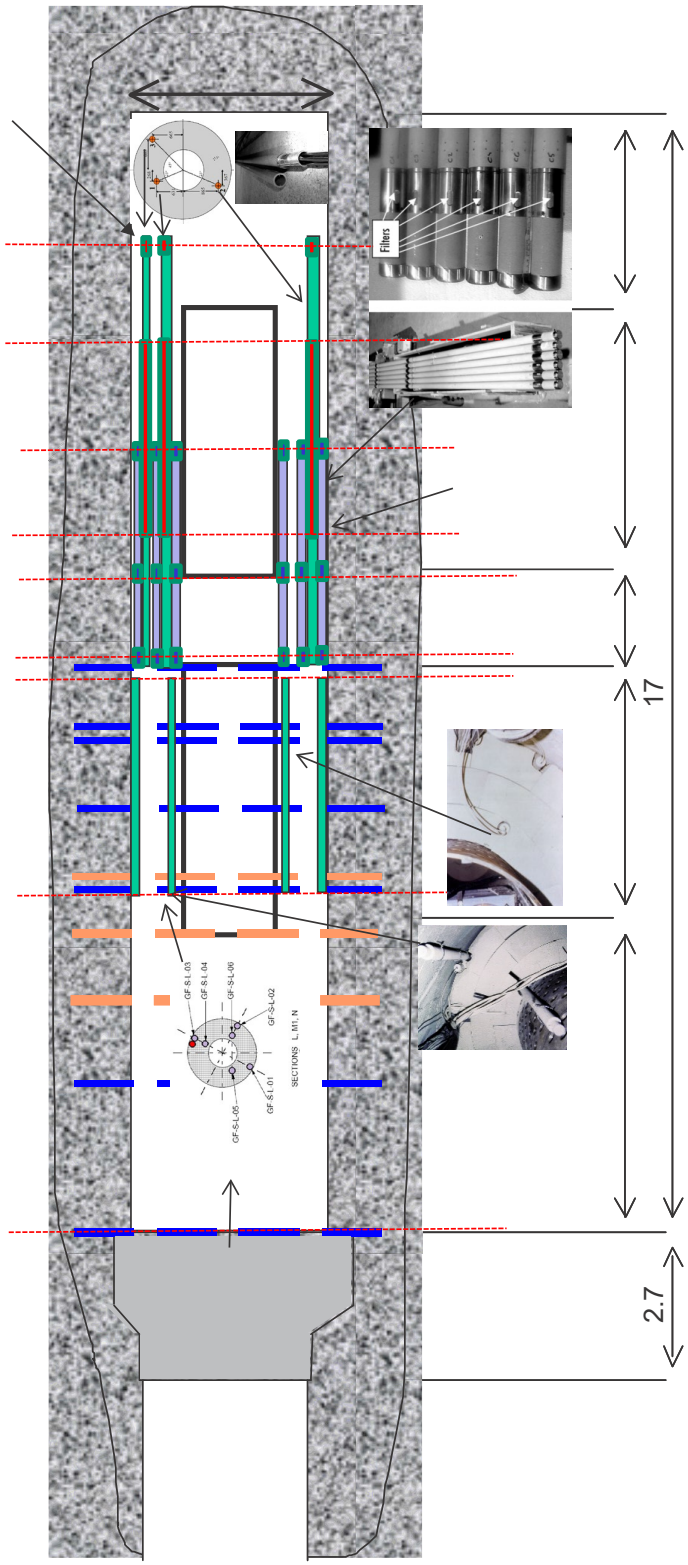

Fig. 14: *In situ* test configuration and location of the gas/water (GRS) and porewater sampling pipes (CIEMAT) during the First and Second Operational Phases

GRS: green colour pipes, CIEMAT: purple colour pipes)

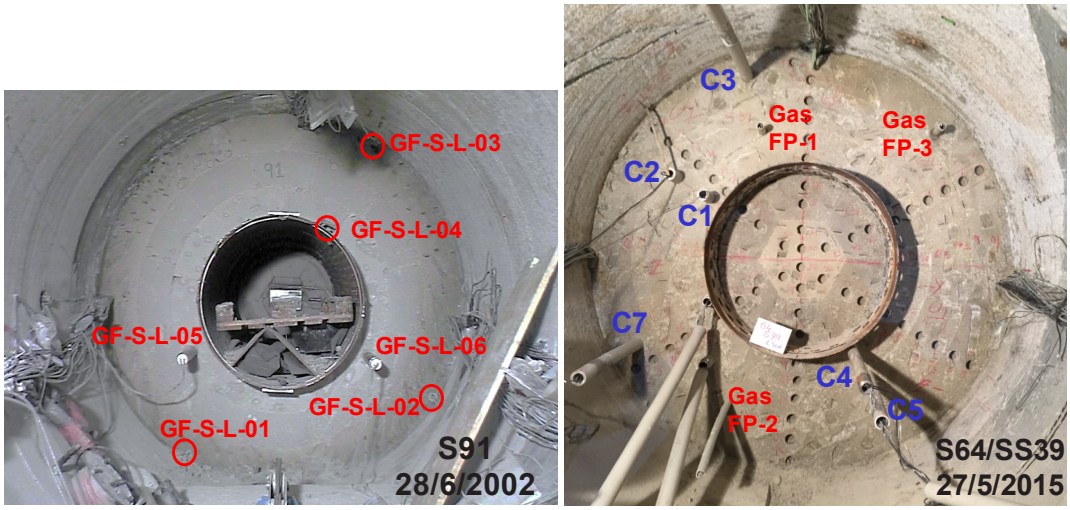

Fig. 15: a) GRS pipes inserted in the bentonite buffer during the First Operational Phase (around the Heater #1: 1996 – 2002) and b) GRS (FP-x) and CIEMAT (Cx) pipes inserted during the Second Operational Phase (around the Heater #2: 2002 – 2015)

Photos taken after dismantling of the Heater #1 and Heater #2 in bentonite Sections 91 and 64, respectively.

1.5.2 Porewater composition of the FEBEX bentonite

An understanding of bentonite's properties and of the processes occurring within the near field is essential for evaluating the performance assessment of a HLW repository. In this context, the knowledge of the porewater chemistry of the bentonite is of special importance for the long-term safety evaluation of a repository, in particular for understanding sorption and diffusion processes, assessing the influence of long-term groundwater/bentonite interactions, the corrosion rate of the canister, and also predicting near-field solubilities.

The processes in the near field are complex, especially in the early, non-isothermal and unsaturated period, when thermal and hydraulic gradients affect the physical-chemical properties of the bentonite barrier and its performance. The mechanical and hydraulic performance of the bentonite barrier is dependent to some extent on the chemical conditions in the near field; and the chemical state of the barrier is controlled by the bentonite-water interactions and defined by the bentonite composition (clay minerals and accessory minerals) and the chemical composition of the porewater.

Numerous experimental studies on the water interaction processes in bentonites have been conducted for decades and the key geochemical processes have been identified. Reactions between bentonite and different groundwaters have been investigated at low (aqueous extracts) (e.g., Wieland et al. 1994), and high (squeezing tests) solid to liquid ratios (e.g., Muurinen & Lehikoinen 1999, Fernández et al. 2001). These studies have shown that the chemical composition of the porewater depends on the solid to liquid ratios involved in the system, and is basically controlled by the exchange reactions and by the dissolution/precipitation of the soluble accessory minerals in the bentonite (see Fernández & Villar (2010) for further references). However, few studies have been carried out on: a) the chemical composition of compacted bentonite at the initial and saturated states of the bentonite barrier (e.g., Bradbury & Baeyens 1998, Muurinen &

Lehikoinen 1999, Fernández et al. 2004); and b) the porewater composition of compacted bentonite subjected to simultaneous thermal and hydration processes (e.g., Cuevas et al. 1997, Poinssot et al. 1998, Muurinen 2003), where the duration of these experiments encompass only short periods of time relative to the long-term safety requirements of HLW repositories.

One of the most important problems in the study of the porewater chemistry in bentonites and clayrocks is the validity of the sampling procedures (Sacchi et al. 2001, Tournassat et al. 2015). Recovering the porewater solution representative of *in situ* conditions from low permeable and low water content systems is very difficult and seems sometimes impossible. Research efforts over the last 15 years have focused on developing techniques for determining the porewater composition of bentonites and clayrocks in the context of waste disposal (Pearson et al. 2003, Pearson et al. 2011; Wersin et al. 2011, Vinsot et al. 2008, Fernández et al. 2014, Mazurek et al. 2015, Tournassat et al. 2015b), including both direct methods (from borehole core samples or *in situ* dedicated experiments carried out in underground research laboratories, URL) and indirect methods (from geochemical modelling).

The approach used for analysing the porewater chemistry of FEBEX compacted bentonite have been squeezing tests at laboratory conditions or by means of geochemical modelling (Fernández et al. 2004, Fernández & Rivas 2005), but porewaters have never been obtained at *in situ* conditions and analysed. The FEBEX *in situ* test offered a unique opportunity to check the chemical conditions and the evolution of the porewater chemistry of compacted bentonite subjected to simultaneous heating and hydration from porewater collected directly from the bentonite over time from a real full-scale field test.

2 Description of the pipes for gas and water sampling introduced in the FEBEX *in situ* test

In order to collect gas and porewater from the bentonite barrier different pipes were inserted inside the bentonite during the First (1996 – 2002) and the Second Operational (2002 – 2015) Phases.

For determining the gas content and the permeability of the bentonite buffer, six ceramic filter pipes 3 m long were installed around Heater #1 by GRS in 1996. After dismantling of Heater #1 in 2002, GRS installed three draining pipe systems made of sintered stainless steel with a length of about 3 m around Heater #2 in April 2003. At this time, CIEMAT inserted also six sintered stainless steel pipes 5.3 m length with the aim of recording the relative humidity and temperature of the FEBEX bentonite over time, as well as to collect and characterize the chemistry of the bentonite porewater.

2.1 GRS Pipes for gas and water analyses from the bentonite barrier

2.1.1 Installation of the GRS pipes in the First Operational Phase (1996 – 2002)

In the First Operational phase (FEBEX-I and FEBEX-II projects), six ceramic filter pipes of 60 mm outer diameter, 40 mm inner diameter and 3 m long (Total volume, V = 3.78 L) were installed by GRS in the bentonite buffer around Heater #1 (Fig. 16). Three of them were located near the heater surface, named GF-S-L-04, GF-S-L-05 and GF-S-L-06; and another three at the gallery wall, named GF-S-L-01, GF-S-L-02 and GF-S-L-03. From these filter pipes flexible PFA (perfluoroalkoxy alkane polymer) tubes run through the backfill and the concrete plug to a valve panel located in the access gallery. At the valve panel, gas and water samples were collected for analyses.

All the sampling pipes were made of sintered ceramic material with an average pore size of 65 µm (Fig. 17). The ceramic pipes have a porosity of 42.5 % and a permeability of 2×10^{-9} m^2, allowing the easy gas and moisture sampling from the buffer as well as gas injection into the buffer. Each 3-m long pipe consisted of three single pipes pieces of 1 m and 40 mm inner diameter, which were connected by Teflon tubes (200 mm length, 20 mm inner diameter, 40 mm outer diameter), and inserted and secured by screws at the interfaces of the pipes. The rear end was closed by a ceramic lid, while the front end was closed by a 20 mm long Teflon plug, secured by a screw. At the front-end plug of each single pipe assembly, two holes were drilled (Fig. 17c) in order to insert two PFA tubes (1/4" diameter) which run through the buffer and the concrete plug to a transducer cabinet in the access gallery. One of the PFA tubes was led to the rear end and the other to the front end of the ceramic pipe so that the residual volume could be flushed by inert gas (GRS 1996, Jockwer & Wieczorek 1999).

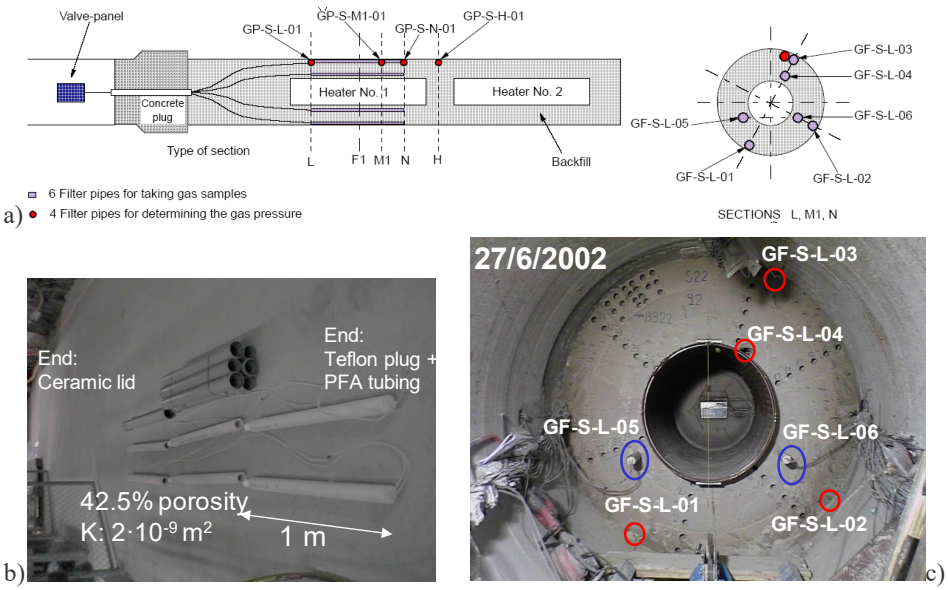

Fig. 16: a) Principal drawing of the FEBEX test gallery with the GRS pipes. b) Visual aspect of the GRS draining pipes for gas sampling and gas pressure measurements prior to installation (Jockwer & Wieczorek 2001). c) GRS pipes observed in the bentonite Slice 92 (bentonite Sampling Section 22) during the dismantling of the Heater #1 in 27 June 2002

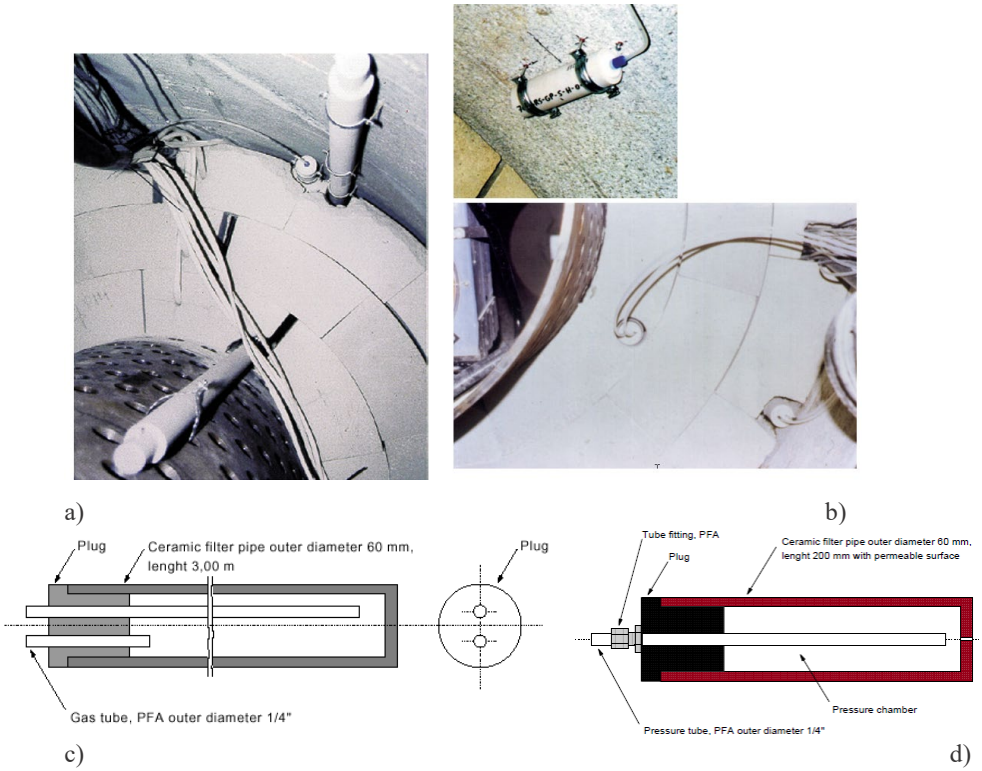

Fig. 17: a) and b) GRS ceramic filters at the bentonite/granite interface and inside the barrier for the sampling and measurement of gas flows. c) Schematic of draining pipe for gas sampling and gas injection. d) Draining pipes for pressure measurements

The six tubes from the rear ends of the gas sampling/injection pipes were closed by valves. The 12 PFA tubes coming from the ceramic pipes were connected to a transducer cabinet located in the access gallery (Fig. 18), where pressure transducers (WIKA type 891.34.500) were introduced for measuring relative pressure up to 25 bar, as well as three parallel mass flow meters (Brooks 5860S) with different measuring range (100, 1'000 and 10'000 mL/min). The pressure transducers and mass flow meters were connected to a data acquisition system. All tubings and connectors within the transducer cabinet are made of stainless steel 316L.

For gas sampling, a sampling circuit provided with a manual or peristaltic pump was plugged via a quick connector to the valve of the PFA tube running to the back end of the draining pipe. Before the gas was taken out of the draining pipes for analyses, about half a litre was removed from the system and discarded in order to purge the PFA tubes. Then one litre of gas was taken and transferred into a second Linde Plastigas® bag. These bags were closed gastight with a special valve and sent to the GRS laboratory for analyses. Samples were collected from 30 November 1996 to 25 February 2002. Sometimes, after the analysis of the gas phase in GRS the water inside the gas bags was sent to the CIEMAT's Porewater Laboratory for performing the analysis of the water phases.

Additionally to the draining pipes for gas sampling/injection tests, four smaller ceramic pipes were installed for pore pressure measurements in Sections L, M1, N and H (named GP-S-L-01, GP-S-M1-01 GP-S-N-01 GP-S-H-01), at the top part of the bentonite (Fig. 16a). They have a length of 200 mm, an outer diameter of 60 mm and an inner diameter of 40 mm each. The rear end is closed by a ceramic lid, while the front end is closed by a 20-mm long Teflon plug, secured by screws. The plug contains a fitting for a ¼" PFA tube, running to the transducer cabinet (Fig. 17d).

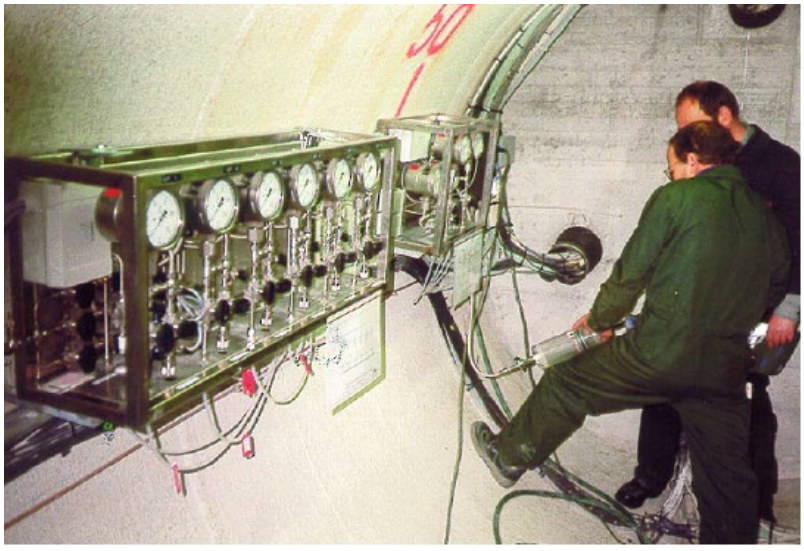

Fig. 18: Transducer cabinet with valves and pressure gauges for gas sampling

During the installation of the bentonite slices and the gas pipes, a water outflow appeared from the granite (Fig. 19a), which may have implications on the gas tightness of the barrier system. The drilling of radial borehole SI2 (x = 10.23 m, y = -8.12, z = -1.54 m of the test zone, Fig. 4) in 1996 produced the entrance of unexpected water (Fig. 19a), with a contributing flow of around five litres/day. This borehole cut the large lamprophyre dike of the test site (Fig. 4a). According to AITEMIN, it was impossible to seal this flow, and water flow was always present on the granite surface in the lower right-hand part of the drift up to the plug (Fig. 19). In placing the bentonite blocks, a rapid hydration of the bentonite at the contact was produced, but apparently the hydrated zone did not penetrate any further than 2 to 3 cm into the blocks. The swelling of the affected material was towards the free surface, but no movements of bentonite mass sections were detected in the radial direction. The water was channelled by the bundle of cables on the right, apparently closing the vertical joints between slices. However, the water appeared up to the last bentonite slice, and even on the outside of the plug (Fig. 19e,f), flowing by capillarity between the different cables, and also on the inside of some psychrometer cables (Fuentes-Cantillana & García-Siñeriz 1998).

Polyurethane foam filled the existing interstices in the bundle of cables on the outside of the PVC tubes, the inside was filled afterwards with a fine slightly expansive mortar (Fig. 19f). This solution did not solve the water outflow of the right lateral tube, as borehole SI2 continued to flow, channelled by the bundle of cables. The exterior mouth of this tube had to be sealed with a hot polyurethane resin, after a laborious operation of first closing it with melted silicone. Even so, a good sealing of this tube could not be achieved (Fuentes-Cantillana & García-Siñeriz 1998).

Indeed, water collected through the cables after the concrete plug sealing could be analysed over time (Tab. 4). The chemical composition indicates the interaction of the granitic groundwater with the bentonite porewater over time due to the changes in pH, alkalinity, pCO_2, Cl and Na, mainly. There is an increase in the pCO_2 and, consequently, a decrease of pH tending to be equivalent to air or even higher.

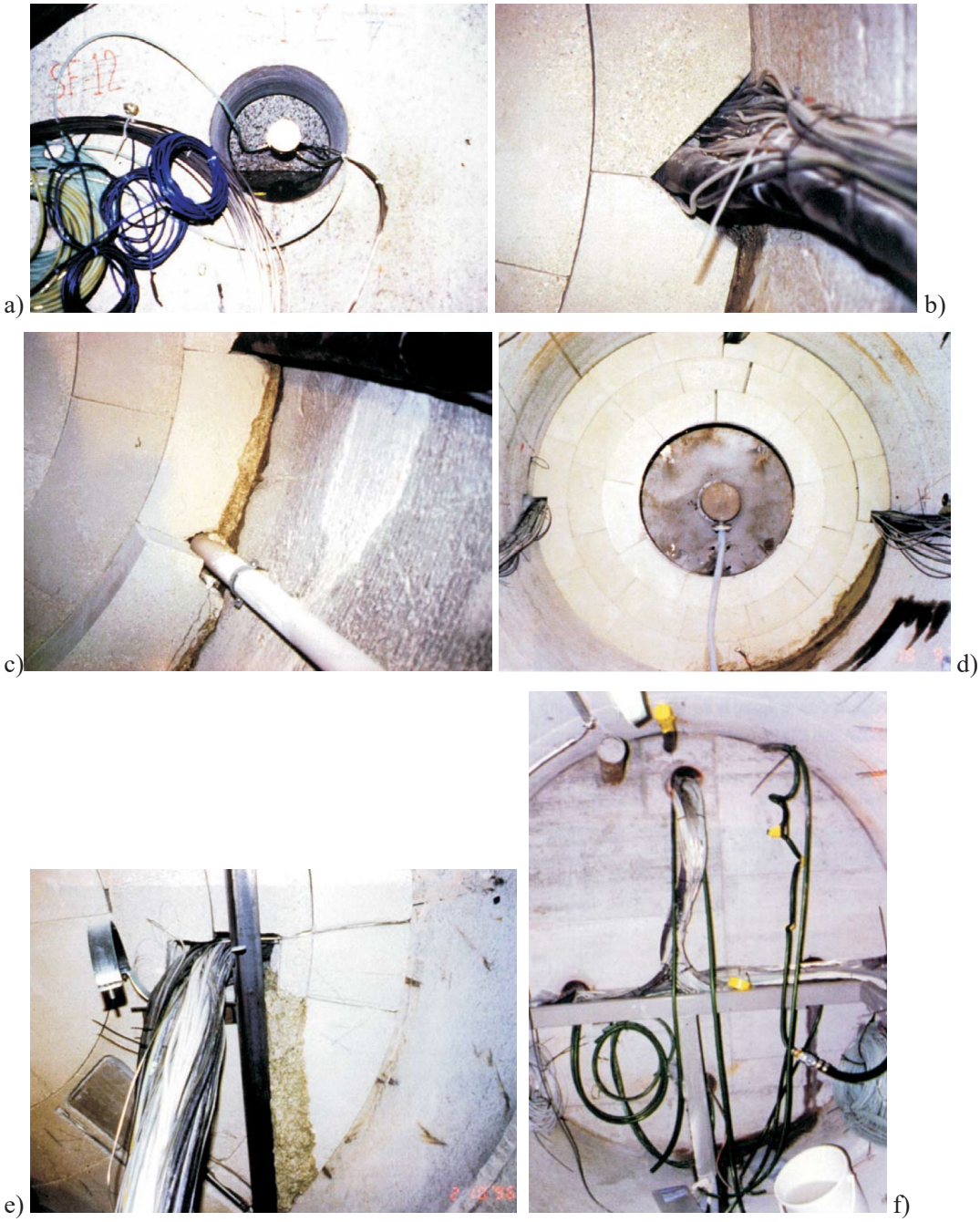

Fig. 19: a) Water outflow caused by the drilling of borehole SI-2, where an extensometer was placed in the granitic rock. b) Water flow at the right-hand side around the boxes placed in the bentonite for cable runs. c) Effect of water flow from borehole SI-2 on the bentonite blocks around the gas pipe GF-SL-02; d) water flow along the cable channel on the right part after insertion of Heater #1. e) Presence of water in the last slice of bentonite before the plug. f) Water outflow along the right-hand plug cable run tube, following completion

The hoses used for the mortar refill of the tube can be seen as well (Fuentes-Cantillana & García-Siñeriz 1998).

Tab. 4: Chemical composition of the water collected through the cables after the concrete plug sealing (CIEMAT) and comparison with a Grimsel granitic groundwater

Sample	**Grimsel GW***	**SI-2/M1**	**SI-2/M12**	**SI-2/M13**	**SI-2/M14**	**SI-2/M15**
Date	-	25.10.1996	16.10.1997	29.1.1998	16.10.1998	12.11.1998
Water-type	$Na\text{-}HCO_3\text{-}F$	$Na\text{-}Ca\text{-}HCO_3$	$Na\text{-}Ca\text{-}HCO_3$	$Na\text{-}K\text{-}HCO_3$	$Na\text{-}HCO_3\text{-}Cl\text{-}SO_4$	$Na\text{-}HCO_3\text{-}Cl\text{-}SO_4$
Flow Rate	7 – 12 L/day	5 L/day	2.5 L/day	1.5 L/day	1.5 L/day	4 L/day
I (M)	0.0012	0.0016	0.0055	0.0135	0.0177	0.0051
TDS (mg/L)	-	76	207	453	711	207
Eh (mV, SHE)	-382	n.d.	n.d.	n.d.	n.d.	n.d.
pH	9.59	9.7	9.1	9.5	8.9	8.4
pCO_2	-5.47	-5.46	-3.85	-3.94	-3.96	-3.39
Cl^- (mg/L)	5.5	4.3	21	48	210	48
SO_4^{2-} (mg/L)	5.5	13	22	54	165	45
Br^- (mg/L)	< 0.1	< 0.01	< 0.1	0.16	0.40	0.13
NO_3^- (mg/L)	-	0.02	< 0.1	6.1	1.1	< 0.1
Alk (meq/L)	0.42	0.8	3.74	9.51	6.72	2.21
F^- (mg/L)	6.1	4.6	2.6	3.8	6.4	3.6
I^- (mg/L)	-	< 0.02	0.07	0.08	0.07	0.034
SiO_2 (mg/L)	12	18.5	22.7	23.6	34.4	22.1
Na (mg/L)	16	19	80	190	320	87
K (mg/L)	0.22	5.9	17	110	24	11
Ca (mg/L)	5.6	6.5	21	19	19	6.3
Mg (mg/L)	0.044	0.22	0.4	0.64	0.8	< 0.4
Fe (mg/L)	-	0.55	0.04	0.11	0.65	< 0.03
Al (mg/L)	0.012	1.8	1.6	1.1	2.5	0.91
NH_4^+ (mg/L)	0.42	< 0.1	n.d.	n.d.	n.d.	n.d.

* BOMI 87.009 (see Appendix A)

2.1.2 Installation of the GRS pipes in the Second Operational Phase (2002 – 2015)

In the Second Operational Phase, after dismantling Heater #1 and during operation of Heater #2, three draining pipe systems of sintered stainless steel with a length of about 4.5 m and outer diameter of 40 mm (34 mm internal diameter, ID) were installed around the Heater #2 in April 2003 (Fig. 20). Each pipe consists of a 3 m long (total volume V = 3.2 L), stainless steel sintered filter that was centred with the heater in the longitudinal direction, and another short filter of the same type at the end of the pipe, connected by equal-diameter tubes.

For transportation reasons, the filter pipes systems were manufactured in single parts with a length of 1 to 1.5 m each (Fig. 21b). After assembling in the main gallery, the pipes were inserted in three boreholes 45 mm diameter and 8.3 m length, as it can be seen in Fig. 21a,d immediately after extraction of the drilling rod used for drilling the boreholes.

The boreholes were drilled in the buffer parallel to the drift axis on April 2003 (days 1, 3 and 7 of April, respectively), up to 0.7 m beyond the rear part of heater #2 (Tab. 5). For borehole drilling, a hydraulic drilling machine type Cordian M60 (and/or Hilti DCM2) was used, with connection for a drilling rod of 1 ¼" UNC by using an adapter, as well as 20 drill rods with 18 mm square connection, 45 mm diameter and 500 mm length of the company Schmidt, Kranz & Co GmbH, D 37445 Walkenried. The drilling crown was a rotary drill bit with 18 mm square pin connection, 44 mm diameter. Different tests were performed beforehand in May 2002 for a successful insertion of the pipes inside the partially-saturated bentonite (Fig. 22). After extraction of the drilling rod, the remaining drilling debris was extracted by a vacuum cleaner over the whole length with an additional 9 m long plastic tube (Fig. 21c), which was introduced without problems, indicating that the borehole was rectilinear without drilling debris.

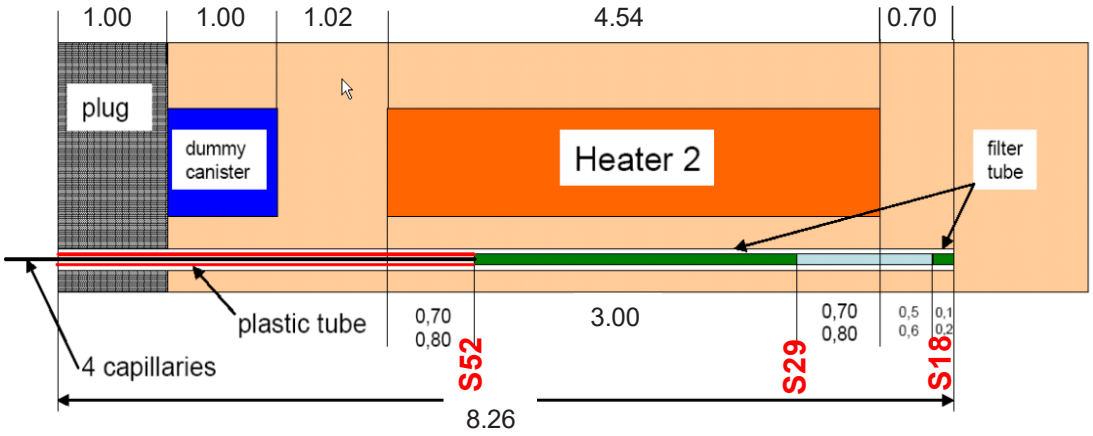

Fig. 20: Structure of one of the stainless steel filter pipes for gas injection and collection between bentonite Section 52 and Section 29 and in Section 18

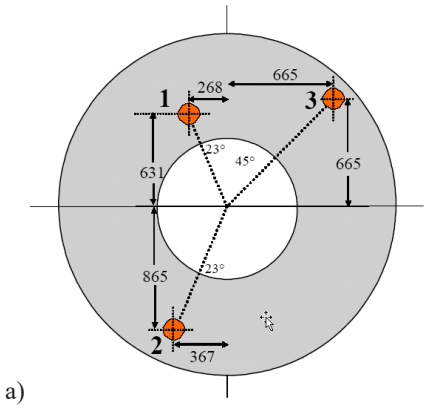

a)

b)

c)

d)

Fig. 21: a) Final position of the boreholes for the three pipes for gas injection and collection (dimensions in mm). b) Sinter stainless steel pipes. c) View of one gas pipe (right), plastic pipe used for borehole checking (left). d) Installation of the gas pipes by Norbert Jocker (GRS) in April 2003

Tab. 5: Coordinates of the boreholes for inserting pipes FP1, FP2 and FP3

Boreholes	**Location**	**Y- coord.** (cm)	**Z-coord.** (cm)	**Angle** (°)	**Distance from wall** (cm)	**Initial date**	**Borehole length**	**Length of extracted concrete**
Borehole 1	Up-left (FP-1)	27.4	64.4	67	44	01.04.2003	8.26	1.05
Borehole 2	Bottom-left (FP-2)	36.7	-86.5	293	20	03.04.2003	8.26	1.16
Borehole 3	Up-right (FP-3)	-66.5	66.5	135	20	07.04.2003	8.26	1.07

For each pipe four 1/8″ stainless steel tubes (capillaries) run a length of 10 m though the backfill and the concrete plug to the valve panel in the access gallery for extracting and injecting gases (Fig. 20, Fig. 23b, Fig. 24). These capillaries were protected inside a plastic tube (type ALPHAPLUS Druckrohr Polypropylen Homopolymer (PP-H) 100 SDR Grau, 40 × 3.7 mm diameter and length of 3.8 m), which was glued to the front end of each draining pipe system. In August 2003, the pipes were connected to a valve panel with pressure gauges and flowmeters (Fig. 23a) used previously in the First Operational Phase.

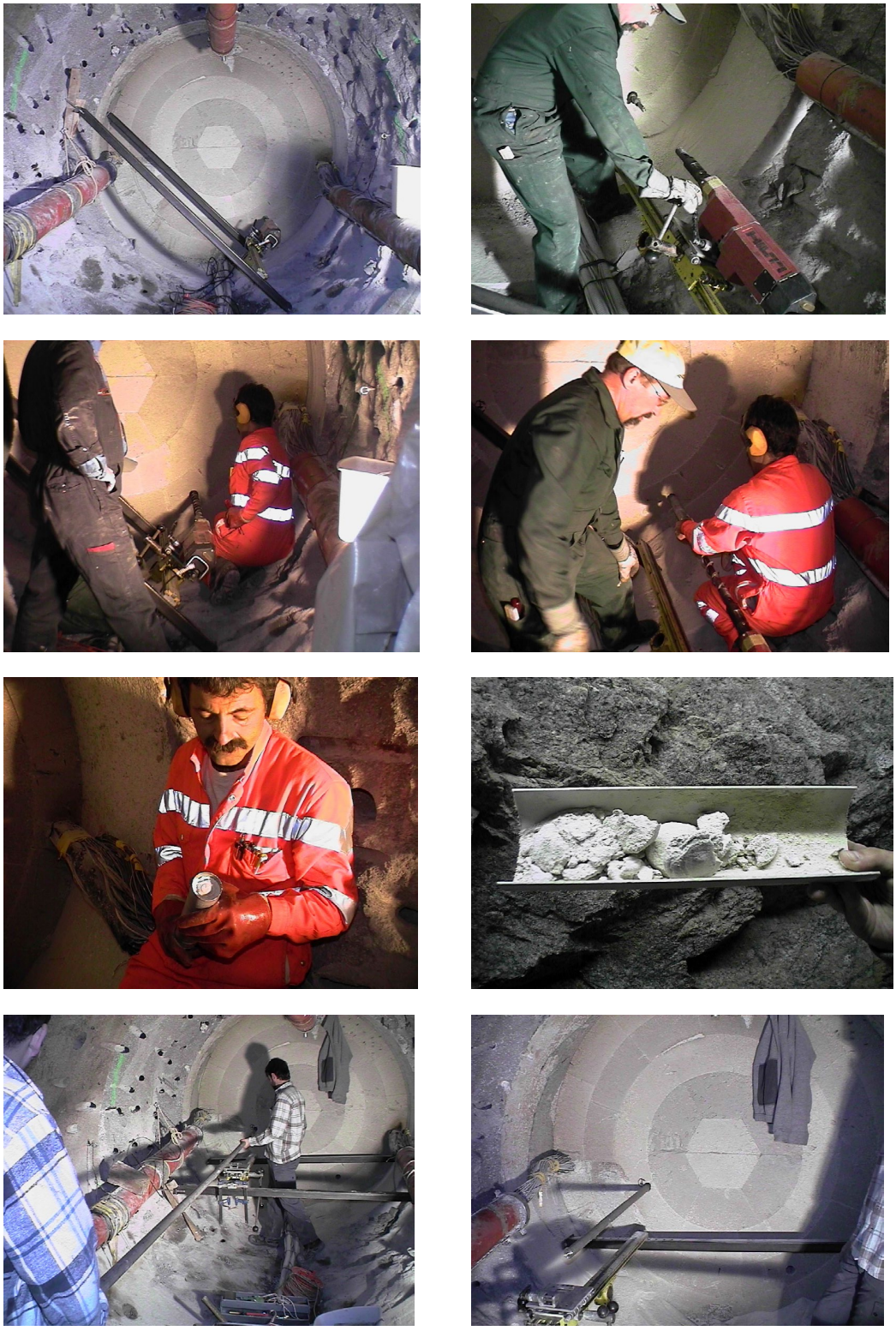

Fig. 22: Front end of the bentonite Slice 131 with the two steel grinders and the mounted machine for drilling boreholes in the bentonite: drilling tests performed on 29 May

2002 during dismantling of the Heater #1 for future installation of the gas pipes around the second heater (Heater #2)

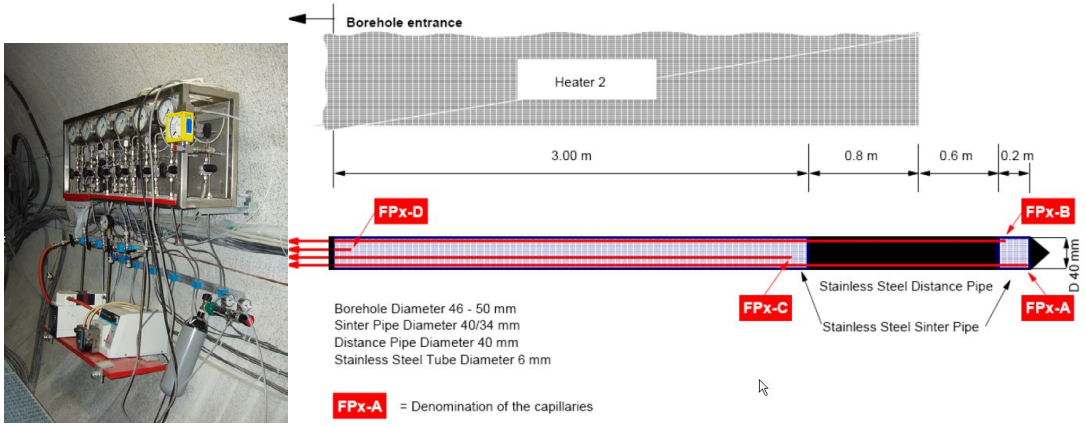

Fig. 23: a) Valve panel with the pressure gauges, flow meters and capillaries from the draining pipes. b) Overview of the draining pipe system

Jockwer & Wieczorek (2008)

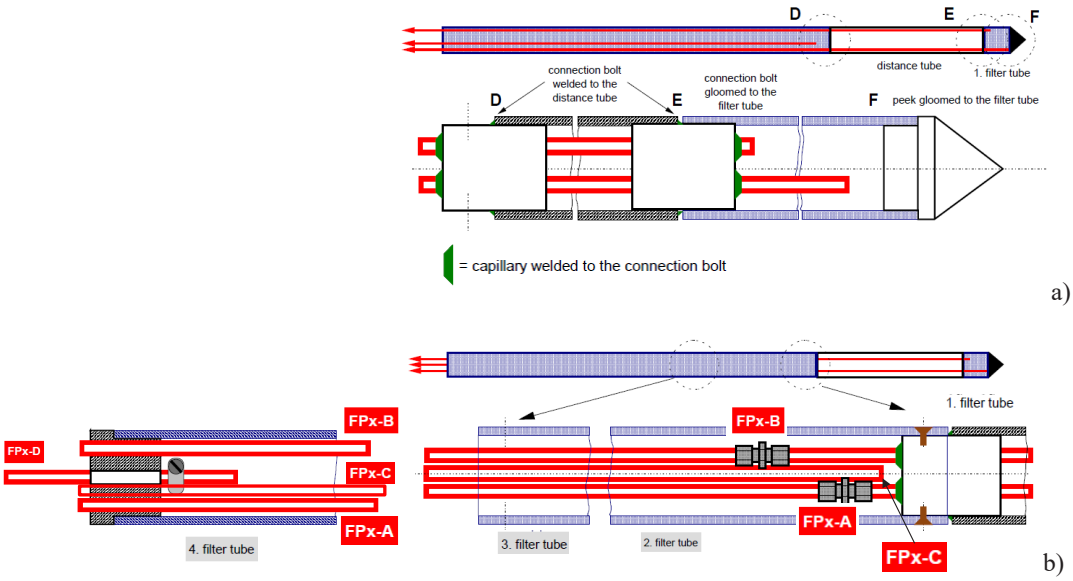

Fig. 24: a) Detail of the draining pipe system from the first filter. d) Detail of the draining pipe system showing the FPx-A, FPx-B, FPx-C and FPx-D 1/8" stainless steel tubings or capillaries for gas/water sampling and pressure measurements

Jockwer & Wieczorek (2008)

The system worked from September 2003 through February 2015. Gas samples for analyses were taken in different sampling campaigns from October 2003 to December 2007 (each 3 – 9 months), and on 11 August 2011 (44 months after the previous campaign). Two additional campaigns were performed on 14 August 2014 and 29 January 2015 during the FEBEX-DP Project. From October 2003 to December 2007, before gas was taken out of the draining pipes the fluid inside the pipes was recirculated and then, about half a litre was removed from the system inside a Linde Plastigas® aluminum foil bag and discarded in order to purge the capillaries. Then, one litre of gas was taken inside a second Al-bag. The procedure for gas/water sampling used from 2011 to 2015 is described in Section 3.1.

During the Second Operational Phase, no leaks were observed through the cables, as observed during the First Operational Phase, which suggested that the cable connection boxes were better sealed with resin, preventing the water leakage across the inner part of the cables. However, after the bentonite barrier was sealed with the concrete plug, a new water outflow was observed. A constant water flow rate of 3.5 L/day coming from the bottom of the gallery was detected. Because of this high water flux, an automatic pump was installed in the drift to collect the water from the bottom of the gallery surface and transfer it into a plastic container. The weight of the water volume recovered being measured over time. This water was analysed in June 2005, resulting a K-Na-Ca-TIC water-type with a high pH 12.1 (Tab. 6). The composition indicates the interaction of the granitic groundwater (due to the F^- and NH_4^+ contents) with the concrete porewater (high pH, K, Ca and alkalinity), which is different from the granitic/bentonite interaction waters observed during the First Operational Phase (Tab. 4). Therefore, at this time, it was not possible to clarify if the water comes from the inner part of the bentonite barrier through the concrete or from the granitic surface around the concrete plug. However, it must be taken into account that the plug was constructed with a higher gas/water tightness than the concrete plug present during the First Operational Phase (Tab. 2), and that the new concrete plug was located in a zone of higher water inflow due to the presence of a lamprophyre (Fig. 4, Fig. A-2 from Appendix A).

Tab. 6: Chemical composition of the water (in mg/L) collected from the bottom of the gallery close to the concrete plug in June 2005

Fernández et al. (2007), Hoehn (1990)

Parameter	**Eh** (mV, SHE)	**I** (M)	**pH**	**Cl^-**	**SO_4^{2-}**	**Br^-**	**Alk** (meq/L)	**pCO_2** (bar)	**F^-**	**SiO_2**	**NH_4^+**
Grimsel GW	-382	0.001	9.6	5.5	5.5	< 0.1	0.42	-5.69	6.1	12	0.42
Collected water	-17.4	0.015	12.1	17	11.3	< 0.1	16.2	-9.69	0.67	4.1	4.0
Parameter	**E.C.** (µS/cm)	**Na**	**K**	**Ca**	**Mg**	**Sr**	**Ba**	**Fe**	**Fe(II)**	**Al**	
Grimsel GW	108	16	0.22	5.6	0.04	0.18	n.d.	< d.l.	n.d.	0.01	
Collected water	1'556	115	245	82.5	< 0.4	1.65	0.08	0.23	0.16	1.15	

Fig. 25: Detail of the second concrete plug after dismantling of Heater #1 and the location of the water flow coming from the granite

2.2 CIEMAT Pipes for bentonite pore water characterization

Six pipes were installed from April to May 2003 with the aim of collecting water from the bentonite buffer for determining the chemical evolution of the bentonite porewater subjected to simultaneous heating and hydration, as well as to recording the evolution of the relative humidity and temperature.

Each pipe was made of four high pressure polypropylene rods (PP-H 100, PN10) with an outer dimeter (OD) of 63 mm of and a length of 1 m. In each of these rods a PP-H100 tube with an OD of 50 mm was inserted to strengthen both the instrumentation and the filtration system. These six pipes with an average total length of 4.30 m each were inserted into the bentonite buffer, parallel to the drift axis up to the instrumented Section F2 (Fig. 26). Each of these pipes has three sections made of a sintered porous 316L stainless steel filters 20.1 cm length (Fig. 27), located at depths corresponding to the instrumented sections G (x = 8.91 m, at the end of the dummy heater, Slice 67: S67, bentonite sampling section: BSS38), I (x = 9.85 m, at the frontal part of heater 2, S59, BSS42) and F2 (x = 12.015 m, at the middle part of Heater #2, S42, BSS48). Next to the porous stainless steel sampling section, three humidity sensors (Vaisala HMP 237, capacitive type) were included for measuring the relative humidity and temperature in each section (Fig. 27).

The pipes were inserted inside different boreholes (Tab. 7), which were drilled on 9 April 2003 immediately after the installation of the gas pipes. A hydraulic drilling machine (Cordian M60) with a 74 mm-diameter drill rod (Fig. 28, Fig. 29) was used for drilling up to a total length of about 5.30 m each. Boreholes B1 and B2 were first drilled by using a 64 mm diameter drill bit, but it proved to be too tight for the pipes. The boreholes were then re-drilled with a 74 mm-diameter drill bit. During the drilling of the borehole Nº 4F, the drill rod broke and the drill bit could not be retrieved, so this borehole was discarded. The drilling works resumed on 19 May 2003 and all boreholes were re-drilled and the pipes intersected. The final location of the six boreholes is shown in Fig. 30.

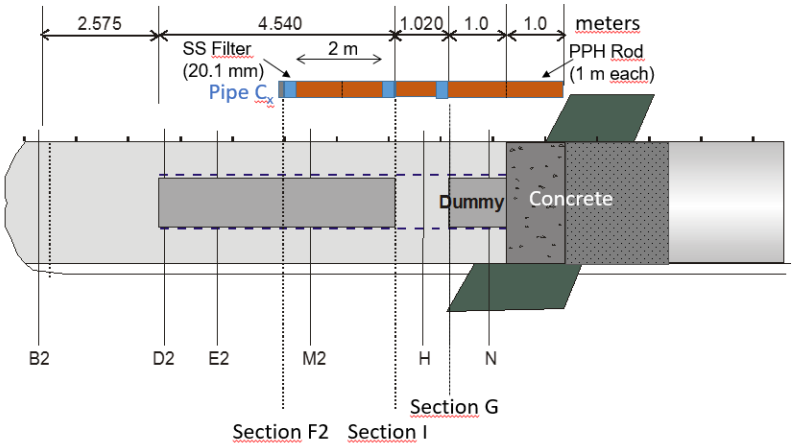

Fig. 26: Location of the 316L stainless steel filters at Sections G, I and F2 in the C_x pipes

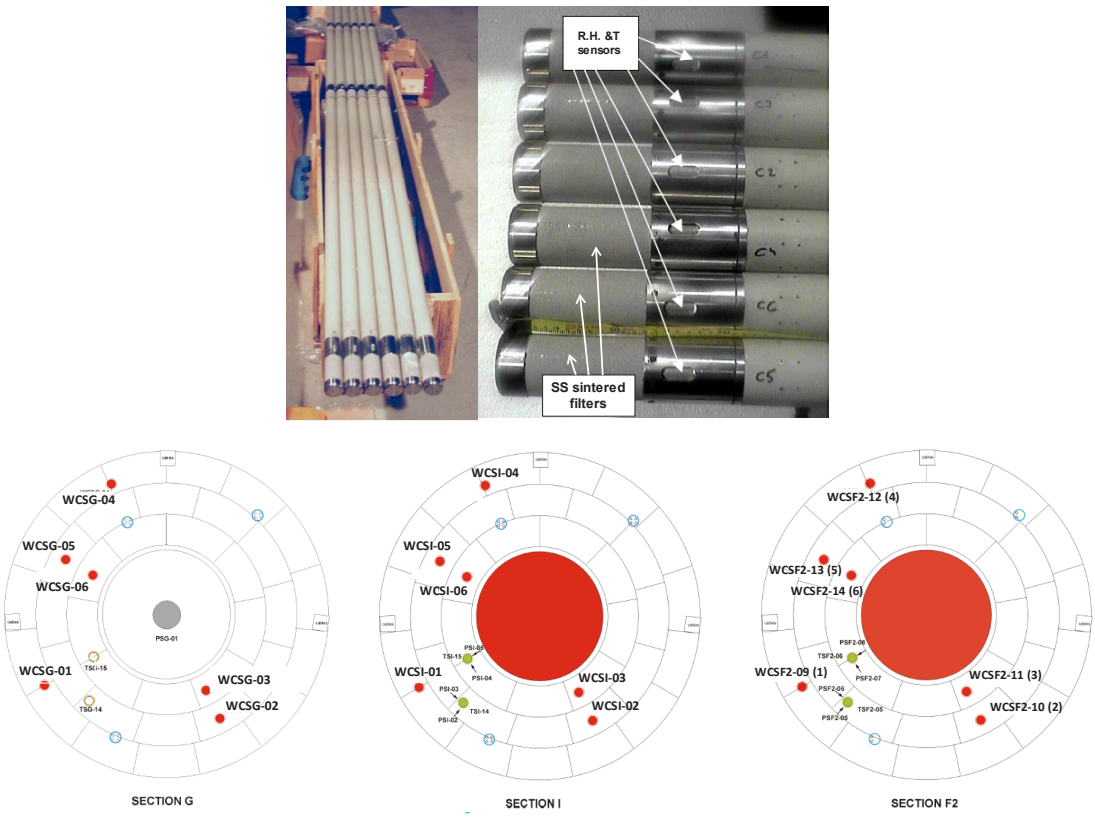

Fig. 27: General view of the CIEMAT's pipes (red circles), detail of stainless steel sintered filters for measuring relative humidity (RH) and collecting the bentonite porewater; location of the pipes at Sections G, I and F2 from the bentonite buffer with the corresponding name of the RH & Temperature sensors

Tab. 7: Coordinates of the boreholes for inserting CIEMAT pipes

Boreholes	**Location of the rods**	**Initial drilling date**	**Y-coord.** (m)	**Z-coord.** (m)	**Angle** (°)	**Distance from wall** (cm)	**Borehole length** (m)	**Bentonite length** (m)	**Length of extracted concrete** (m)
Borehole 1 (B1)	Internal, up (rod C1)	09.04.2003 and 20.05.2003	52.1	27.7	28	55	5.3	4.2	1.1
Borehole 2 (B2)	Internal, bottom (C4)	09.04.2003 and 20.05.2003	-27.7	-52.1	242	55	5.3	4.2	1.1
Borehole 3-F (failed)	External, up	10.04.2003	87.4	46.5	28	15	4.45	3.35	1.05
Borehole 4 (B4)	External, up (rod C3)	19.05.2003	38.7	91.1	67	15	5.3	4.2	1.1
Borehole 5 (B5)	Middle, up (rod C2)	19.05.2003	71.5	38	28	33	5.3	4.2	1.1
Borehole 6 (B6)	Middle, bottom (C5)	21.05.2003	-38.0	-71.5	242	33	5.5	4.45	1.05
Borehole 7 (B7)	External, bottom (C7)	22.05.2003	85.7	-49.5	330	15	5.8	4.4	1.4
Borehole Aitemin-1	Internal (rod A1)	26.05.2003	51.1	-29.5	330	55	5.5	4.38	1.12
Borehole Aitemin-2	External (rod A2)	26.05.2003	54.2	-60.2	321	33	5.62	4.38	1.24

At the top and at the bottom of each sintered filter (Fig. 31 and Fig. 32), two AISI 316 stainless steel tubes (1/8" outer diameter) were connected to AISI 316L tubes (1/16" OD) allowing gas injection in each filter (line-in) and the collection of water from the line-out point. There were, therefore, a total of 18 water sampling points in the clay barrier. The 36 slim stainless steel tubes (18 × 2) ran though the bentonite barrier and the concrete plug to the access gallery where porewater could be extracted. On 21 July and 22 July 2004, the water sampling tubes were connected to stainless steel two-ways valves which were maintained closed over time, except for sampling. Six valves were connected close to the cable pass box named I (at the roof), eighteen valves close to the cable pass box named II (at the left side), and twelve valves close to the cable pass box named III (at the right side) (Fig. 30). The position of the Vaisala HMP 237 humidity sensors at each section is shown in Fig. 33.

Fig. 28: Drilling machine, rod and bit used for drilling boreholes where the gas and water sampling pipes were inserted

Fig. 29: Drilling of boreholes and insertion of the six C_x pipes for water sampling in May 2003

a) b)

Fig. 30: a) Location of the CIEMAT pipes (C_x), Aitemin's pipes (A-1 and A-2: for measuring total pressure and temperature at Sections I and F2), and the broken drilling rod. b) The corresponding water sampling points from each pipe at the gallery entrance

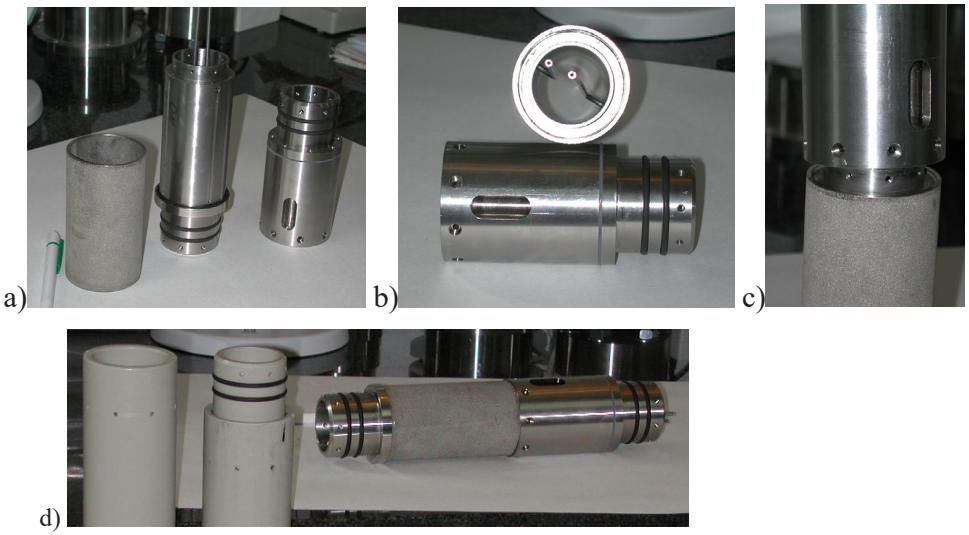

Fig. 31: Fluid sampling assembly of elements: a) parts, b) detail, c) insertion, d) element and rods

Fig. 32: Fluid sampling element and rod: a) after dismantling, b) element without the porous 316L stainless steel sintered filter, and c) detail of the 1/8 to 1/16" tube reduction

Photo taken during dismantling activities in 2015.

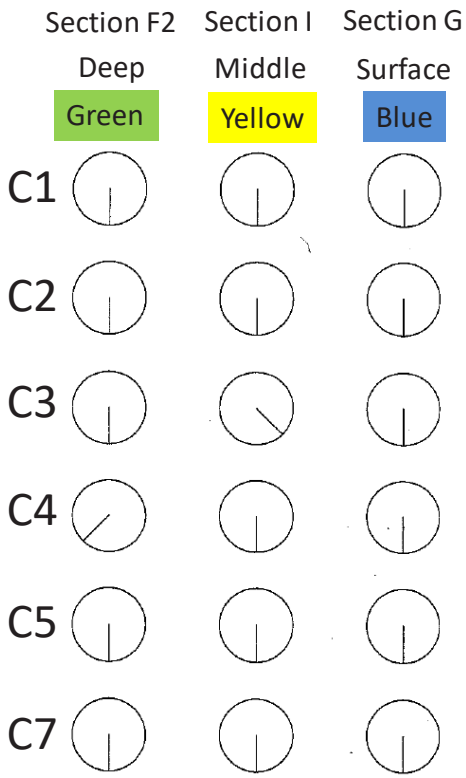

Fig. 33: Position of the VAISALA sintered filters for RH & T measurements in each pipe at Sections F2 (deep interval: at the middle of Heater #2), I (middle interval: at the frontal part of the Heater #2) and G (surface interval: at the rear-end of the dummy); and related colours of the sampling lines at different bentonite sections

It must be stressed that the labels of the different pipes (C1, C2, ...C7) inserted in the bentonite buffer (Fig. 34) are different from the borehole names where the pipes were inserted (Fig. 35), as well as from the relative humidity sensors' labels (Fig. 27). During the final concrete plug installation some of the references labelling the sampling lines were lost or erased leading to the confusion in the labels for the installed pipes, especially in the sampling lines C1, C2 and C7, as well as in the location of the sampling intervals (G, I and F2). Although the collected waters were obtained following the same order and location in all sampling campaigns, this should be taken into account for the interpretation of the results.

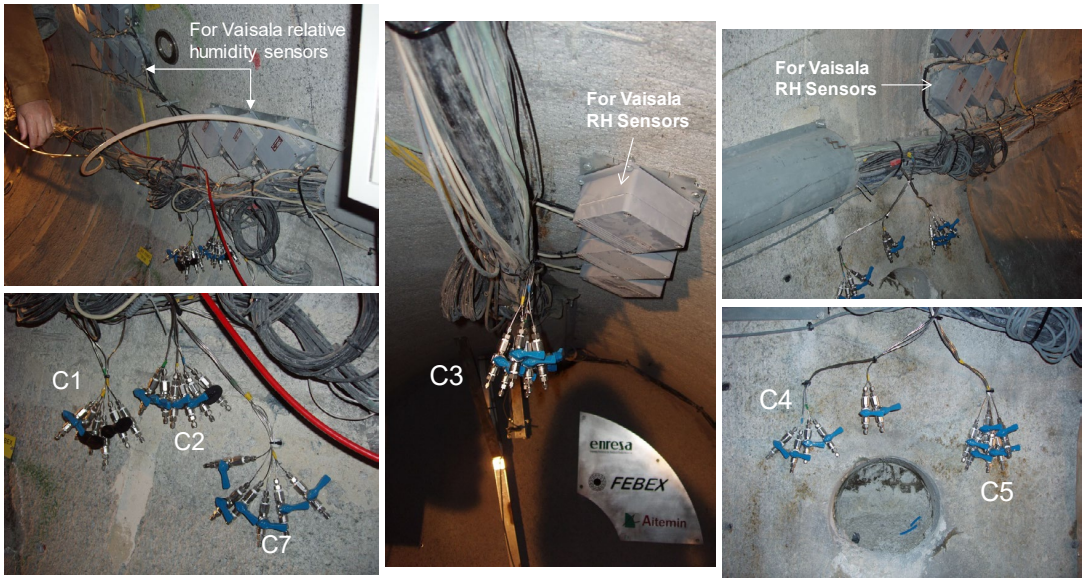

Left side **At the top of the gallery** **Right side**

Fig. 34: Labelled sampling points in the CIEMAT pipes showing the valves from each sampling interval (yellow colour: Section F2 (deep interval: at the middle of Heater #2), green colour: Section I (middle interval: at the frontal part of the Heater #2) and blue colour: Section G (surface interval: at the rear-end of the dummy)

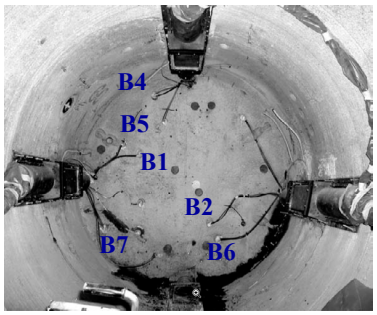

Name of the pipes in AITEMIN's nomenclature	Name of the Sampling points in the gallery	Associated RH sensor
B4	C3 at the top	WCS-x-04
B2	C4 at the right	WCS-x-03
B6	C5 at the right	WCS-x-02
B5	C2 at the left	WCS-x-05
B1	C1 at the left	WCS-x-06
B7	C7 at the left	WCS-x-01

Fig. 35: Boreholes drilled for insertion of the Cx pipes and the correlation to the water sampling points in the gallery and to the humidity sensors. x: Sections G, I or F2

3 Methodology

This section describes the methodology of the sampling campaigns performed in 2014 and 2015 for collecting and analysing the gas and water from the GRS and CIEMAT pipes installed during the Second Operational Phase. Additional information about the methods used by GRS during the First Operational Phase is also given.

3.1 Gas/water sampling from the GRS pipes around the Heater #2

Three draining pipe systems of sintered stainless steel with a length of about 4.5 m and 40 mm diameter were installed around Heater # 2 in April 2003 (Fig. 14, Fig. 36). Details of the installation are given in Section 2.1.2. The tubes from the 0.2 m interval were labelled FPx-A and FPx-B (x being the number of the pipe or probe: 1, 2 or 3). The sampling tubes from the 3 m interval were labelled FPx-C and FPx-D.

These tubes were connected to the valve panel with pressure gauges and flowmeters in August 2003, and the system started operating in September 2003. Gas samples for analyses were taken from October 2003 until December 2007; every three months at the beginning and every six to nine months later. Another campaign was performed in August 2011, 44 months after the previous one. For sampling each pipe, a gas/water sampling circuit (Fig. 37, Fig. 38) or equipment made of stainless steel was connected to the respective connectors FPx-C (Swagelok SS-QF4-B-400 quick connector, female), and FPx-D (tube clip connector) located at the valve panel (Fig. 36).

For the sampling campaign of August 2014 (in the context of the FEBEX-DP Project), the valve panel was in operation but the external sampling circuit for collecting gas and water from the GRS pipes had been dismantled already (Fig. 36). Therefore, it was necessary to clean the area and the rack panel first, and to insert the circuit for the gas/water sampling in the whole system. The setup of the circuit system is shown in Fig. 37 and Fig. 38 and is the same used by the GRS team in previous campaigns. However, now two high precision digital manometers (Keller, LEX1 model) were mounted on the circuit for the measurement of the pressure inside the FPx-C and FPx-D lines (Fig. 39). Furthermore, helium instead of nitrogen gas was used as carrier gas for flushing/cleaning the sampling circuit. Helium gas was used for checking and discarding air contamination during the collections of gas/water samples.

The sampling system was composed of:

a) a stainless steel collecting circuit with different Swagelok connectors and valves

b) an Ismatec BVP-Z ISM 446 peristaltic pump for circulating around 0.5 – 3 L of gas/water fluid from the sintered steel pipe for homogenization and for retrieving the sample, at a flow rate of 100 – 500 mL/min for 30 minutes

c) a Rotary Vane Pump FB54915 Fisher Scientific vacuum pump for evacuating the sampling system prior to sampling: 2×10^{-3} mbar ultimate pressure, 4.6 m^3/h pumping speed, 1 bar maximum outlet pressure)

d) two high precision digital manometers Keller LEX-1 (0 – 10 bar absolute, 0.025 % accuracy)

e) Super^{TM}–Inert Foil Gas sampling bags and/or Tedlar® bags for collecting gas/water (Fig. 41)

f) FEP (fluorinated ethylene propylene) tubes (6 × 4 mm diameter), chemically inert to most industrial fluids and gases and having the lowest permeability to gases, which were connected to the connectors FPx-C and FPx-D on the transducer rack for the recirculation and collection of gas and water from inside the pipes

g) gas bottles with helium gas (99.9999 % purity) with a 0 – 10 bar manometer

The total internal volume of the sampling circuit, including all tubings was around 0.2 L. Briefly, before sampling each pipe, the sampling circuit was connected to: the valve panel, the digital manometers, the vacuum pump, the peristaltic pump and the gas bottle (Fig. 37, Fig. 38). Then, the sampling system was cleaned with circulating distilled water, and gas-dried by means of several cycles of gas flushing and subsequent evacuation. The sampling bags were also filled with gas and evacuated several times, for avoiding O_2 contamination from air, and left at vacuum. Then, the sampling circuit was filled with gas at an overpressure of 1 bar (for avoiding degassing during the collection of samples). Prior to open the sampling circuit to the pipe system, valves FPx-C and FPx-D were opened for measuring the interval pressure. Then, the valves connecting the sampling circuit and the valves FPx-C and FPx-D were opened, and the fluid inside the filter was recirculated for homogenization during 30 min. Finally, one of the two sampling bags connected to the system was opened for filling with gas or gas/water mixture coming from the bentonite buffer (Fig. 40, Fig. 41, see complete procedure in Appendix C). This bas was sent for gas/water analyses at Hydroisotop. Additional water samples were collected by using the second Al-bag inserted in the sampling circuit (Fig. 38). If further water samples could be collected, the FPx-C line of each pipe was flushed with carrier gas for collecting the water through the FPx-D line inside Al-bags or septum vials. At the end of each sampling campaign all the pipes were left under vacuum.

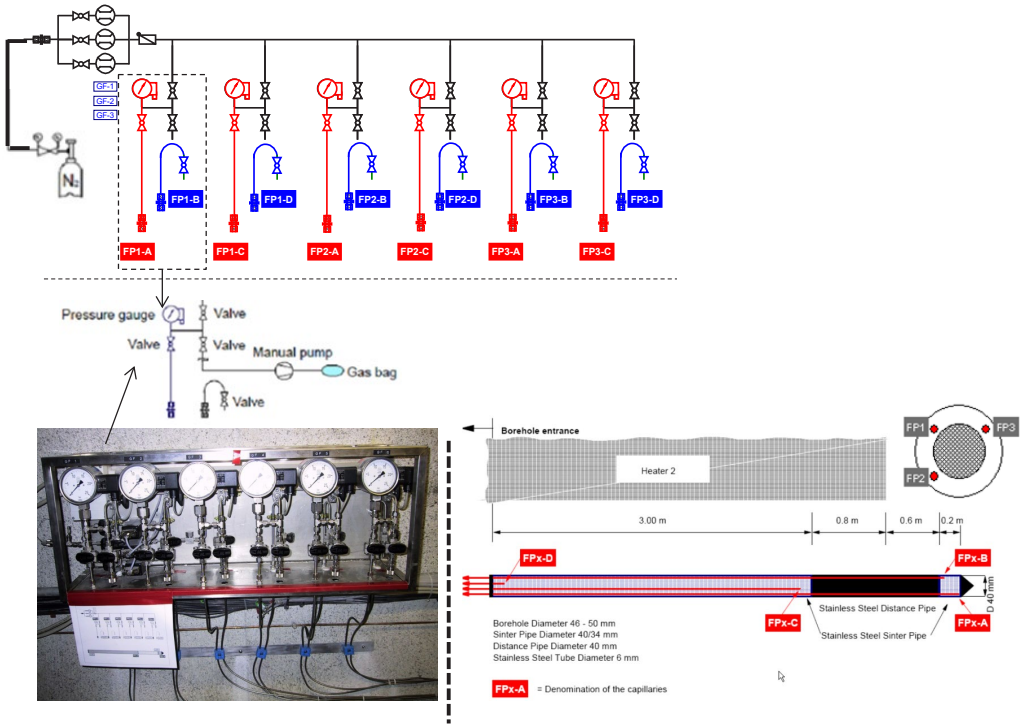

Fig. 36: Valve panel with the pressure gauges, flow meters and SS tubings from the GRS pipes, and overview of the draining pipe system

Jockwer & Wieczorek (2001)

In the sampling campaign of January 2015, due to the presence of some amount of oxygen in the gas analysed during the 2014 campaign, the sampling circuit was modified to allow control the tightness of the system better by changing the quick connectors and tube clip connectors by Swagelok two-way and three-way ball valves (Fig. 42). Furthermore, stainless steel 500 cm^3 gas cylinders with internal PTFE coating were used for collecting the fluid (gas/water) from the pipes instead of the Al coated plastic bags (Fig. 43). Another modification was the introduction of a sub-circuit inside the collecting circuit system, which would allow the insertion of additional multilayer Al-foil sampling bags for extra water collection, when needed, preserving the anoxic conditions in the system.

Fig. 37: Set-up of the system for collecting gas and water in the GRS pipes in 2014

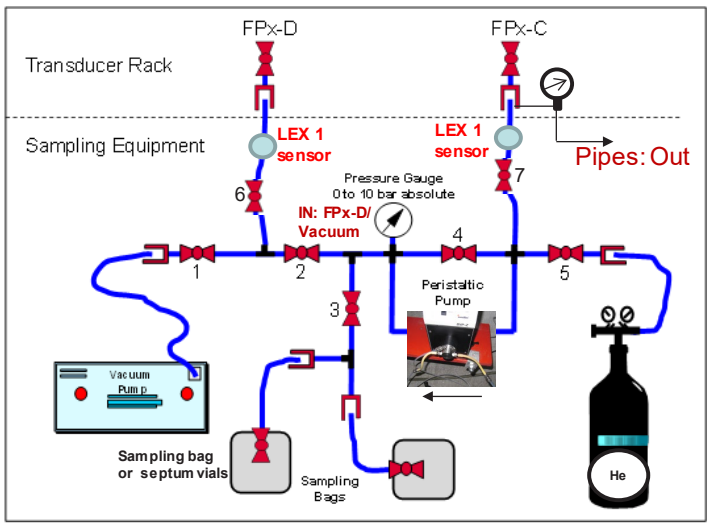

Fig. 38: Sampling circuit for gas/water sampling used in the GRS pipes during the sampling campaigns from 2003 to 2014 (LEX type manometers were introduced in 2014)

Total internal volume of tubings: ~0.2 L

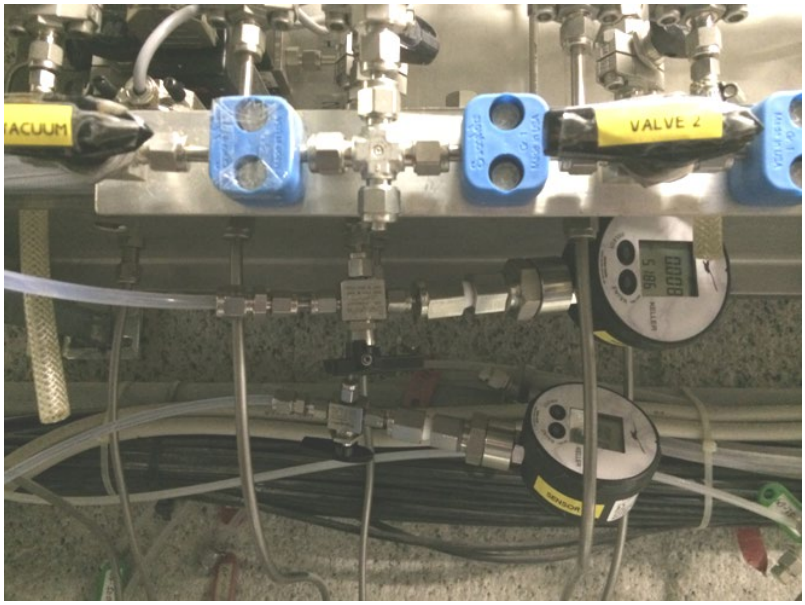

Fig. 39: Detail of the connection of the LEX1 manometers to the connectors FPx-C and FPx-D of the sampling lines of each pipe

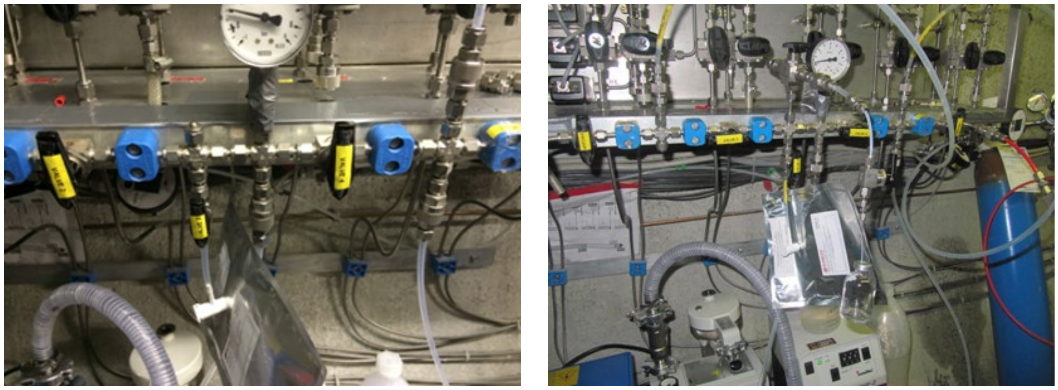

a) b)

Fig. 40: a) Detail of the gas and water sampling by using a multilayer foil bag in the FP1 pipe in 2014. b) Detail of the water sampling inside septum vials in the FP3 pipe by flushing the lines with He gas prior to sampling

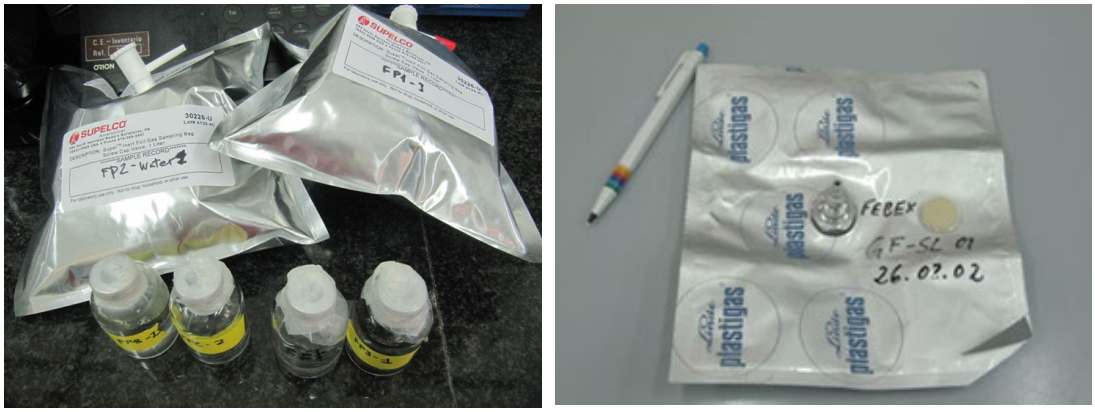

Fig. 41: a) Porewater collected inside SuperTM–Inert Al-Foil Gas sampling bags and septum vials from the GRS pipes in 2014, which were analysed at CIEMAT. b) Linde Plastigas® bags used for collecting gas and water from 2002 to 2011 from the GRS pipes

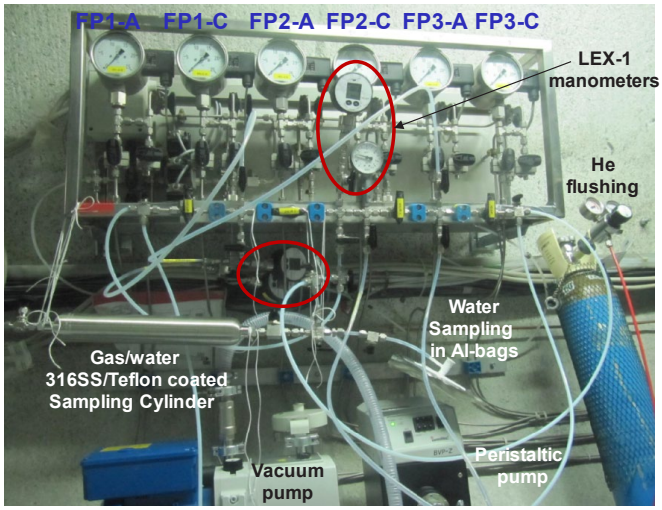

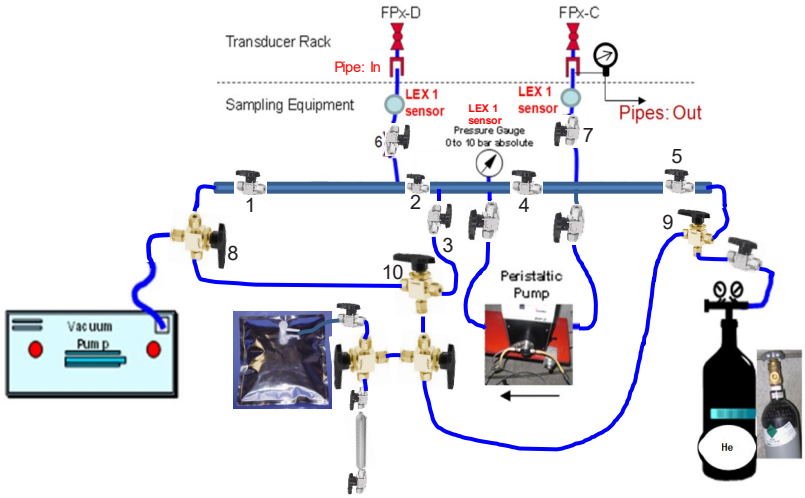

Fig. 42: Sampling circuit for gas/water sampling used in the GRS pipes in January 2015

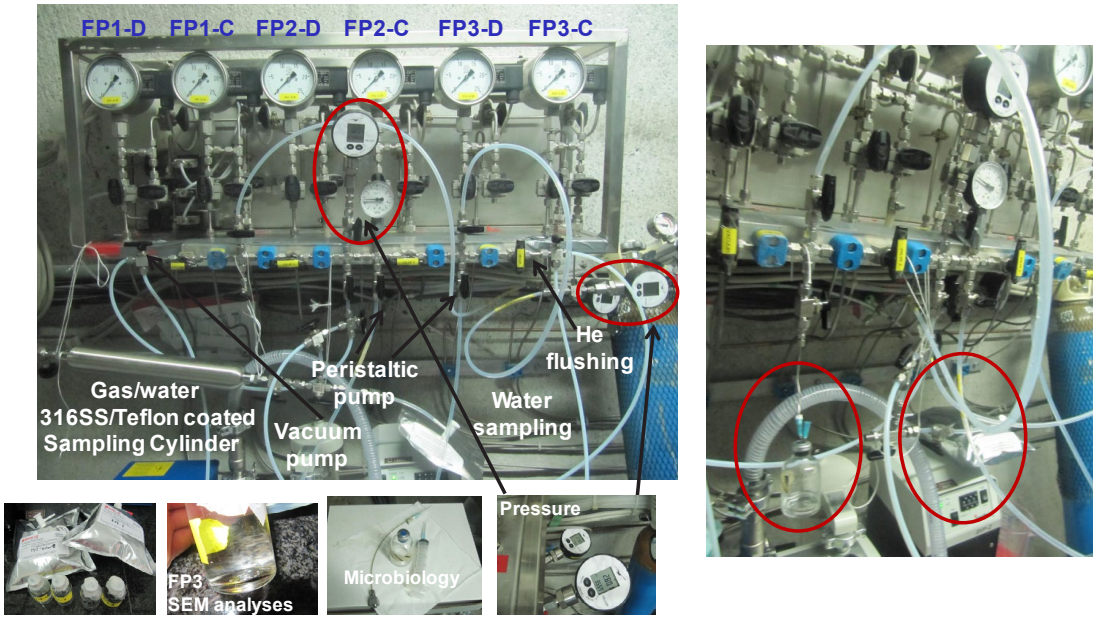

Fig. 43: Detail of the gas/water sampling during the January 2015 campaign

3.2 Porewater sampling from the CIEMAT pipes

Six pipes were installed in April 2003 with the aim of collecting porewater from the bentonite buffer for chemical analysis. Each of these pipes has three sections made of a sintered porous 316L stainless steel, located at depths corresponding to the instrumented Sections G, I and F2 (see Fig. 14, Fig. 26). At the bottom and at the top of each sintered filter, two AISI 316 stainless steel tubes (1/8" outer diameter) connected to AISI 316L tubes (1/16" OD) were present, which allowed gas injection in each filter (line-in) and the collection of water from the line-out point, giving a total of 18 water sampling points in the clay barrier.

In order to collect the porewater from these pipes, a sampling system was designed for measuring the pressure inside each interval and maintaining and preserving the redox conditions during water sampling. The final setup is shown in Fig. 44. The system has different two- and three-way stainless steel valves and tubes for connecting to: a) the two sampling lines coming from each pipe: in-gas pipe line (first blue valve) and out-water pipe line (second blue valve); b) a high precision digital manometer Keller LEX-1, c) a vacuum pump, d) a gas bottle for flushing the lines with helium gas (99.9999 % purity), and e) the sampling bags (Super^{TM}–Inert Foil Gas sampling bags).

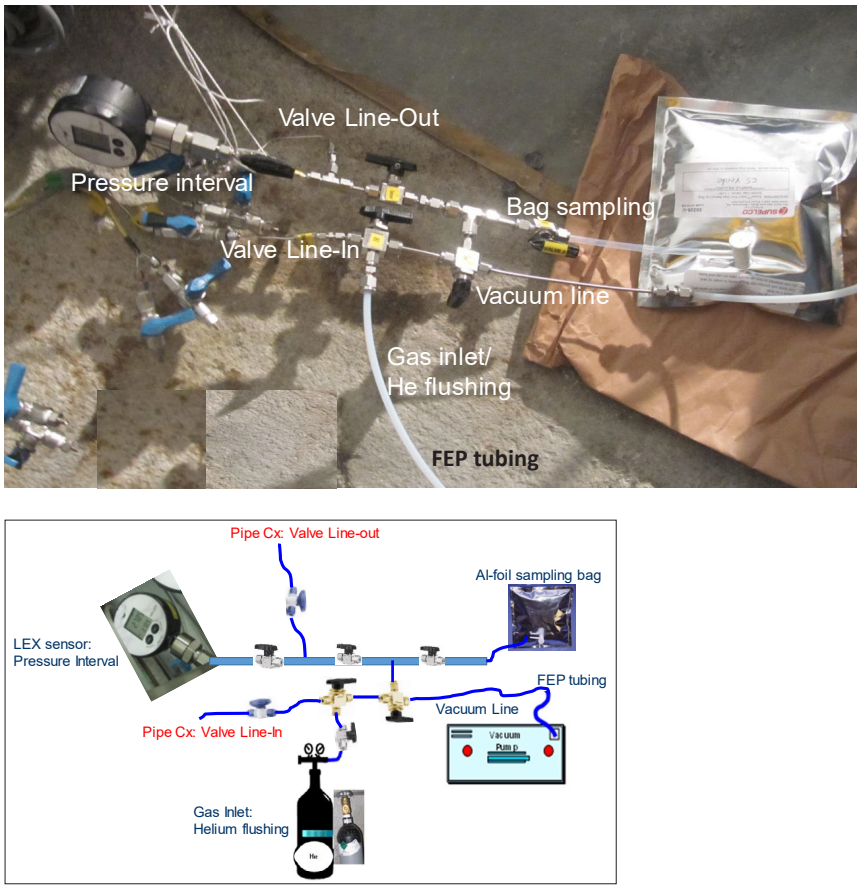

Fig. 44. Setup for the water sampling from the CIEMAT pipes

In each pipe and prior to sampling, the sampling circuit (Fig. 44) was installed and checked for tightness according to the procedure described in Appendix D. During the first checks, it was observed that the whole system was tight, except in the tube connection of the sampling bag, where a very small loss of pressure was observed over time. However, due to the small sampling time required for the water collection, this leak was considered negligible.

In each pipe, the sampling system was cleaned by circulating distilled water, and gas-dried by means of several cycles of gas flushing and subsequent evacuation. The sampling bags were also filled with gas and evacuated several times, for avoiding O_2 contamination from air. Then, the whole collecting system was left under vacuum. Prior to sampling the water, the pipe line going out, was opened for checking the interval pressure. Afterwards, the sampling bag was opened for collecting the bentonite porewater. In the case of no water could be collected from the interval, the in-sampling line was flushed with He carrier gas at a maximum pressure of 1 bar, with the aim of collecting some water from the out-sampling line.

Two sampling campaigns were performed with this procedure in August 2014 and January 2015. Previous sampling campaigns were performed on March 30th 2006, July 4 – 9th 2007 and August 19th 2011 by using stainless steel cylinders or septum vials. The extraction method at that time consisted on applying a vacuum to the system (Fig. 45).

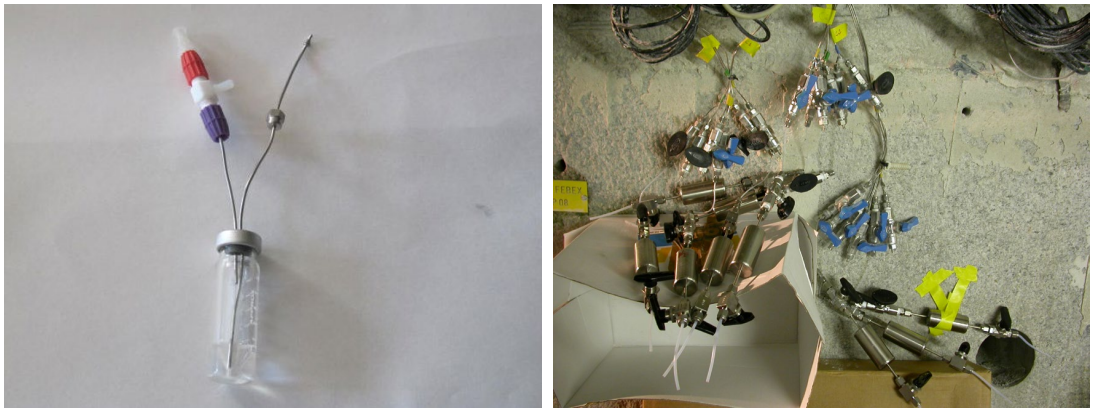

Fig. 45: Porewater sampling in CIEMAT pipes from 2006 to 2011: a) Septum vials. b) Stainless steel cylinders of 40 cm^3 with double end

3.3 Gas and water chemical analyses

Two laboratories were involved in the gas and chemical analyses in the 2014 and 2015 sampling campaigns. Hydroisotop GmbH laboratory analysed the gas and porewater composition from the GRS pipes, whereas the chemical analyses of the porewater from both GRS and CIEMAT pipes were carried out at CIEMAT laboratories.

At Hydroisotop GmbH laboratory (Germany), the gas and water samples were analysed according to the following methods:

- The gas composition was obtained via gas chromatography (GC) and various detectors (GC-TDR, GC-FID).
- pH value (20 °C) was determined according to the standard method DIN 38404-5: 1984-01 (C5).
- Cations (Na^+, K^+, Ca^{2+}, Mg^{2+}, Li^+, Sr^{2+}, Ba^{2+}) by ion chromatography: DIN EN ISO 14911 (E34).
- Anions (Cl^-, SO_4^{2-}, NO_3^-, PO_4^{2-}, F^-, Br^-, I^-, $S_2O_3^-$, acetate, formate) by ion chromatography: DIN EN ISO 10304-1 (D20).
- Alkalinity at pH 4.3 and pH 8.2 by potentiometric titration: DIN 38409-7: 2004-03.
- DOC, TOC, TIC according to the standard method DIN EN 1484-H3.
- Fe, silica and NH_4^+ by photometry.
- Trace elements (Ag, Al, As, B, Cd, Co, Cr, Cu, Hg, Mo, Nb, Pb, Rb, Se, Si, Sn, Th, U, V, Zn, Zr) by ICP-Ms (DIN EN ISO 17294-2 (E29).
- Nitrogen-15 ($\delta^{15}N$-N_2) by isotope ratio mass spectrometry (IRMS), related to Air, the standard deviation of the measurement being ± 0.2 ‰.
- Oxygen-18-CO_2 ($\delta^{18}O$-CO_2) by isotope ratio mass spectrometry (IRMS), related to VSMOW, the standard deviation of the measurement being ± 0.2 ‰.
- Carbon-13-CO_2 ($\delta^{13}C$-CO_2) by isotope ratio mass spectrometry (IRMS), related to VPDB, the standard deviation of the measurement being ± 0.3 ‰.
- Carbon-13-CH_4 ($\delta^{13}C$-CH_4) by isotope ratio mass spectrometry (IRMS), related to VPDB, the standard deviation of the measurement being ± 1.5 ‰.
- Deuterium-CH_4 ($\delta^{2}H$-CH_4) by isotope ratio mass spectrometry (IRMS), related to VSMOW, the standard deviation of the measurement being of ± 10 ‰.
- Oxygen-18-SO_4 ($\delta^{18}O$-SO_4) was determined by isotope ratio mass spectrometry (IRMS), related to VSMOW, the standard deviation of the measurement being ± 0.6 ‰.
- Sulfur-34-SO_4 ($\delta^{34}S$-SO_4) by isotope ratio mass spectrometry (IRMS), related to V-CDT, the standard deviation of the measurement being ± 0.5 ‰.
- Sulfur-34-SO_4 ($\delta^{34}S$-H_2S) by isotope ratio mass spectrometry (IRMS), related to V-CDT, the standard deviation of the measurement being ± 0.5 ‰.

At CIEMAT, the sampling bags and septum vials obtained during the sampling campaigns were handled inside a JACOMEX anoxic glove box (< 1 ppm O_2), where different aliquots were used for several determinations (Fig. 46, Fig. 47). The water samples were filtered through 0.45 µm syringe filters, except those for pH, electrical conductivity (EC) and redox measurements.

- The pH was measured by means of an ORION 720A pH-meter equipped with a Metrohm 6.0224.100 combined pH micro-electrode. Merck pH buffer solutions of pH 4.00 and 7.00 were used for pH-meter calibration.
- Electrical Conductivity measurements (EC) were performed by an ORION 115 conductimeter. The conductivity cell was checked/calibrated with a standard solution of 1413 µS/cm or 12.6 mS/cm(NaCl). The measurements were automatically adjusted to a temperature of 25 °C.
- The redox potential (Eh) was measured by means of a combined platinum-ring electrode (Metrohm, ref. 6.0451.100) with a built-in Ag/AgCl reference electrode. The calibration was carried out by using a redox buffer, $Fe(CN)_6^{4-}/Fe(CN)_6^{3-}$ (10^{-3} M), at + 250 ± 5 mV vs the Ag-AgCl 3 M KCl electrode.
- The total *alkalinity* of the water samples was determined with a specific Dynamic Equivalence point Titration (DET) method for analysing samples of 1 – 2 mL. The instrumentation consists of a Metrohm 888 Titroprocessor equipped with a 5 mL burette and a 6.0224.100 Metrohm combined pH micro-electrode.
- The *major, trace cations and silica* were analysed by Inductively Coupled Plasma-Optical Emission Spectrometry (ICP-OES) with a Varian 735ES spectrometer. Sodium and potassium were determined by atomic absorption spectrometry with an Agilent AA 240 FS spectrometer, and *ultratrace elements* were determined by ICP-MS (Finningan Mat SOLA).
- A*nions* were analyzed by ion chromatography (Dionex ICS-2000).
- Fe(II)/Fe(III) ratio was determined by UV-Vis spectrophotometry with the ferrozine method after acidification of the samples to pH < 1 with HCl. Spectrometric determination of the Fe(II)-ferrozine complex was performed on separated aliquots before and after reduction step with hydroxylamine. Fe (III) was obtained from the difference between total Fe and Fe(II).
- *The NPOC* (non-purgable organic carbon) which refers to organic carbon present in a non-volatile form was analysed with a TOC-V_{CSH} analyser (Shimadzu Scientific Instruments, Kyoto, Japan). Samples were acidified with HCl 2 M and sparged with synthetic compressed air (99.999 % purity) to remove inorganic carbon. The samples were then injected into a reaction chamber heated at 720 °C packed with platinum catalyst. The CO_2 formed was transported to the detector by a carrier gas stream (high-purity oxygen) and measured directly by a non-dispersive infra-red (NDIR) gas analysis system. The amount of detected CO_2 is directly proportional to the TOC content in the sample.

The error in the measurements is the standard deviation of at least three individual runs. The analytical error for major anions, cations, alkalinity and TOC is ± 5 % (including necessary dilution steps).

Fig. 46: Jacomex anoxic glove box (< 1 ppm O_2) for pH and redox measurements in the porewaters from the FEBEX bentonite collected inside the sampling bags from the GRS and CIEMAT pipes

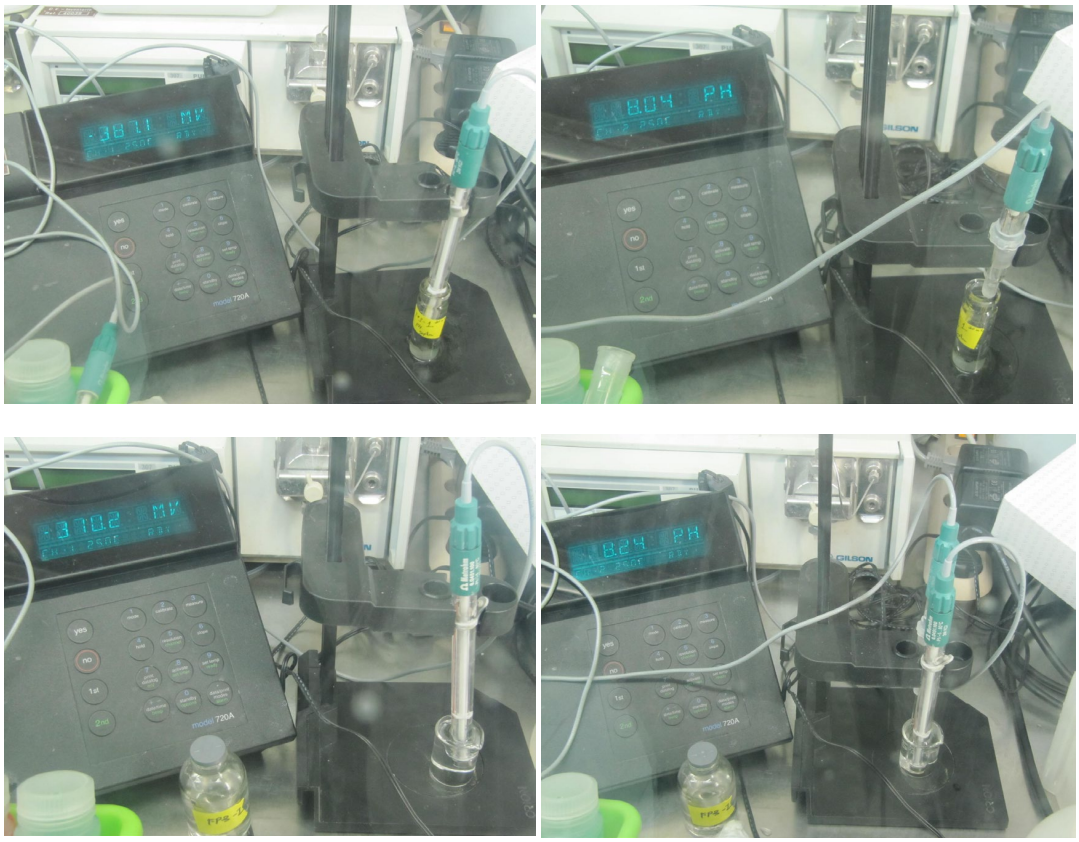

Fig. 47: Redox potential and pH measurements inside the anoxic glove box (< 1 ppm O_2) of the water samples collected in septum vials FP3-1 (upper part: -386 mV, pH 8.04) and FP3-2 (bottom part: -370 mV, pH 8.24), respectively

These Eh measurements correspond to those performed the 24th November 2014 from closed septum vials preserved inside the anoxic glove box.

From 1996 to 2011, the gas samples were analysed in GRS laboratories, where the gas chromatography system consisted of four independent GC channels, each of which was optimised for detecting a special class of gases. Each channel was equipped with two chromatographic columns in series, a guard column and a separation column. The guard column was used only to remove components which might interfere with the detection, while the components of interest passed through this column quickly. After all analytes had passed through the guard column, a multi-position valve was switched in order to backflush the guard column. The analytes were then separated on the separation column having different detectors (Column A: FPD: flame photometric and TCD: thermal conductivity detectors for analysing sulfur-containing gases; Column B: TCD detector for analysing He, N_2O and H_2; Column C: TCD detector for analysing O_2 and N_2; Column D: FID or Flame ionization detector for analysing C1-C4 hydrocarbons, CO and CO_2). The measuring signals were recorded and analysed. Calibration was performed using commercially available test gas mixtures, having a certified accuracy of ± 2 %.

Gas contents for O_2, N_2, and CO_2 are given in vol.-%, whereas for the rest of gases their content in given in vpm (or ppmv: parts per million by volume). The analytical error of the gas measurements performed both in the GRS and Hydroisotop laboratories is in the range of 5 % to 10 % for all gases, except for hydrocarbons for which the uncertainty in the analytical determination is lower than 5 %.

4 Results

4.1 Visual aspect of the sampling pipes and their surrounding after dismantling

The dismantling of the FEBEX *in situ* test in April 2015 after 18 years of continuous heating and natural resaturation of a compacted bentonite offered a unique opportunity to check the final aspect of the pipes (integrity, location, etc.), as well as the geochemical and physical environment in the bentonite barrier around the gas pipes and porewater sampling intervals, which may help interpreting the results.

The most important aspects are the damages of the ceramic filters observed after dismantling of Heater #1 and the corrosion products halos observed, probably influenced by the higher water content and Cl-content around the ceramic and the stainless steel pipes. The pipes GF-S-L-01, GF-S-L-02 and GF-S-L-03, located close to the granite, and the pipe GF-S-L-04, located close to the liner contact, were broken as a result of the bentonite swelling and a heterogeneous mechanical stress (Fig. 48). Nevertheless, the porosity and the permeability of the ceramic filters remained sufficient intact and a residual volume was present between the broken pieces (with sizes between 1 and 10 cm), allowing the gas/water sampling and pore pressure measurements (Jockwer & Wieczorek 2008). The pipes GF-S-L-05 and GF-S-L-06 were not damaged because they were inserted inside perforated stainless steel (SS) tubes (Fig. 48b). The corrosion halos observed around the ceramic pipes are probably due to the corrosion of bolts and anchors made of low alloyed steel, especially at the granite contact (Fig. 49). The inner tubes where the pipes GF-S-L-05 and GF-S-L-06 were inserted seem to show only a partial and localized corrosion on surface with adhered corrosion products. However, other metals (liner, Heater #1, sensors) were partially corroded as shown in Madina & Azkárate (2004). On the other hand, the PFA (PerFluoroalkoxy) tubes did not show any evidences of alteration, even in the heated zones, where they supported ~ 90 °C during five years.

After dismantling of Heater #2 the displacement along the X-axis is something clearly observed for both the GRS and CIEMAT sampling pipes (Fig. E-9 from Appendix E). The displacement of the sampling points with respect to the initial location was probably due to the displacement of bentonite layers along the x-coordinate, as observed by García Siñeriz et al. (2016) and Villar et al. (2016). According to AITEMIN, the displacement of the bentonite sections with respect to the x-coordinate could be related to a potential decompression of the outer bentonite section (~1 m) during the dismantling of Heater #1 in 2002, when the bentonite was open to the gallery during three months.

Several sensors were placed in the instrumented Sections I, M2, F2, E2 and D2 (Fig. 50, Fig. 51, see also Appendix E). The different corrosion processes of these sensors during the FEBEX experiment, which were checked and analysed by TECNALIA (Madina, 2016: NAB 16-54), are a source of gases. Further information about the final state of the sensors and on the sensor corrosion in the FEBEX *in situ* test can be found in Rey et al. (2016: NAB 16-20) and in Wersin & Kober (2016: NAB 16-16). Another possible source of gases was the possible degradation of the plastic tubings and organic materials placed in the test (e.g., cellulose filter papers (total mass: 1.371 kg) for tracers deposition (Fig. 52)).

During the dismantling of Heater #2 no significant signs of corrosion were visually observed at the external part of the stainless steel gas pipes along the whole sampling intervals (Fig. 53), as well as in the CIEMAT pipes (see Appendix E). Exception was the CIEMAT pipe C4 in the Instrumented Section G, where obvious signs of corrosion were observed around the sampling filter, which are possibly related to a higher water inflow due to the presence of the lamprophyre

dike (Fig. 54). Powder scratch from the C4 sampling pipe was later analysed by XRD; showing the presence of aragonite, calcite, quartz, feldspars, iron sulfur, hematite and magnetite as corrosion products (Fig. 55, Fig. E-22, Fig. E-23). Furthermore, a clear deformation damage of pipe C4 in Section I (Fig. 56), probably related to thermal stress from an overheating incident (such an event took place during 2009 when maximum temperatures around Heater #2 may have reached between 120 – 130 °C for about 62 hours). This could also affect the extraction of water from this pipe.

Fig. 48: Visual aspect of the GRS pipes during the dismantling of the Heater #1: bentonite Slice 96 (BSS20, Instrumented Section L) in 25 June 2002, and Slice 94 (Bentonite Sampling Section BSS21) in 26 June 2002

The pipes GF01, GF03, GF02 and GF04 were broken due to bentonite swelling and a heterogeneous stress.

a)

b)

Fig. 49: Visual aspect of the GRS pipes for water pressure measurements during the dismantling of the Heater #1: a) GP-S-L-3 in the bentonite Sections 96 and 79 (Instrumented Sections L and M1, respectively). b) GP-S-H-3 for pore pressure measurements during the dismantling of the Heater #2 (29/5/2015) in the Slice 63 (BSS40, Instrumented Section H)

Fig. 50: Location of pipes FP-1 and FP-3 around the Heater # 2 (carbon steel) and visual aspect of the internal part of the liner during dismantling

Fig. 51: Types of sensors potentially corroded and degraded in the bentonite barrier close to gas pipes FP-1, FP-2 and FP-3

Fig. 52: Possible source of gases due to plastics and organic matter degradation: a) Visual aspect of the plastic tube close to the porous SS FP1-D sampling port at Section 53 (Sampling Section 44), showing a black colour. b) Filter papers of cellulose for tracers deposition located at the bentonite-granite interface at Sections S70, S74, S37, S32 and S31

A greenish discoloration near iodide paper was observed at the bentonite-granite interface in Section 37 (BSS50); b) Iodide filter deposition at Sections S37 (BSS50), S32 (BSS51/E2) and S31(BSS52).

García-Gutiérrez (2001)

Fig. 53: Visual aspect of the stainless steel pipes with no evidences of external corrosion

Fig. 54: Visual aspect of both the corroded sintered filter from pipe C4 and the non-corroded filter from the pipe C5 at Section G (close to a lamprophyre area)

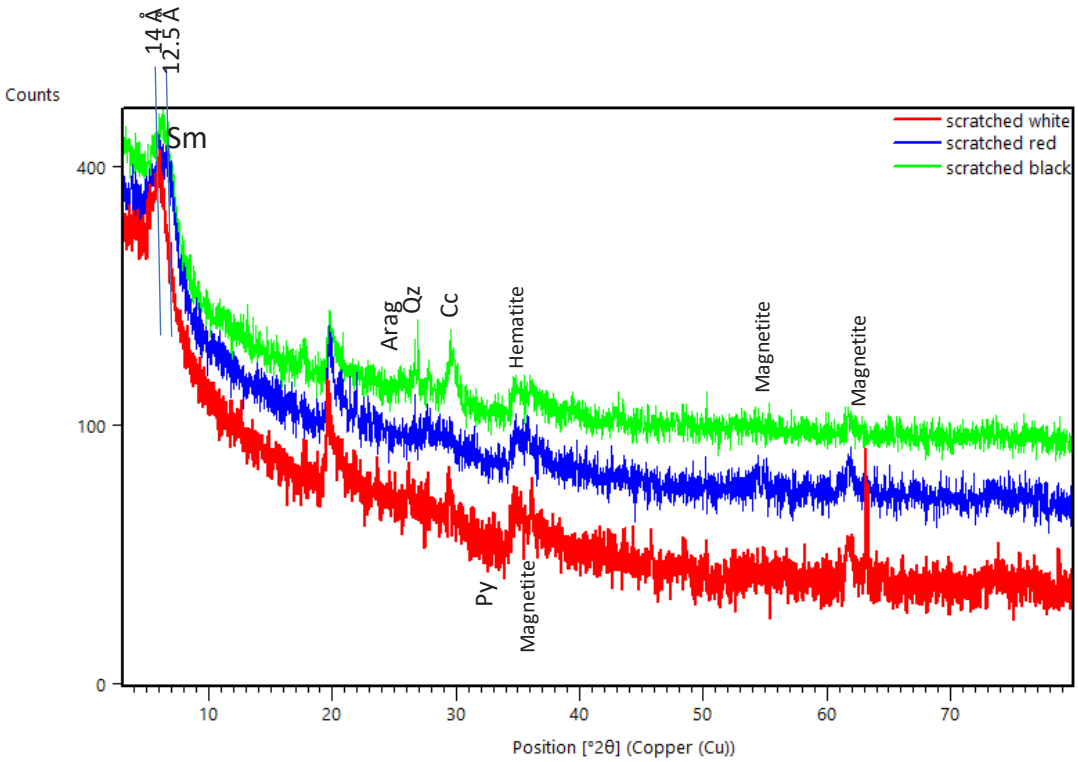

Fig. 55: XRD patterns from the scratched powders (white, red, black) from the corroded C4 filter at Section G showing smectite, aragonite, calcite, quartz, iron sulfur, hematite and magnetite as corrosion products

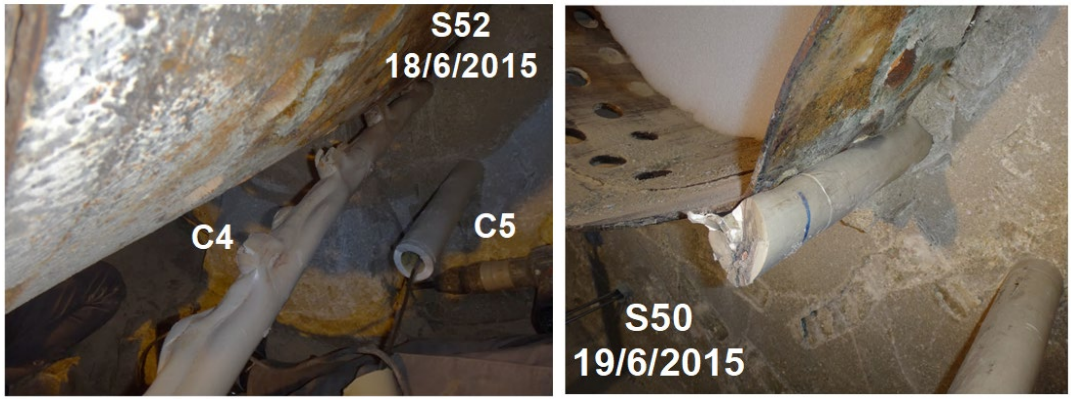

Fig. 56: Visual aspect of the pipe C4 from Section 55 to Section 45 (from the frontal part to centre of the heater): deformation probably due to thermal stress by overheating

4.2 Results from gas and water sampling (GRS pipes)

GRS analysed the gas composition from the FEBEX *in situ* test from 1996 with the aim of determining the gas content and the pore pressure of the bentonite buffer. Ceramic filter pipes were inserted around the Heater #1 allowing the collection of gas/water from 30 November 1996 to 25 February 2002 (Heater #1 was switched on in 27 February 1997 (taken as Day 0) and switched off in 28 February 2002). After the dismantling of the Heater #1, three sintered stainless steel filter pipes were introduced around the Heater #2 and gas/water samples were collected in different *in situ* sampling campaigns from 21 October 2003 until 30 January 2015 (Heater #2 was switched off in 24 April 2015). In this section, a global overview of the main gas and porewater composition results over time are described. It is necessary to point out here that the gas pipes were only focused on obtaining and analysing the gases generated/consumed in the bentonite barrier; and most of the water samples were discarded and not analysed. Geochemical analysis of the porewater collected from the pipes was incidental until 2011. Only in the last three sampling campaigns performed in 2011, 2014 and 2015, the gas and water samples were collected specifically for analysing the geochemical processes in the FEBEX *in situ* test.

4.2.1 Results obtained during the First Operational Phase (1996 – 2002)

Sampling started in December 1996, almost 3 months prior to switching on the electrical heaters in 28 February 1997. Sampling continued from January 1997 to January 1999 (each month) and from August 2000 until the dismantling of Heater #1 (every 2 – 4 months).

Gas samples were obtained directly from the gas pipes GF-S-L-01 and GF-S-L-02, located at the granite interface, until 20 October 1997 and 11 August 1997, respectively. After this, these pipes filled with water. The higher water flow from borehole SI-2 may have contributed to a faster filling with water in pipe GF-SL-02 in comparison to pipe GF-SL-01 (Fig. 19). Afterwards, gas samples were obtained after extracting about 1 L of water. Sometimes, no gas (gas phase) could be sampled even after extracting 3 L of water. In these cases, gas sampling was stopped in order not to disturb the system. The gas pipe GF-S-L-03 was filled with water between February and May 1997. No more water was found in the pipe after this period, and gas sampling started on 19 June 1997. In February 2000 it became flooded again. No dissolved gases in the porewater were analysed in this phase. In the pipes GF-S-L-04 (located at liner contact), GF-S-L-5 and

GF-S-L-6 (both located in the inner part of the bentonite barrier), water was never detected, so gas samples were taken until dismantling in 2002 (Jockwer & Wieczorek 2001, 2003, 2008).

Fluid pressures inside the pipes were measured by pressure transducers linked to a data acquisition system. The values ranged between 804 and 842 mbar, showing a fluctuation of 5 to 30 mbar within one week. These values are similar to either vapour pressure at temperatures higher than 94 °C or to the atmospheric pressure. These pressures were observed in the inner gas pipes (GF-S-L-04, GF-L-S-L-05 and GF-S-L-06) over time until dismantling of Heater #1; and in the external pipes located at the granite interface (GF-S-L-01, GF-S-L-02 and GF-S-L-03), until they were flooded with water. Pressure increases were detected in the pipes GF-S-L-02, GF-S-L-01 and GF-S-L-03 in July 1997, October 1997 and February 2000, respectively (Fig. 57), clearly coinciding with water inflow in the pipes (Jockwer & Wieczorek 2001, 2008). The pressures observed in these external pipes were between 2.5 and 4.5 bar. The difference in values observed between the pipe located in the upper part (GF-S-L-03) and the pipes located in the lower part (GF-S-L-01 and GF-S-L-02) of the bentonite barrier is probably related to the difference in height (height of water column of around 2 m, i.e., 0.2 bar).

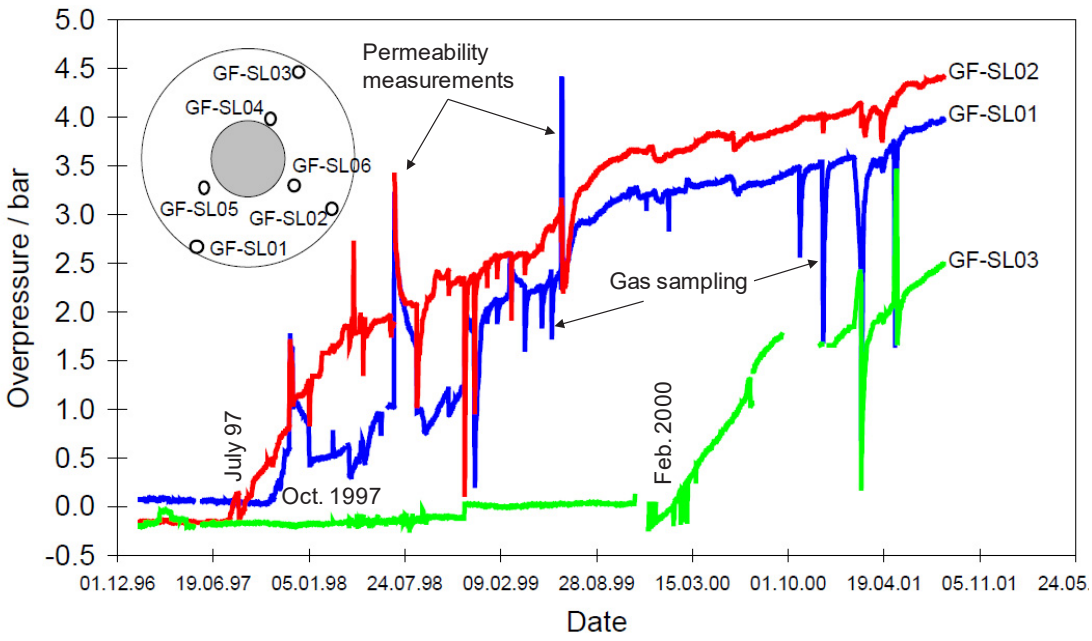

Fig. 57: Fluid pressure development in the gas pipes GF-S-L-01, GF-S-L-02 and GF-S-L-03

The other pipes located at the inner part of the bentonite showed pressures ranging from 804 to 842 mbar (Jockwer & Wieczorek 2001). Note: peaks and drops of the pressure in the figure are caused by gas injections for determining gas permeability and by pressure recovery tests for determining water permeability.

The gas concentration obtained in the different sampling campaigns are shown in Fig. 58 and Fig. 59 (see data in Appendix B). The gases released from the bentonite and collected from the pipes were oxygen, hydrogen, carbon dioxide, methane and other hydrocarbons. Oxygen is depleted over time from the concentration of air (20.95 vol.-%) to 2 vol.-%; the peaks observed in the figures are a consequence of oxygen infiltration during the performance of other tests (gas and water permeability tests). O_2 values above atmospheric are in the range of the uncertainty in

the measurements (5 – 10 %). Carbon dioxide and methane contents increase along the test duration, whereas hydrogen first increases and afterwards decreases over time.

When the pipes GF-S-L-01, GF-S-L-02 and GF-S-L-03, located at the granite/bentonite contact, became flooded, some water samples were also sampled for chemical analyses. The water was collected during three different sampling campaigns: 24 February 1998, 11 December 2001 and 25 January 2002. The water was collected inside the gastight gas/water Al-sampling bags and, therefore, away from any contact with the air. The GRS team sent these preserved bags to CIEMAT for the chemical analysis. Another water sample trapped in one tube of the most external gas pipe (GF-S-L-03) was collected during dismantling of the Heater #1 (July 2002) and analysed. This water was obtained at air conditions and preserved in a polyethylene vial.

The chemical composition of the samples is shown in Tab. 8 and compared with Grimsel groundwater and squeezed bentonite pore water. The results show a large variation of chemical concentrations over time. The GF-SL-01 and GF-SL-02 waters are Na-Cl water-type, while the GF-SL-03 water is Na-Cl-SO_4 water-type. The ionic strength of the waters ranges between 0.02 and 0.09, and the pH are neutral to slightly alkaline (7.7 – 8.4). The chloride content in the porewater, which represents the salinity of the FEBEX bentonite porewater (Fernández et al. 2018; 2004), slightly increased over time, due to bentonite-granite groundwater interactions. Fluor is always detected in the porewaters (coming from the granite groundwater), as well as, some tracers (I^-, Re, Se, etc.), coming from different tracers deposition systems introduced in the FEBEX *in situ* test. A high alkalinity value in the porewaters sampled in 2002 can be seen for all locations. Sulfate content in the pipe GF-SL-02 decreased over time and Fe(II) was detected in all pipes in the 2001 campaign. The redox values measured always point to oxidized values, although there is no absolute certainty on the perfect sample preservation prior to each measurement at CIEMAT after the gas measurements in GRS.

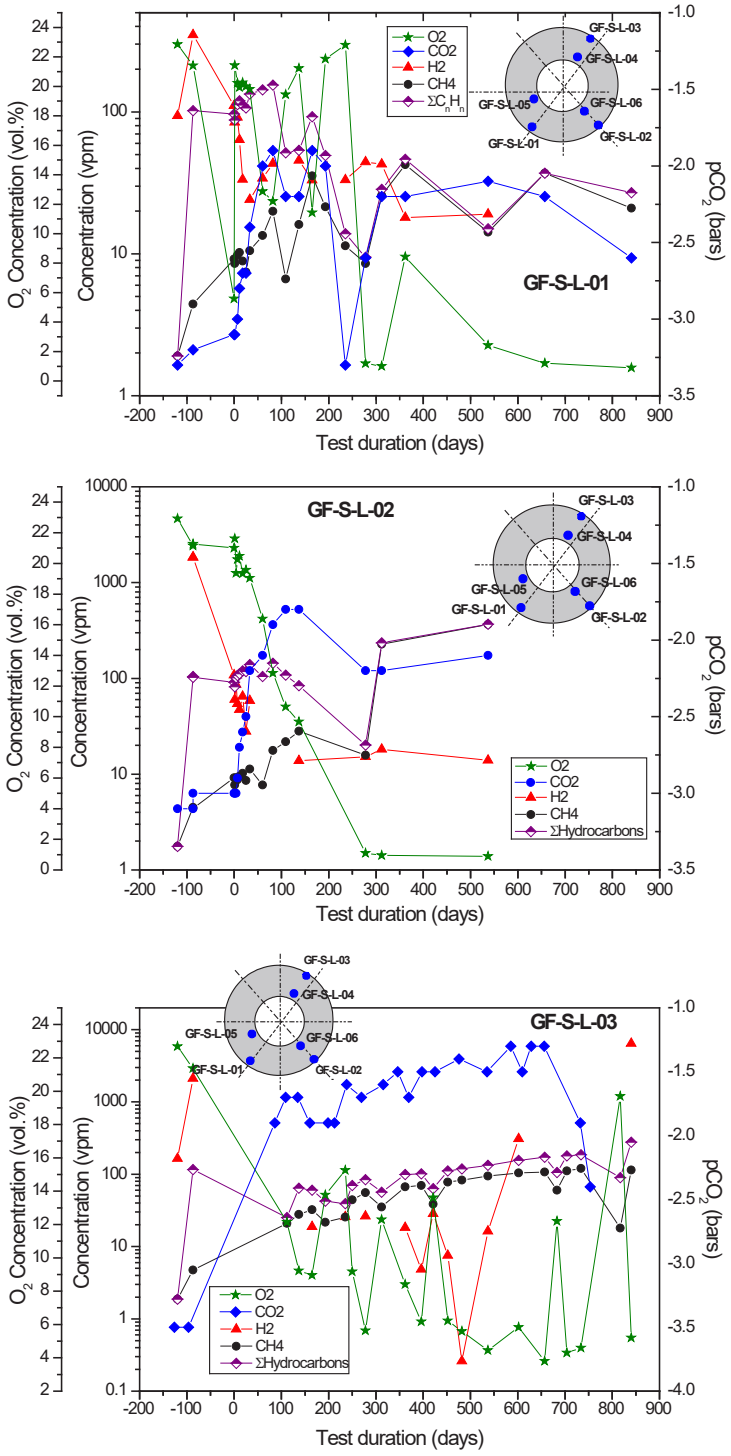

Fig. 58: Gas concentration in the gas pipes GF-S-L-01, GF-S-L-02 and GF-S-L-03 located at the bentonite/granite interface

Day 0: 27.02.1997 when heaters were switched on.

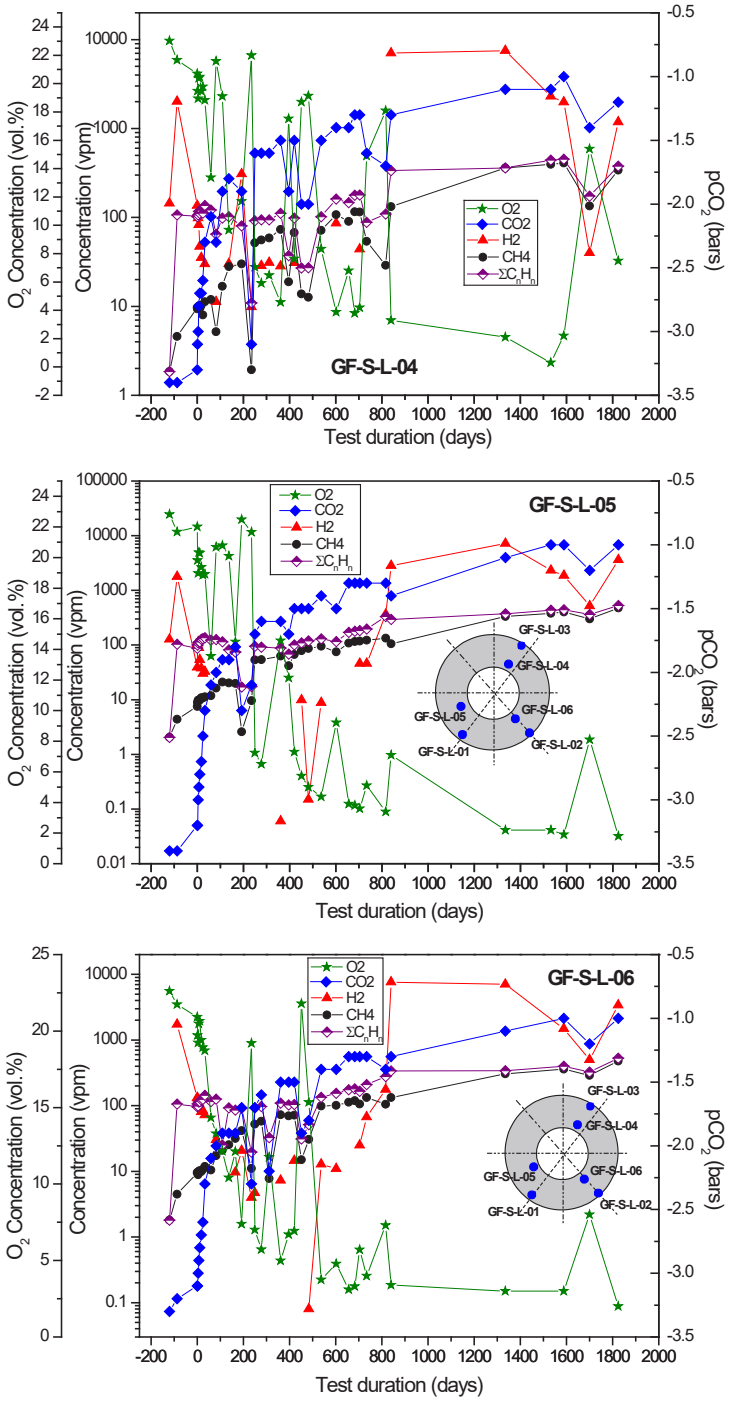

Fig. 59: Gas concentration in the gas pipes GF-S-L-04, GF-S-L-05 and GF-S-L-06 located at the inner part of the bentonite barrier

Day 0: 27.02.1997 when heaters were switched on.

Tab. 8: Chemical composition of the water from the gas pipes surrounding Heater #1

		Grimsel GW*	Sq. water BB-19-1**	GF-SL-01	GF-SL-01	GF-SL-02	GF-SL-02	GF-SL-02	GF-SL-03	GF-SL-03	GF-SL-03 Dismantling
Date		27.10.1987	January 2003	11.12.2001	25.02.2002	24.02.1998	11.12.2001	25.02.2002	11.12.2001	25.02.2002	15.07.2002
Water type		Na-HCO_3-F	Na-Cl	Na-Cl	Na-Cl	Na-Cl	Na-Cl	Na-Cl	Na-Cl-SO_4^{2-}	Na-Cl-SO_4^{2-}	Na-Cl
I.S.	(M)	0.0012	0.07	0.07	0.05	0.02	0.06	0.03	0.09	0.06	0.07
pH		9.59	7.5	7.9	7.9	7.7	7.8	7.7	7.8	7.5	8.4
Eh (mV)	(SHE)	-382 ± 17	n.d.	107	n.d.	n.d.	28	384	64	413	n.d.
Alkalinity	(meq/L)	0.42	2.57	-	9.70	3.95	-	8.08	-	5.92	4.64
pCO_2	(bar)	-5.62	-2.39	-	-2.21	-2.35	-	-2.06	-	-2.03	-3.07
Cl^-	(mg/L)	5.5	1'500	1'300	1'500	356	1'100	876	1'500	1'500	2'100
SO_4^{2-}	(mg/L)	5.5	883	281	310	121	27	43	818	752	770
Br^-	(mg/L)	-	2.6	2.8	3.0	0.9	2.0	1.4	2.8	2.6	4.7
NO_3^-	(mg/L)	< 0.3	1.5	< 1	< 1	< 0.1	< 1	< 1	< 1	< 1	< 1
F^-	(mg/L)	6.1	n.d.	1.6	1.3	3.7	2.3	2.9	1.8	1.7	n.d.
I^-	(mg/L)	-	-	1.0	1.1	1.4	2.5	1.8	0.75	0.7	n.d.
Si	(mg/L)	12	n.d.	12.5	n.d.	36.4	10.7	67.3	5.1	65.8	n.d.
Ca	(mg/L)	5.6	106	29	16	10	20	16	57	64	50
Mg	(mg/L)	0.044	67	29	39	5.5	18	17	47	62	< 4
Na	(mg/L)	16	1'200	2'400	1'200	365	1'900	700	2'800	1'300	1'600
K	(mg/L)	0.22	13	19	20	8.7	17	13	23	22	34
Mn	(mg/L)	-	0.17	< 0.03	< 0.03	n.d.	< 0.03	< 0.03	0.06	0.05	< 0.3
Al	(mg/L)	0.012	0.65	< 0.01	0.1	0.06	< 0.01	< 0.05	< 0.01	< 0.05	< 0.5
B	(mg/L)	-	0.63	3.2	3.1	n.d.	2.8	2.0	2.7	2.4	0.75
Ba	(mg/L)	-	-	< 0.05	< 0.05	n.d.	< 0.05	< 0.05	< 0.05	< 0.05	< 0.5
Fe	(mg/L)	-	0.25	0.04	< 0.05	0.03	0.04	< 0.05	0.03	< 0.05	< 0.3
Fe^{2+}	(µg/L)	-	-	44	< 0.05	n.d.	47	< 0.05	25	< 0.05	n.d.
Sr	(mg/L)	0.18	1.7	0.79	0.56	n.d.	0.53	0.30	1.4	1.0	< 0.5
Cs	(µg/L)	-	-	0.5	0.2	n.d.	0.5	0.2	0.5	0.2	n.d.
Se	(µg/L)	-	-	≤ 10	n.d.	n.d.	≤ 10	n.d.	20	n.d.	n.d.
As	(µg/L)	-	-	7.0	5.1	n.d.	2.6	3.4	6.0	5.5	n.d.
Re	(µg/L)	-	-	6.2	5.9	n.d.	< 0.5	0.5	3.5	5.3	n.d.
U	(µg/L)	-	-	0.7	< 1	n.d.	n.d.	< 0.5	0.9	0.9	n.d.
Th	(µg/L)	-	-	< 0.5	< 1	n.d.	≤ 0.5	0.5	< 0.5	0.5	n.d.

* Grimsel granitic groundwater BOMI 87.009 (see Appendix A)

** Squeezed bentonite porewater at 25 MPa from a compacted block at contact with the granite (first bentonite ring) in Sampling Section 19 taken after dismantling of Heater #1 (Fernández et al. 2018)

4.2.2 Results obtained during the Second Operational Phase (2002 – 2015)

4.2.2.1 Pressure measured in the sampling interval

The fluid pressure was monitored from October 2003 until June 2008. Then, the system was dismantled. From the installation of the gas sampling pipes in 2003, no significant increase of pressure was observed in the three pipes. The gas pressure recorded was almost identical to the atmospheric gas pressure value in the galleries of the Grimsel Test Site, showing a slight fluctuation. Only a slight gas pressure increase was detected in 2004 (Jockwer & Wieczorek 2008). Pressures similar to atmospheric values were also measured in the three pipes during the 2011 sampling campaign.

In both the August 2014 and January 2015 campaigns, the pressure inside the filter pipes was measured *in situ* by means of a LEX-1 high precision manometer (range: -1 to 10 bars, accuracy: 0.025 % FS). Prior to opening the FPx-C and FPx-D valves of the sampling lines, the tightness of the sampling circuit/system was checked during some hours (even overnight in the FP3-C/D pipe). This checking was performed both while applying an overpressure (P = 1 – 3.6 bar) and under vacuum conditions in different cycles. For example, in the FP3 pipe, the pressures measured under vacuum were between 0.018 and 0.029 bar in the FP3-D and FP3-C lines, respectively, even with the gas/water sampling bags connected. The pressures in both LEX manometers connected to both FPx-C and FPx-D lines in each pipe were similar, with a difference of ± 0.05 – 0.1 bar (Fig. 60).

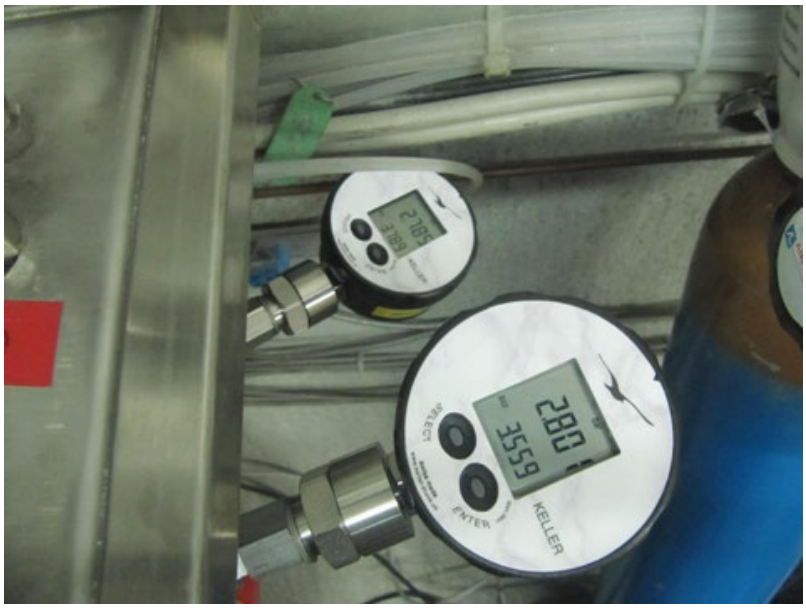

Fig. 60: LEX-1 type manometers: pressure measurements in the FPx-C/D lines while applying an overpressure in the sampling system for tightness checking of the sampling circuit.

The pressures measured inside the intervals of the three pipes FP1, FP2 and FP3 ranged between 0.805 and 0.929 bar absolute pressure in the August 2014 campaign, and between 0.746 and 0.887 bar absolute pressure in the January 2015 campaign. These values (Tab. 9, Fig. 61) are similar or slightly lower than the atmospheric pressure value (0.804 – 0.842 bar in the gallery), except in the FP2 gas pipe, where slightly higher values were measured in both campaigns (0.925 bar in 2014 and 0.887 bar in 2015). Therefore, small fluctuations (~ 0.132 bar) on pressures over time were detected in the pipes. This was also observed in the First Operational Phase, where the fluctuations ranged between 0.038 and 0.080 bar (see Section 4.2.1).

In spite of the low pressures registered, gas (or gas/water mixture) and water samples could be collected from the pipes in August 2014 (three years after the last sampling campaign in 2011). However, in the January 2015 campaign (~ 5 months later), the pressures values were slightly lower than in the August 2014 campaign, and mainly gas and very little water could be sampled inside the stainless steel cylinders, which were sent to Hydroisotop. Additional small amount of water could be extracted inside Al-sampling bags from each pipe after flushing the sampling tubings with He as carrier gas. The volume of water collected was not enough for microbiological determinations, and only chemical analyses could be performed at CIEMAT.

Tab. 9: Pressures (in bar) measured in the GRS pipes (FP1, FP2 and FP3): *on site* and inside the gas sampling bag measured at the Hydroisotop Lab. prior to gas analysis

Pipe-interval	**August 2014**		**January 2015**	
	On site	**Hydroisotop**	**On site**	**Hydroisotop**
FP1-D	0.865	0.960*	0.836	0.902
FP1-C	0.862		0.837	
FP2-D	0.925	0.960*	0.887	0.868
FP2-C	0.929		0.841	
FP3-D	0.845	-	0.759	0.886
FP3-C	0.842		0.746	
Atmospheric	0.826**	0.960	0.810**	0.960

* Pressure in gas bags measured at Hydroisotop laboratory (500 m a.s.l)
** Pressure inside the gallery (AITEMIN's sensor)

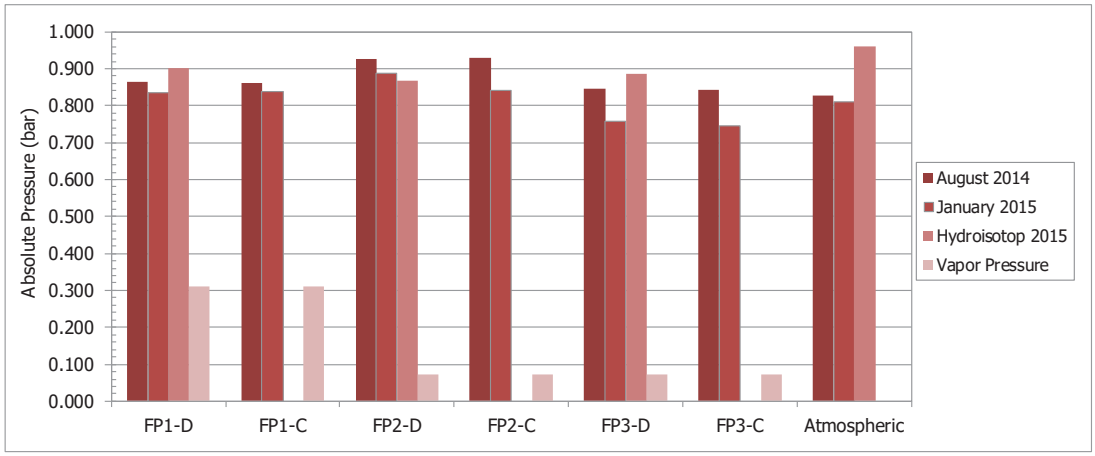

Fig. 61: Pressure (bar, abs.) inside the D and C sampling lines from the GRS pipes FP1, FP2 and FP3

Comparison with atmospheric pressure at Grimsel Test Site: 823 ± 16 mbar (range taken: 804 – 842 mbar), at Hydroisotop laboratory: 960 mbar; and with vapour pressure at bentonite temperature (~ 70 °C for FP-1 and ~ 40 °C for FP-2 and FP-3 pipes)

4.2.2.2 Gas and Porewater composition

GRS started gas sampling from November 2003 until December 2007 (every six months). CIEMAT performed three additional sampling campaigns in 2011, 2014 and 2015. Until 2014 gases were analysed by gas chromatography at the GRS laboratory, and the water samples at CIEMAT laboratories. In the 2014 and 2015 sampling campaigns, gas and water phases were analysed by Hydroisotop (gas/water mixture) and CIEMAT (only water phase).

The results for gas contents, isotope signals and chemical composition obtained in 2014 and 2015 are shown in Tab. 10, Tab. 11 and Tab. 12. The complete gas content dataset obtained during the Second Operational Phase is given in Appendix B, whereas the chemical composition of the porewaters obtained from the GRS pipes over time is shown in Tab. 13.

The gases released from the bentonite and collected from the pipes from 2003 to 2015 were the same as during the first phase: oxygen, hydrogen, nitrogen, carbon dioxide, methane and other hydrocarbons: n-alkanes up to C5 chains and n-alkenes (Fig. 62, Fig. 63 and Fig. 64), except CO which was not detected. In 2014 and 2015, oxygen is practically consumed. Measurements of 0.8 – 4.5 % and higher are probably due to some air contamination during collection and/or analysis, which are practically unavoidable or due to no air-tight conditions through the concrete plug. Carbon dioxide content is high, with a partial pressure of CO_2 much higher than the atmospheric one (pCO_2 =-3.5 bar). Methane content increases along the test duration, the content of other hydrocarbons being higher than that of methane only at the beginning of the experiment. Hydrogen seems to decrease over time, following an inverse correlation with respect to methane in the pipes FP2 and FP3. A different pattern is observed in pipe FP1, where the highest values of H_2 were measured, increasing H_2 and methane as the same time until 2014. Then, methane and hydrogen contents increase and decrease, respectively (Fig. 62, Fig. 63 and Fig. 64). Contrary to pipes FP2 and FP3, H_2 was always detected over time in pipe FP1.

In the 2014 sampling campaign, more than 36 months after the last campaign in 2011, a high amount of water was collected inside the pipes. Indeed, the FP3 sample was mainly water, and

the gas concentration is referred as gases in the water phase. The FP1 and FP2 samples were a mixture of gas and water but analyses correspond to content in the gas phase. After gas/water collection, additional water samples were collected inside septum vials preserved from oxygen by flushing with gas the lines of all pipes (Fig. 40 and Fig. 41). Thus, a comparison of the water analyses obtained by Hydroisotop and CIEMAT could be performed from both types of extractions: multilayer Al-bags and septum vials (Tab. 11); the chemical results being quite similar.

During the collection of water inside the septum vials, a hydrogen sulfide smell appeared, and black particles were observed at the bottom, especially in the FP-3 water sample (Fig. 65). It was not possible to dilucidated if these particles were in the water or precipitated during sampling due to a perturbation of the system, such as degassing and change of pH. These particles, analysed by the SEM technique at CIEMAT (Fig. 66 to Fig. 69), were composed mainly of S, Fe and Cu, i.e., sulfide particles of Fe and Cu. However, other elements such as C, Cr, Ni and Mn were also detected. Furthermore, clay particles were found. C is due to the syringe filters used for separating the particles from water. Fe, Cr and Ni derive from the corrosion of the stainless steel filters. However, the huge amount of S, may indicate a corrosion process mediated by SRB bacteria, which reduce the sulfate from the bentonite porewater to sulfide. The black particles were also observed by Hydroisotop in the FP1 and FP3 water samples. The FP1 water sample was also slightly turbid, indicating the presence of some organic material, whereas FP2 and FP3 samples were clear (Tab. 11). The redox potential (Eh) of the porewaters, measured inside an anoxic glove box (Fig. 47), gave negative values indicating a reducing environment.

During the January 2015 campaign, 5.5 months after the last campaign, only the gas phase could be collected (Fig. 43). These samples were analysed by Hydroisotop. Only a small amount water could be collected inside additional Al-sampling bags after flushing the sampling lines with He carrier gas, which was analysed at CIEMAT (Tab. 12). A water sample was extracted for microbiological analysis. However, due to the low amount of water collected, this was not possible. Furthermore, at this time the water samples were quite clear, so the presence of organic matter at that time was discarded.

Tab. 10: Gas composition from the FP1, FP2 and FP3 pipes collected in 2014 and 2015

Pipe			**FP1 pipe**		**FP2 pipe**		**FP3 pipe**	
Sampling campaign			1st	2nd	1st	2nd	1st	2nd
Note			Gas	Only Gas	Gas	Only gas	Gas + water*	Only gas
Description			Gas bag	Inox cell	Gas bag	Inox Cell	Gas bag	Inox Cell
Volume (mL)			1'000	500	1'000	500	1'000	500
Date			14.08.2014	29.01.2015	14.08.2014	29.01.2015	14.08.2014	29.01.2015
Gases								
Hydrogen	H_2	vol.-%	0.26	0.14	< 0.1	< 0.1	0.002	< 0.1
Helium	He	vol.-%	8.6	45.6	4.0	80.0	2.1	70.1
Oxygen	O_2	vol.-%	1.5	2.3	0.8	2.6	1.3	4.5
Nitrogen	N_2	vol.-%	59.4	46.5	90.1	16.4	92	24.6
Argon	Ar	vol.-%	0.4	0.6	0.5	0.2	0.5	0.3
Carbon dioxide	CO_2	vol.-%	1.7	0.6	2.7	0.3	1.3	0.17
Methane	CH_4	vol.-%	27.7	4.1	1.35	0.0265	1.8	0.207
Ethane	C_2H_6	vpm	4	1	8	5	26	4
Propane	C_3H_8	vpm	57	20	155	8	78	8
i-Butane	i-C_4H_{10}	vpm	15	10	42	9	69	11
n-Butane	n-C_4H_{10}	vpm	45	67	80	10	25	10
i-Pentane	i-C_5H_{12}	vpm	< 2	< 1	2	< 1	< 1	< 1
n-Pentane	n-C_5H_{12}	vpm	4	1.1	8	0.5	3	0.3
Ethene	C_2H_4	vpm	n.m.	1	-	5	-	1
Propene	C_3H_6	vpm	n.m.	5	-	3	-	5
1-Butene	1-C_4H_8	vpm	n.m.	210	-	2	-	1
Hydrogensulfide	H_2S	vpm	< 5	< 5	< 5	< 5	< 5	< 5
Gas isotopes								
Nitrogen-15 -N_2	$\delta^{15}N$-N_2	Air-‰	-0.3	-0.5	-1.1	0.6	-1.4	1.6
Carbon-13-CO_2	$\delta^{13}C$-CO_2	V-PDB-‰	-8.4	-13.8	-8.8	-20.0	-19.7	-17.6
Oxygen-18-CO_2	$\delta^{18}O$-CO_2	V-PDB-‰	38	34.4	36.8	33.2	-	37.3
Carbon-13-CH_4	$\delta^{13}C$-CH_4	V-PDB-‰	-65.2	-70.6	-57.6	-54.2	-71.9	-59.3
Deuterium-CH_4	$\delta^{2}H$-CH_4	V-SMOW-‰	-377	-384	-373	n.m.	-378	-377
O_4/H_2S isotopes								
Sulfur-34 of sulfate	$\delta^{34}S$-SO_4	V-CDT-‰	-	-	-	-	13.3	-
Oxygen-18 of sulfate	$\delta^{18}O$-SO_4	V-SMOW-‰	-	-	-	-	11.9	-
sulfur-34 of sulfide	$\delta^{34}S$-H_2S	V-CDT-‰	-	-	-	-	-6.1	-

* Gas values measured in a gas/water mixed sample and values correspond to gas dissolved in water. The gas contents showed in the rest of columns correspond to concentration in gas phase. vpm: volume per million.

** Argon content in atmosphere = 0.934 vol.-% (Lide 1997)

Tab. 11: Chemical composition of the porewater collected from the GRS filter pipes FP-1, FP-2 and FP-3 in the August 2014 sampling campaign

Pipe			**FP3**	**FP3**	**FP3**	**FP2**	**FP2**	**FP1**	**FP1**	**FP1**	**FP1**
Laboratory			Hydroisotop	CIEMAT	CIEMAT	Hydroisotop	CIEMAT	Hydroisotop	Hydroisotop	Hydroisotop	CIEMAT
Sample No.			[2]	Septum V.	Septum Vial	[4]	Sampling bag	[5]	[6]	[7]	Septum Vial
Note			Agua-2	Agua -3	Agua-4	Gas and water 2	Agua	Water	Agua 1 flushed with He	Agua 2 flushed with He	Agua
Sort			1 L gas bag	FP3-1	FP3-2	1 L gas bag	FP2-water 1	1 L gas bag	1 L gas bag	1 L gas bag	FP1- water 4
Weight		g	163	60	60	17.8	60 (+ 60)	14.4	38.2	25	60 (+ 3)
Sensoric parameter lab											
Color			No color	No color	No color	No color	No color		No color		
Turbidity			Clear, black particles	Clear, black particles	Clear, black particles	Clear	Clear		Slightly turbid with few black particles		Clear
Smell			Organic	-	Hyd. sulfide	-	-		organic, moldy		-
Physical-chemical parameter lab											
pH value (20 °C) Lab. (Glove box/lab)	pH		7.82 (CIEMAT: 8.4)	8.0/7.5	8.24/ 8.25	8.44	7.7/7.9		11.74	11.68	10.6/10.5
Redox potential	Eh (SHE)	mV	90 (CIEMAT: -103)	- 210	-193	n.d.			112	-138	-1.6
Spec. electr. conductivity (25 °C) lab.	Cond.	µS/cm		11'360							
Alkalinity (pH 4.3) Lab.	Alk.4.3	meq/L	5.66	5.15	5.91	4.6	< 1		53.5		59.1
Alkalinity (pH 8.2) Lab.	Alk.8.2	meq/L	-	-	-	0.13	-		24		17.9
Main ions											
Sodium	Na^+	mg/L	3'170	3'100	3'200	129	68		1'430		1'700
Potassium	K^+	mg/L	34.8	50	47	78	28		898		900
Calcium	Ca^{2+}	mg/L	482	444	501	6.9	6.6		15.5		1.8
Magnesium	Mg^{2+}	mg/L	339	301	330	2.1	1.0		< 0.5		0.85
Ammonium	NH_4^+	mg/L	0.44	-	-	8.8	-		13.3		-
Chloride	Cl^-	mg/L	2'800	2'700	2'700	82	39		836		1'100
Sulfate	SO_4^{2-}	mg/L	5'240	5'000	5'000	87.3	24		549		672
Nitrate	NO_3	mg/L	< 1	12	< 1	< 1	0.5		1.9		12
Bromide	Br^-	mg/L	7.9	7.0	7.8	< 0.5	< 0.1		1.7		2
Fluoride	F^-	mg/L	n.d.	n.d.	1.8	n.d.	n.d.		n.d.		n.d.
Thiosulfate	$S_2O_3^{2-}$	mg/L	< 1	< 0.5	1.8	< 1	< 0.5		5.5		7.4
Trace compounds											
Aluminium	Al	mg/L	< 0.025	0.2	< 0.3	0.09	< 0.3		27		19
Silicon	Si	mg/L	43.5	54	63	1.6	2.9		12		8.4
Iron	Fe	mg/L	2.45	0.22	< 0.3	0.1	< 0.3		1.5		1.9
Strontium	Sr	mg/L	7.6	8.0	8.5	0.14	< 0.3		0.44		< 0.3
Organic parameter											
Total organic carbon	TOC	mg C/L	57.4	61.1	35.6	n.d.	15.8		1'390		1'280
Acetate	$CH_3\text{-}COO^-$	mg/L	41	67	2.8	16	n.d.		1'600		1'299

Tab. 12: Chemical composition of the porewater collected from the GRS filter pipes FP-1, FP-2 and FP-3 in the January 2015 sampling campaign

Pipe			**FP3**	**FP3**	**FP2**	**FP2**	**FP2**	**FP1**	**FP1**	**FP1**
Laboratory			CIEMAT	CIEMAT	CIEMAT	CIEMAT	CIEMAT	CIEMAT	CIEMAT	CIEMAT
Sample No.			Sampling bag - 1	Sampling bag - 2	Sampling bag	Septum vial microbiology	Bottle 2	Sampling bag	Septum vial microbiology	Septum Vial
Weight		g	3	1		3	0.3	0.5	0.5	2
Sensoric parameter lab										
Colour/turbidity										
Smell						Hydr. sulfide				
Physical-chemical parameter lab										
pH value (20 °C) Lab. (Glove box/lab)	pH		7.17/7.5	8.22/7.4	3.76/4.2	6.04/6.5	/ n.d.	8.54/n.d.	/ n.d.	8.45/8.4
Redox potential	Eh (SHE)	mV	-161.1	-	-	-5.3	-	-65	-	-
Spec. electr. conductivity (25 °C) lab.	Cond.	µS/cm								
Alkalinity Lab.	Alk.	meq/L	3.88	2.44	< 0.5	< 0.5	n.d.	n.d.	n.d.	3.45
Main ions										
Sodium	Na^+	mg/L	3'400	3'100	7.9	4.3	9.0	84	42	14
Potassium	K^+	mg/L	41	50	2.2	2.4	5.4	33	23	12
Calcium	Ca^{2+}	mg/L	474	469	12	2.1	< 18	12	15	15
Magnesium	Mg^{2+}	mg/L	328	362	8.5	< 0.3	< 18	< 10	< 4	0.89
Ammonium	NH_4^+	mg/L	n.d.	n.d.	n.d.	n.d.	n.d.	n.d.	n.d.	n.d.
Chloride	Cl^-	mg/L	2'600	2'700	5.2	2.4	6.8	72	32.6	8.4
Sulfate	SO_4^{2-}	mg/L	5'100	5'200	45	7.8	16	53	24	9.9
Nitrate	NO_3	mg/L	8.3	1.1	0.74	< 0.6	< 5	< 3	1.3	< 0.8
Bromide	Br^-	mg/L	7.1	9.4	< 1	0.25	< 5	< 3	2.6	< 0.8
Thiosulfate	$S_2O_3^{2-}$	mg/L	13	5.0	< 0.5	< 0.5	< 5	1.4	7.2	8.2
Trace compounds										
Aluminium	Al	mg/L	< 0.3	< 0.6	< 0.3	≤ 0.3	< 18	< 10	< 4	0.53
Silicon	Si	mg/L	56	48	2.4	1.3	< 18	< 10	6.9	1.4
Iron	Fe	mg/L	≤ 0.3	< 0.6	1.6	0.63	< 18	< 10	< 4	< 0.3
Strontium	Sr	mg/L	8.6	8.7	< 0.3	< 0.3	< 18	< 10	< 4	< 0.3
Organic parameter										
Total organic carbon	TOC	mg C/L	689.7	n.d.	52.8	n.d.	n.d.	n.d.	n.d.	n.d.
Acetate	$CH_3\text{-}COO^-$	mg/L	n.d.	n.d.	n.d.	n.d.	n.d.	n.d.	n.d.	n.d.

Tab. 13: Chemical composition of the porewater collected from the GRS filter pipes FP-1, FP-2 and FP-3 surrounding Heater #2 over time

Pipe			**FP1**	**FP1**	**FP1**	**FP1**	**FP2**	**FP2**	**FP2**	**FP3**	**FP3**	**FP3**
Date			24.05.2005	12.08.2011	15.08.2014	29.01.2015	12.08.2011	18.08.2014	30.01.2015	12.08.2011	18.08.2014	29.01.2015
Laboratory			CIEMAT	CIEMAT	Hydroisotop	CIEMAT	CIEMAT	Hydroisotop	CIEMAT	CIEMAT	Hydroisotop	CIEMAT
Weight		g	250	10 (+10)	38.2	44.55	5	17.8	14.9	35 (+20)	163	29
Physical-chemical parameter lab												
pH value (20 °C) (glove box/lab.)	pH		9.4/9.12	8.7	11.7	8.54 – 8.45/ n.d.-8.4	8.4	8.44	3.76 – 6.04/ 4.2 – 6.5	7.8	7.8	7.17 – 8.22/ 7.5 – 7.4
Redox potential	Eh (SHE)	mV	-284.2	n.m.	-138	-65	n.m.	n.m.	-5.3	-124	-210	-161
Alkalinity lab.	Alk.	meq/L	18.3	30.5	53.5	n.d.-3.45	4.76	4.6	< 0.5	3.5	5.66	3.88 – 2.44
Main ions												
Sodium	Na^+	mg/L	1'071	664	1'430	84 – 14	209	129	4.3 – 9.0	3831	3170	3'400 – 3'100
Potassium	K^+	mg/L	262	441	898	33 – 12	188	78	2.2 – 5.4	69	34.8	41 – 50
Calcium	Ca^{2+}	mg/L	< 5	9.7	15.5	12 – 15	17	6.9	2.1 – 12	578	482	474 – 469
Magnesium	Mg^{2+}	mg/L	22.5	12	< 0.5	0.89 – < 10	11	2.1	8.5 – < 0.3	426	339	328 – 362
Strontium	Sr^{2+}	mg/L	< 0.5	< 0.24	0.44	< d.l.	< 0.3	0.14	< d.l.	10	7.6	8.6 – 8.7
Fe total/Fe(II)	Fe/Fe^{2+}	mg/L	0.145/0.145	< 0.24	1.5	< d.l.	< 0.3	0.1	0.63 – 1.6	< 0.3	2.45	< d.l.
Silicon	Si	mg/L	n.d.	11	12	6.9 – 1.4	4.5	1.6	1.3 – 2.4	44	43.5	56 – 48
Ammonium	NH_4^+	mg/L	9.2	n.m.	13.3	n.d.	n.m.	8.8	n.d.	n.m.	0.44	n.d.
Chloride	Cl^-	mg/L	914	438	836	72 – 8.4	153	82	2.4 – 6.8	4'800	2'800	2'600 – 2'700
Sulfate	SO_4^{2-}	mg/L	590	31	549	53 – 9.9	234	87.3	7.8 – 45	4'700	5'240	5'100 – 5'200
Nitrate	NO_3	mg/L	< d.l.	0.2	1.9	< 3 – 1.3	1.2	< 1	< 0.6 – 0.74	25	< 1	1.1 – 8.3
Bromide	Br^-	mg/L	< 1	1	1.7	< 3 – 2.6	0.38	< 0.5	0.25 - < 1	13	7.9	7.1 – 9.4
Fluoride	F^-	mg/L	1.6	n.d.	n.d.	n.d.	n.d.	n.d.	n.d.	n.d.	1.8	n.d.
Thiosulfate	$S_2O_3^{2-}$	mg/L	n.d.	n.d.	n.d.	1.4 – 8.2	n.d.	n.d.	n.d.	n.d.	n.d.	13 – 5
Total organic carbon	TOC	mg C/L	n.d.	n.d.	1390	n.d.	n.d.	15.8	52.8	n.d.	57.4	690
Acetate	$CH_3\text{-}COO^-$	mg/L	n.d.	n.d.	1600	n.d.	n.d.	n.d.	n.d.	n.d.	41	n.d.
Iodide	I^-	mg/L	n.d.	0.35	n.d.	n.d.	0.29	n.d.	n.d.	2.4	n.d.	n.d.
Boron	B	mg/L	0.66	1.3	4.4	< d.l.	0.62	< 0.3	< 0.3	11	8.2	7.9
Caesium	Cs	mg/L	n.m.	n.m.	n.m.	n.m.	n.m.	n.m.	n.m.	$\leq 2 \times 10^{-3}$	n.m.	n.m.

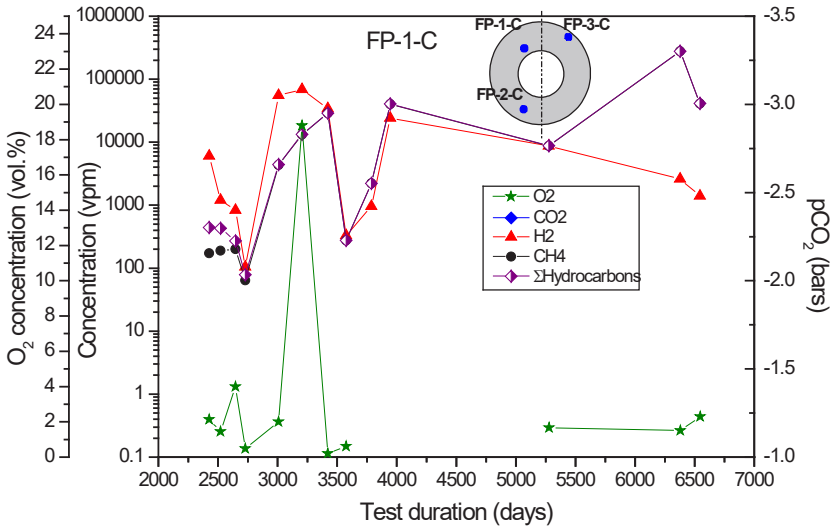

Fig. 62: Gas composition in the GRS pipe FP-1

Day 0: 27.02.1997 when heaters were switched on. First measurement during the second phase: 21.10.2003.

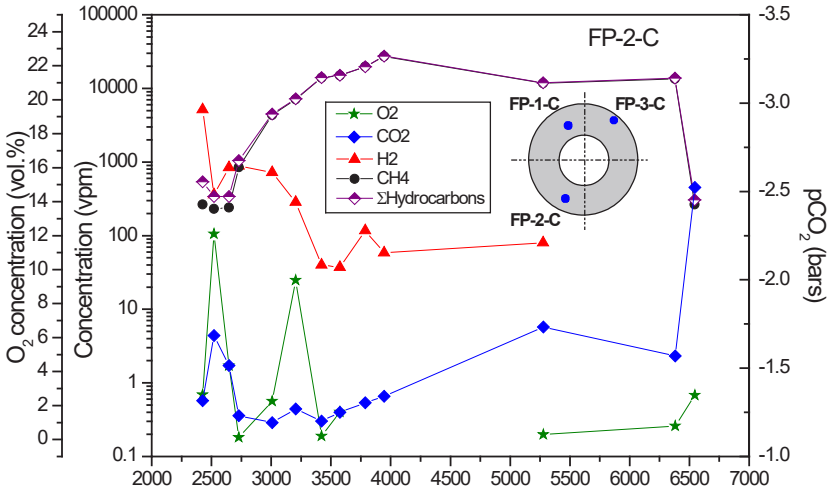

Fig. 63: Gas composition in the GRS pipe FP-2

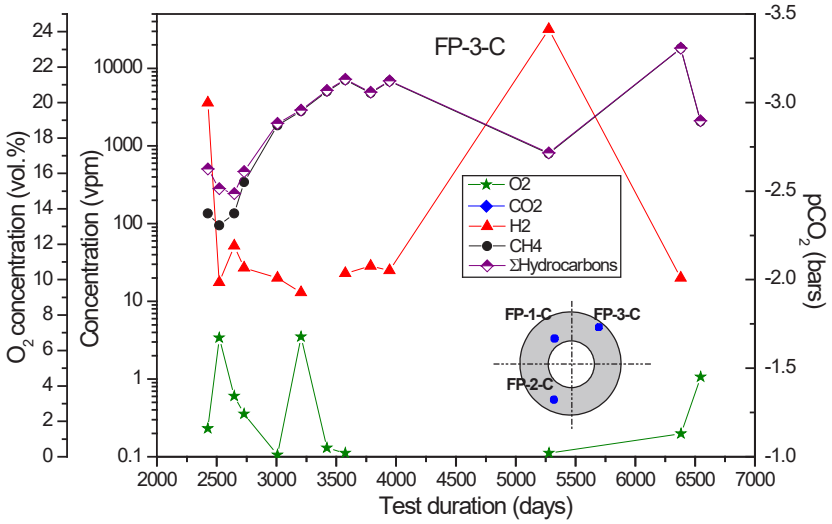

Fig. 64: Gas composition in the GRS pipe FP-3

Fig. 65: Black particles observed at the bottom of the septum vial -1 from the FP3 pipe, which were analysed by scanning electron microscopy (SEM)

The black particles were observed both *on site* after water collection and at CIEMAT.

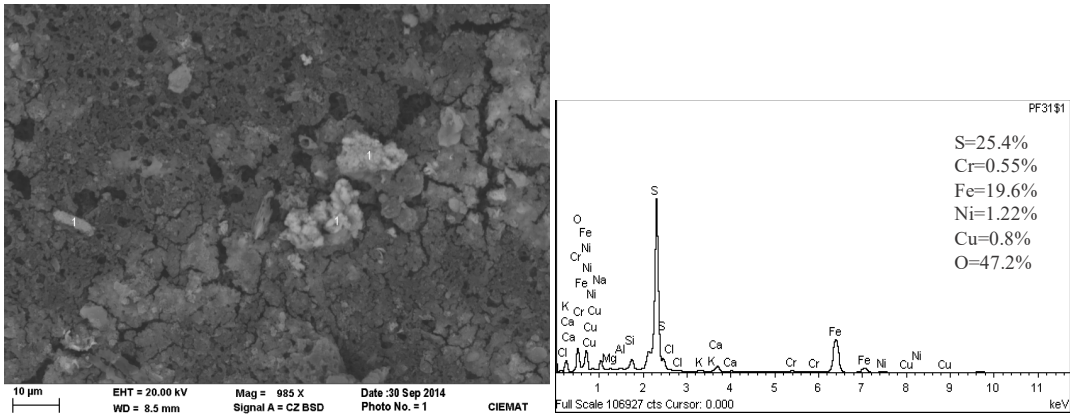

Fig. 66: SEM photomicrographs: black particles of Fe, S, Cu observed in the FP3 water

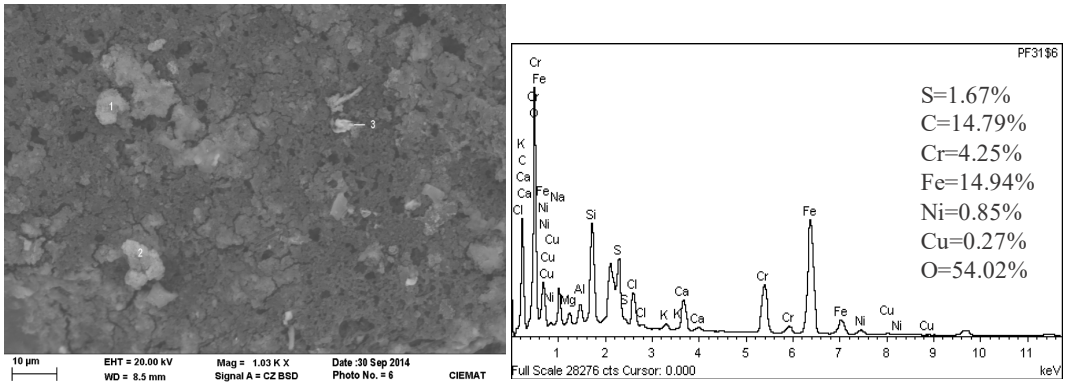

Fig. 67: SEM photomicrographs: black particles observed in the FP3 water: 1) Fe, Cr, Ni, Cu, S (EDAX). 2) S, Fe, and 3) Fe, Cr, Ni

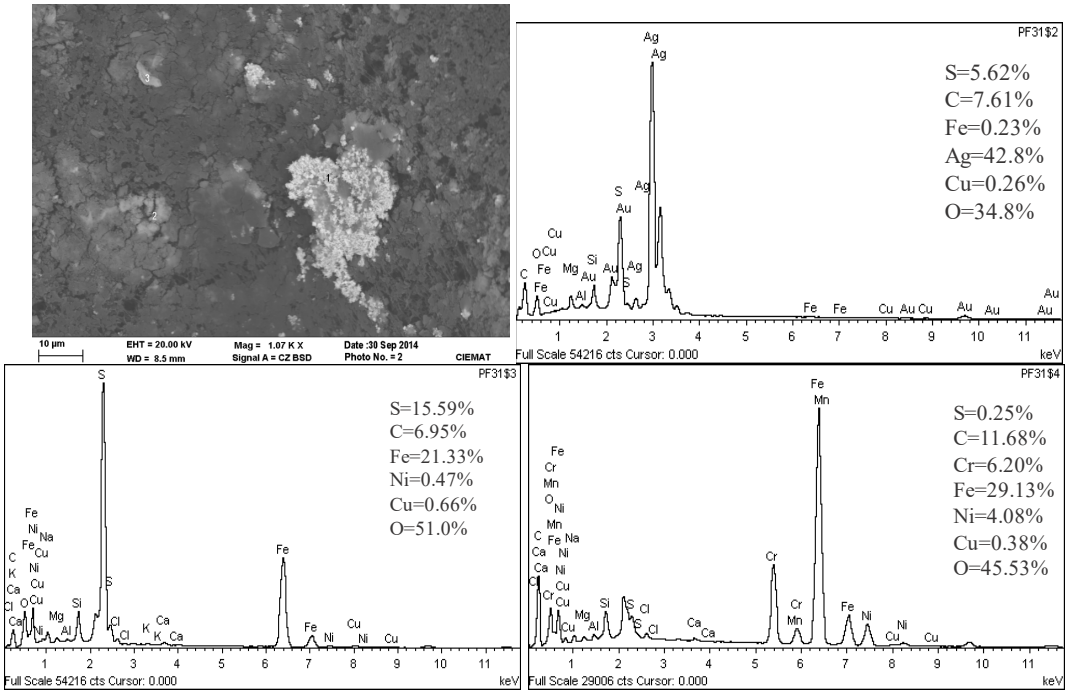

Fig. 68: SEM photomicrographs: black particles observed in the FP3 water: 1) S, Fe, Ag, C, Cu. 2) S, Fe, Cu, and 3) S, Fe, Cr, Cu, Ni

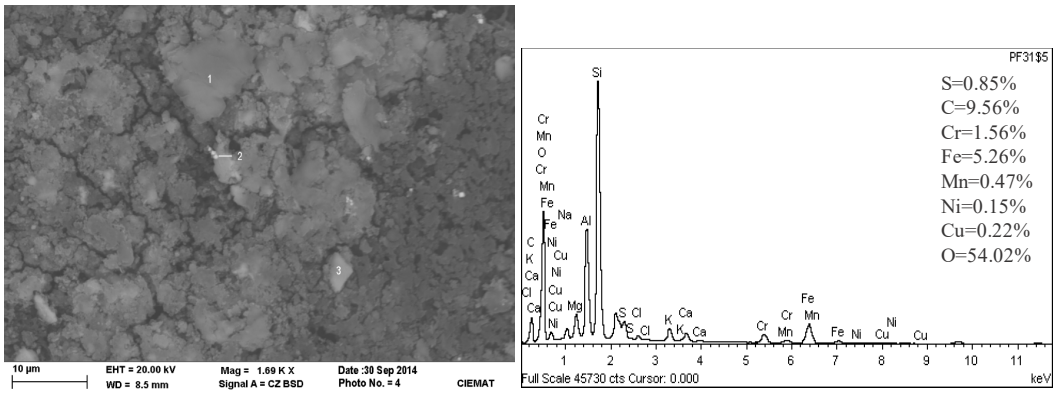

Fig. 69: SEM photomicrographs: black particles observed in the FP3 water: 1) silicates and (S, Fe, Cr, Mn, Cu) (EDAX). 2) S, Ag, and 3) Fe, Cr, Cu, Ni, S

A comparison of the chemical data obtained from the pipes over time during the Second Operational Phase is shown in Tab. 13.

Even though the FP2 pipe was located at the bottom part of the bentonite barrier close to the granite interface and that the bentonite was saturated at that interface (Fig. 11), no water could be collected and analysed until 2011. The small volume of water analysed indicates that the chemical composition of water inside the sintered filters (with an internal total volume of V = 3.2 L) may be diluted over time, especially in the external pipes, located close to the granite interface. The salinity is low, with a maximum chloride concentration of 153 mg/L, which decreased to ~5 mg/L in 2015. pH ranged from alkaline (~ 8.4) in 2011 to acidic (~ 4 – 6) conditions in 2015; alkalinity and sulfate concentration decreased, whereas TOC values slightly increased. Acidic conditions and low alkalinity values indicate oxidation processes.

In the case of the FP3 pipe, located at the upper part of the saturated bentonite barrier close to the granite interface, the chemical composition of waters presents an unexpected much higher salinity than that observed in FP2 and FP1. Nevertheless, the overall concentration is also diluted over time but at much lower rate. The chloride concentrations range from 4'800 to 2'600 mg/L from 2011 to 2015. pH values are slightly alkaline (~ 7.8), and Eh values indicate reduced conditions (~-200 mV SHE). TOC values increase with time (57 mg C/L in 2014 and 690 mg C/L in 2015). Ammonium (0.44 mg/L) was detected in 2014 and thiosulfate (13 mg/L) in 2015. Alkalinity increased from 2011 to 2014, but decreased in 2015. Sulfate concentrations (> 4'700 mg/L) are higher than those found in the other pipes and higher than expected from this pipe located close to granite interface. At this point a dilution of the porewaters due to the granite groundwater inflow is supposed, increasing the salinity towards the internal part of the barrier.

The porewaters from pipe FP1, located at the upper and inner part of the bentonite barrier, closer to the liner/Heater #2, have a highly alkaline pH (between 9.1 and 11.7 over time), reduced Eh values (~ -200 mV, SHE), very high alkalinity values (18 – 54 meq/L), and high concentrations of thiosulphate (1.4 – 8.2 mg/L), acetate (1600 mg/L) and TOC (1'600 mg/L), increasing over time. The salinity of the waters is slightly lower than that observed in the porewaters from pipe FP3 but higher than those of the pipe FP2, with chloride concentrations ranging between 914 and 72 mg/L. Sulphate concentrations seem to increase and decrease over time, ranging between 590 and 31 mg/L. Alkalinity increases over time from 18.3 to 54 meq/L in 2014, and decreases to 3.45 meq/L in 2015. Ammonium was detected in 2011 and 2014 (around 10 mg/L) and Fe(II) in 2005 (0.15 mg/L).

4.2.3 Comparison of data obtained along 18 years of experiment

4.2.3.1 Evolution of pressures

The fluid pressures (gas and water pressures) from each gas pipe measured by pressure transducers connected to a data acquisition system during the 18-years of the FEBEX *in situ* test are shown in Fig. 70. During the First Operational Phase when Heater #1 was running small fluid pressure fluctuations were observed. Fluid pressures were only detected in the pipes located at the granite interface, which were related to porewater pressures during the saturation phase of the barrier. Water pressures between 2.5 and 4.5 bar were observed in the pipes located in the outer bentonite ring in contact with the granite interface: GF-S-L-02, GF-S-L-01 and GF-S-L-03, which coincided with the appearance of water inside the pipes (Fig. 57 and Fig. 70). These overpressures are much lower than the pore pressures measured inside the bentonite buffer over time, which ranged between 20 and 60 bar in the external bentonite rings and from 5 to 20 bar in the internal ones (Martínez et al. 2016: NAB 16-19). The different time evolution of observed water pressures in the different GF-S-L-xx pipes indicated that saturation did not take place homogeneously during the First Operational Phase. The upper-right part of the bentonite needed more time to be saturated than the rest of the barrier.

In the Second Operational Phase (Heater #2 running), the measured fluid pressures indicated either low gas production rates and/or low total gas pressures inside the bentonite buffer. Fluid pressures maintained values similar to atmospheric pressure, with values ranging between 0.805 and 0.929 bar (variations in the range of atmospheric pressure fluctuations). The highest values were observed in pipe FP2 located at the bottom of the bentonite barrier, which may be related to the influence of hydrostatic pressure (Fig. 70).

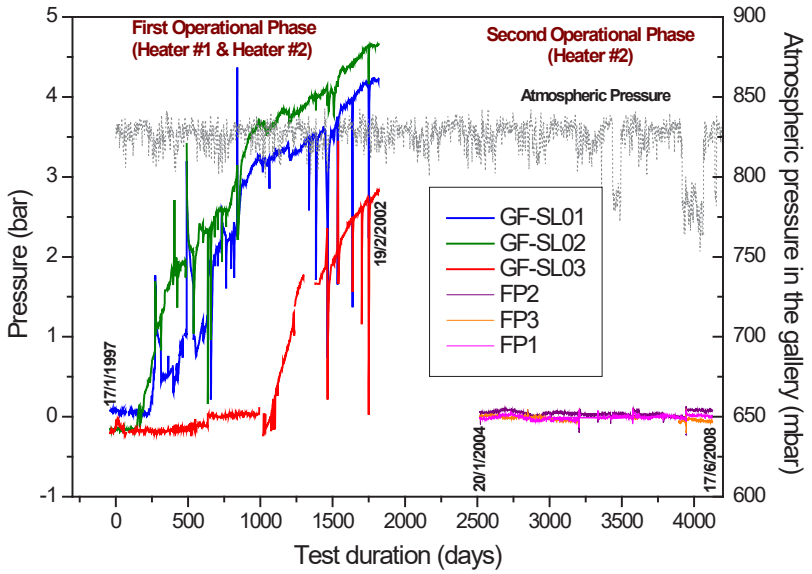

Fig. 70: Pressures measured in the gas pipes around Heater #1 (GF-SL-0x) and Heater #2 (FP-x, interval C-D)

Atmospheric pressures inside the gallery recorded *on site* by AITEMIN are also shown (average: 823 ± 16 mbar). Day 0: 27.02.1997 when heaters were switched on.

4.2.3.2 Evolution of the gas composition

The main gases collected from the FEBEX *in situ* test were O_2, N_2, CO_2, CO, H_2, CH_4 and other light hydrocarbons, such as ethane (C_2), propane (C_3), and isobutane (iC_4). In the two last 2014 and 2015 sampling campaigns, n-alkanes up to C5 chains (saturated) and n-alkenes (unsaturated) hydrocarbons were also detected. The evolution of the gas composition as a function of time is described in this section.

Gases were sampled at ambient temperature (~ 15 °C inside the tunnels of the Grimsel Test Site) but analysed at laboratory temperature, so the gas composition was transformed from vpm (or/%) to mmol/L units of gas by using the Universal Gas Law at 1 atmosphere and 25 °C. As first approximation and for only comparison purposes, dissolved gas contents in porewater were obtained by using Henry's Law (for ideal gases the solubility of a gas is directly proportional to the partial pressure of the gas in the vapour phase) and the program Phreeqc (Parkhurst & Appelo 2013) at 1 atmosphere and 25 °C by using the Thermoddem database (Blanc 2017). It should be taken into account that gas solubilities in water increase with hydrostatic pressure and decreasing temperature (Appelo & Postma 2005). In this report, a constant temperature of 25 °C was considered in the interpretation of results because: a) the effect of temperature in the range 12 °C to 25 °C is low; b) the highest temperatures affecting the gas pipes were lower than 55 °C, and c) the water temperature is not very different from 25 °C, because the obtained water is a mix of water originating from different zones (outer and middle bentonite rings located between the frontal to the rear-end of the heater, temperature ranging from 36 to 72 °C, Tab. 3).

Oxygen evolution

At the initial stage of the FEBEX *in situ* test, aerobic conditions were prevailing in the bentonite barrier, showing oxygen values of around 22.95 vol.-%, slightly higher than atmospheric, although in the range of the measurement uncertainty (5 – 10 %). However, oxygen was rapidly depleted (around 83 % lower than atmospheric value) and, after about one year (Fig. 71), oxygen kept decreasing or consuming, measuring low dissolved oxygen concentration ranging between 3.2 and 0.3 vol.-% (Fig. 72). The lowest values were reached in the pipes located at the bottom part of the bentonite barrier (GF-SL-01 and GF-SL-02).

Many oxygen measurements obtained during the First Operational Phase were discarded in Fig. 71 due to the high levels of oxygen measured probably due to sampling artefacts and/or during the gas injection tests. Exception was the GF-SL-02 pipe, located at the bottom part of the bentonite, where values decreased from 22 vol.-% to 1 vol.-% in one year, and none O_2 increments or fluctuations were observed, values being maintained lower than 1 vol.-% (from 1.1 wt.-% to 0.89 wt.-%) during the next one year (Zone 3). On the other hand, the FEBEX *in situ* test cannot be considered as gas-tight at all.

In the Second Operational Phase, oxygen contents ranged between 2.6 vol.-% (Zone 2, when "quasi anoxic" conditions may be stablished) to 0.2 vol. % (Zone 3); O_2 being never completely consumed. Artefact measurements or major shifts in O_2 contents (values discarded in the figure) were almost absent with respect to those observed during the First Phase, most O_2 values being between 2.6 to 0.2 vol.-%. The shifts ranged up to 7, 9 – 12 and 4 vol.-% in pipe FP-3, FP-2 and FP-1, respectively in only one sampling campaign along time, indicating the good sampling performance and the higher tightness of the second concrete plug. However, the presence of a remaining O_2 may be due to atmospheric air income, transported from the gallery access towards the barrier through the concrete plug, responding to atmospheric pressure variations.

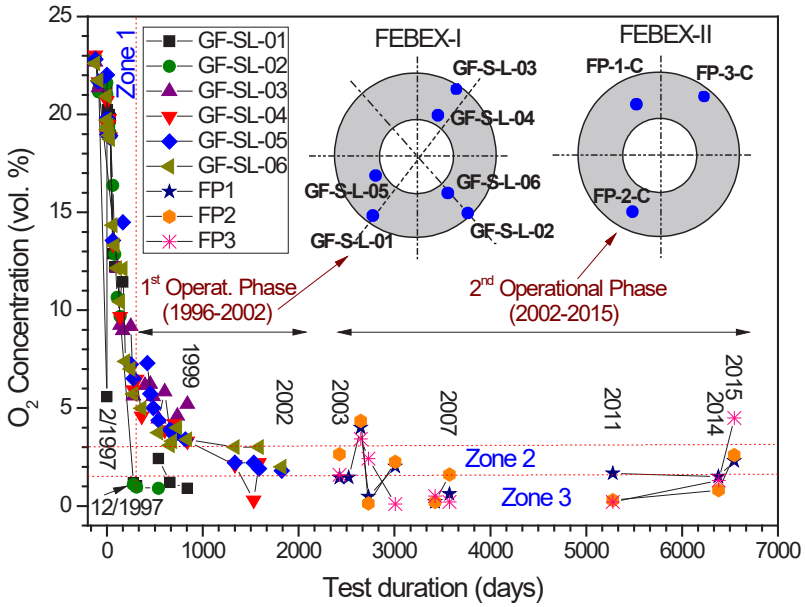

Fig. 71: Concentration of oxygen gas (in vol.-%) in the different GRS pipes obtained during the First (1996 – 2002, FEBEX-I) and Second (2002 – 2015, FEBEX-II) Operational Phases

Zone 1, Zone 2 ("quasi-anoxic conditions") and Zone 3 indicate different oxygen levels over time. Day 0: 27.02.1997 when heaters were switched on.

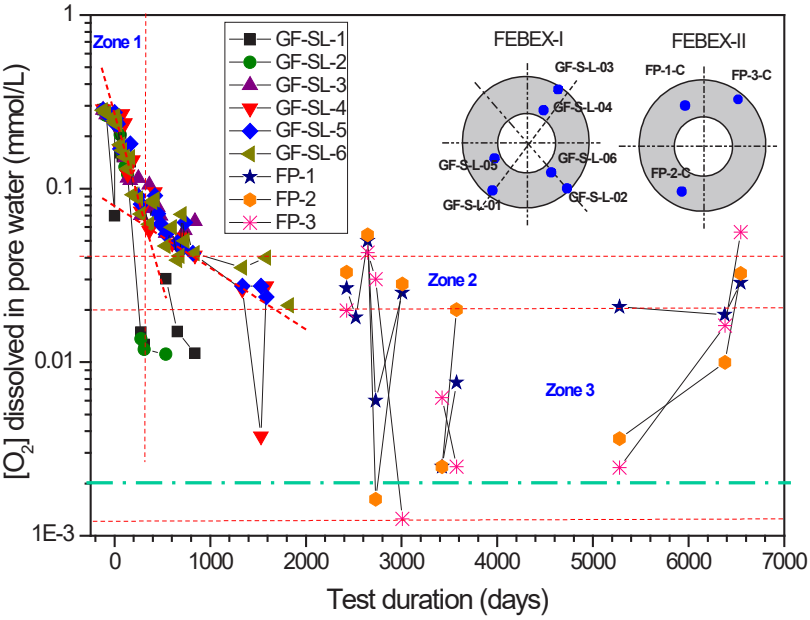

Fig. 72: Concentration of dissolved oxygen in porewater at 25 °C in the different GRS pipes obtained during the First (1996 – 2002, FEBEX-I) and Second (2002 – 2015, FEBEX-II) Operational Phases

It is interesting to note that the oxygen contents at the beginning of the Second Operational Phase were similar to those obtained at the end of the First Operational Phase. This may indicate that either the oxygen income was quite limited, probably due to the low gas permeability of the partially saturated bentonite; or that the oxygen consumption rate could have increased in response to a new influx of O_2. Oxygen could income either by advective flow though preferential pathways or by diffusion from the access gallery towards the inner part of the bentonite during the dismantling operations of Heater #1 (from 25 April 2002 to 24 July 2002 when the first part of the shotcrete plug was constructed, see Tab. 2). Additional oxygen intrusions may be also related to other monitoring activities: gas permeability measurements, water or colloids sampling from radial and parallel boreholes, which ended in the test interval of the FEBEX *in situ* experiment (Fig. 4) or were very close to the bentonite barrier (see Garralón et al. 2017: NAB 16-14, Missana et al. 2014), and/or Excavation Damage Zone (EDZ) effects.

Regarding dissolved O_2 contents, three zones can be defined over time (Fig. 72): Zone 1 with O_2 contents higher than 4×10^{-2} mmol/L; Zone 2 with O_2 contents between 4×10^{-2} and 2×10^{-2} mmol/L; and Zone 3 with O_2 contents below $2 \cdot 10^{-2}$ mmol/L. Real anaerobic conditions with dissolved O_2 values below $1 \cdot 10^{-3}$ mmol/L were never reached after 18 years of experiment. However, "quasi anaerobic" conditions can be considered in Zone 2. This small presence of oxygen can be explained both by atmospheric air fluctuations because the bentonite barrier system was not gas-tight (at least at the concrete interface through the cables for instrumentation) or by unavoidable oxygen artefacts during sampling. Therefore, oxygen values lower than 2×10^{-2} mmol/L can be considered for establishing "quasi anaerobic/anoxic" conditions in the FEBEX *in situ* test, i.e., after 1.5 years of switching on the heaters for the pipes located at the bottom of the gallery.

Apparently, the zones firstly saturated due to gravity or hydrostatic pressure, i.e., those located at the bottom of the gallery, reached "quasi" anaerobic conditions in less time than the inner and upper-right parts of the buffer, which were saturated at lower rates.

Nitrogen evolution

The evolution of the nitrogen content in the gas phase during the FEBEX *in situ* test is shown in Fig. 73. At the beginning of the experiment, atmospheric air conditions were present in the unsaturated bentonite barrier, where pores and gaps were, therefore, filled with 78.09 vol.-% of nitrogen, with constant compositions of isotopes $\delta^{14}N$ and $\delta^{15}N$ of 99.63 ‰ and 0.37 ‰, respectively. Then, nitrogen concentration seems to accumulate rapidly and increase exponentially above the atmospheric value from the beginning of the experiment until "quasi anoxic" conditions are established, from which steady state values are maintained or slightly decrease over time, especially in pipes located at the inner part of the bentonite. Therefore, the N_2 increase seems to be related with the water saturation process and the O_2 consumption.

It should be noted that the sampling circuit for collecting the gas/water samples (internal volume of 0.2 L), was filled with nitrogen gas at a maximum pressure of 1 bar, except in the 2014 and 2015 sampling campaigns when helium gas (99.9999 % purity) was used. From 2011 all the pipes were left under vacuum after the sampling campaigns, but this cannot be assured for the other campaigns. In addition, stainless steels cylinders were used in 2015 for collecting the gas/water samples instead of Al-foil bags as in the rest of sampling campaigns since 1996.

In the second phase N_2 values are always higher than 92 vol.-% in average in all pipes, except in the last sampling campaign, where He is another major gas phase with values of 40, 80 and 70 vol.-% in the pipes FP1, FP2 and FP3, respectively (Tab. 10). The major content of gases (> 95 vol.-%) is nitrogen and oxygen (plus He in the two last campaigns), the sum of remaining

gases being only between 0.5 and 6.7 vol.-% (Tab. 14). When oxygen decreases (or is consumed), the amount of nitrogen (Fig. 73) and/or helium (Tab. 10) increases in vol.-%, indicating the low generation rate of other gases (CO_2, H_2, CH_4, etc.) in the test (especially in 2015), the total gas content of these other gases being higher when Heater # 2 was running, higher as a function of the heater source, and higher in pipe FP1 than in the rest of pipes (average values of 6.7, 5.1 and 2.9 vol.-% for pipes FP-1, FP-2 and FP-3, respectively; whereas in GF-SL-x pipes the values ranged from 0.5 (GF-SL-1) to 3 vol.-% (GF-SL-5)). It is interesting to note that nitrogen was also measured in 2015, with contents ranging between 46 and 16 vol.-%, even though He was used as gas carrier since 2014.

Apart from low gas content of other gases, the increase of N_2 over time until almost a plateau value (~95 vol.-%), may be related with the drop of total pressure during O_2 consumption, enhancing the gas inflow into the barrier, and the entrance of atmospheric air from the access gallery due to no airtight conditions. However, N_2 could be also introduced inside the barrier during the saturation process of the bentonite due to Grimsel groundwater contains dissolved nitrogen (Hoehn et al. 1990; see Appendix A). The main gases dissolved in Grimsel groundwaters are nitrogen (~ 17.62 mg/kg, implying a N_2 gas content of 98.5 vol.-% or $P_{N2} = 10^{-0.0065}$ atm), argon (~ 0.79 mg/kg; i.e. 1.37 vol.-% or $P_{Ar} = 10^{-1.86}$ atm), and helium (~ 4×10^{-4} mg/kg; i.e. 306 ppmv or $P_{Ar} = 10^{-3.51}$ atm). Indeed, granitic rocks can have nitrogen concentrations up to 250 mg N/kg and $\delta^{15}N$ from 1.7 to 14.9‰; with ammonium partitioned into the feldspar orthoclase to a greater extent than muscovite or biotite (Holloway & Dahlgren 2002, Boyd et al. 1993). Therefore, the increase of the nitrogen content inside the bentonite over time can be also related with the entrance of dissolved nitrogen from the granitic groundwater during the saturation process of the barrier and/or with air infiltrations. In some periods of time nitrogen decreased being oxygen also depleted. Therefore, variations of nitrogen concentrations and isotopic signals should be due, in turn, to biogeochemical interactions inside the bentonite barrier.

To identify possible biogeochemical processes, $\delta^{15}N$ isotope data were obtained during the 2014 and 2015 gas/water sampling campaigns from the pipes FP-1, FP-2 and FP-3 (Fig. 74). In 2014, the isotopic values are negative (-0.3, -1.1 and -1.4 ‰ for pipes FP-1, FP-2 and FP-3, respectively). These values changed in the 2015 campaign towards most enriched values of 0.6 and 1.6 ‰ in the pipes FP2 and FP3, respectively; and towards slightly depleted values of -0.5 ‰ in the FP1 pipe. Then, $\delta^{15}N–N_2$ data seem to indicate different geochemical reactions in each pipe. A relationship between $\delta^{15}N–N_2$ and $\delta^{13}C–CH_4$ is observed in Fig. 75.

Tab. 14: Average concentration of gases in the different pipes

Gas pipe	**O_2+N_2** (vol.-%)	**O_2+N_2+He** (vol.-%)	**Rest of gases** (vol.-%)
GF-SL-1	98.81		0.49
GF-SL-2	99.26		0.55
GF-SL-3	95.44		2.39
GF-SL-4	96.20		2.58
GF-SL-5	95.97		3.00
GF-SL-6	95.96		2.72
FP-1	95.22	93.13	6.70
FP-2	94.36	94.76	5.11
FP-3	96.92	96.97	2.87

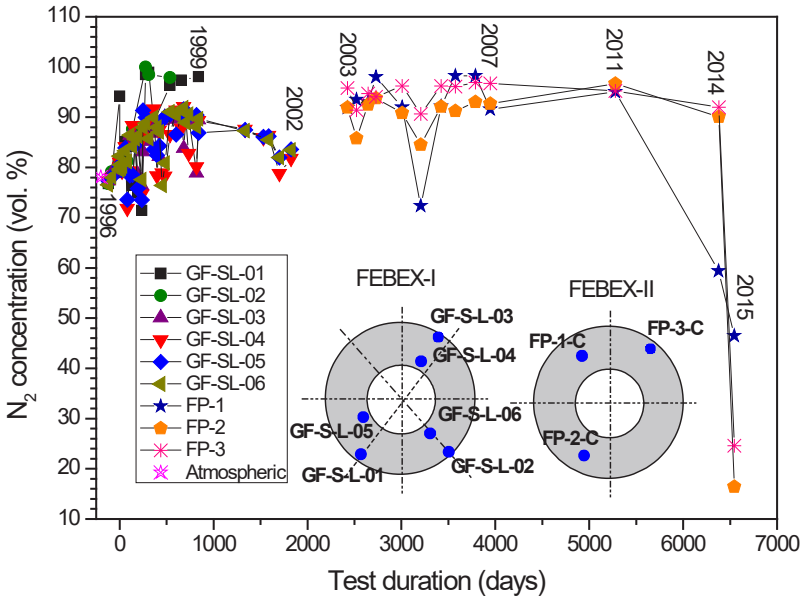

Fig. 73: Evolution of nitrogen in the gas phase (in vol.-%) during the FEBEX *in situ* test
Day 0: 27.02.1997 when heaters were switched on.

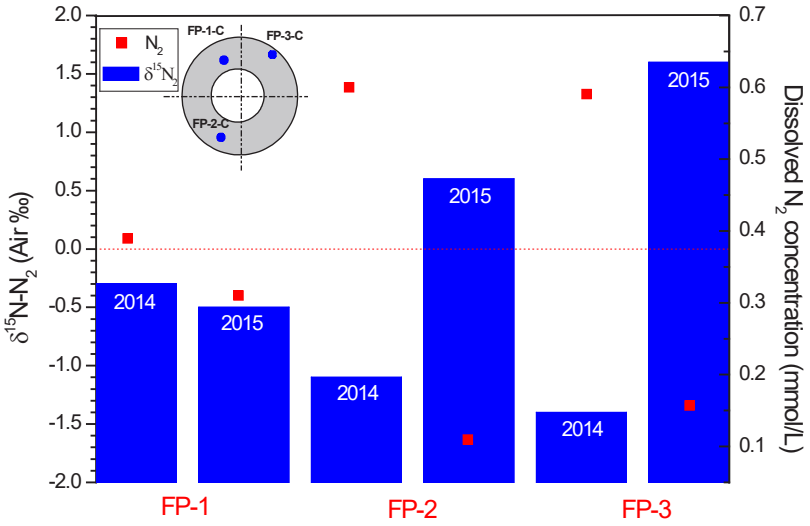

Fig. 74: $\delta^{15}N\text{-}N_2$ values and dissolved N_2 concentration (mmol/L) obtained from the pipes FP-1, FP-2 and FP-3 located around Heater #2

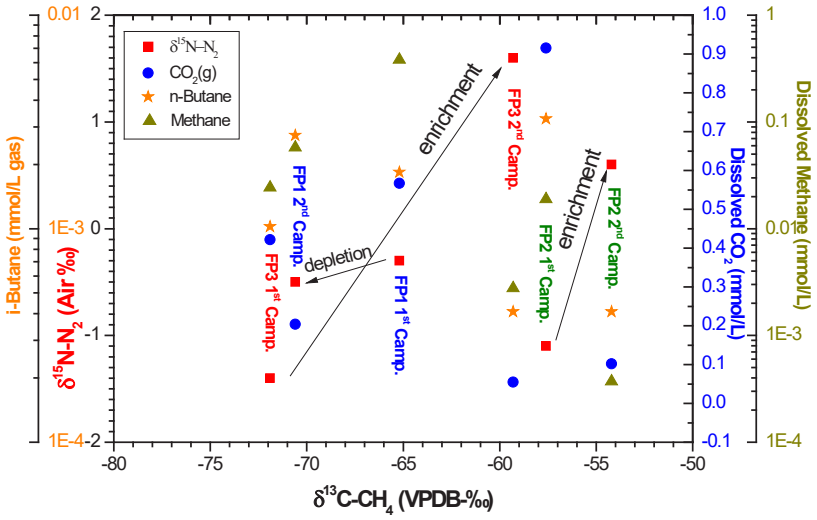

Fig. 75: $\delta^{15}N\text{-}N_2$, $CO_2(g)$, i-Butane and methane composition as a function of the $\delta^{13}C\text{-}CH_4$ isotopic composition obtained from the pipes FP-1, FP-2 and FP-3 located around Heater #2

CO_2 and CO evolution

The evolution of the CO_2 and CO contents during the FEBEX *in situ* test is shown in Fig. 76 and Fig. 77. It should be taken into account that dissolved CO_2 concentrations in the porewater depend on pH and temperature. In all pipes, the concentration of CO_2 increases rapidly towards a plateau during the First Operational Phase. However, the slope of the steeply increasing curve changes when "quasi anoxic" conditions are almost established after about one year (with pCO_2 = -1.6 bar.). The CO_2 generation rate slows afterwards. A maximum amount of pCO_2 = -1.0 bar was reached during the First Operational Phase (Heater #1 and Heater #2 running). The pipes close to the granite interface showed a lower amount of CO_2 over time probably due to a CO_2 loss by dilution after the bentonite interaction with granite groundwater.

During the Second Operational Phase (Fig. 76), a decrease of CO_2 is observed after the dismantling of Heater #1, probably due to CO_2-degassing because the system remained open to the air at least during three months during the dismantling of Heater #1. The initial values of CO_2 when Heater #2 was only running were higher in the pipe FP1 (FP1: pCO_2 = -1.27 bat; FP2: pCO_2 = -1.32 bar; FP3: pCO_2 = -1.66 bar). Indeed, the high concentrations measured during the First Operational Phase were never recovered, and less variations in pCO_2 were observed in this second phase with a tendency to a slight decrease. The variations in CO_2 concentration may be produced inside the bentonite barrier due to different water/bentonite interactions (carbonates dissolution) and/or organic matter degradation since CO_2 is practically absent in the granite groundwater. Granite groundwater of pH 9.59 and pCO_2 -5.47 bar (Tab. 8) could act as a sink for CO_2, escaping from the bentonite barrier system.

CO content was only measured during the First Operational Phase (Fig. 77), and it was always higher than atmospheric content (0.2 vpm), increasing rapidly from 1996 to 1997 before switching on the heaters (27.02.1997: Day 0). After a slight decrease, CO increased over time, except in pipe GF-SL-02.

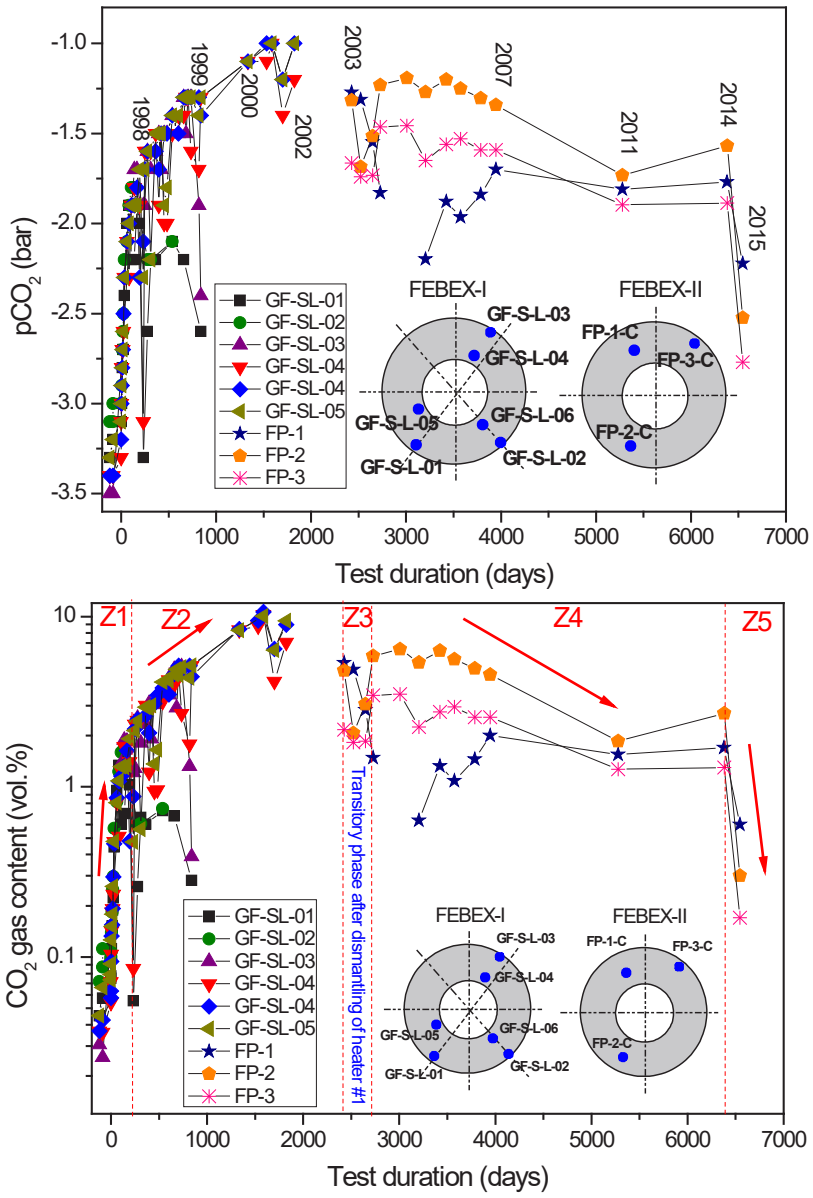

Fig. 76: Carbon dioxide gas content expressed as pCO_2 (bar) and in vol.-% in the different GRS pipes obtained during the First (1996 – 2002) and Second (2002 – 2015) Operational Phases.

Day 0: 27.02.1997 when heaters were switched on.

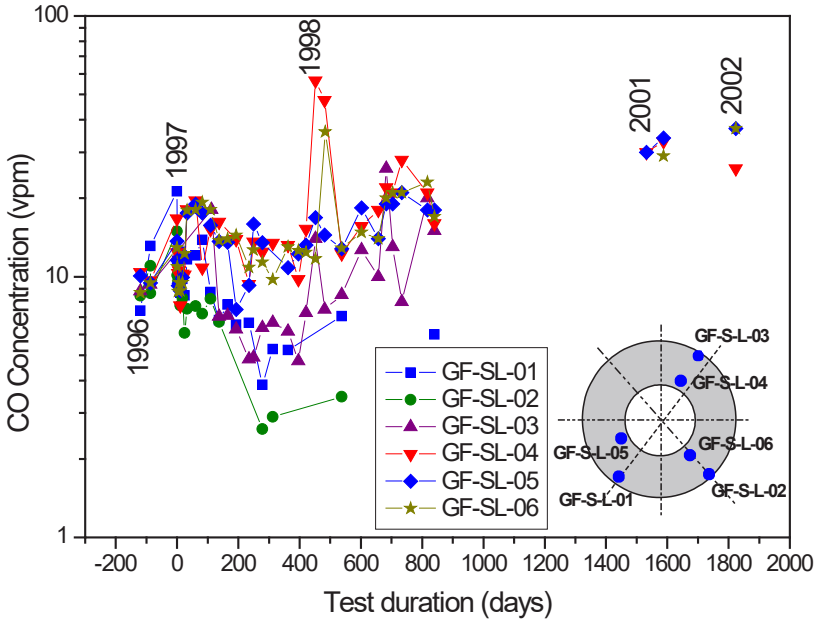

Fig. 77: Carbon monoxide gas content in the different GRS pipes obtained during the First (1996 – 2002) Operational Phase in vpm (or ppmv: parts per million by volume) of gas

Day 0: 27.02.1997 when heaters were switched on.

The study of the carbon isotopic composition may allow to understand the biogenic or abiogenic origin of the carbon species. The isotopic $\delta^{13}C$-CO_2 signals were only obtained from the last two campaigns (Tab. 10, Fig. 78), which makes difficult the interpretation of results. The measured $\delta^{13}C$-CO_2 content of pipe FP3 approached to -20‰ in 2014 and enriched to -18‰ in 2015. In the case of the pipes FP1 and FP2 a large depletion of $\delta^{13}C$–CO_2 is observed between both campaigns (from -8.4 to -13.8 ‰ in FP1, and from -8.8 to -20.0 ‰ in FP2).

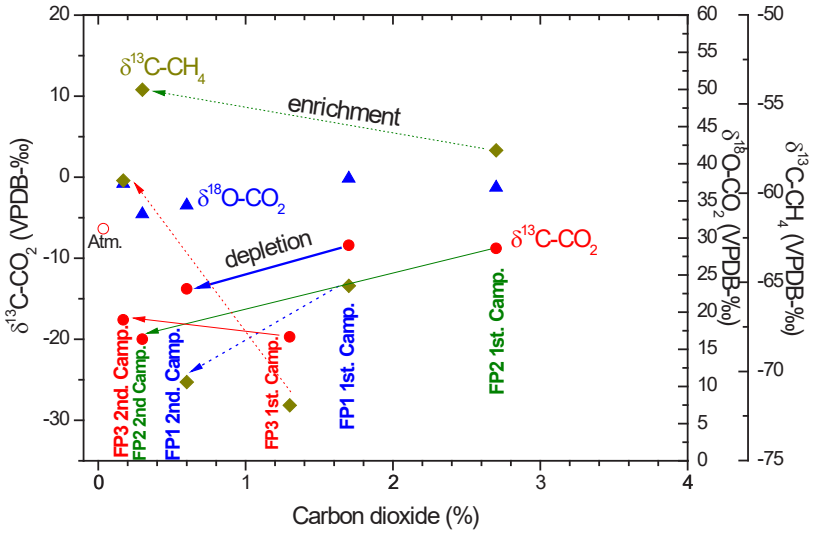

Fig. 78: Cross plots of $\delta^{13}C$–CO_2 versus carbon dioxide content for the gas samples obtained from the GRS pipes FP-1, FP-2 and FP-3 in the FEBEX *in situ* test

Methane and hydrocarbons evolution

Methane and other light hydrocarbons, such as ethane (C_2), propane (C_3) and isobutane (iC_4), were detected from the beginning of the experiment (Fig. 79, Fig. 80). Methane (CH_4) production is indicative of the presence of strongly reduced redox conditions, i.e., anoxic conditions although thermodynamically other hydrocarbons (alkanes, alkenes, carboxylic acids, etc.), with standard reduction potentials near that of methane, will be present. n-alkanes up to C5 chains (saturated) and alkenes (unsaturated) hydrocarbons were also detected in the two last 2014 and 2015 sampling campaigns. (Tab. 10). In principle, GRS Chromatograph could only detect hydrocarbons up to C4 chains.

The evolution of methane generation in the FEBEX *in situ* test is shown in Fig. 79. Methane, present in the atmosphere at a concentration of 1.7 vpm (Lide, 1997) and absent in Grimsel groundwaters (see Appendix A), increased over time at different rates. During the First Operational Phase, i.e., during the hydration of the bentonite, there was a rapid increase of methane related with the progressive consumption of O_2 and decrease of hydrogen (Zone Z1). After 500 days, there is a slope change in the concentration curve, showing a decrease at the same time that "quasi anoxic" conditions are established, and an increase of hydrogen is observed (Zone Z2). In the Second Operational Phase, the methane contents are slightly lower than those at the final period of the experiment prior to the dismantling of Heater #1, probably due to some oxidation process during the dismantling of Heater #1, when the bentonite barrier was open to the atmosphere during at least three months (Zone Z3). Next, a new increase of methane concentration is seen, with values always higher than those generated in the First Operational Phase, and reaching values of around 4.0 vol.-% of CH_4 (Zone Z4), except in FP-1 pipe where an abrupt decrease is observed (not related with an increase of O_2). From 4000 days onward, the methane concentration is either constant or decreasing in some sampling points, except in FP-1 pipe (Zone Z5). The lower values are found in the pipes located at the contact with the granite interface. It is interesting to note that at the beginning of both phases of the FEBEX *in situ* test the sum of the concentration of light hydrocarbons (C2, C3, iC4), was higher than methane concentration during the first months of the experiment or until "quasi anoxic" conditions were established (Fig. 81, Fig. 82).

Stable isotopes are especially valuable for identifying the origin and cycling of organic matter in the biosphere (Schoell 1988, Whiticar 1990, 1999). Considerable carbon isotope fractionation (commonly 60‰–70‰) is associated with methanogenesis. Thermogenic CH_4 typically has $\delta^{13}C_{CH4}$ values more positive than –55‰ and methane to ethane ratios less than 100 (Bernard et al. 1977). In addition, δD_{CH4} values are used to distinguish between the two major microbial methane production pathways (Schoell 1980, Whiticar et al., 1986). Stable isotopes were analysed in the two last sampling campaigns with the aim of identifying the origin of methane (Tab. 10). Values ranged from -54.2 to -71.9 ‰ for $\delta^{13}C$-CH_4 and from -373 to -384 ‰ for $\delta^{2}H$-CH_4. According to the isotopic signals of $\delta^{13}C_{CH4}$ and δD_{CH4}, acetoclastic methane production (from acetate/organics) prevails over autotrophic methane production (from bicarbonate or CO_2). Therefore, methane seems to be originated from organic degradation/oxidation processes (Fig. 84, Fig. 85) from materials introduced in the bentonite barrier and not from the bentonite itself. This is because experiments performed at laboratory conditions for analysing the release of gases from compacted FEBEX bentonite (which were done at 20, 50 and 100 °C for 100 days in air and nitrogen atmosphere and in dry and water saturated conditions), indicated that carbon dioxide was the only main gas component released from the bentonite both in aerobic and anoxic conditions (due to carbonate dissolution and/or organic matter oxidation), increasing the content with temperature and water saturated conditions. The hydrocarbons content generated (due to organic matter fermentation/decarboxylation) was insignificant, less than 10 mL per 1000 kg bentonite (Jockwer & Wieczorek 2003, 2008).

As organic material to be degraded over time inside the barrier can be mentioned cellulose filters for tracers deposition (Fig. E-13, 1.371 kg as total amount) placed at the bentonite-granite interface, the initial organic matter present in the bentonite (0.096 wt.-%; i.e. 111 kg of organic carbon in the total barrier), the degradable resins or the plastics from cables and tubings (Fig. 12). However, large amounts of hydrocarbons from these sources should not be expected due to their content and the temperatures (< 100 °C).

On the other hand, different processes seem to be involved in each pipe since the concentration of methane and hydrocarbons of higher chains (n-butane) in pipe FP-1 are higher and lower, respectively, than those in FP-2 and FP-3 (Fig. 79, Fig. 80). Pipe FP1 was close to a highly corroded fissurometer (Fig. 83, see also Wersin & Kober 2017). The higher contents of NH_4^+, TOC, and H_2 in pipe FP-1 in 2014 with respect the other pipes, as well as the depletion of $\delta^{15}N–N_2$, $\delta^{13}C–CH_4$ and $\delta^{13}C–CO_2$ from 2014 to 2015 may point to a corrosion of steels (abiotic or microbially mediated), and/or organic matter oxidation as main process involved in the generation/consumption of these gases.

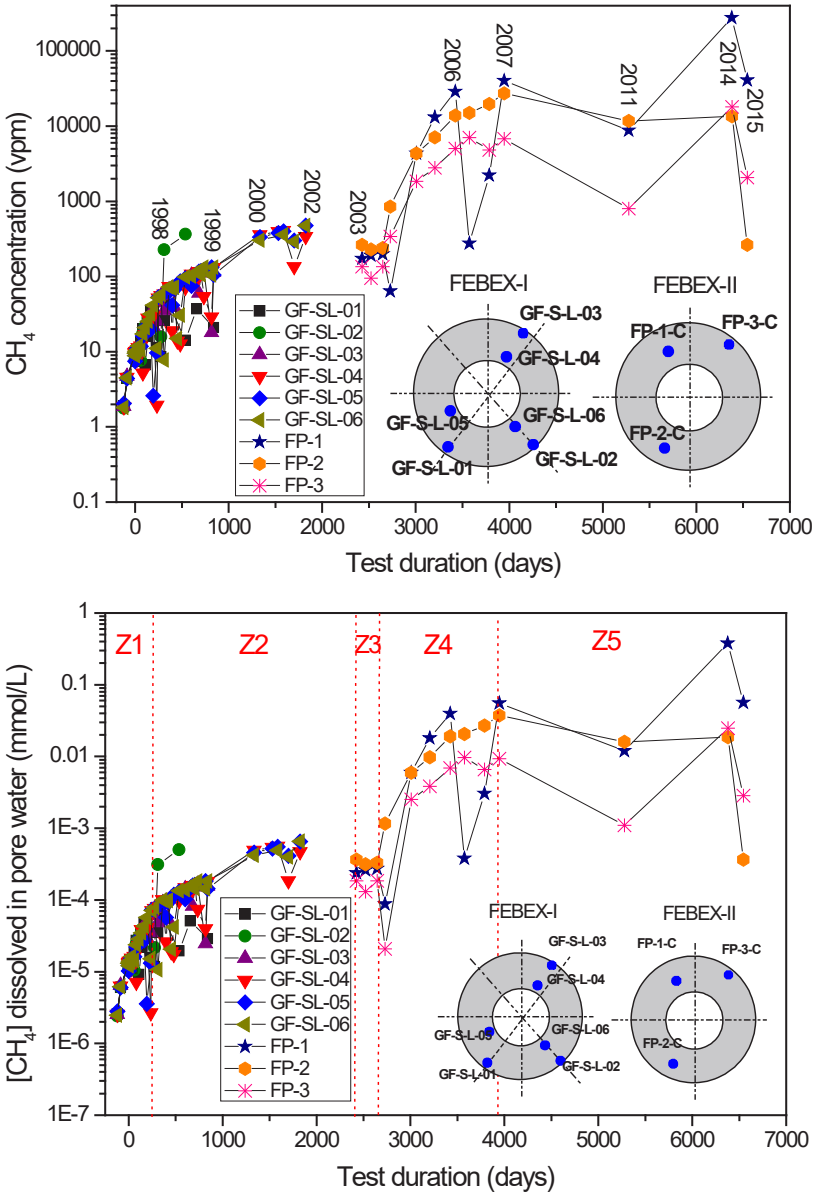

Fig. 79: Concentration of methane in the different GRS pipes obtained during the First (1996 – 2002) and Second (2002 – 2015) Operational Phases in vol.-% of gas and in mmol/L of gas dissolved in porewater (25 °C, 1 atm.)

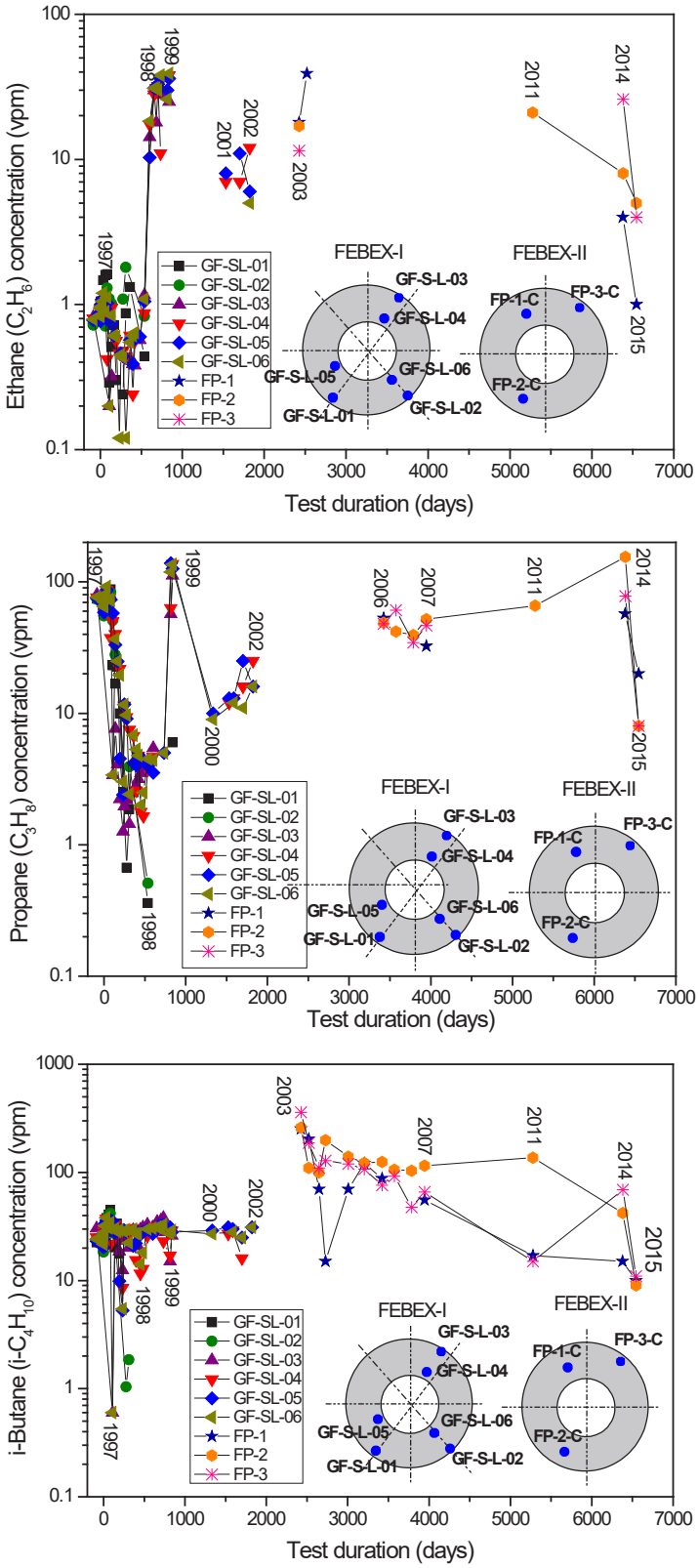

Fig. 80: Gas concentration of ethane, propane and butane in the different GRS pipes obtained during the First (1996 – 2002) and Second (2002 – 2015) Operational Phases

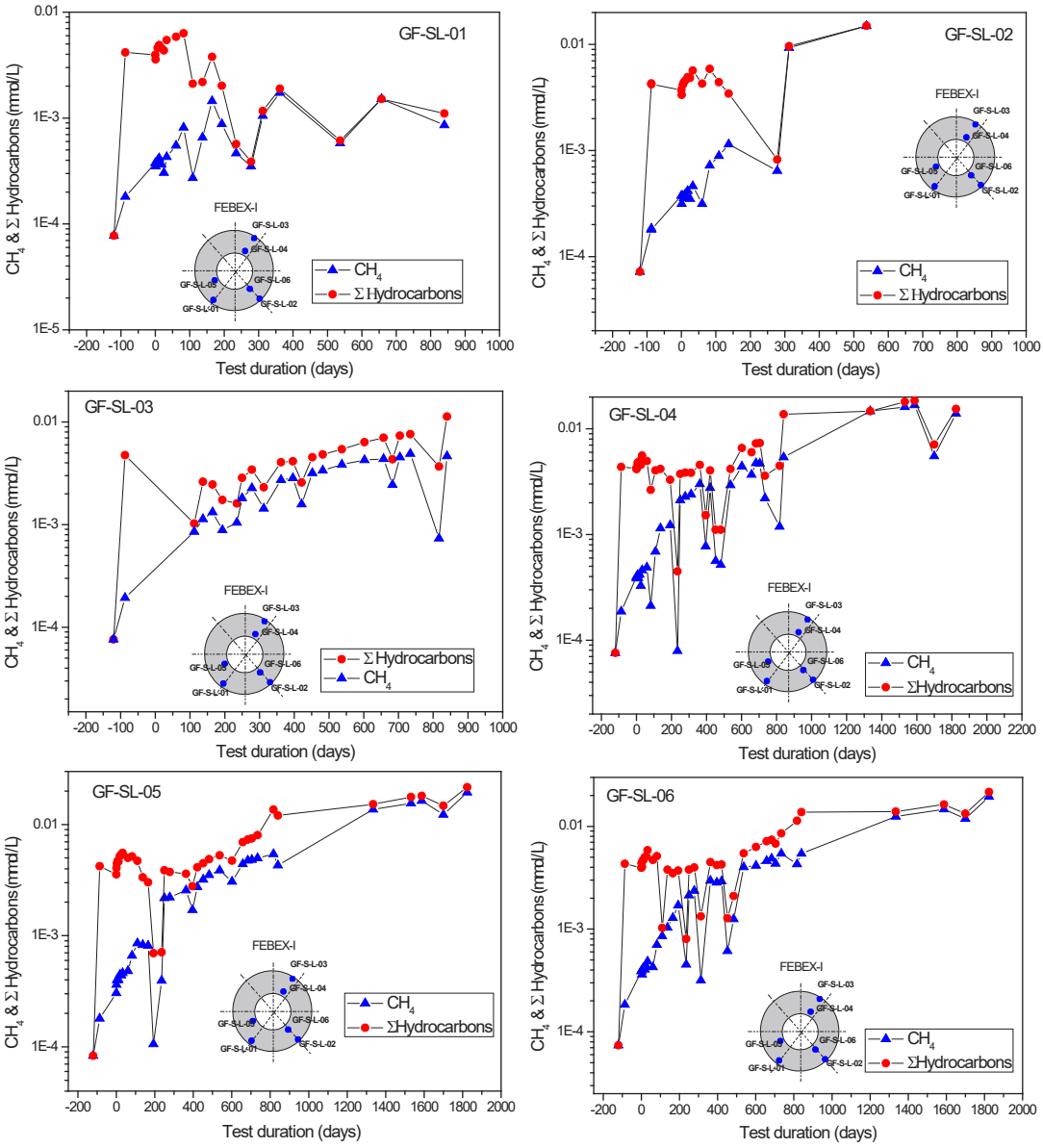

Fig. 81: Gas concentration of methane and total hydrocarbons (methane, ethane, propane and butane) in the different GRS pipes obtained during the First Operational Phase (1996 – 2002), in mmol/L of gas (25 °C, 1 atm.)

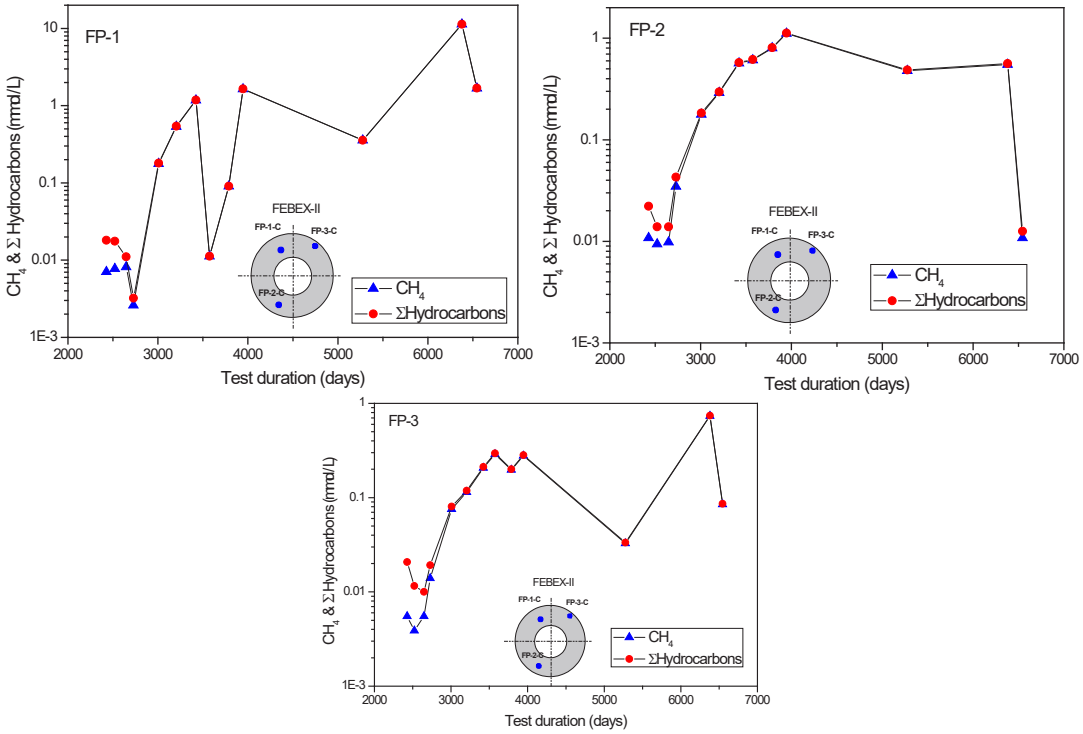

Fig. 82: Gas concentration of methane and total hydrocarbons (methane, ethane, propane and butane) obtained in the different GRS pipes obtained during the Second Operational Phase (2002 – 2015), in mmol/L of gas (25 °C, 1 atm.)

Fig. 83: Influence of the corroded fissurometer from bentonite Section 47 to Section 40, which was located close to pipe FP1

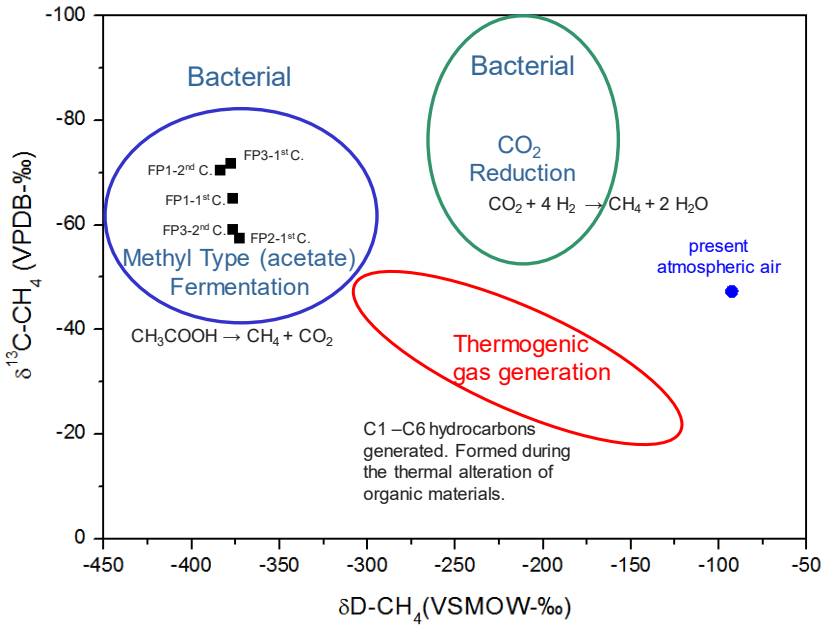

Fig. 84: ^{13}C-D diagram for the gas samples obtained from the GRS pipes FP-1, FP-2 and FP-3 in the FEBEX *in situ* test

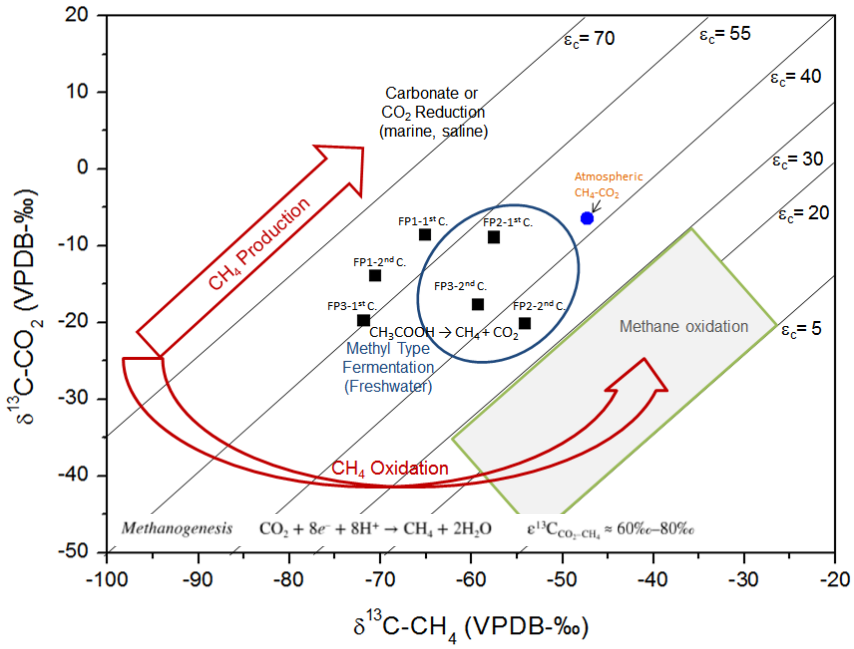

Fig. 85: Cross plots of $\delta^{13}C–CH_4$ versus $\delta^{13}C–CO_2$ for the gas samples obtained from the GRS pipes FP-1, FP-2 and FP-3 in the FEBEX *in situ* test

H_2 evolution

The evolution of hydrogen during the FEBEX *in situ* test is shown in Fig. 86, where large fluctuations in the concentration are observed over time. There are two main periods clearly defined for the hydrogen variation during the First Operational Phase. Starting from a high H_2 content (up to 2'000 vpm), measured at the beginning of the test, i.e. before switching on the heaters, there is a large decrease of hydrogen, correlated with the decrease of oxygen and the increase of methane and CO_2 (Zone Z1). The second period is after oxygen consumption, where hydrogen increases and its concentration is more or less maintained over time or decreasing slightly, with values ranging between 0.76 vol.-% to 0.24 vol.-% (Zone Z2). During the Second Operational Phase, hydrogen values are high at the beginning, with concentrations similar to those measured at the end of the First Operational Phase. But these values decrease slowly over time with a rate dependent on the location of the pipe, except for some sampling point. The higher H_2 values were measured in pipe FP-1, (maximum value of 6.9 vol.-%), and the lowest in pipe FP-3, located close the contact granite interface (maximum of 3.1 vol.-%). The variations of H_2 seems to be correlated with and methane (positively or inversely), which may imply that different mechanisms were controlling both species over time.

It is interesting to note that pipe FP1 is close to the corroded fissurometer (Fig. 83) and between an expansion sensor (Fig. E-14), and pipe FP3 close to a corroded displacement sensor (Fig. 51). In pipe FP1, H_2 contents were detected even in the last sampling campaign, which indicates the progressive corrosion of this instrumentation (see Wersin & Kober 2017: NAB 16-16).

It is unexpected the high content of hydrogen generated at the beginning stages of the test. Hydrogen generation by iron corrosion is only produced under anoxic conditions. However, corrosion of Al- and Zn-alloys are produced at oxygenated conditions. Most of the bolts and fittings in the FEBEX *in situ* test were made of Al- and Zn-alloys and were located at the granite interface for supporting cables, where water was available from the beginning. Furthermore, cellulose filters for tracers (1.371 kg as total amount) were also placed at the bentonite-granite interface (Fig. E-13), allowing the possible proliferation of microorganisms, which produced corrosive metabolic products and, as a consequence, the corrosion of the bolts and fittings. Indeed, most of the bolts found after dismantling suffered corrosion (Fig. 48, Fig. 49). Therefore, at the beginning of the experiment (Zone 1), the high amount of H_2 may be due to Al- and Zn-alloys corrosion. However, another possibility maybe the fermentation of organic matter in its acidogenesis phase, where H_2 is a common fermentation product:

$$(CH_2)_n + nH_2O \leftrightarrow CO_2 + 2nH_2$$

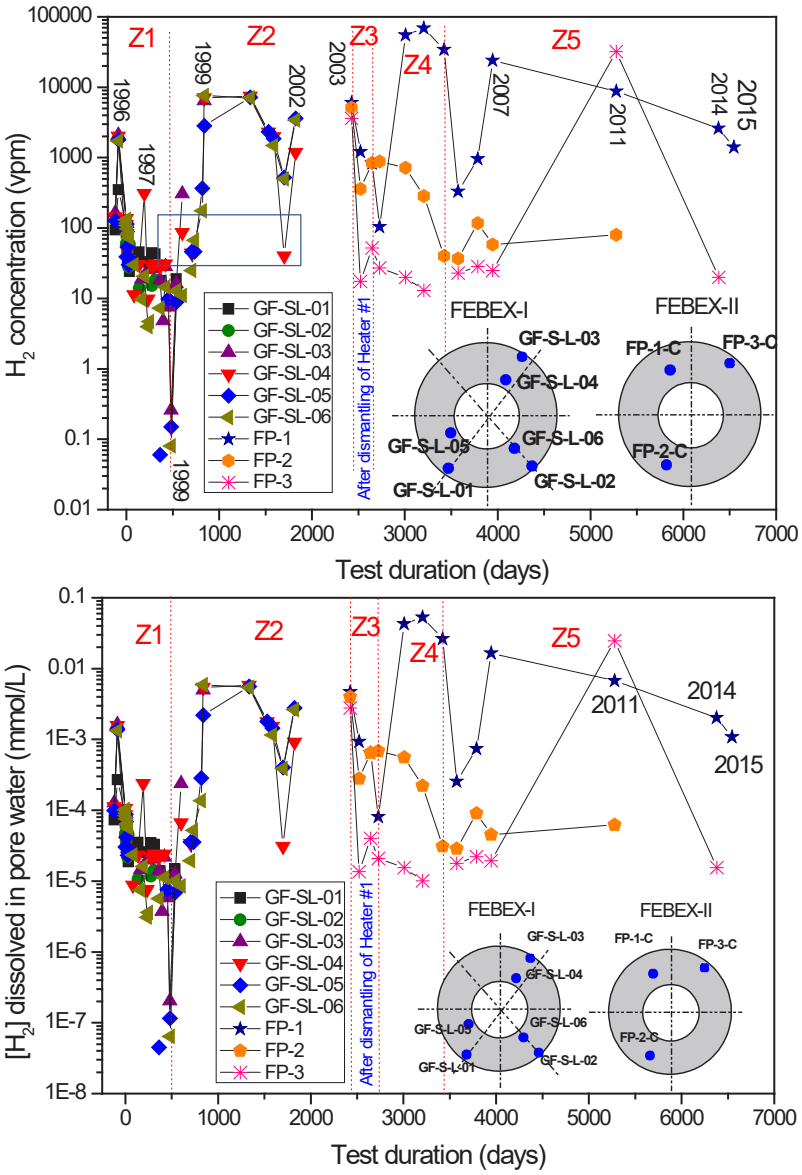

Fig. 86: Concentration of hydrogen in the different GRS pipes obtained during the First (1996 – 2002) and Second (2002 – 2015) Operational Phases in vpm of gas and in mmol/L of gas dissolved in porewater (25 °C, 1 atm.)

Hydrogen-sulfide (H_2S)

Hydrogen-sulfide was not measured in any gas sampling campaign, except in the last two ones, where values were always below detection limits. However, when collecting some water samples inside septum vials a strong hydrogen sulfide smell was detected which indicated that hydrogen-sulfide or mercaptan (organo-sulfides) were present in the system (Tab. 11, Tab. 12). Black particles were observed in some samples from FP3 samples (Fig. 65), sulfurs being precipitated as detected by SEM analyses (Fig. 66 to Fig. 69). A microbiological analysis of the water samples could not be performed. However, the water from pipes FP1 and C4 showed some turbidity (e.g., see Tab. 11, Fig. 106) in the 2014 sampling campaign indicating the presence of organic matter.

The analysis of stable sulfur isotopes is usually used as potential tracers of microbial activity. $\delta^{34}S$-H_2S and $\delta^{34}S$-SO_4^{2-} could be determined only in the water sample from pipe FP3 collected in 2014. Isotopic compositions $\delta^{34}S$-H_2S of -6.1‰ and $\delta^{34}S$-SO_4^{2-} of 13.3‰ were obtained, showing a sulfur fractionation ε (SO_4^{2-}-H_2S) = 19.5 (Fig. 87).

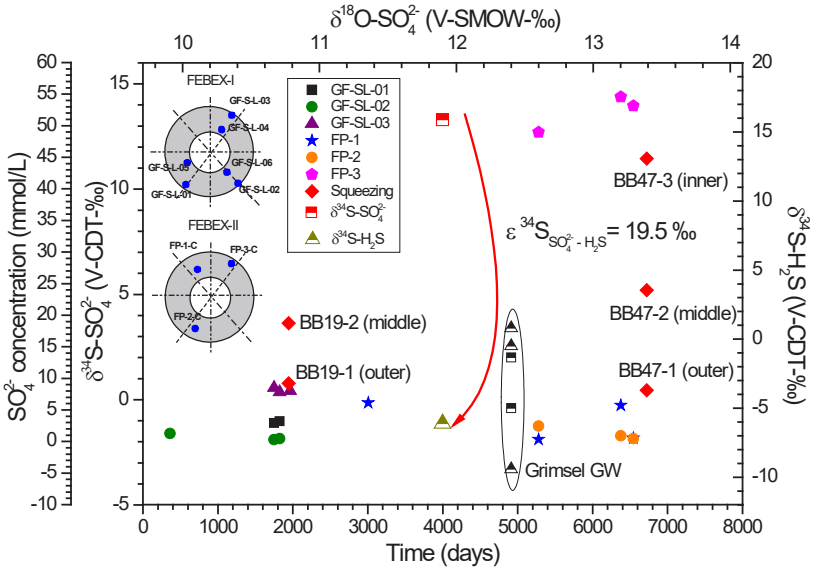

Fig. 87: $\delta^{34}S$-SO_4^{2-} and $\delta^{34}S$-H_2S versus $\delta^{18}O$-SO_4^{2-} obtained in the porewater from the FP-3 located around Heater #2 at the contact with the granite interface

Sulfate reduction $SO_4^{2-} + 8e^- + 8H^+ \rightarrow H_2S + 4H_2O$ $\varepsilon^{34}S_{SO4\text{-}H2S} \approx 10 - 40$ ‰

Data were compared with $\delta^{34}S$-SO_4^{2-} and $\delta^{34}S$-H_2S values of Grimsel granitic groundwaters from boreholes BOUS85 02, BOADUS 96.001 and JGP0 002 (see Appendix A, $\delta^{18}O$-SO_4^{2-} was taken arbitrarily because it is unknown). Sulfate concentrations were compared with data obtained from squeezed bentonite blocks taken as a function of the distance from Heater #2 contact (Fernández et al. 2018). ε is the isotopic fractionation, in per mil, associated with this reaction.

4.2.3.3 Porewater chemistry in the GRS pipes

The chemical composition of the porewater from the FEBEX bentonite barrier was only measured in some sampling campaigns. This is because the water samples were collected randomly since the main objective of the GRS group was the analysis of the gas phase. Exceptions were the sampling campaigns performed in 2005, 2011, 2014 and 2015, where a special effort was done for collecting both gas and water samples, maintaining strict anoxic conditions.

The evolution of the main physico-chemical parameters of the water samples and the concentration of major dissolved species over time are shown in Fig. 88 and Fig. 89 as a function of time. The porewaters are NaCl water-type with a variable salinity, with ionic strengths (I) ranging from 0.01 to 0.2 M. Chloride, and sodium as counterion, are the main ions in the porewater (Fig. 88). The high content of chloride in the FEBEX bentonite allows us to follow the solute movement through the bentonite during hydration due to its conservative behaviour. The porewaters obtained from these pipes were compared to those obtained from squeezing experiments from bentonite block samples (outer, middle and inner blocks) located at the heated sections Section 19 and Section 47 (Fernández et al. 2018: NAB 16-25). Apart from increments in salinity due to evaporation at zones close to the heaters, chloride contents should increase towards the inner parts of the bentonite barrier due to the infiltration of granite groundwater, dilution/dissolution process and subsequent transport, as is observed in the squeezing porewaters (Tab. 16) and aqueous leaching experiments (Fig. 90). However, the results from porewater analysis seem not to depend on the pipe location; the difference is small between samples close to the granite interface or at an inner position at the bentonite.

At the First Operational phase, the chloride content is similar to those found in squeezed waters. In the Second Operational Phase, the lower salinities or ionic strengths, I (I = 0.01 – 0.06 M) are located at pipe FP-2 (at the bottom) and then in pipe FP-1 (at the top), with composition similar to the squeezed porewaters from the external bentonite ring. However, the highest salinities are found at the FP-3 pipe (I = 0.2 M). This FP-3 pipe is located at the right-upper part close to granite interface, where the porewaters should be more diluted than the inner pipe FP-1, due to the mixing with incoming granitic groundwater. The high amounts of chloride and sulfate in pipe FP-3 compared to FP-1 and FP-2 (Tab. 15, Fig. 88) were not expected and not well-understood. Therefore, a dilution of the porewaters seems to have occurred in the pipes FP-1 and FP-2, especially if the data are compared with those obtained from the CIEMAT pipes and the squeezed waters from bentonite blocks.

On the other hand, it can be seen that chloride contents decrease in subsequent aliquots sampled at the same sampling campaign (see Pipe FP-2) or during a next sampling campaign performed shortly after the last one (e.g. August 2014 and January 2015: FP-1 and FP-2). This is probably related with the large internal volume of the pipes, the final composition being diluted over time. The higher dilution of the pore water is observed in pipe FP2, probably due to a higher water inflow in this zone or to the hydrostatic pressure since this pipe is located at the bottom of the gallery.

In all pipes sodium concentration is always higher than chloride concentration, although the difference is lower in pipe FP2. This is probably due to the exchange reactions at interlayers. Carbonate dissolution during hydration should provoke sodium to be replaced by calcium at exchange sites, increasing the sodium content in the porewater.

Sulfate is not a conservative element so, although it is affected by the advective transport towards the internal part of the bentonite, sulfate is controlled by gypsum dissolution/precipitation processes. In the First Operational Phase sulfate contents are diluted when compared to the results from squeezed waters, except those found in pipe GF-SL-03 (right, upper part), which are in good

agreement (Fig. 88). In the Second Operational Phase, the sulfate concentrations in pipes FP-1 and FP-2 are also lower than those found in squeezed porewaters, except pipe FP-3 (right, upper part). A decrease of sulfate is observed over time in pipes FP-1 and FP-2, indicating either a dilution of the porewaters during the hydration process (a decrease of chloride is also observed) or a possible sulfate reduction process. According to the saturation indices (Tab. 15), the porewaters are always in disequilibrium with gypsum, except in pipe FP-3. This means that a source of sulfate is maintained over time in this part of the bentonite barrier. More interesting is that sulfate data are similar to those observed in the pipe GF-SL-3 from the First Operational Phase, located at the same position, and in those found in the CIEMAT pipes C1 and C7 (located close to the granite interface) at Sections G and F2 (see below). Therefore, the differences in composition among pipes FP1, FP2 and FP-3 is not well-understood. The dilution effect of the porewaters over time due to the granitic groundwater infiltration and the large internal volume of the pipes, should be the same for the three pipes. However, the chemical concentrations found in samples from pipes FP1 and FP2 are lower than that in FP-3 and lower than the concentrations found in CIEMAT pipes C1 and C7 (see below) or in the squeezed porewaters.

Regarding the carbonate system, there are clear differences between the results obtained for pipe FP-1 and the pipes FP-2 and FP-3 (Fig. 89). The alkalinity values are in agreement with the squeezing results for pipes FP-2 and FP-3, but high pH (9 – 11.7) and alkalinity values are observed in pipe FP-1, which is correlated with increments in the TOC values and/or acetate contents. Carbonate dissolution/precipitation processes seem to control the alkalinity, the pH and the concentration of cations via exchange reactions at interlayers. However, in pipe FP-1, located close to a fissurometer and an extension sensor, both highly corroded, another process seems to be involved.

Acetate concentrations were found in all GRS porewaters, correlated with the TOC values and high alkalinity values. VFAs, such as acetate and formate, are produced as fermentation products through the degradation of organic matter under anaerobic conditions or by abiotic reactions induced by corrosion processes. High concentrations of VFAs are correlated with a depletion of sulfate in pipes FP-1 and FP-2. Other redox-sensitive species in the porewaters obtained during the Second Operational Phase are shown in Tab. 15. Different terminal electron acceptors (TEAs) and electron donors (Fe^{2+}, NH_4^+, acetate, etc.) could be measured in the porewaters as well (Fig. 91).

By assuming that the gas composition obtained in the pipes could be dissolved in the porewater (at least in the Second Operational Phase this is true), the relationship between the main gases and alkalinity and sulfate concentrations in the porewater can be useful for distinguishing different biogeochemical processes over time (Fig. 92). Again, it is clear that processes in pipe FP-1 are quite different from those in pipe FP-2 and FP-3 due to the higher hydrogen and acetate concentration even in the last campaign at 2015. Indeed, FP-1 pipe is located in between an expansion sensor (SBF2-2, partially corroded, Fig. E-14) and close to the highly corroded fissurometer (Fig. 83), so both parameters are related with a corrosion process. However, it is not clear if the decrease of sulfate in the porewater is the result of a dilution and/or a reduction process, because there is also a decrease of chloride in the porewaters compared to FP-3 waters, water samples from the CIEMAT pipes and squeezed waters.

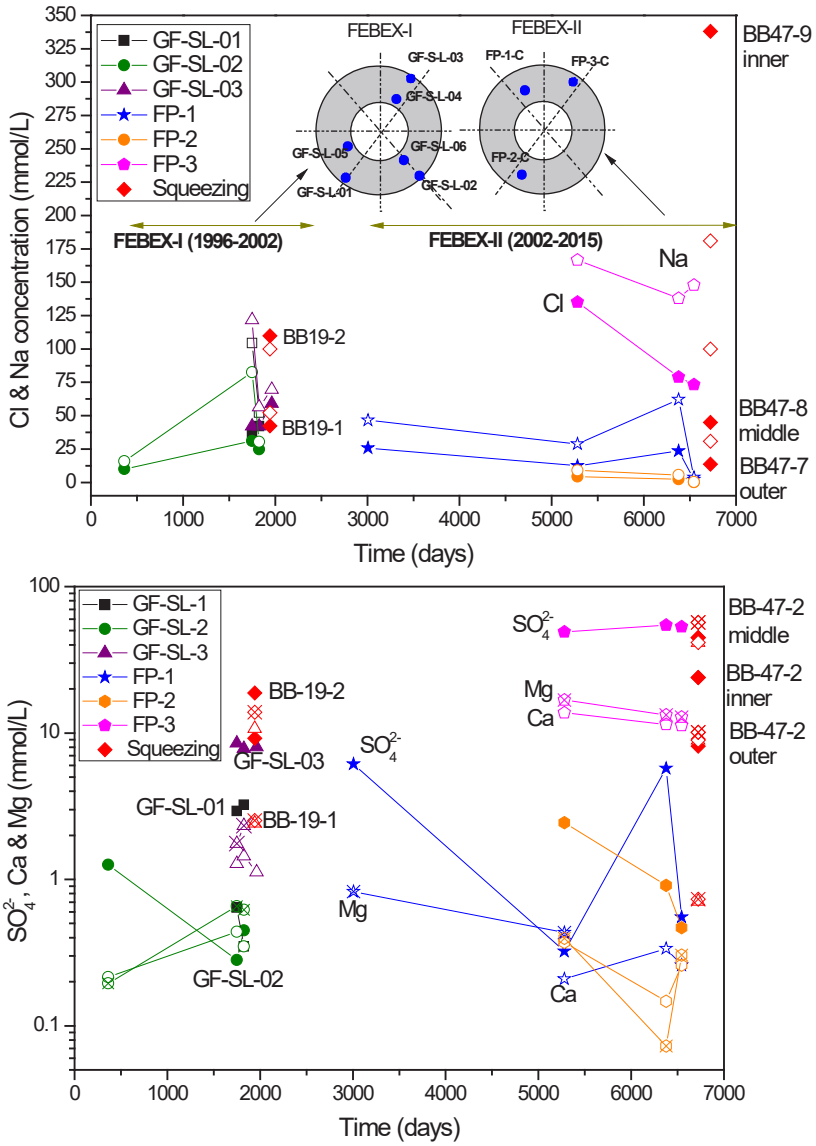

Fig. 88: Cl, Na, SO_4^{2-}, Ca and Mg concentrations from water samples collected from the GRS pipes over time

Data are compared with porewater samples extracted by the squeezing technique from bentonite blocks (Fernández et al. 2018) after dismantling of Heater #1 in 2002 (bentonite Sampling Section 19, Tab. 8) and Heater #2 in 2005 (bentonite Sampling Section 47: Tab. 16).

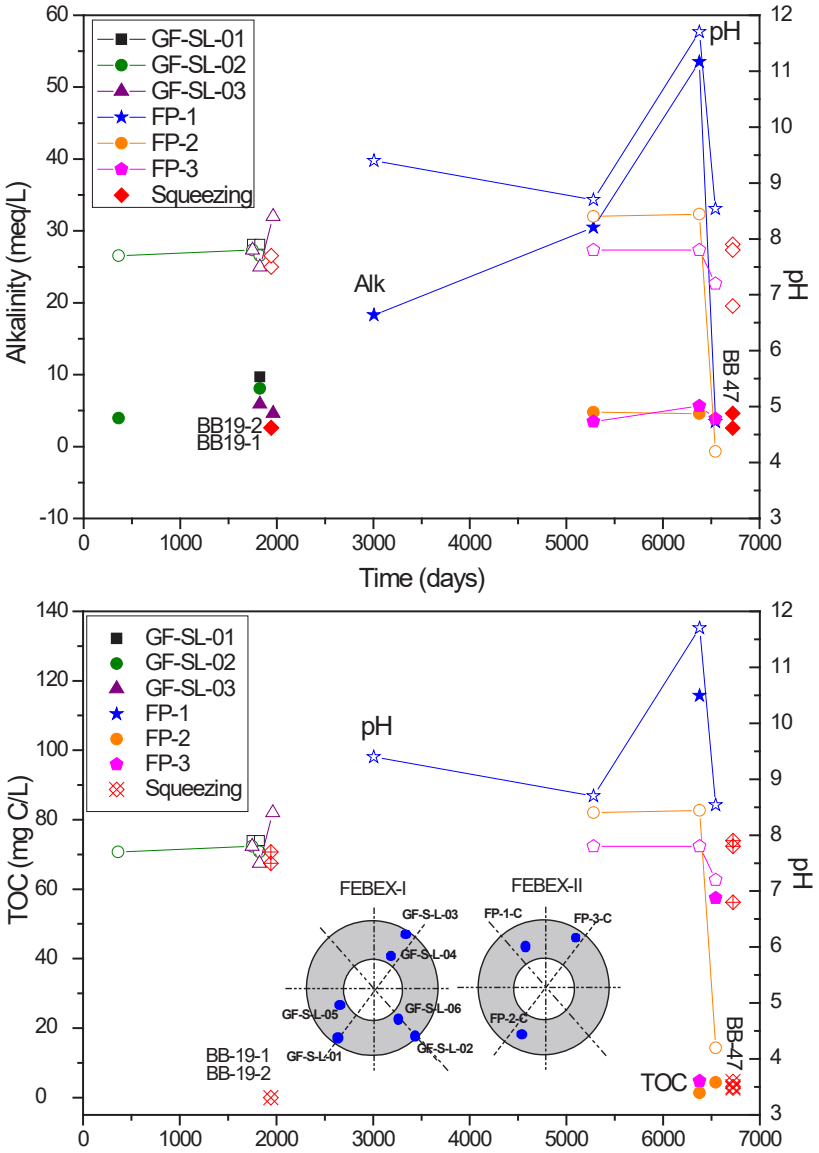

Fig. 89: pH, alkalinity, TOC (total organic carbon) and major anions and cations from water samples collected from the GRS pipes over time

Data are compared with porewater samples extracted by the squeezing technique from bentonite blocks (Fernández et al. 2018) after dismantling of Heater #1 in 2002 (bentonite Sampling Section 19, Tab. 8) and Heater #2 in 2005 (bentonite Sampling Section 47: Tab. 16).

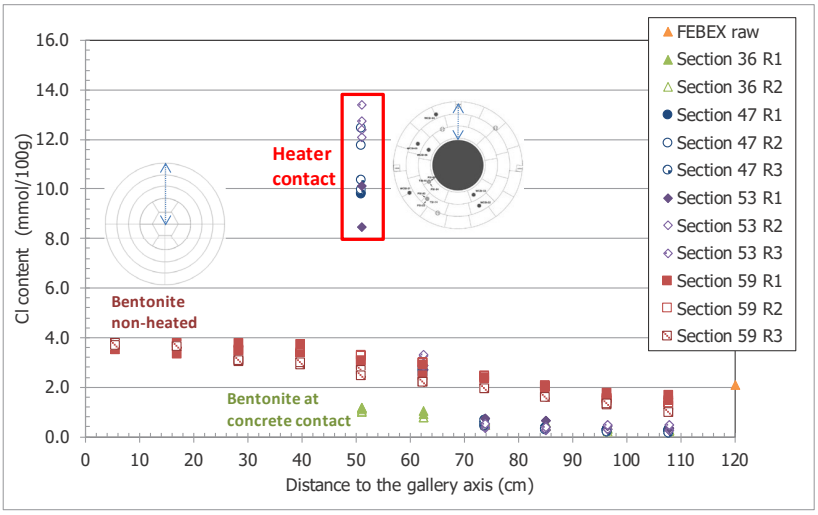

Fig. 90: Chloride distribution in aqueous extracts as a function of the distance to gallery in the heated bentonite Sampling Sections 47 and 53, and in non-heated Sections 36 and 59

Fernández et al. (2018): NAB 16-25

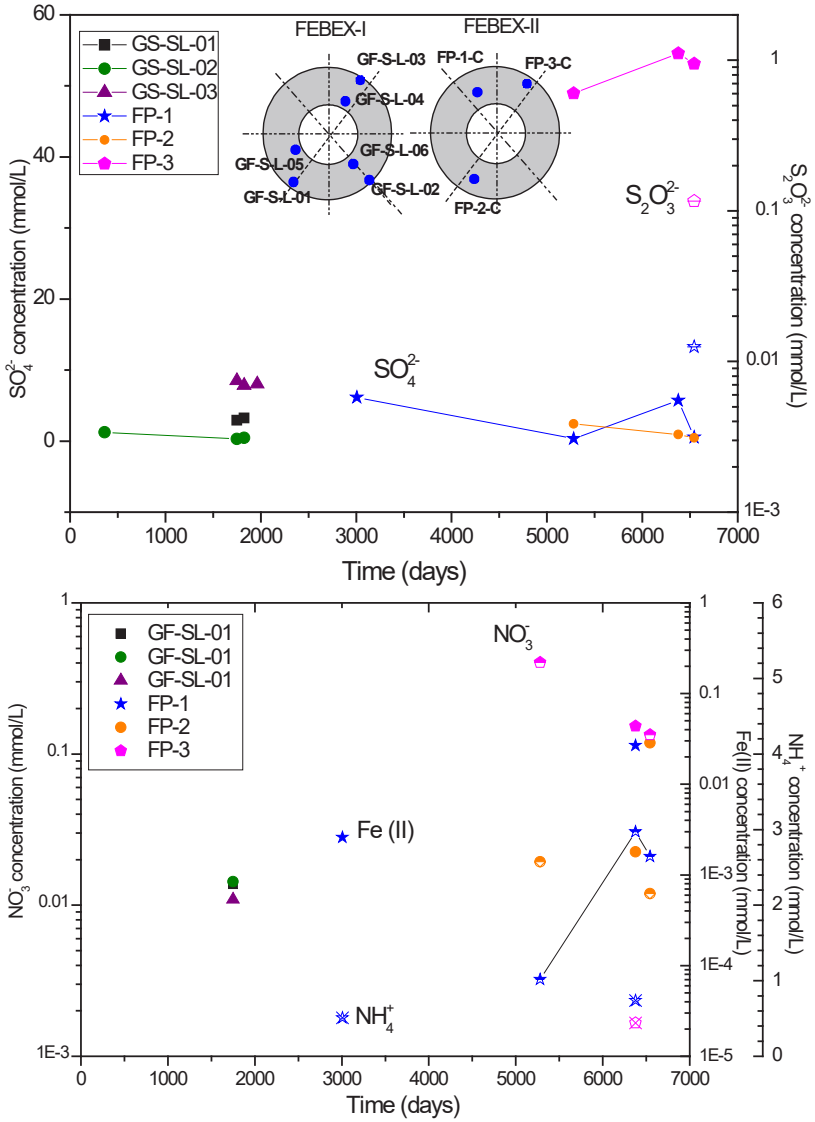

Fig. 91: Evolution of different electron donors and acceptors in the porewater over time

Tab. 15: Concentration of species in the porewater and gases from pipes FP1, FP2 and FP3

Pipe	**FP-1**				**FP2**			**FP3**		
Sampling campaign	2005	2011	2014	2015	2011	2014	2015	2011	2014	2015
Ionic Strength	0.0589	0.041	0.090	0.0079	0.017	0.0093	1.86×10^{-3}	0.221	0.188	0.197
a_w	0.998	0.999	0.997	1.000	1.000	1.000	1.00	0.995	0.996	0.995
pH	9.4	8.7	11.7	8.54	8.4	8.4	4.2	7.8	8.0	7.2
Redox potential (mV, SHE)	-284	n.d.	-138	-65	n.m.	n.d.	-5.3	124	-210	-161
Alk. (meq/L)	18.3	30.5	53.5	n.d.	4.76	4.6	< 0.5	3.50	5.15	3.88
DIC (mmol/L)	16.0	29.6	24.0	-	4.73	4.57	-	3.61	5.23	4.40
Cl (mg/L)	914	438	836	72	153	82	2.6	4'800	2'800	2'600
Sulfate (mg/L)	590	31	549	83	234	87.3	45	4'700	5'000	5'100
Nitrate (mg/L)	< d.l.	0.2	1.9	1.3	1.2	0.5	0.74	13	< 1	8.3
$S_2O_3^{2-}$ (mg/L)	n.d.	n.d.	5.5	1.4	n.m.	< 1	< 0.5	n.m.	< 0.5	13
NH_4^+ (mg/L)	9.2	n.d.	13.3	n.d.	n.m.	8.8	n.d.	n.m.	0.44	n.d.
Fe/Fe^{2+} (mg/L)	0.15/0.15	-	0.15	-	< 0.3	0.10	1.60	< 0.3	2.45	< d.l.
TOC (mg C/L)	n.d.	n.d.	1390	n.d.	n.m.	15.8	52.8	n.m.	61.1	690
Acetate (mg/L)	n.d.	n.d.	1600	n.d.	n.m.	n.d.	n.d.	n.m.	67	n.d.
O_2 (aq, µmol/L)	2.53×10^{-2}	2.11×10^{-2}	1.878×10^{-2}	2.934×10^{-5}	3.622	0.0102	3.32×10^{-2}	2.405×10^{-3}	1.59×10^{-2}	5.50×10^{-2}
H_2 (aq, µmol/L)	4.26×10^{-2}	6.77×10^{-3}	1.997×10^{-3}	1.096×10^{-3}	61.31	-	-	0.02378	1.50×10^{-5}	-
CH_4 (aq, µmol/L)	6.02×10^{-3}	1.22×10^{-2}	3.81×10^{-1}	5.751×10^{-2}	16.07	0.0189	3.72×10^{-4}	1.068×10^{-3}	0.02422	2.78×10^{-3}
CO_2 (aq, µmol/L)	1.51×10^{-2}	5.20×10^{-1}	5.65×10^{-1}	0.2034	0.6264	0.9152	0.1018	0.4090	0.4197	5.51×10^{-2}
$Log(pO_2)$ (atm)	-1.70	-1.78	-1.82	-1.64	-2.54	-2.10	-1.59	-2.70	-1.89	-1.35
$Log(pH_2)$ (atm)	-1.26	-2.06	-2.59	-2.85	-4.10	-	-	-1.50	-4.70	-

Tab. 15: Cont.

Pipe	**FP-1**				**FP2**			**FP3**		
Log(pCH_4) (atm)	-2.36	-2.06	-0.56	-1.39	-1.93	-1.87	-3.58	-3.10	-1.74	-2.68
Log(pCO_2) (atm)	-3.35	-1.81	-1.77	-2.22	-1.73	-1.57	-2.52	-1.90	-1.89	-2.77
Total CO_2 (mmol/L)	16.57	30.68	27.11	6.091	5.405	5.536	2.108	3.895	5.399	3.776
pH cal	9.21	8.02	7.90	7.77	7.12	7.01	7.60	7.09	7.24	7.99
Eh cal (mV)	-343	-273	-270	-260	-204	-203	745	712	-213	-263
SI Calcite	0.88	0.54	0.43	0.00	-0.72	-1.19	0.00	0.08	0.41	0.90
SI Dolomite	1.91	0.62	-	-1.78	-2.20	-4.24	-1.38	-0.54	0.12	1.09
SI Siderite	-0.85	-	0.28	-	-	-1.27	-8.88	-	-0.02	-
SI Quartz	-	0.33	0.37	0.13	-0.06	-0.50	-0.33	0.94	0.93	1.03
SI Gypsum	-2.58	-3.31	-2.13	-2.52	-1.94	-2.62	-1.94	-0.01	-0.01	-0.04
SI Strontianite	-	-	-	-	-	-2.44	-	-1.26	-0.96	-0.41
SI Pyrite	3.96	-	9.62	-	-	7.13	-	-	8.39	-
SI Pyrrhotite	-0.92	-	1.77	-	-	-0.59	-	-	0.70	-
SI Goethite	0.08	-	-0.45	-	-	-1.95	8.05	-	-0.27	-
SI Magnetite	0.57	-	-0.93	-	-	-5.68	7.59	-	-0.76	-

Tab. 16: Chemical composition of the pore water collected from the heated sections Section 19 (around Heater #1): BB-19-1 and BB-19-2 bentonite blocks; and Section 47 (around Heater #2): BB-47-7, BB-47-8 and BB-47-9 blocks as a function of the distance to gallery axis

Fernández et al. (2018)

Sample			**BB-19-1**	**BB-19-2**	**BB-47-7**	**BB-47-8**	**BB-47-9**
Distance from the gallery axis	d	cm	102.15	79.45	102.15	79.45	56.75
Physical-chemical parameter lab							
pH value (20 °C) lab.	pH		7.4	7.5	7.9	7.8	6.8
Alkalinity	Alk.	meq/L	2.57	2.64	4.63	2.58	< 5
Main ions							
Sodium	Na^+	mg/L	1'200	2'300	710	2'300	4161
Potassium	K^+	mg/L	13	13	9.2	24	23
Calcium	Ca^{2+}	mg/L	106	453	32	380	1'700
Magnesium	Mg^{2+}	mg/L	67	353	20	260	1'400
Chloride	Cl^-	mg/L	1'500	3'900	481	1'600	12'000
Sulfate	SO_4^{2-}	mg/L	883	1800	779	4'300	2'300
Nitrate	NO_3^-	mg/L	1.5	38	1.9	15	124
Nitrite	NO_2^-	mg/L	< 1	< 1	< 1	< 1	< 1
Phosphate	PO_4^{3-}	mg/L	< 1	< 1	< 1	< 1	< 0.1
Bromide	Br^-	mg/L	2.6	7.4	1.1	2.5	12.7
Fluoride	F^-	mg/L	< 1	< 1	< 1	< 1	< 1
Thiosulfate	$S_2O_3^{2-}$	mg/L	< 1	< 1	< 1	< 1	< 1
Trace compounds							
Aluminium	Al	mg/L	0.65	0.56	< 0.1	< 0.3	< 2.9
Silicon	Si	mg/L	n.d.	n.d.	23	22	15
Iron	Fe (II/III)	mg/L	0.25	< 0.3	< 0.1	< 0.3	< 2.9
Strontium	Sr	mg/L	1.7	7.1	0.59	6.7	29
Copper	Cu	mg/L	-	-	0.15	1.4	< 2.9
Boron	B	mg/L	0.63	< 0.5	1.5	1.8	< 2.9
Manganese	Mn	mg/L	0.17	0.83	0.15	0.70	5.6
Nickel	Ni	mg/L	-	-	0.09	0.41	< 2.9
Lead	Pb	mg/L	-	-	0.18	< 0.3	< 2.9
Zinc	Zn	mg/L	-	-	0.08	0.59	< 2.9
Organic parameter							
Total organic carbon	TOC	mg/L	n.d.	n.d.	38	n.d.	n.d.
Acetate	$CH_3\text{-}COO^-$	mg/L	n.d.	n.d.	< 0.1	86	142
Formate	$HCOO^-$	mg/L	n.d.	n.d.	0.36	25	1.3
Oxalate	$(COO)_2^{2-}$	mg/L	n.d.	n.d.	n.d.	n.d.	17.7

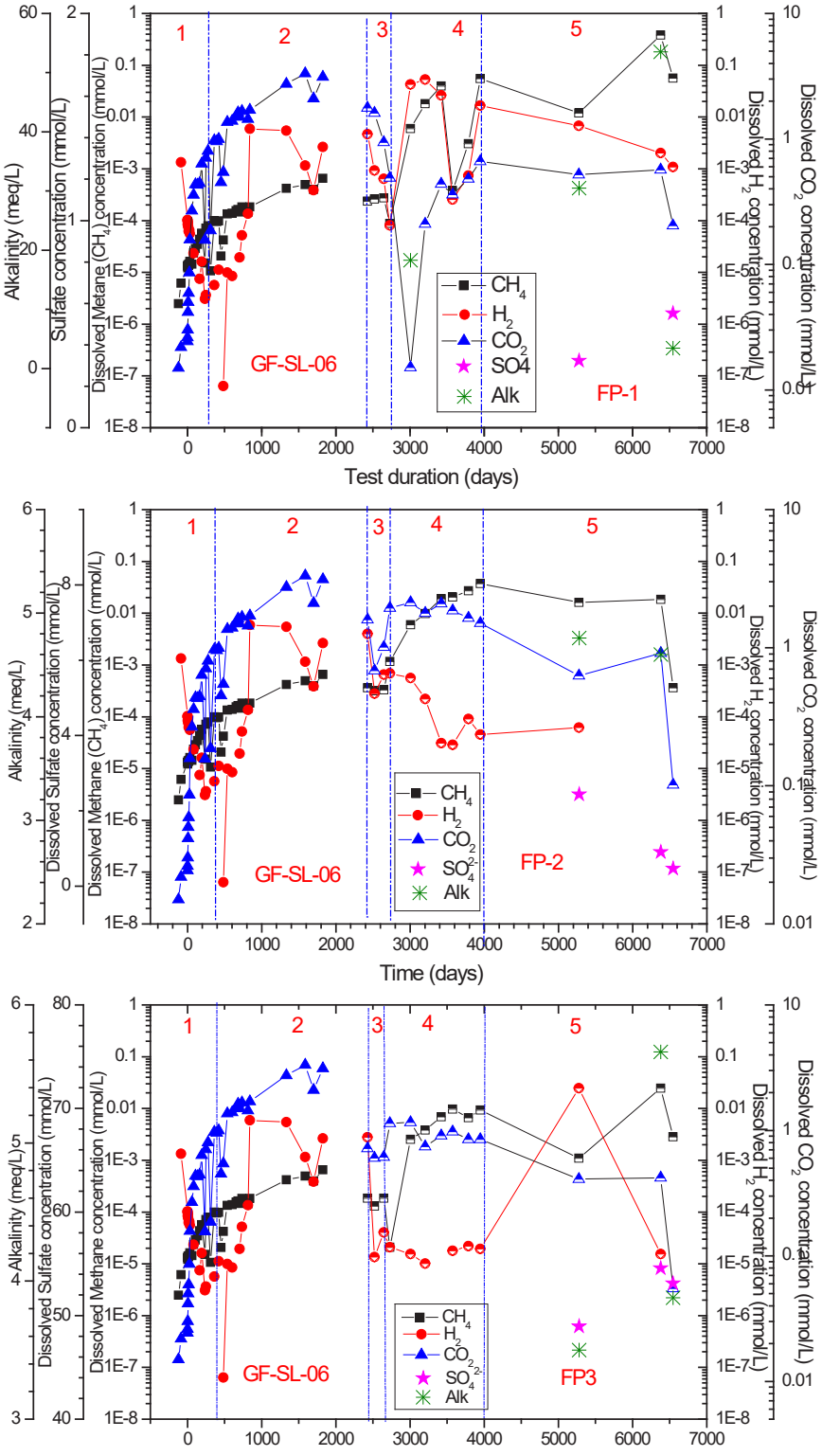

Fig. 92: Ion concentration and gases in the pipes FP-1, FP-2 and FP-3, as well as different geochemical periods (1 to 5) observed in the FEBEX *in situ* test

4.3 Porewater sampling from the CIEMAT pipes

Six pipes were installed in 2003 for collecting water from the bentonite buffer, determining the relative humidity and the chemical evolution of the porewater from the bentonite barrier in the FEBEX *in situ* test. In this section, a global overview of the main results of these parameters measured in the CIEMAT pipes over time (relative humidity, temperature, fluid pressure and porewater chemistry) are described.

4.3.1 Relative humidity and temperature

The values of relative humidity and temperature were measured *online* from relative humidity sensors located inside the filters at Sections G, I and F2 (Fig. 93, Fig. 94, Fig. 95). These VAISALA capacity sensors measure total suction through the pore air relative humidity (R.H.), taking into account the temperature, i.e., a temperature value is needed to obtain values of R.H.

The sensors located at Section G are not affected directly by the heater, while the sensors located at Sections I and F2 are affected by the Heater #2 environment. Therefore, the temperature evolution in Section G is quite different from the other sections. In Section G the temperature ranged from 25 to 32 °C, while in Sections I and F2 the temperature ranged from 32 to 100 °C (Fig. 96). The evolution of the temperatures and the relative humidity values of each sensor changed according to the radial position in the bentonite barrier (from granite contact to heater). Temperatures at the bottom part of the barrier were slightly lower than those at the upper part in Sections G, I and F2, and increased towards the inner part of the bentonite barrier.

The sensors had a short life time as indicated in Fig. 96. Some of them because they flooded, as suggested by the sensors F2-04 and F2-01 located at the outer bentonite ring. However, in the case of sensor I-03 from Section I erratic signals were recorded, probably as a consequence of damage from the start of the measurements (Fig. 97). The highest temperature (~ 100 °C) was recorded by sensor I-06, located close to the liner at the upper-frontal part of the heater. This value is high taken into account the position of the pipe, which is close to liner but not at the liner contact. Lower values were measured at the middle of the heater, around 90.3 °C and 77 °C in sensors F2-03 (bottom part) and F2-06 (upper part), respectively. It seems that in Section I (frontal part of the heater) the highest temperatures were registered inside the barrier. In any case, the temperatures obtained with these sensors are always much lower than those measured in other *in situ* sensors, as seen in Martínez et al. (2006).

Relative humidity values changed as granitic groundwater coming from the outer region of the bentonite barrier infiltrated at the sensor positions (Fig. 97). The sensors located in the outer periphery reached high values of relative humidity quickly. R.H. values higher than 99 – 100 % are indicative that the sensors are almost flooded, and that free water can be collected from the pipes (Fig. 93). When the sensors are flooded, the electrical signal fails, given values of 0 %, i.e., the sensors are out of order.

At the outer bentonite ring, sensors 04 (at the top) were flooded slower than sensors 01 (at the bottom) at Sections I and F2. The opposite was observed in Section G, where sensor G-01 lasted a long time before being flooded, which is also observed in the other *in situ* measurements (Martínez et al. 2016). It should be noted here that corrosion processes consume water; a high corrosion of the dummy canister was observed in Section G. In the middle ring, sensors 05 (at the top) were flooded much faster than sensors 02 (at the bottom) in Sections G and F2, but the opposite is observed in Section I.

The sensors located around the heater (Sections I and F2) have a lower relative humidity. The bentonite is dried by the high temperatures and the hydration process is very slow. The Sensor 03 (at the bottom) has a lower R.H. with respect to Sensor 06 (at the top). Sensor I-03 seems to be damaged. The sensors 03 and 06 at Section G (not affected by heat) were flooded over time (03 faster than 06). From these measurements, it is clear that the hydration of the bentonite barrier did not occur homogeneously, but that a variability in relative humidity (and temperature) is observed at the top and the bottom.

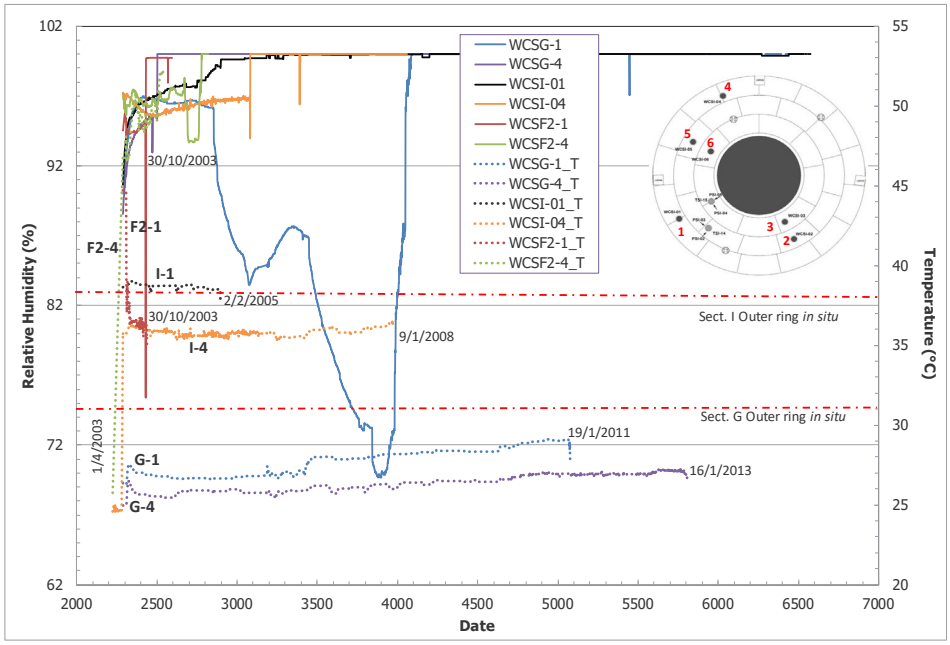

Fig. 93: Relative humidity and temperature in the pipes from the outer bentonite ring (sensors 1 and 4) at Sections G, I and F2

Comparison with average temperature values (red dashed lines) obtained from other *in situ* sensors (Martínez, 2016). Location of the sensors 1 to 6 in red (take into account that the number of the sensors does not coincide with the number of the pipes, see Fig. 35).

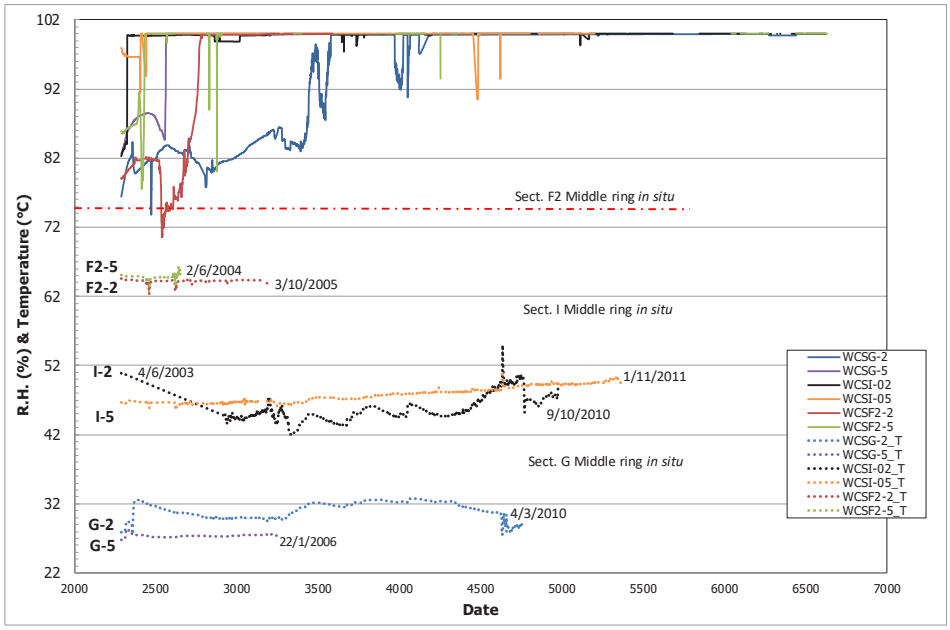

Fig. 94: Relative humidity and temperature in the pipes from the middle bentonite ring (sensors 2 and 5) at Sections G, I and F2

Comparison with average temperature values (red dashed lines) obtained from other in situ sensors (Martínez et al. 2016).

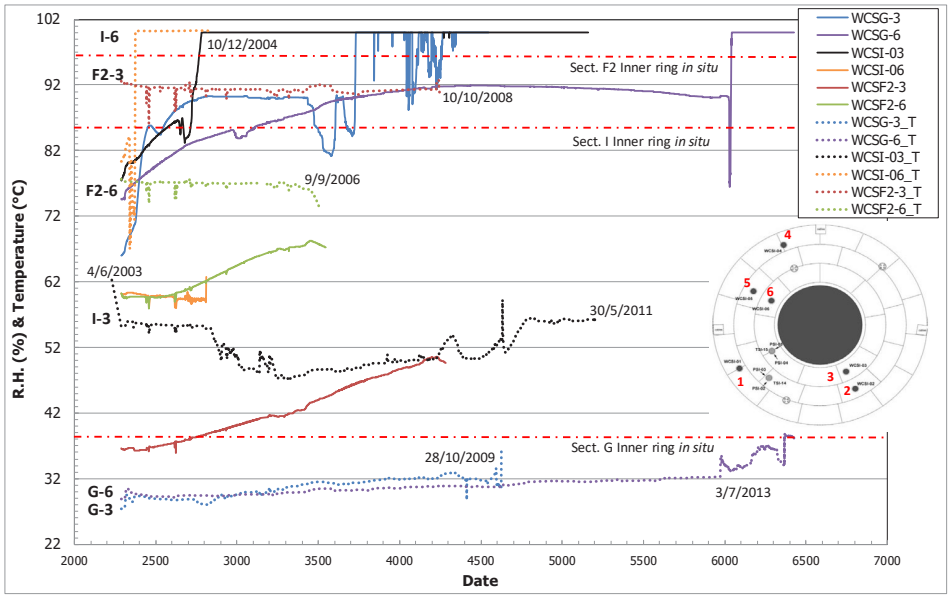

Fig. 95: Relative humidity and temperature in the pipes from the inner ring (Sensors 3 and 6) at Sections G, I and F2

Comparison with average temperature values (red dashed lines) obtained from other in situ sensors (Martínez et al. 2016). Location of the sensors 1 to 6 in red (take into account that the number of the sensors does not coincide with the number of the pipes, see Fig. 35).

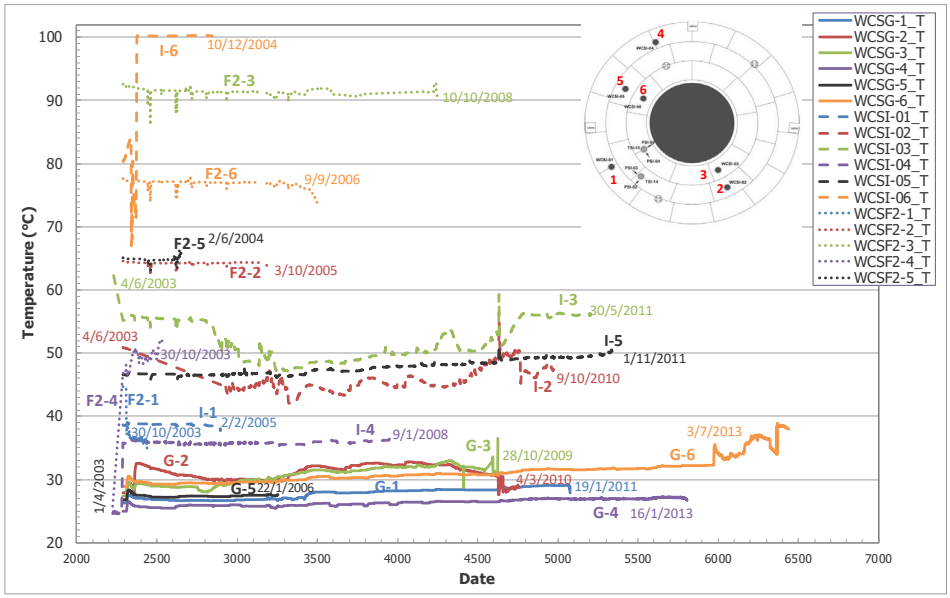

Fig. 96: Comparison of temperature values from the Sensors 1 to 6 at Sections G, I and F2

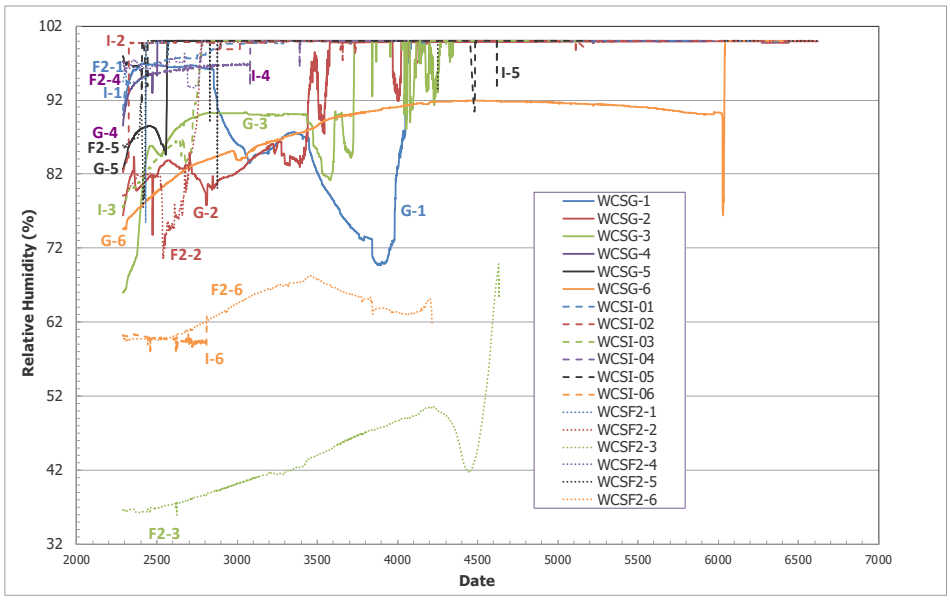

Fig. 97: Comparison of R.H values from the Sensors 1 to 6 at Sections G, I and F2

4.3.2 Fluid pressure measurements

Fluid pressure measurements from the CIEMAT pipes were obtained in the sampling campaigns of August 2014 and January 2015. The same designed sampling circuit (Fig. 44) was used in both water sampling campaigns at each pipe, the water being obtained after several cycles of washing of the circuit with deionized water, vacuum and gas drying (see Section 3.2 and Appendix D).

Prior to opening each sampling line (two blue valves: in-gas, out-water), the tightness of the sampling system was checked over time. This checking was performed both by means of an overpressure (P = 2 – 3 bar) and under vacuum. During this operation a slight loss of pressure was detected when connecting the sampling system to the sampling bag. However, this was always very slow, so the water sampling could be successfully performed.

The fluid pressure measurements obtained from the CIEMAT pipes are shown in Tab. 17. These values range between 0.775 and 2.320 bar (absolute pressure). The comparison of pressures obtained in both campaigns are shown in Fig. 98, Fig. 99 and Fig. 100. In general, the lowest pressures were observed in the C1 pipe located close to the heater at the top part of the bentonite buffer; and the higher pressures in the pipes located at the bottom of the gallery (C5) and close to the granite interface (C3 and C7). In these last pipes, where the highest amount of water could be extracted, pressures are due to water pressure, because of granitic groundwater inflow.

Regarding the behaviour along the x-coordinate of the barrier, the higher pressures were registered in the Section I, located at the frontal part of the heater. The lower pressures were noted in Section F2, which is located at the middle of the Heater #2, except in the pipes C3 and C7, which were located close to the granite and were easily filled with water. In Section F2 no water could be obtained from pipes C1, C2, C4 and C5 in the 2014 and 2015 sampling campaigns. In the rest of campaigns some water could be ever sampled from each filter, except from pipes C2 and C4 from which porewater could never be collected.

Tab. 17: Pressures (absolute, bar) measured in the Cx pipes

Section G				**Section I**				**Section F2**			
Pipe	**T.** (°C)	**August 2014**	**January 2015**	**Pipe**	**T.** (°C)	**August 2014**	**January 2015**	**Pipe**	**T.** (°C)	**August 2014**	**January 2015**
C1 Blue	39	0.960	0.858	C1 Yellow	86	1.366	0.940	C1 Green	97	0.814	0.792
C4 Blue	39	1.084	0.991	C4 Yellow	86	1.068	1.082	C4 Green	97	0.826	0.840
C2 Blue	37	1.548	1.146	C2 Yellow	59	1.928	1.264	C2 Green	75	0.775	0.825
C5 Blue	37	1.347	1.035	C5 Yellow	59	1.661	0.991	C5 Green	75	0.807	0.854
C3 Blue	32	1.186	1.480	C3 Yellow	38	1.817	1.602	C3 Green	45	1.805	2.320
C7 Blue	32	1.274	1.187	C7 Yellow	38	2.057	1.190	C7 Green	45	1.548	1.597
Atmospheric pressure inside the gallery (from AITEMIN sensor)										0.826	0.810

Because the FEBEX *in situ* test is a non-isothermal test, the development of pressure due to water vapour is expected, especially in the inner bentonite parts at contact with the heaters. In the case of the CIEMAT pipes, the pressures measured may be related to water pressure in the pipes located at the external part of the barrier (C3 and C7, especially in the Section G non-affected by heat), and to vapour pressure in addition to water pressure in the pipes close to Heater #2 (C1, C4).

The vapour pressures at the temperature reached in each bentonite ring (inner ring: 94 – 99 °C, intermediate ring: 54 – 75 °C and outer ring: 37 – 45 °C, see Tab. 3) is shown in Fig. 98, Fig. 99 and Fig. 100. The vapour pressure at 90 °C ($P_{90\,°C}$ = 0.815 bar) is similar to the atmospheric pressure at Grimsel gallery ($P_{atm,\ average}$ = 0.823 bar, $P_{atm,\ min}$ = 0.823 bar, $P_{atm,max}$ = 0.843 bar), whereas the vapor pressure at 96 °C is slightly higher, $P_{96\,°C}$ = 0.877 bar.

The fluid pressures in CIEMAT pipes were always higher (Fig. 101) than those measured in the GRS pipes (FP1, FP2 and FP3), which it is probably related to the internal volume of the pipes: 5 – 10 mL in CIEMAT pipes and 3.2 L in GRS pipes. Hence, it is easier to fill the internal volume of the CIEMAT tubes.

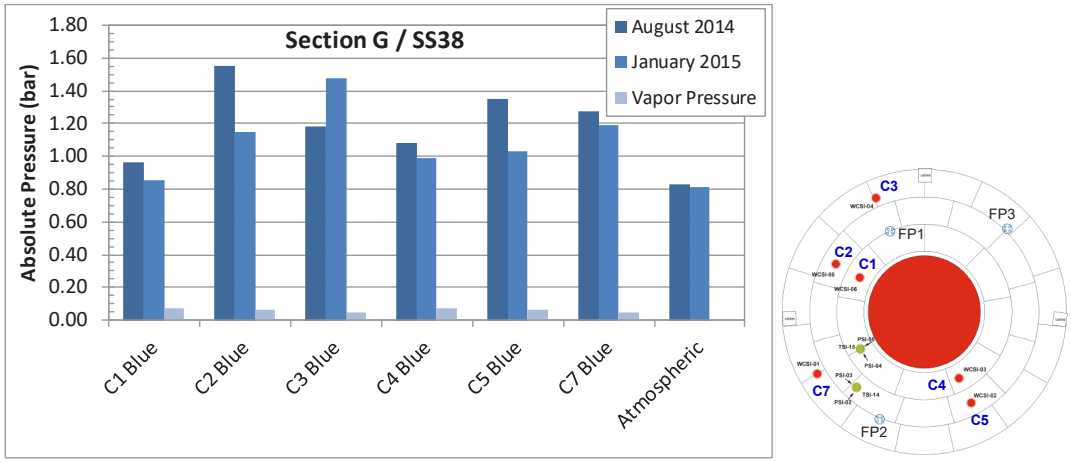

Fig. 98: Pressure (bar, abs.) inside the surface interval (blue colour) from the CIEMAT pipes Cx located in the instrumented Section G (slice S67, Sampling Section 38)

Comparison with atmospheric pressure in the gallery (823 ± 16 mbar, range taken: 804 – 842 mbar), and vapour pressure at the temperature of each bentonite ring.

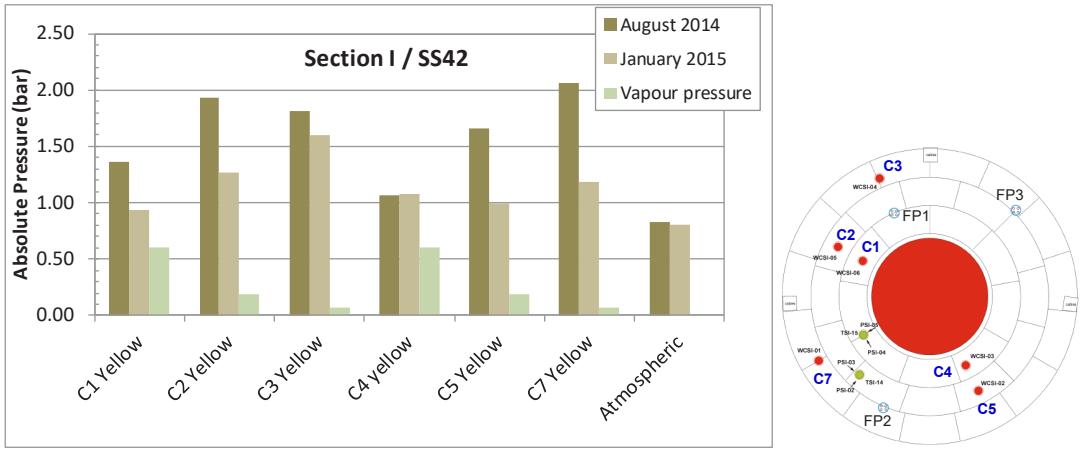

Fig. 99: Pressure (bar, abs.) inside the middle interval (yellow colour) from the CIEMAT pipes Cx located in the instrumented Section I (slice S59, Sampling Section 42)

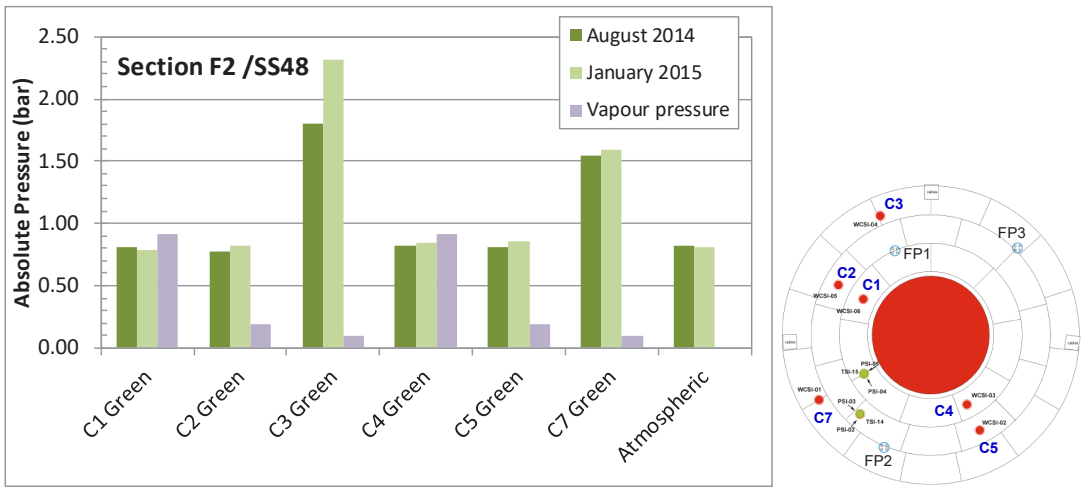

Fig. 100: Pressure (bar, abs.) inside the deep interval (green colour) from the CIEMAT pipes Cx located in the instrumented Section F2 (slice S42, Sampling Section 48)

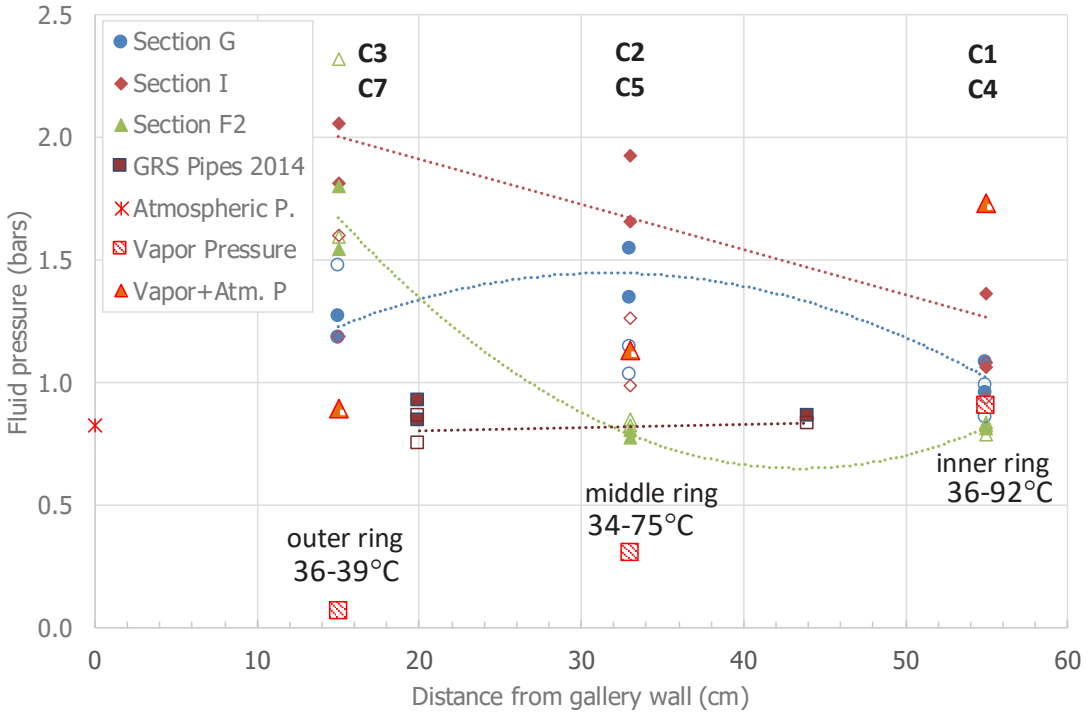

Fig. 101: Pressures measured in GRS and CIEMAT Cx pipes in 2014 and 2015 (open symbols)

Section G: close to the dummy heater; Section I: at the frontal part of Heater #2; Section F2: at the middle part of Heater #2. Temperatures are the minimum and maximum values obtained in each bentonite ring for Sections G, I and F2.

4.3.3 Porewater chemistry

Water sampling from these pipes was performed in 2006, 2011, 2014 and 2015. The optimised sampling conditions made the samples collected during the 2014 and 2015 sampling campaigns the best.

In 2014 and 2015, all the water samples were collected under anoxic conditions inside multilayer Al-foil sampling bags (Fig. 102, Fig. 103, Fig. 104), except those from the C4/yellow and C3/yellow pipe/interval in 2014, where Tedlar® sampling bags were used (Fig. 105, Fig. 106). A detail of the extraction of water from the pipes and the pressure interval measurement is shown in Fig. 107. Only the water sample from the C4/yellow pipe (I section) at both campaigns showed a slight turbidity, indicating the possible presence of organic matter (Fig. 106). In January 2015, the water sample from the C1/yellow pipe (I section) also showed a slight turbidity. Once at the laboratory, all the bags were introduced inside an anoxic glove box for pH and Eh measurements prior to their distribution for chemical analysis. The chemical composition of the porewaters in each pipe/interval, as well as the pH and redox measurements are shown in Tab. 18 and Tab. 19.

The ion concentrations from both the 2014 and 2015 samplings campaigns are quite similar in all intervals, with some exceptions, especially pH. The same intervals were sampled in 2014 and 2015, except the C3 Section I, where no water could be collected. The lowest salinities are found in the C3 and C7 pipes located close to the granite interface, with chloride contents ranging between 1'000 and 7'800 mg/L. The highest salinities are found in the pipes C1 and C4 at Section I, located close to the liner/heater interface (Cl contents from 11'000 to 15'700 mg/L). pH

values are higher in the 2015 sampling campaign (pH 7.9 – 8.8) than in the 2014 campaign (pH 5.5 – 8.6), indicating some type of oxidation in the 2014 porewaters, probably induced by a degassing process. Most of the Eh values measured are reduced and TOC and acetate were always detected, when enough water could be sampled for their determination. Especially high alkalinity values were found (> 15 meq/L) in the interval C3 from Section G.

The evolution of the porewater composition at each sampling interval over time is given in Tab. 20 to Tab. 24. However, it should be taken into account for the interpretation of the results that during the final concrete plug installation some of the references labelling the sampling lines were lost or erased leading to the confusion in the labels for the installed pipes, especially in the sampling lines C1, C2 and C7, as well as in the location of the sampling intervals (G, I and F2). In any case, the collection of water for each sampling line was performed maintaining the same labelling criteria from the beginning of the sampling campaigns.

Fig. 102: Collection of porewater in the August 2014 sampling campaign from the pipes located: a) at the right side of the gallery, b) at the left side of the gallery and c) at the top of the gallery

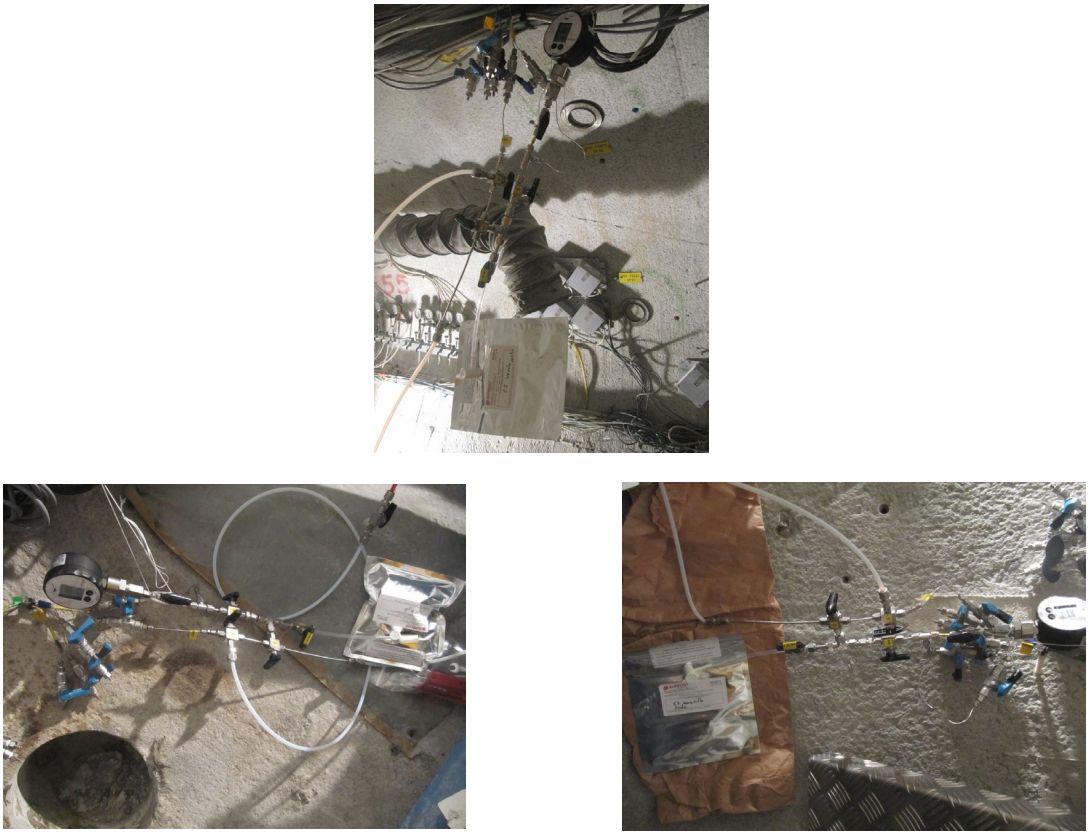

Fig. 103: Collection of porewater in the January 2015 sampling campaign from the pipes located: a) at the top of the gallery (C3 pipe), b) at the right side of the gallery (C2 and C5 pipes), and c) at the left side of the gallery (C1, C2 and C7 pipes)

Fig. 104: Sampling bags with porewater collected from the CIEMAT pipes after their reception in the Pore Water Chemistry Laboratory at CIEMAT

Fig. 105: Collection of porewater on August 2014 from some intervals of different pipes by using multilayer foil sampling bags (most of the samples) and Tedlar® sampling bags (only C3 yellow and C4 yellow samples)

Fig. 106: Detail of the appearance of water collected in the August 2014 inside Tedlar® sampling bags from the sintered filters C3-Section I (yellow colour) and C4-Section I (yellow colour)

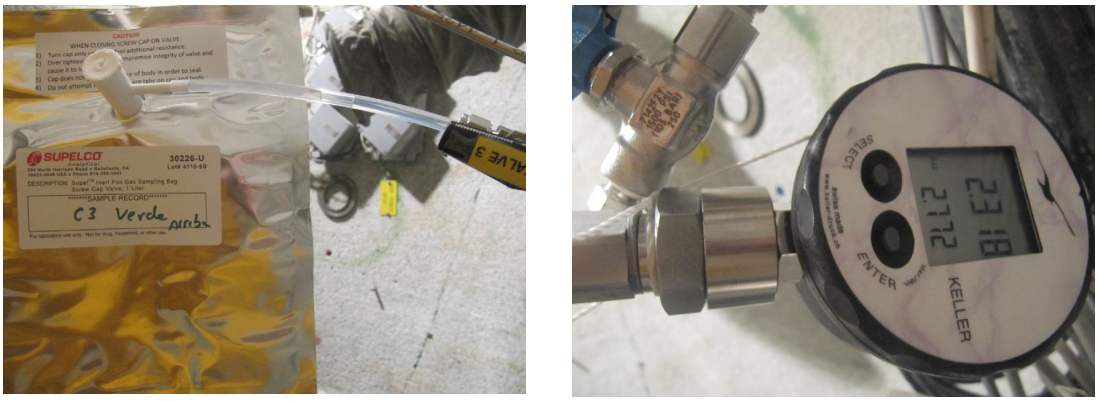

Fig. 107: Detail of the extraction of porewater from the pipe C3 at Section F2 (green colour) and detail of the corresponding interval pressure measurement

Tab. 18: Chemical composition of the porewater collected from the CIEMAT pipes in August 2014

Section			**G**	**I**	**F2**	**G**	**I**	**I**	**G**	**I**	**F2**	**I**	**G**	**G**
Pipe			C3 BLUE	C3 YELLOW	C3 GREEN	C4 BLUE	C4 YELLOW	C5 YELLOW	C7 BLUE	C7 YELLOW	C7 GREEN	C1 YELLOW	C1 BLUE-GREEN	C2 BLUE
Laboratory			CIEMAT	CIEMAT	CIEMAT	CIEMAT	CIEMAT	CIEMAT	CIEMAT	CIEMAT	CIEMAT	CIEMAT	CIEMAT	CIEMAT
Sampling bag type			Al Foil	Al Foil	Tedlar®	Al Foil	Tedlar®	Al Foil	Al Foil	Al Foil	Al Foil	Al Foil	Al Foil	Al Foil
Weight		2	16		12	1	7	7	5		6	1	0.5	0.5
Sensoric parameter lab														
Colour/turbidity			Clear	Clear	Clear	Clear	Slightly turbid	Clear	Clear	Clear	Clear	Clear	Clear	Clear
Physical-chemical parameter lab														
pH value (20 °C) (glove box/lab.)	pH		8.2/7.1	7.9	8.6/8.3	6.4	5.5/5.1	7.9	8.4	7.9	8.3/8.1	6.2	6.5	6.5
Redox potential	Eh (SHE)	mV	-206	n.m.	-231	n.m.	+63	n.m.	n.m.	n.m.	-80	n.m.	n.m.	n.m.
Spec. elect. conductivity (25 °C) lab.	Cond.	µS/cm	12'240	n.m.	n.m.	n.m.	n.m.	n.m.	n.m.	n.m.	n.m.	n.m.	n.m.	n.m.
Alkalinity lab.	Alk.	meq/L	3.46	6.27	15.58	< 0.12	< 1	2.11	1.85	2.45	6.12	< 0.12	< 0.12	< 0.12
Main ions														
Sodium	Na^+	mg/L	3'100	6'200	1200	5'400	5'300	5'200	3'300	3'900	2'200	5'600	2'900	3'900
Potassium	K^+	mg/L	47	79	24	109	1'200	83	49	47	34	96	52	69
Calcium	Ca^{2+}	mg/L	390	589	22	224	1'200	1'400	351	606	131	1'500	170	332
Magnesium	Mg^{2+}	mg/L	313	653	51	727	1'000	1'200	296	466	124	1'800	410	536
Ammonium	NH_4^+	mg/L	n.m.	n.m.	n.m.	n.m.	n.m.	n.m.	n.m.	n.m.	n.m.	n.m.	n.m.	n.m.
Chloride	Cl^-	mg/L	4'800	10'200	1'400	9'400	15'500	13'200	5'500	7'800	2'700	15'700	5'000	6'000
Sulfate	SO_4^{2-}	mg/L	3'200	5'100	460	1'700	118	3'200	3'300	3'300	2'600	2'400	1'400	3'400
Nitrate	NO_3	mg/L	< 1	28	1.7	65	103	204	< 1	4.7	< 1	191	47	56
Bromide	Br^-	mg/L	10.9	22.7	2.9	27	36.1	34.1	11.1	16.9	5.6	44	12	15
Thiosulfate	$S_2O_3^{2-}$	mg/L	< 0.5	2.1	3.3	< 0.5	< 0.5	1.4	2.3	< 0.5	1.6	< 0.5	< 0.5	< 0.5
Trace compounds														
Aluminium	Al	mg/L	< 0.3	< 0.3	< 0.3	< 2.0	< 0.3	< 0.3	< 0.4	< 0.3	< 0.3	< 2.0	< 2.0	< 2.0
Silicon	Si	mg/L	35	66	47	75	37	54	35	27	45	64	54	52
Iron	Fe (II/III)	mg/L	< 0.3	< 0.3	< 0.3	< 2.0	37	< 0.3	< 0.4	< 0.3	< 0.3	< 2.0	< 2.0	< 2.0
Strontium	Sr	mg/L	7.9	15	0.76	5.5	19	22	7.1	12	3.3	29	4.0	8.5
Boron	B	mg/L	4.1	4.8	7.2	9.0	5.2	3.5	4.6	2.5	5.5	3.9	5.2	7.0
Organic parameter														
Total organic carbon	TOC	mg/L	33.7	41.6	135	n.m.	302	119	55.3	55.3	74.5	n.m.	n.m.	n.m.
Acetate	CH_3-COO^-	mg/L	< 10	< 20	152	163	174	< 10	< 10	< 10	< 10	142	103	82

* Section G: surface interval (S67, BSS38); Section I (S59, BSS42): middle interval; Section F2: deep interval (S42, BSS48)

Tab. 19: Chemical composition of the porewater collected from the CIEMAT pipes in January 2015

Section			**G**	**I**	**F2**	**G**	**I**	**I**	**G**	**I**	**F2**	**I**	**G**	**G**	**I**
Pipe			C3 BLUE	C3 YELLOW	C3 GREEN	C4 BLUE	C4 YELLOW	C5 YELLOW	C7 BLUE	C7 YELLOW	C7 GREEN	C1 YELLOW	C1 BLUE-GREEN	C2 BLUE	C2 YELLOW
Laboratory			CIEMAT	CIEMAT	CIEMAT	CIEMAT	CIEMAT	CIEMAT	CIEMAT	CIEMAT	CIEMAT	CIEMAT	CIEMAT	CIEMAT	CIEMAT
Sampling bag type			Al Foil	Al Foil	Al Foil	Al Foil	Al Foil	Al Foil	Al Foil	Al Foil	Al Foil	Al Foil	Al Foil	Al Foil	Al Foil
Weight		3	6		5	0.5	3	4	4		4	3	0.1	2.5	4
Sensoric parameter lab															
Colour/turbidity			Clear	Clear with black spots	Clear	Clear	Slightly turbid	Clear	Clear	Clear	Clear	Slightly turbid	Clear	Clear	Clear
Physical-chemical parameter lab															
Ph value (20 °C) (Glove box/lab.)	pH		8.11/7.9	8.62/8.1	8.83/8.8	8.31/n.d	8.04/7.7	8.18/7.7	8.43/8.1	8.29/7.9	8.77/8.4	7.9/7.6	8.59/n.d.	8.23/8.1	8.24/7.9
Redox potential	Eh (SHE)	mV	-7.4	-139	-127		+288	-225	-170		-169	-64		-90.6	-152
Spec. electc Conductivity (25 °C) lab	Cond.	µS/cm													
Alkalinity lab.	Alk.	meq/L	3.78	1.59	16.63	n.d.	1.36	1.57	2.04	1.81	5.11	1.34	n.d.	3.05	1.72
Main ions															
Sodium	Na^+	mg/L	3'100	3'500	1'200	4'600	4'500	5'200	3'600	3'900	2'100	6'300	4'600	3'800	5'600
Potassium	K^+	mg/L	40	39	19	102	90	68	46	39	24	96	105	69	62
Calcium	Ca^{2+}	mg/L	363	479	21	388	901	1'300	462	708	107	1'800	469	453	1.2
Magnesium	Mg^{2+}	mg/L	285	366	31	704	814	1'000	379	536	113	1'700	684	560	1'100
Ammonium	NH_4^+	mg/L	n.d.	n.d.	n.d.	n.d.	n.d.	n.d.	n.d.	n.d.	n.d.	n.d.	n.d.	n.d.	n.d.
Chloride	Cl^-	mg/L	4'100	5'100	1'000	8'200	11'000	12'700	5'200	7'200	2'000	14'400	8'600	6'400	11'300
Sulfate	SO_4^{2-}	mg/L	2'500	2'600	298	1'500	97	2'900	3'100	2'900	1'900	2300	2'200	3'500	3'000
Nitrate	NO_3	mg/L	< 1	< 0.5	1.9	< 3	< 1	132	2.9	< 1	1.2	68	< 10	1.2	145
Bromide	Br^-	mg/L	16	15	2.5	24	43	35	19	28	7.3	47	20	20	33
Thiosulfate	$S_2O_3^{2-}$	mg/L	< 0.5	< 0.5	8.1	< 0.5	2.1	7.2	< 0.5	< 0.5	< 0.5	2.3	< 10	< 0.5	< 0.5
Trace compounds															
Aluminium	Al	mg/L	< 0.3	< 0.3	< 0.3	< 10	< 0.3	< 0.3	< 0.3	< 0.3	< 0.3	< 0.3	< 36	< 0.3	< 0.6
Silicon	Si	mg/L	38	33	52	106	33	59	49	29	49	56	165	64	51
Iron	Fe (II/III)	mg/L	< 0.3	< 0.3	0.97	< 10	< 0.3	2.4	< 0.3	< 0.3	< 0.3	0.59	< 36	< 0.3	< 0.6
Strontium	Sr	mg/L	7.3	10	0.38	< 10	16	23	8.6	14	2.4	32	< 36	9.3	22
Boron	B	mg/L	4.6	2.1	6.3	< 10	4.3	< 3.0	5.0	2.5	4.8	4.3	< 36	6.6	2.6
Organic parameter															
Total organic carbon	TOC	mg/L	33.7	n.d.	119.9	n.d.	141.1	n.d.	51.8	43	46.2	n.d.	n.d.	n.d.	83.1
Acetate	CH_3-COO^-	mg/L	n.d.	n.d.	n.d.	n.d.	n.d.	n.d.	n.d.	n.d.	n.d.	n.d.	n.d.	n.d.	n.d.

* Section G: surface interval (S67, BSS38); Section I: middle interval (S59, BSS42); Section F2: deep interval (S42, BSS48)

Tab. 20: Chemical composition of the porewater collected from the CIEMAT pipes in different sampling campaigns over time

Section			**Section G** (Surface Interval, S67)				**Section I** (Middle Interval, S59)			**Section F2** (Deep Interval, S42)		
Pipe			C3 BLUE	C3 BLUE	C3 BLUE	C3 BLUE	C3 YELLOW	C3 YELLOW	C3 YELLOW	C3 GREEN	C3 GREEN	C3 GREEN
Laboratory			CIEMAT	CIEMAT	CIEMAT	CIEMAT	CIEMAT	CIEMAT	CIEMAT	CIEMAT	CIEMAT	CIEMAT
Date			30.03.2006	11.08.2011	20.08.2014	28.01.2015	11.08.2011	20.08.2014	28.01.2015	11.08.2011	20.08.2014	28.01.2015
Sampling bag type			Septum V.	Septum V.	Al Foil	Al Foil	Septum V.	Tedlar®	Al Foil	Septum V.	Al Foil	Al Foil
Weight		g	3	10	16	6	2	2	3	2	12	5
Physical-chemical parameter lab												
pH value (20 °C) (glove box/lab.)	pH		n.m.	7.8	8.2/7.1	8.11/7.9	8.3	7.9	8.62/8.1	8.6	8.5/8.3	8.83/8.8
Redox Potential	Eh (SHE)	mV	n.m.	n.m.	-206	-7.4	n.m.	n.m.	-139	n.m.	-231	-127
Alkalinity Lab.	Alk.	meq/L	n.m.	4.48	3.46	3.78	18.75	6.27	1.59	17.84	15.58	16.63
Main ions												
Sodium	Na^+	mg/L	2'800	3'196	3'100	3'100	1'391	6'200	3'500	1'119	1'200	1'200
Potassium	K^+	mg/L	54	71	47	40	32	79	39	25	24	19
Calcium	Ca^{2+}	mg/L	6.4	4'800	390	363	36	589	479	39	22	21
Magnesium	Mg^{2+}	mg/L	< 2	4'100	313	285	55	653	366	41	51	31
Ammonium	NH_4^+	mg/L	n.m.	n.m.	n.m.	n.d.	n.m.	n.m.	n.m.	n.m.	n.m.	n.m.
Chloride	Cl^-	mg/L	3'400	4'500	4'800	4'100	1'700	10'200	5'100	1'300	1'400	1'000
Sulfate	SO_4^{2-}	mg/L	3'300	3'300	3'200	2'500	147	5'100	2'600	178	460	298
Nitrate	NO_3	mg/L	n.m.	< 0.4	< 1	< 1	2.7	28	< 0.5	0.42	1.7	1.9
Bromide	Br^-	mg/L	9.4	19	10.9	16	3.9	22.7	15	3.0	2.9	2.5
Thiosulfate	$S_2O_3^{2-}$	mg/L	n.m.	n.m.	< 0.5	< 0.5	n.m.	2.1	< 0.5	n.m.	3.3	8.1
Trace compounds												
Aluminium	Al	mg/L	n.m.	< 1.5	< 0.3	< 0.3	< 1	< 0.3	< 0.3	< 1.0	< 0.3	< 0.3
Silicon	Si	mg/L	n.m.	298	35	38	35	66	33	40	47	52
Iron	Fe (II/III)	mg/L	n.m.	< 1.5	< 0.3	< 0.3	< 1	< 0.3	< 0.3	< 1.0	< 0.3	0.97
Strontium	Sr	mg/L	n.m.	88	7.9	7.3	< 1	15	10	< 1.0	0.76	0.38
Boron	B	mg/L	n.m.	60	4.1	4.6	12	4.8	2.1	10	7.2	6.3
Iodide	I^-	mg/L	n.m.	1.0	n.m.	n.m.	1.2	n.m.	n.m.	1.1	n.m.	n.m.
Caesium	Cs	mg/L	0.15	2.4	n.m.	n.m.	< 1	n.m.	n.m.	< 1	n.m.	n.m.
Organic parameter												
Total organic carbon	TOC	mg/L	n.m.	n.m.	33.7	33.7	n.m.	41.6	n.m.	n.m.	135	119.9
Acetate	CH_3-COO^-	mg/L	n.m.	n.m.	< 10	n.m.	n.m.	< 20	n.m.	n.m.	152	n.m.

Tab. 21: Chemical composition of the porewater collected from the CIEMAT pipes over time (continuation: 1)

Section			**Section G** (Surface interval, S67)				**Section I** (Middle Interval, S59)			
Pipe			C4 BLUE	C4 BLUE	C4 BLUE	C4 BLUE	C4 BLUE	C4 YELLOW	C4 YELLOW	C4 YELLOW
Laboratory			CIEMAT	CIEMAT	CIEMAT	CIEMAT	CIEMAT	CIEMAT	CIEMAT	CIEMAT
Date			30.03.2006	040.7.2007	11.08.2011	14.08.2014	27.01.2015	11.08.2011	13.08.2014	27.01.2015
Sampling bag type			Septum V.	Septum V.	Septum V.	Al Foil	Al Foil	Septum V.	Tedlar®	Al Foil
Weight		g	drops	13	1	1	0.5	2	7	3
Physical-chemical parameter lab.										
Ph value (20 °C) (glove box/lab.)	pH		n.m.	8.3 /8.2	8.2	6.4	8.31/n.d.	7.9	5.5 /5.1	8.04/7.7
Redox potential	Eh (SHE)	mV	n.m.	n.m.	n.m.	n.m.		n.m.	+63	+288
Alkalinity lab.	Alk.	meq/L	n.m.	3.52	25.36	< 0.12	n.d.	10.3	< 1	1.36
Main ions										
Sodium	Na^+	mg/L	203	3'000	n.m.	5'400	4'600	4'443	5'300	4'500
Potassium	K^+	mg/L	60	48	n.m.	109	102	133	1'200	90
Calcium	Ca^{2+}	mg/L	< 17	436	178	224	388	1'000	1'200	901
Magnesium	Mg^{2+}	mg/L	< 5	369	570	727	704	1'100	1'000	814
Ammonium	NH_4^+	mg/L	n.m.	n.m.	n.m.	n.m.	n.d.	n.m.	n.m.	n.d.
Chloride	Cl^-	mg/L	369	3'900	8'300	9'400	8'200	11'400	15'500	11'000
Sulfate	SO_4^{2-}	mg/L	95	3'500	1'300	1'700	1'500	757	118	97
Nitrate	NO_3	mg/L		< 1	72	65	< 3	135	103	< 1
Bromide	Br^-	mg/L	< 20	4.3	22	27	24	28	36.1	43
Thiosulfate	$S_2O_3^{2-}$	mg/L	n.m.	n.m.	n.m.	< 0.5	< 0.5	n.m.	< 0.5	2.1
Trace compounds										
Aluminium	Al	mg/L	n.m.	< 0.3	< 0.7	< 2.0	< 10	< 1	< 0.3	< 0.3
Silicon	Si	mg/L	n.m.	n.m.	79	75	106	40	37	33
Iron	Fe /Fe(II)	mg/L	n.m.	0.3/0.3	< 0.7	< 2.0	< 10	< 1	37	< 0.3
Strontium	Sr	mg/L	n.m.	9.0	4.7	5.5	< 10	17	19	16
Boron	B	mg/L	n.m.	3.5	13	9.0	< 10	8.4	5.2	4.3
Iodide	I^-	mg/L	n.m.	n.m.	n.m.	n.m.	n.m.	7.1	n.m.	n.m.
Caesium	Cs	mg/L	1.3	n.m.	< 1	n.m.	n.m.	< 1	n.m.	n.m.
Organic parameter										
Total organic carbon	TOC	mg/L	n.m.	n.m.	n.m.	n.m.	n.m.	n.m.	302	141.1
Acetate	CH_3-COO^-	mg/L	n.m.	n.m.	n.m.	163	n.m.	n.m.	174	n.m.

Tab. 22: Chemical composition of the porewater collected from the CIEMAT pipes over time (continuation: 2)

Section			**Section G** (Surface Interval)		**Section I** (Middle Interval)		**Section F2** (Deep I.)		**Section G** (Surface I., S67)		**Section I** (Middle Interval, S59)		**Section F2** (Deep Interval, S42)	
Pipe			C5 BLUE	C5 BLUE	C5 YELLOW	C5 YELLOW	C5 GREEN	C1 BLUE	C1 BLUE	C1 YELLOW	C1 YELLOW	C1 YELLOW	C1 GREEN	C1 GREEN
Laboratory			CIEMAT	CIEMAT	CIEMAT	CIEMAT	CIEMAT	CIEMAT	CIEMAT	CIEMAT	CIEMAT	CIEMAT	CIEMAT	CIEMAT
Date			30.03.2006	11.08.2011	19.08.2014	27.01.2015	11.08.2011	19.08.2014	29.01.2015	11.08.2011	19.08.2014	28.01.2015	30.03.2006	11.08.2011
Sampling bag type			Septum V.	Septum V.	Al Foil	Al Foil	Septum V.	Al Foil	Al Foil	Septum V.	Al Foil	Al Foil	Al foil	Septum V.
Weight		g	drops	0.5	5	3	0.1	0.5	drops	1	1	3	drops	1
Physical-chemical parameter lab														
Ph value (20 °C) (glove box/lab.)	pH		n.m.	6.1	7.9	8.18/7.7	n.m.	6.5	8.59/n.d.	6.4	6.2	7.9/7.6	n.m.	6.1
Redox potential	Eh (SHE)	mV	n.m.	n.m.	n.m.	-225	n.m.	n.m.		n.m.	n.m.	-64	n.m.	n.m.
Alkalinity lab.	Alk.	meq/L	n.m.	< 6	2.11	1.57	n.m.	< 0.12	n.d.	14.81	< 0.12	1.34	n.m.	3.55
Main ions														
Sodium	Na^+	mg/L	n.m.	136	5'200	5'200	4'408	2'900	4'600	680	5'600	6'300	18	885
Potassium	K^+	mg/L	n.m.	7.9	83	68	n.m.	52	105	25	96	96	23	19
Calcium	Ca^{2+}	mg/L	n.m.	16	1'400	1'300	844	170	469	20	1'500	1'800	< 41	49
Magnesium	Mg^{2+}	mg/L	n.m.	13	1'200	100	1'300	410	684	19	1'800	1'700	< 12	118
Ammonium	NH_4^+	mg/L	n.m.	n.m.	n.m.	n.d.	n.m.	n.m.	n.d.	n.m.	n.m.	n.d.	n.m.	n.m.
Chloride	Cl^-	mg/L	121	41	13'200	12'700	11'100	5'000	8'600	503	15'700	14'400	51	1'400
Sulfate	SO_4^{2-}	mg/L	95	26	3'200	2'900	2'500	1'400	2'200	4	2'400	2'300	9	452
Nitrate	NO_3	mg/L	n.m.	5.1	204	132	232	47	< 10	245	191	68	n.m.	16
Bromide	Br^-	mg/L	< 50	< 2	34.1	32	26	12	20	1.3	44	47	< 5	3.5
Thiosulfate	$S_2O_3^{2-}$	mg/L	n.m.	n.m.	1.4	7.2	n.m.	< 0.5	< 10	n.m.	< 0.5	2.3	n.m.	n.m.
Trace compounds														
Aluminium	Al	mg/L	n.m.	< 2	< 0.3	< 0.3	< 3.6	< 2.0	< 36	< 1.8	< 2.0	< 0.3	n.m.	< 1.3
Silicon	Si	mg/L	n.m.	46	54	59	64	54	165	41	64	56	n.m.	54
Iron	Fe (II/III)	mg/L	n.m.	< 2	< 0.3	2.4	< 3.6	< 2.0	< 36	< 1.8	< 2.0	0.59	n.m.	< 1.3
Strontium	Sr	mg/L	n.m.	< 2	22	23	15	4.0	< 36	< 1.8	29	32	n.m.	1.3
Boron	B	mg/L	n.m.	17	3.5	< 3.0	15	5.2	< 36	14	3.9	4.3	n.m.	9.6
Iodide	I	mg/L	n.m.	n.m.	n.m.	n.d.	n.m.	n.m.	n.m.	n.m.	n.m.	n.m.	n.m.	n.m.
Caesium	Cs	mg/L	9.9	< 2	n.m.	n.d.	< 2	n.m.	n.m.	< 1	n.m.	n.m.	1	< 1
Organic parameter														
Total organic carbon	TOC	mg/L	n.m.	n.m.	119	n.d.	n.m.	n.m.	n.m.	n.m.	n.m.	n.m.	n.m.	n.m.
Acetate	$CH_3\text{-}COO^-$	mg/L	n.m.	n.m.	< 10	n.d.	n.m.	103	n.m.	n.m.	142	n.m.	n.m.	n.m.

Tab. 23: Chemical composition of the porewater collected from the CIEMAT pipes over time (continuation: 3)

Section			**Section G** (Surface interval, S67)			**Section I** (Middle interval, S42)
Pipe			C2 BLUE	C2 BLUE	C2 BLUE	C2 YELLOW
Laboratory			CIEMAT	CIEMAT	CIEMAT	CIEMAT
Date			04.07.2007	19.08.2014	28.01.2015	28.01.2015
Sampling bag type			Septum V.	Al Foil	Al Foil	Al Foil
Weight		g	43	0.5	2.5	4
Physical-chemical parameter lab						
Ph value (20 °C) (glove box/lab.)	pH		8.68/9.4	6.5	8.2/8.1	8.24/7.9
Redox potential	Eh (SHE)	mV	-290	n.m.	-90.6	-152
Alkalinity lab.	Alk.	meq/L	14.4	< 0.12	3.05	1.72
Main ions						
Sodium	Na^+	mg/L	1'400	3'900	3'800	5'600
Potassium	K^+	mg/L	230	69	69	62
Calcium	Ca^{2+}	mg/L	n.m.	332	453	1.2
Magnesium	Mg^{2+}	mg/L	n.m.	536	560	1'100
Ammonium	NH_4^+	mg/L	n.m.	n.m.	n.d.	n.d.
Chloride	Cl^-	mg/L	2'200	6'000	6'400	11'300
Sulfate	SO_4^{2-}	mg/L	65	3'400	3'500	3'000
Nitrate	NO_3	mg/L	< 1	56	1.2	145
Bromide	Br^-	mg/L	2.9	15	20	33
Thiosulfate	$S_2O_3^{2-}$	mg/L	n.m.	< 0.5	< 0.5	< 0.5
Trace compounds						
Aluminium	Al	mg/L	< 0.3	< 2.0	< 0.3	< 0.6
Silicon	Si	mg/L	n.m.	52	64	51
Iron	Fe (II/III)	mg/L	< 0.3	< 2.0	< 0.3	< 0.6
Strontium	Sr	mg/L	< 0.3	8.5	9.3	22
Boron	B	mg/L	6.6	7.0	6.6	2.6
Iodide	I	mg/L	n.m.	n.m.	n.m.	n.m.
Caesium	Cs	mg/L	n.m.	n.m.	n.m.	n.m.
Organic parameter						
Total organic carbon	TOC	mg/L	n.m.	n.m.	n.m.	8.31
Acetate	CH_3-COO^-	mg/L	n.m.	82	n.m.	n.d.

Tab. 24: Chemical composition of the porewater collected from the CIEMAT pipes over time (continuation: 4)

Section			**Section G** (Surface interval, S67)				**Section I** (Middle interval, S59)				**Section F2** (Deep interval, S42)			
Pipe			C7 BLUE	C7 BLUE	C7 BLUE	C7 BLUE	C7 BLUE	C7 YELLOW	C7 YELLOW	C7 YELLOW	C7 GREEN	C7 GREEN	C7 GREEN	C7 GREEN
Laboratory			CIEMAT	CIEMAT	CIEMAT	CIEMAT	CIEMAT	CIEMAT	CIEMAT	CIEMAT	CIEMAT	CIEMAT	CIEMAT	CIEMAT
Date			30.03.2006	04.07.2007	11.08.2011	19.08.2014	28.01.2015	30.03.2006	19.08.2014	28.01.2015	30.03.2006	04.07.2007	19.08.2014	28.01.2015
Sampling bag type			Septum	Septum	Septum	Al Foil	Al Foil	Septum vial	Al Foil	Al Foil	Septum	Septum	Al Foil	Al Foil
Weight		g	drops	5.5	2	5	4	2	4	4	2	4	6	4
Physical-chemical parameter lab														
Ph value (20 °C) (glove box/lab.)	pH		n.m.	8.61 /8.6	8.1	8.4	8.43/8.1	n.m.	7.9	8.29/7.9	n.m.	8.28/8.2	8.3/8.1	8.77/8.4
Redox potential	Eh (SHE)	mV	n.m.	n.m.	n.m.	n.m.	-170	n.m.	n.m.	n.m.	n.m.	165	-80	-169
Alkalinity lab.	Alk.	meq/L	n.m.	8.0	3.22	1.85	2.04	n.m.	2.45	1.81	n.m.	5.03	6.12	5.11
Main ions														
Sodium	Na^+	mg/L	190	1'800	3'223	3'300	3'600	1'800	3'900	3'900	1'100	2'600	2'200	2'100
Potassium	K^+	mg/L	38	45	52	49	46	89	47	39	27	96	34	24
Calcium	Ca^{2+}	mg/L	< 900	59	358	351	462	< 270	606	708	< 192	170	131	107
Magnesium	Mg^{2+}	mg/L	< 280	92	326	296	379	< 83	466	536	< 58	230	124	113
Ammonium	NH_4^+	mg/L	n.m.	n.m.	n.m.	n.m.	n.d.	n.m.	n.m.	n.d.	n.m.	n.m.	n.m.	n.d.
Chloride	Cl^-	mg/L	94	2'300	4'300	5'500	5'200	2'200	7'800	7'200	1'200	3'300	2'700	2'000
Sulfate	SO_4^{2-}	mg/L	98	991	3'000	3'300	3'100	1'100	3'300	2'900	703	2'000	2'600	1'900
Nitrate	NO_3	mg/L	n.m.	< 1	< 2	< 1	2.9	n.m.	4.7	< 1	n.m.	n.m.	< 1	1.2
Bromide	Br^-	mg/L	< 50	2.8	11	11.1	19	< 30	16.9	28	< 20	4.3	5.6	7.3
Thiosulfate	$S_2O_3^{2-}$	mg/L	n.m.	n.m.	n.m.	2.3	< 0.5	n.m.	< 0.5	< 0.5	n.m.	n.m.	1.6	< 0.5
Trace compounds														
Aluminium	Al	mg/L	n.m.	< 0.3	< 0.3	< 0.4	< 0.3	n.m.	< 0.3	< 0.3	n.m.	< 0.3	< 0.3	< 0.3
Silicon	Si	mg/L	n.m.	n.m.	33	35	49	n.m.	29	27	n.m.	n.m.	45	49
Iron	Fe (II/III)	mg/L	n.m.	< 0.3	< 0.3	< 0.4	< 0.3	n.m.	< 0.3	< 0.3	n.m.	0.5	< 0.3	< 0.3
Strontium	Sr	mg/L	n.m.	2.0	6.4	7.1	8.6	n.m.	14	12	n.m.	4.9	3.3	2.4
Barium	Ba	mg/L	n.m.	< 0.3	< 0.3	< 0.4	< 0.3	n.m.	< 0.3	< 0.3	n.m.	0.68	< 0.3	< 0.3
Boron	B	mg/L	n.m.	4.0	7.5	4.6	5.0	n.m.	2.5	2.5	n.m.	3.5	5.5	4.8
Iodide	I^-	mg/L	n.m.	n.m.	1.0	n.m.	n.m.	n.m.	n.m.	n.m.	n.m.	n.m.	n.m.	n.m.
Caesium	Cs	mg/L	0.9	n.m.	< 1	n.m.	n.m.	67×10^{-3}	n.m.	< 0.3	1.4	< 0.4	< 0.3	n.m.
Organic parameter														
Total organic carbon	TOC	mg/L	n.m.	n.m.	n.m.	55.3	51.8	n.m.	55.3	43	n.m.	n.m.	74.5	46.2
Acetate	$CH_3\text{-}COO^-$	mg/L	n.m.	n.m.	n.m.	< 10	n.d.	n.m.	< 10	n.d.	n.m.	n.m.	< 10	n.m.

Porewater from the bentonite barrier could be collected from the different C_x pipes, but not from all sampling intervals. The volume of water collected was very small and ranged between 0.1 and 16 mL, the higher volumes coming from pipes C3 and C7 located close to the granite interface, from which water could be sampled in all sampling campaigns. The low volume of water collected made a complete analysis of the sample difficult. However, taking into account the small size of the filter, not so much water could be extracted during each sampling campaign: ~ 10 mL maximum if they were completely flooded.

The evolution of the main physico-chemical parameters of the water samples and the concentration of species over time is shown in Fig. 108 and Fig. 109 for some parameters as a function of the distance to the gallery axis, as well as a function of time in Fig. 110 to Fig. 112. A Schoeller plot for ion concentration is shown in Fig. 113 for different sampling campaigns.

As the FEBEX reference porewaters (Fernández et al. 2018: NAB 17-25), the porewaters sampled in the CIEMAT pipes are NaCl water-type with a variable salinity. As with the water samples from the GRS pipes, the high content of chloride in the FEBEX bentonite allows us to follow the solute movement through the bentonite during hydration due to its conservative behaviour. In the C_x pipes, the porewater composition depends on the filter location (Section G, I or F2), the pipe location inside the bentonite and the time. Regarding the x-coordinate, the highest salinities are found in the Section I, located at the frontal part of the heater, where the highest chloride content was 15700 mg/L (442.3 mmol/L) in pipe C1, located at the inner part of the bentonite barrier. This may indicate a possible evaporation and concentration of salts at the heater contact as expected. The maximum chloride content at Instrumented Section F2 was 13'200 mg/L (371.8 mmol/L) in pipe C2; and 9'400 mg/L (264.8 mmol/L) in pipe C4 at Section G (Fig. 114).

The pH values are alkaline but in some samples values dropped to values between 6.6 and 5.5 (Fig. 108). These samples correspond to pipes C5, C4, C2 and C1 located at the inner part of the barrier (second and third bentonite blocks); and mainly to Section G, where a high corrosion of the dummy heater took place (Fig. E-8); and to Section I (frontal part of the heater), where some corrosion (Fig. 50) was also observed (Wersin & Kober 2017: NAB 16-16). Because the pH of the reference FEBEX bentonite porewater is neutral to slightly alkaline (Fernandez et al. 2004, 2018), the decreased pHs observed in some samples (below pH 6), indicate an oxidation process.

Regarding the redox state of the bentonite porewater, redox measurements were obtained in some samples, when a high amount of water was obtained. Most of the values are below -50 mV, which indicate a reducing environment. It is interesting to note the presence of $S_2O_3^{2-}$ in some waters (Fig. 108), which implies the presence of the redox pair $SO_4^{2-}/S_2O_3^{2-}$; and the presence of TOC and acetate as well (Fig. 109).

The evolution of the porewaters over time (Fig. 110 to Fig. 112) indicates that chloride, and sodium as counterion, are the main ions in the porewater (Fig. 110, Fig. 113, Fig. 114), increasing the salinity over time. The highest salinities are found in pipes C1 and C4, which are located at the inner part of the bentonite barrier, close to the liner/heater interface. The lower salinities are located in pipes C3 and C7, located close to the granite interface. This behaviour is in agreement with results obtained from aqueous extracts and squeezing tests from bentonite samples obtained after dismantling (Fernández et al. 2018), in which the chloride contents in the heated areas increased towards the internal part of the barrier due to its movement with the hydration front from the granite enhanced by temperature (Fig. 90).

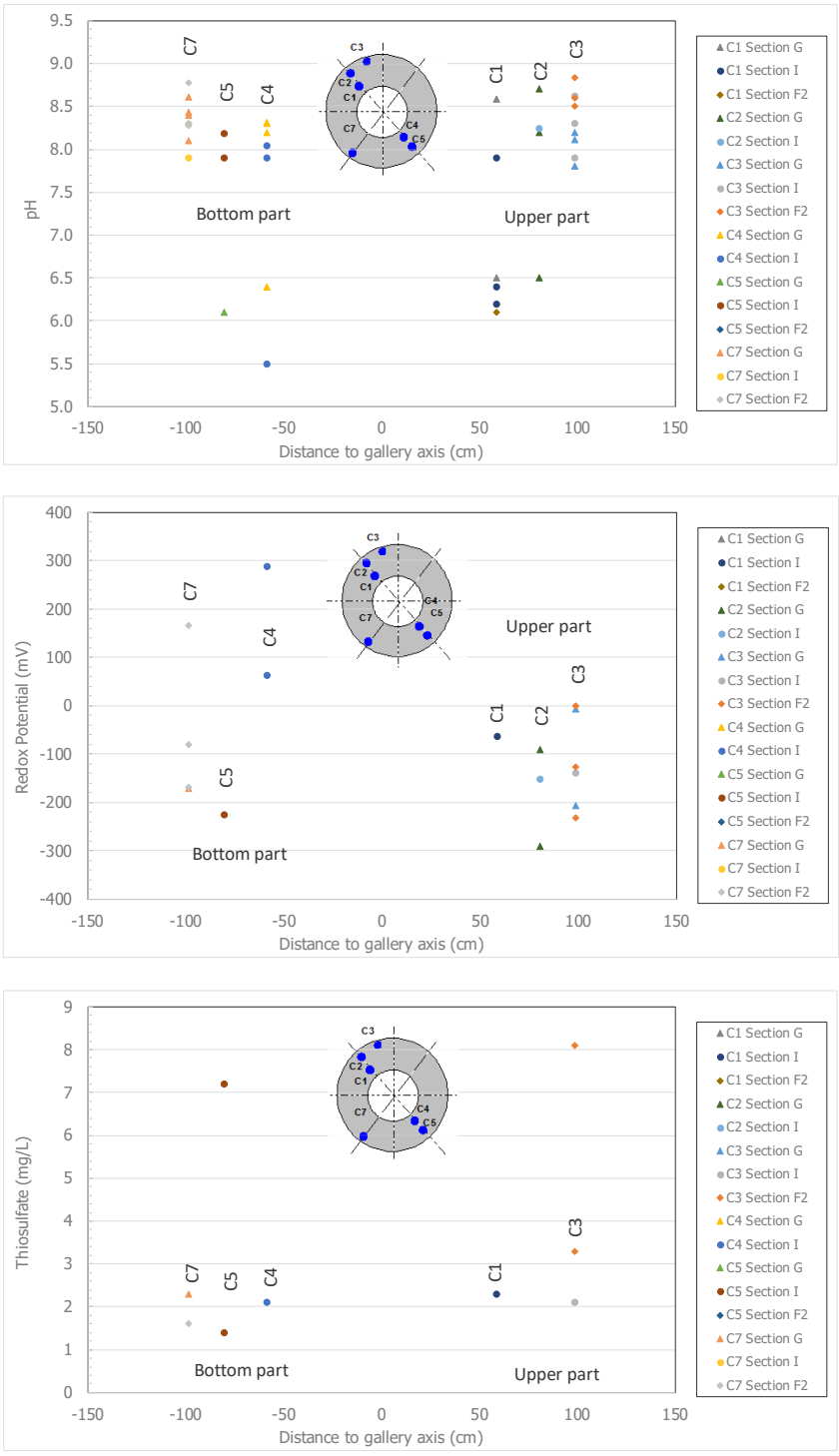

Fig. 108: pH, redox potential and thiosulfate concentration from porewaters in the C_x pipes

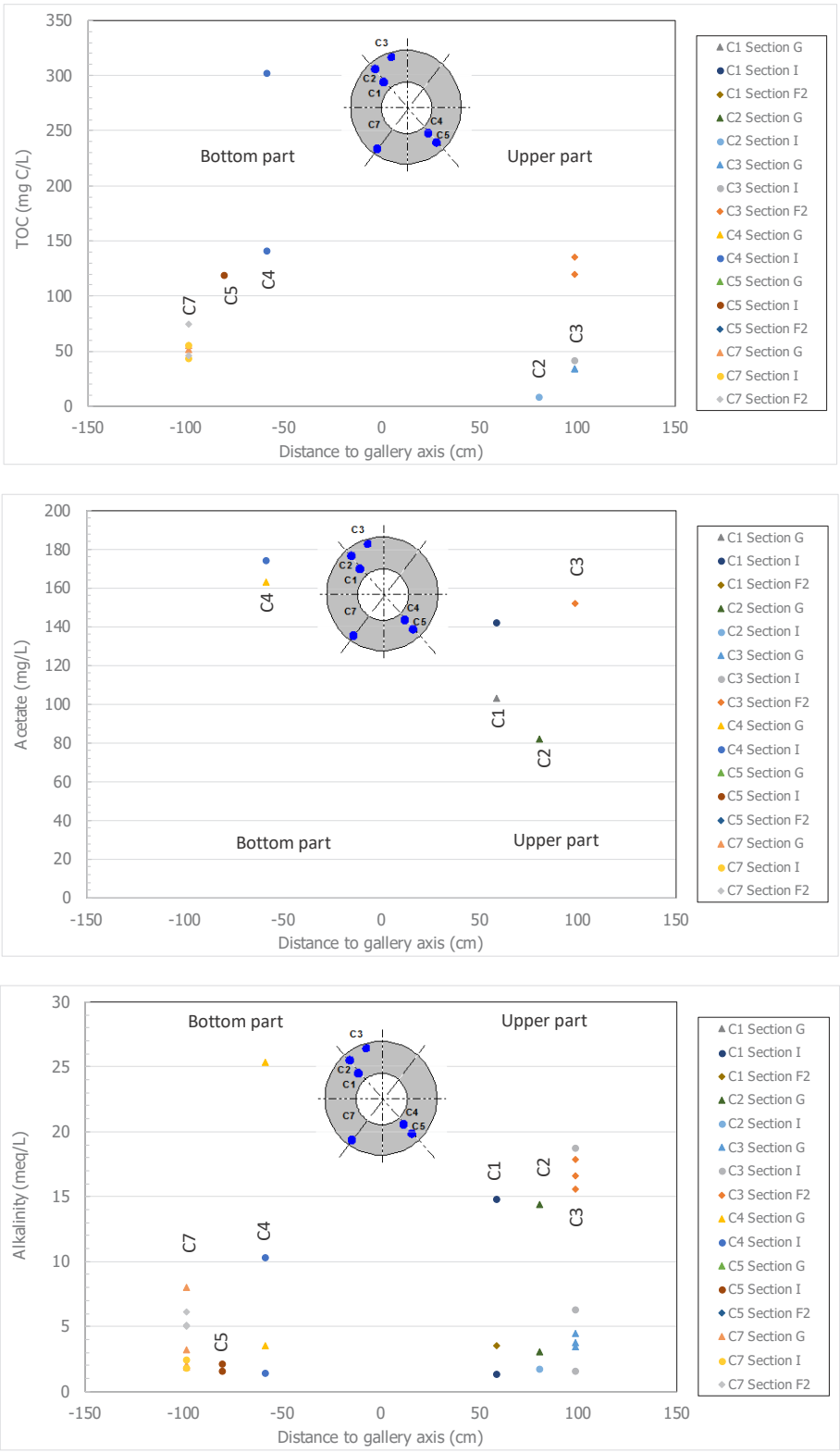

Fig. 109: TOC, acetate and alkalinity from the porewaters in the Cx pipes

The porewaters obtained from the pipes were compared to those obtained from squeezing experiments from bentonite block samples (outer, middle and inner blocks) located at the heated Section BS44/BSS-47 (Tab. 16, Fig. 110); and to those obtained from the gas pipes (Fig. 115, Fig. 116). The chloride and sodium concentrations obtained from the pipes are in the range of porewater compositions obtained from squeezing, but always showing a higher salinity than expected according to the location of the pipe in each bentonite ring (outer, middle, inner). The best agreement is obtained in Section F2, located at bentonite Section BS42 (Fig. 110c), where the more diluted porewaters are from pipes C3 and C7 (at granite contact), and the more concentrated at the inner part of the bentonite (pipe C5). In Section I (Fig. 110b), the samples from the inner Sections C1, C4, C2 and C5 are in agreement with the squeezed waters from the inner bentonite block, whereas the water samples from the external pipes close to granite interface have a higher chloride content with respect to squeezed waters obtained from the middle and outer bentonite blocks. This Section I (BS59) was at the frontal part of the heater with less influence of the heat than in Section BS44 (bentonite Sampling Section 47) according to Tab. 3. However, an overheating incident could affect the salinity of the porewaters, increasing the concentration profiles (see the deformation of pipe C4 in Section I (Fig. 56), probably due to thermal stress). Heat enhanced the transport of solutes towards the Heater #2 (Fernández et al. 2018). Indeed, the salinities at the inner part of the barrier are higher in Section I, than in the non-heated Section G and, finally, in Section F2 (Fig. 110, Fig. 114). It should be taken into account that Section G was a heated section surrounding Heater #1 during the First Operational Phase. With respect to the waters obtained from the gas pipes (FPx), the Cx porewaters are of a much higher salinity (Fig. 115, Fig. 116), which cannot be easily explained, except if the internal volume of both types of pipes is taken into account ($V = 5 – 10 \times 10^{-3}$ L for Cx pipes and V = 3.2 L for gas pipes). What seems to be confusing is that the waters from the FP-3 pipe, the closest to the granitic interface, are of higher salinity than those from other gas pipes FP-1 and FP-2, located at inner parts of the bentonite barrier.

In the pipes located at sections close to the granite interface, sodium is always higher than chloride; whereas in the pipes located at the inner part, chloride is always higher than sodium. This is due to the exchange reactions at interlayers. In the more hydrated zones, carbonates are dissolved, sodium being replaced by calcium at exchange sites, increasing the sodium content in the porewater (Fig. 115, Fig. 116).

The sulfate behaviour is different depending on the location of the pipe along the bentonite radius, as well as the location of each filter along the x-coordinate (Fig. 111, Fig. 117). Sulfate seems to be controlled by gypsum dissolution/precipitation processes according to the saturation indices of the porewaters. Equilibrium seems to be attained in the inner parts of the bentonite, whereas the waters are undersaturated in gypsum in the more hydrated zones (C3 and C7 pipes). However, sulfate contents increased and decreased over time. Therefore, other processes, apart from sulfate transport by advection during the hydration of the bentonite, are involved in the system as well, such as sulfate reduction. In Section G, the sulfate contents are similar to those obtained by squeezing. Thiosulfate was detected in some samples indicating a reduction of sulfate in the system and/or an oxidation of sulfurs produced by the reduction of sulfates. On the other hand, a high amount of nitrate was also detected in some waters.

A high amount of magnesium in the porewaters (Fig. 111, Fig. 120) is observed, with higher concentrations than calcium, and it is correlated with chlorides as observed in the THC studies of the FEBEX in situ test (Fernández et al. 2018: NAB 16-25). In samples not in equilibrium with gypsum, calcium is always below the sulfate concentration, except in the samples from pipes C1 and C4 in Section I, located in the frontal part of the heater.

Carbonate dissolution/precipitation processes control the alkalinity, the pH and the concentration of cations via exchange reactions at interlayers. However, high alkalinities are observed in some waters, which are correlated with a high pH and high contents of total organic carbon and/or acetate contents (Fig. 112). Thus, total alkalinity determined by acid titration consisted of both carbonate alkalinity (HCO_3^- + CO_3^{2-}) and non-carbonate alkalinity (other species such as deprotonated weak organic acids and HS^- (Stumm and Morgan, 1981): $Alk \approx [HCO_3^-] + 2[CO_3^{2-}] + [OH^-] + [SiO(OH)_3^-] + [Ac^-] + [HS^-]$). Therefore, it is expected that organic matter degradation influences the porewater chemistry. Acetate could be detected only in some waters indicating some fermentative/oxidation processes involved in the degradation of organic matter inside the bentonite barrier, as indicated by the slight turbidity in some samples (Fig. 106b). These samples are associated with corrosion of metals (Wersin & Kober 2017). For example, in the 2014 and 2015 campaigns, the water sampled in C4/Section I (slightly turbid as water from C1/Section I) with low pH, high TOC and acetate contents corresponds to a water sample from the frontal part of Heater #2, where a corrosion halo was observed. Madina (2016) analysed the corrosion features from the front part of Heater #2 and indicated that the corrosion morphology in this zone and the presence of sulfurs are due to microbiologically influenced corrosion (MIC). The sample from C3/Section F2, with high alkalinity, pH, TOC and acetate contents, corresponds to a water sample close to a corroded fissurometer with a typical colour pattern formed by aerobic corrosion followed by anaerobic corrosion of steel (Wersin & Kober 2017). The sample from C4/Section G, with a low pH and high acetate content, corresponds to the filter which was found corroded, with the presence of sulfurs, magnetite, hematite, calcite and aragonite. These parameters indicate also, as described for gas pipes, the relationship between corrosion processes and the presence of carboxylic acids, which may further oxidized or reduced depending on oxygen content.

The presence of calcite and aragonite may also indicate biologically induced mineralization (BIM). Microbially induced calcite precipitation is mediated by the metabolic activity of iron-reducing, sulfate-reducing and methanogenic bacteria in anoxic environments (van Lith et al. 2003, Kenward et al. 2009). However, many studies have shown that the presence of a high dissolved magnesium concentration inhibits the formation of calcite and allows only aragonite to form (Zhang and Dawe, 2000). Aerobic and anaerobic (SRB, NRB and IRB) bacteria were found in the non-heated sections of the FEBEX in situ test at the end of the gallery, but were practically absent or very few in the inner part of the bentonite barrier at heated zones (Bengtsson et al. 2017).

The low amount of water obtained for chemical analyses raises some uncertainties in the interpretation of the porewater parameters, especially when compared with the more diluted waters from GRS pipes. The sintered stainless steel filters for recovering water resulted in very small volumes of water and was not always enough for a complete analysis. Some species implied in the redox system were not analysed and the evolution over time of the porewater composition as a consequence of both hydration and heat could not always be followed. Different terminal electron acceptors (TEAs) could be measured in the porewaters, such as SO_4^{2-}, HCO_3^-, and NO_3^-, but electron donors (Fe^{2+}, NH_4^+, acetate, formate, etc.) could not be always measured due to the low amount of water extracted. Furthermore, the possible dehydration/hydration processes close to the heater (evaporation), possible overheatings (such as in 2009 during 62 hours), and/or heating stoppage (in 2011 during 3 days), could have concentrated the porewaters around the stainless steel filters due to vapour migration, precipitating some salts at the filter surface and then dissolving them after rehomogenisation of the water content. Furthermore, preferential gas flow along the pipes cannot be discarded, where desaturated conditions could have occurred. These artefacts may have increased the salinity of the extracted porewaters with respect to those obtained by squeezing and, especially with respect to those obtained from the gas pipes.

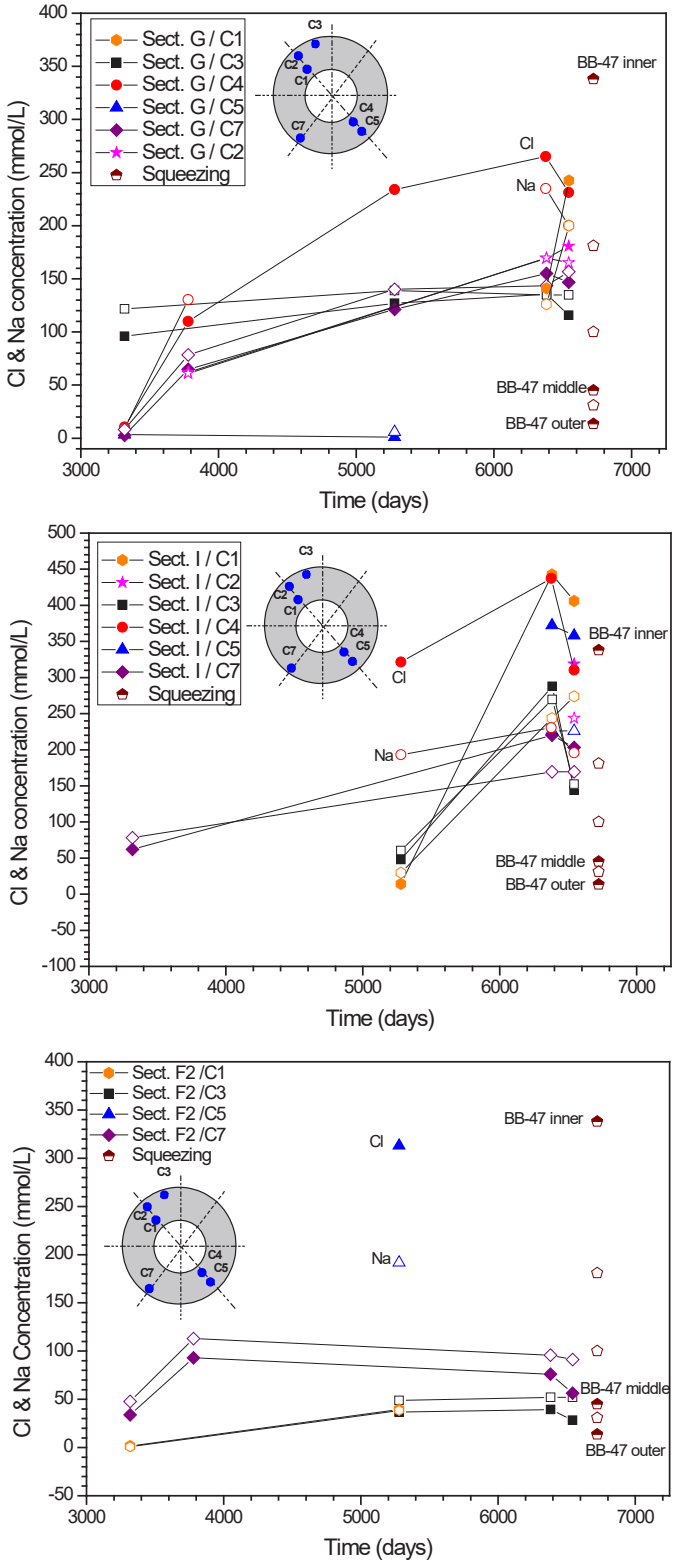

Fig. 110: Cl and Na concentrations as a function of time for the pipes in Sections G, I and F2

Data compared with porewaters obtained from squeezing tests of bentonite blocks from Section 47 (Fernández et al. 2018).

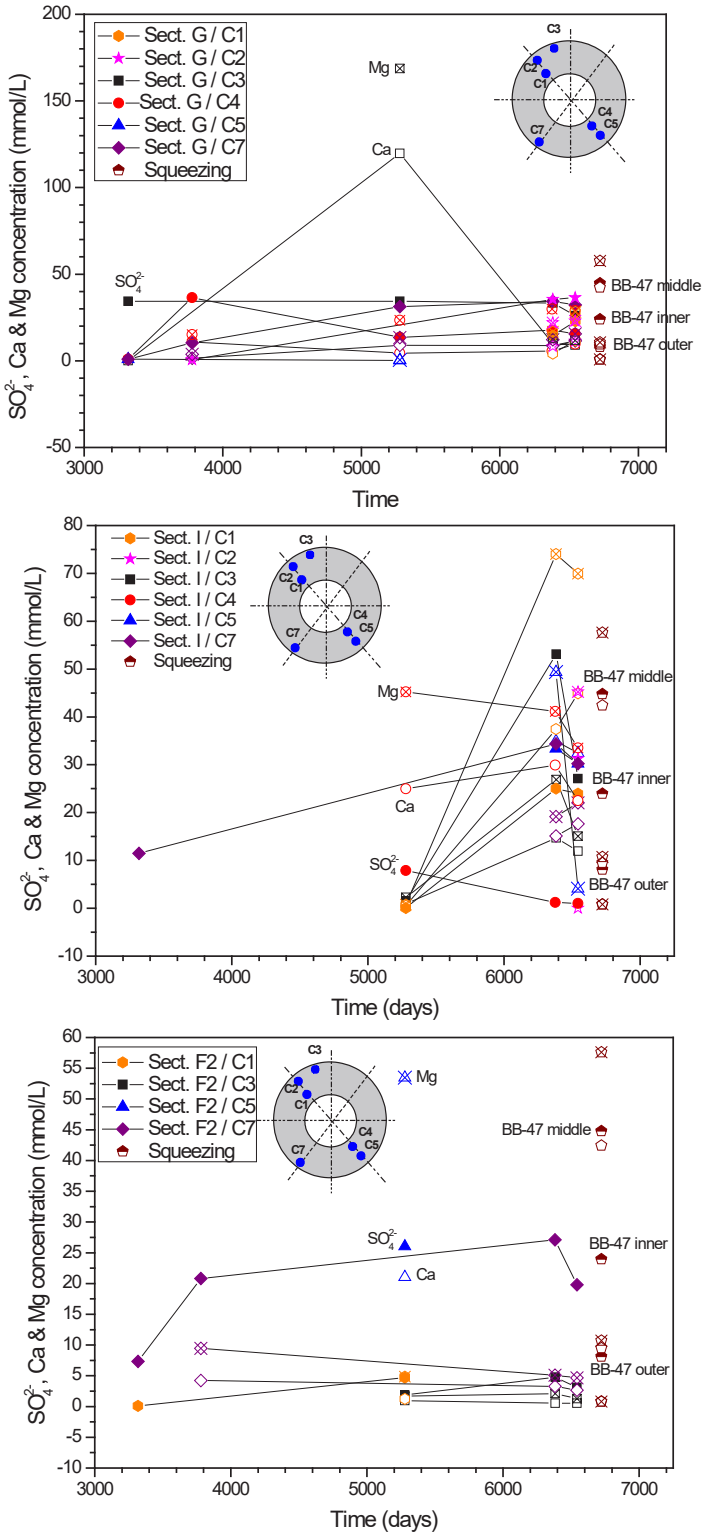

Fig. 111: SO_4^{2-}, Ca and Mg concentrations as a function of time for the pipes in Sections G, I and F2

Data compared with porewaters obtained from squeezing tests of bentonite blocks from Section 47 (Fernández et al. 2018).

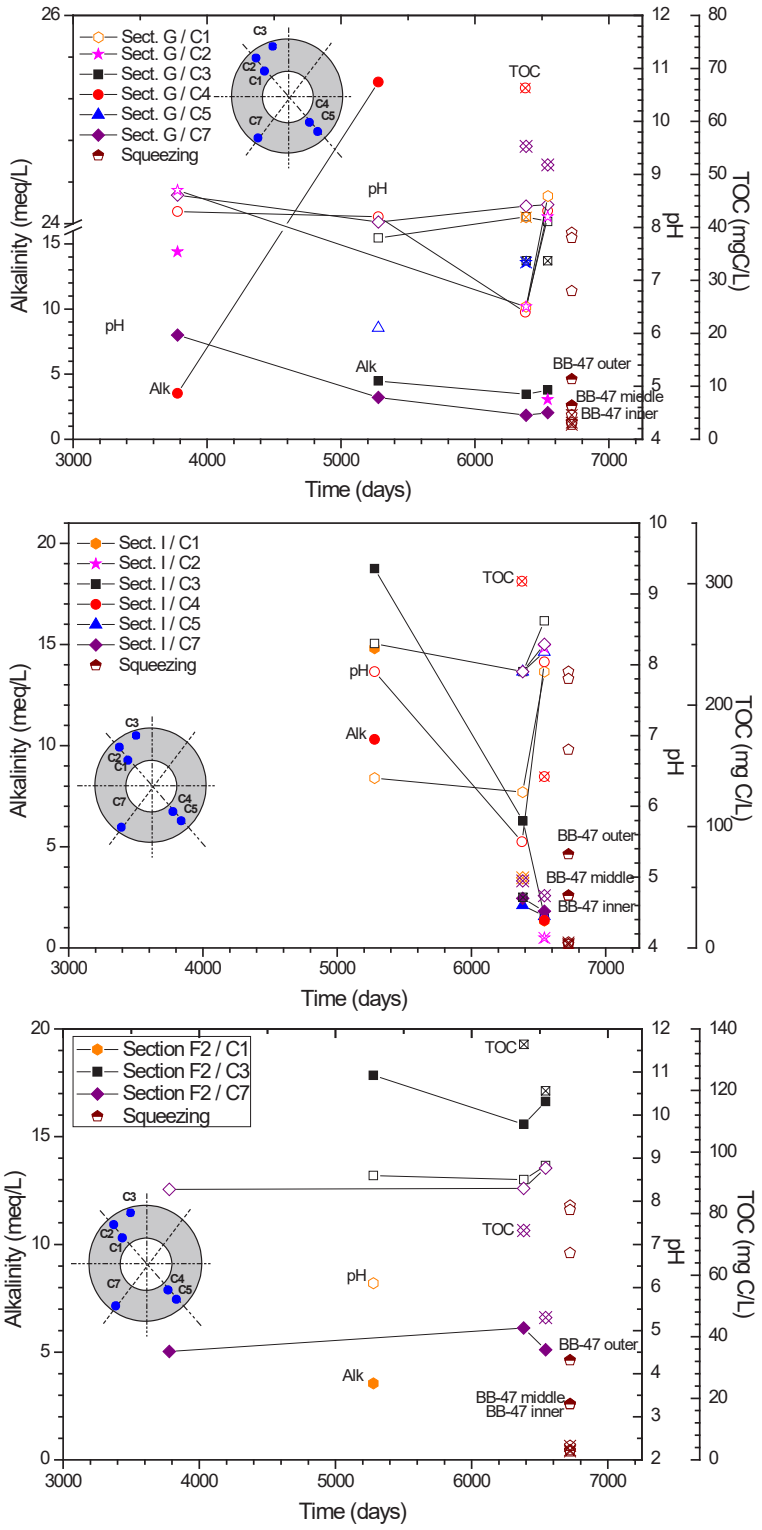

Fig. 112: pH, Alk and TOC contents as a function of time for the pipes in Sections G, I and F2

Data compared with porewaters obtained from squeezing tests of bentonite blocks from Section 47 (Fernández et al. 2018).

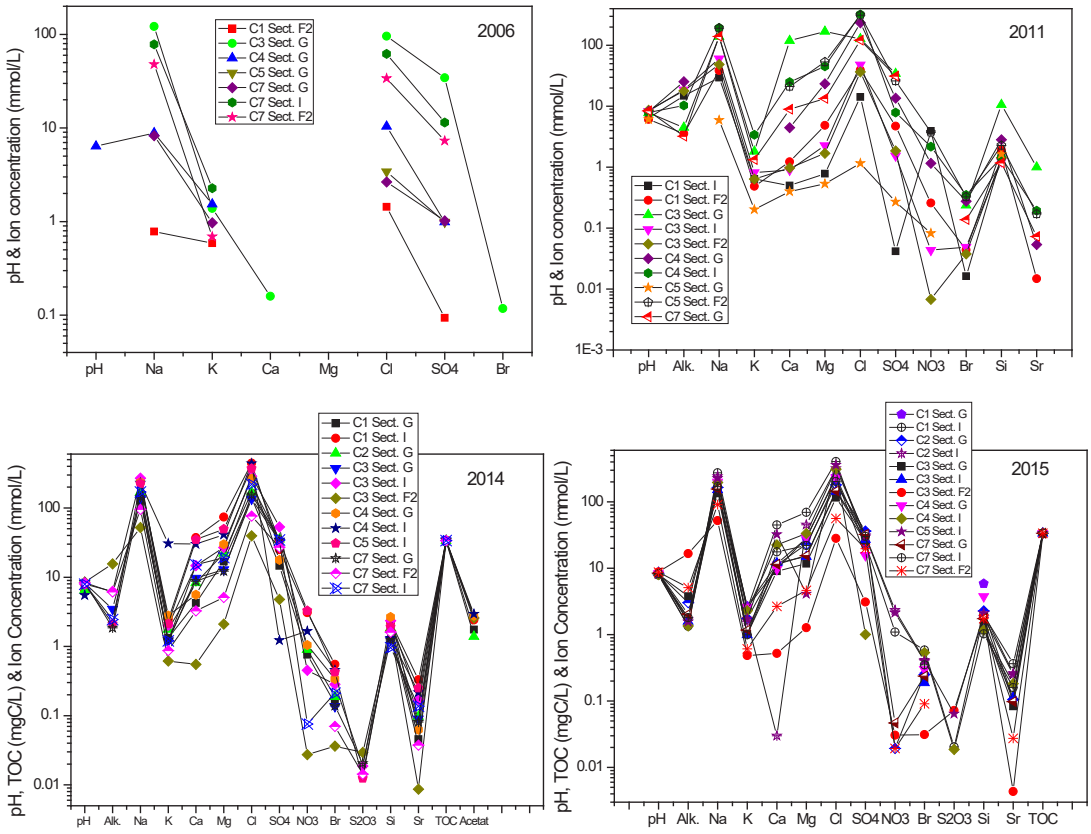

Fig. 113: Schoeller diagram for the porewaters obtained in the Cx pipes over time

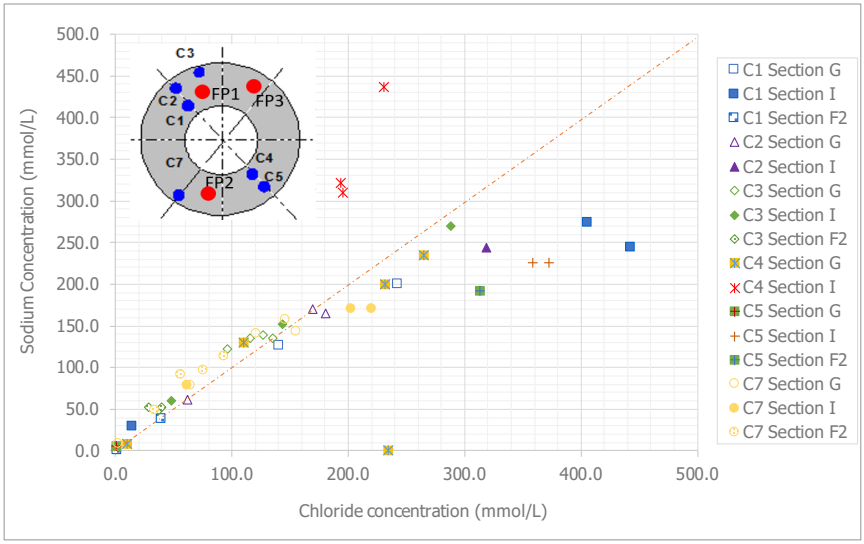

Fig. 114: Chloride versus sodium in Sections G, I and F2 from the different pipes over time

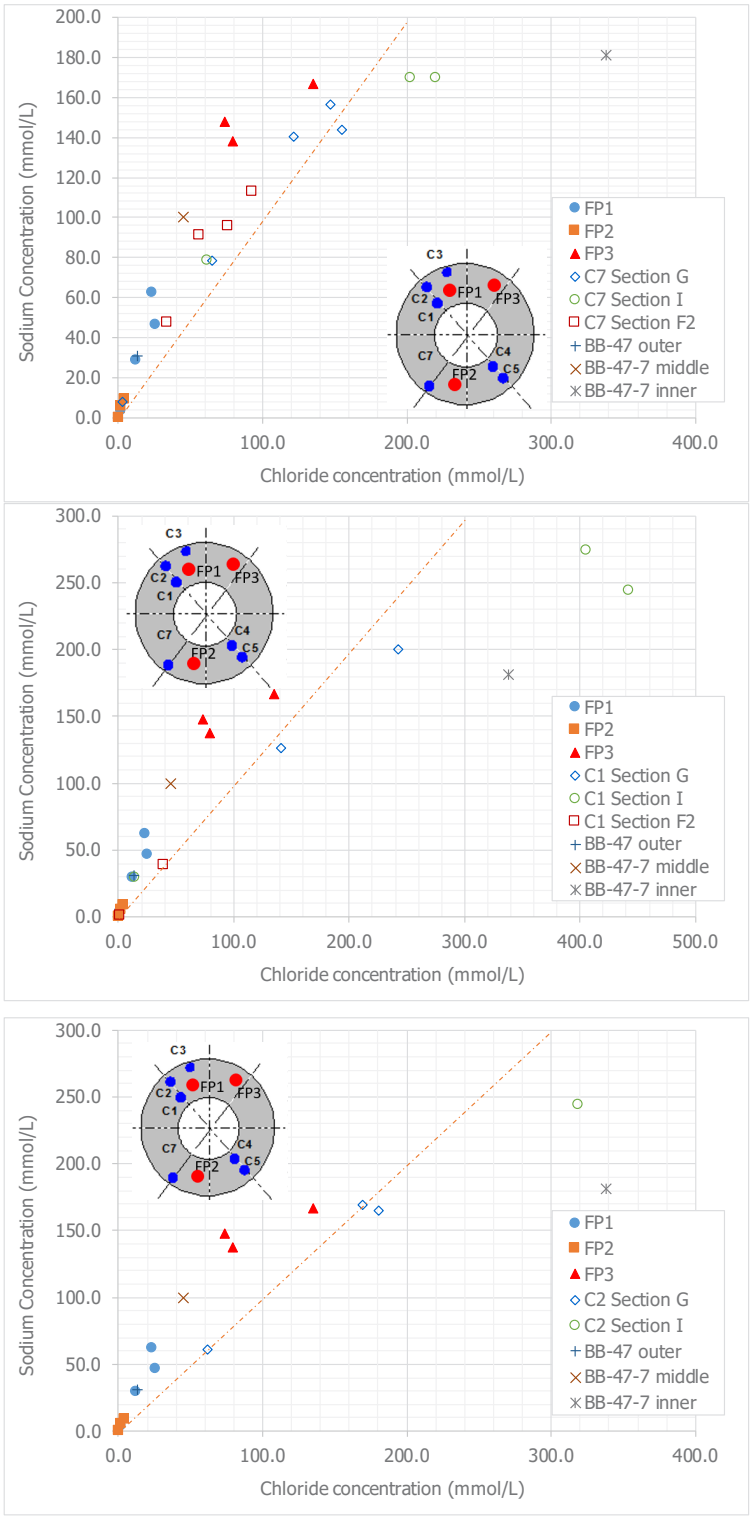

Fig. 115: Chloride versus sodium concentration in the porewater obtained from the gas pipes (FP1, FP2 and FP3) and C7, C1 and C2 pipes

Data are compared with squeezed porewaters in Section 47 at different bentonite rings.

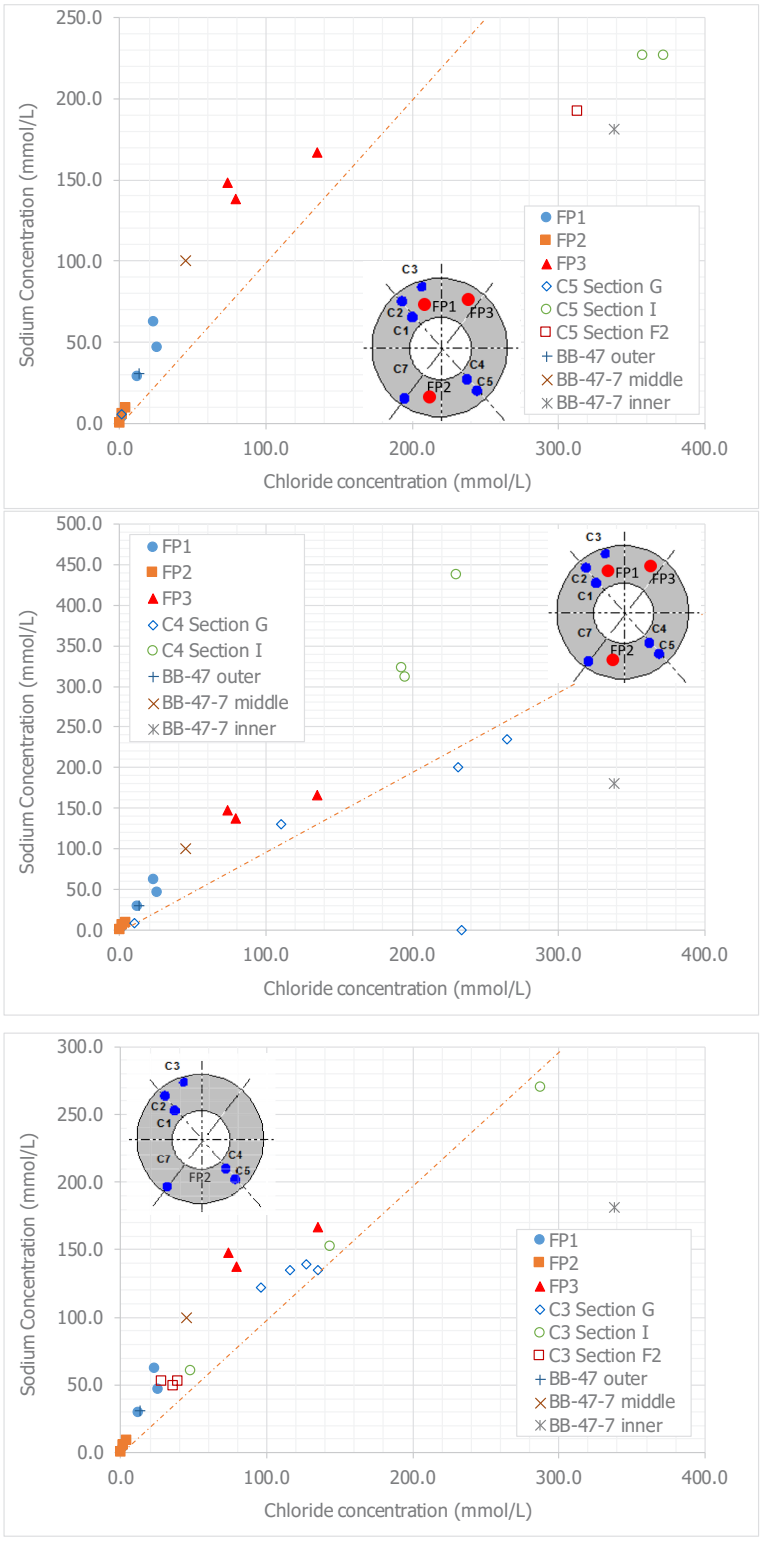

Fig. 116: Chloride versus sodium concentration in the porewater obtained from the gas pipes (FP1, FP2 and FP3) and C5, C4 and C3 pipes

Data are compared with squeezed porewaters in Section 47 at different bentonite rings.

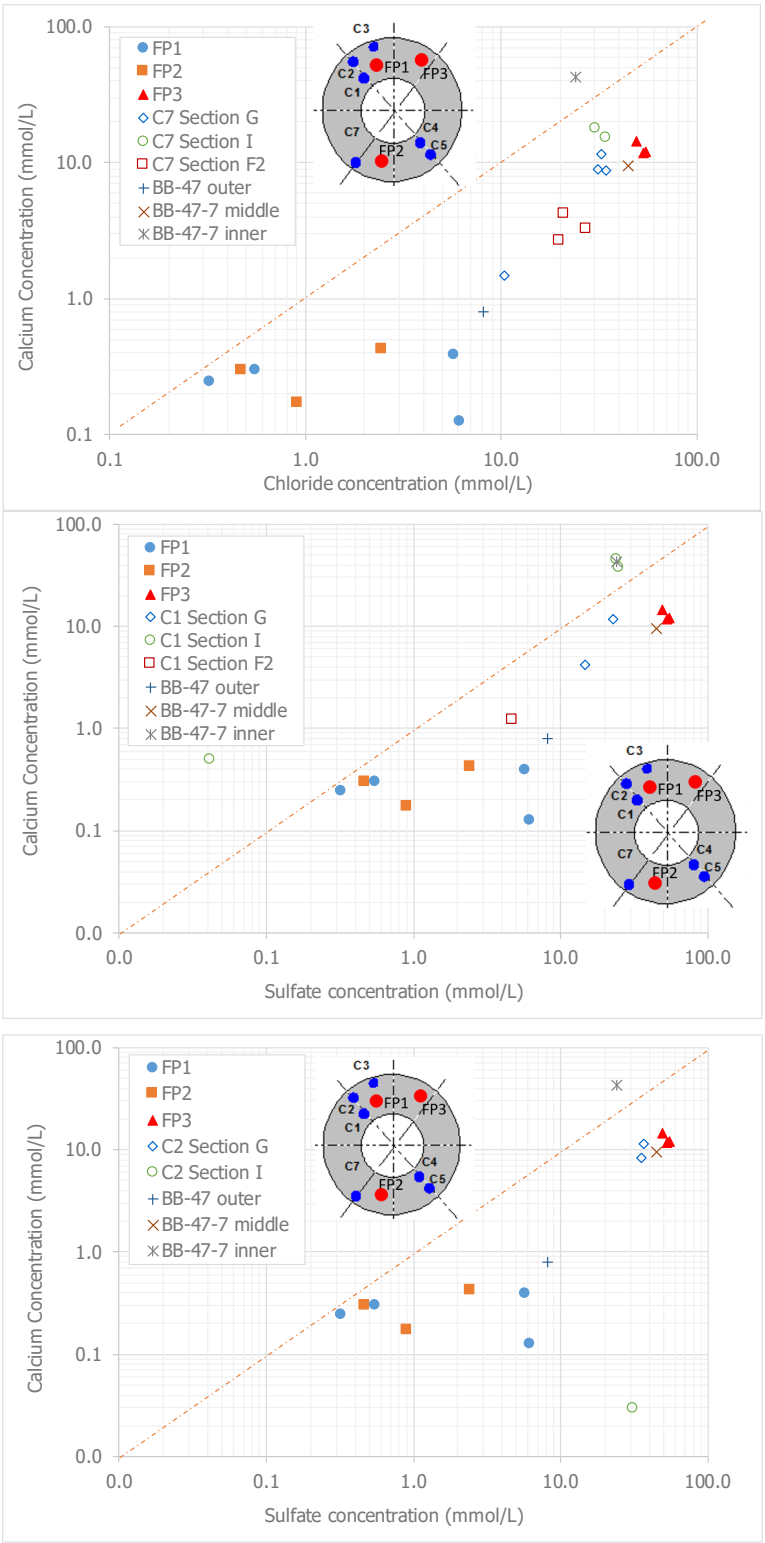

Fig. 117: Sulfate versus calcium concentration in the porewater obtained from the gas pipes (FP1, FP2 and FP3) and C7, C1 and C2 pipes

Data are compared with squeezed porewaters in Section 47 at different bentonite rings.

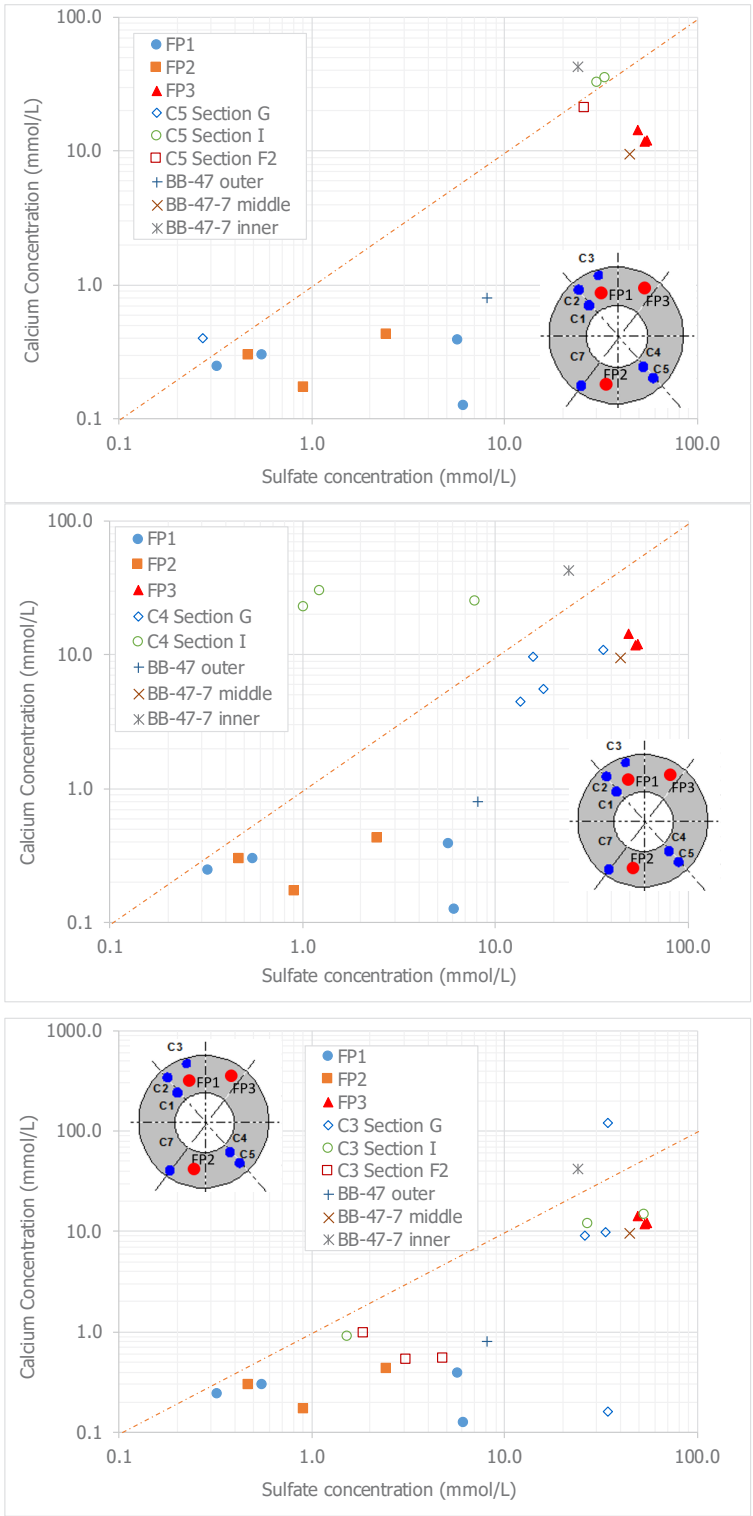

Fig. 118: Sulfate versus calcium concentration in the porewater obtained from the gas pipes (FP1, FP2 and FP3) and C5, C4 and C2 pipes

Data are compared with squeezed porewaters in Section 47 at different bentonite rings.

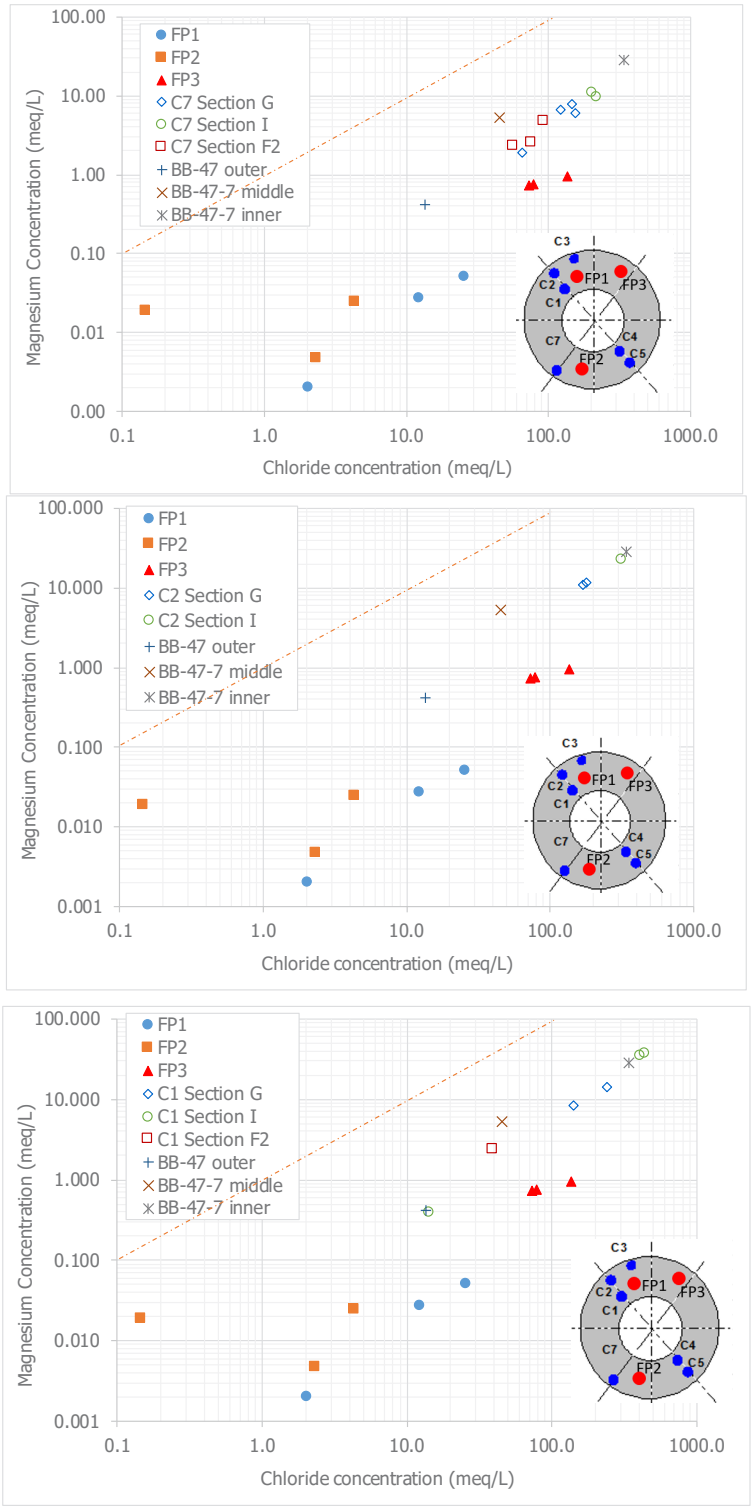

Fig. 119: Chloride versus magnesium concentration in the porewater obtained from the gas pipes (FP1, FP2 and FP3) and C7, C2 and C1 pipes

Data are compared with squeezed porewaters in Section 47 at different bentonite rings.

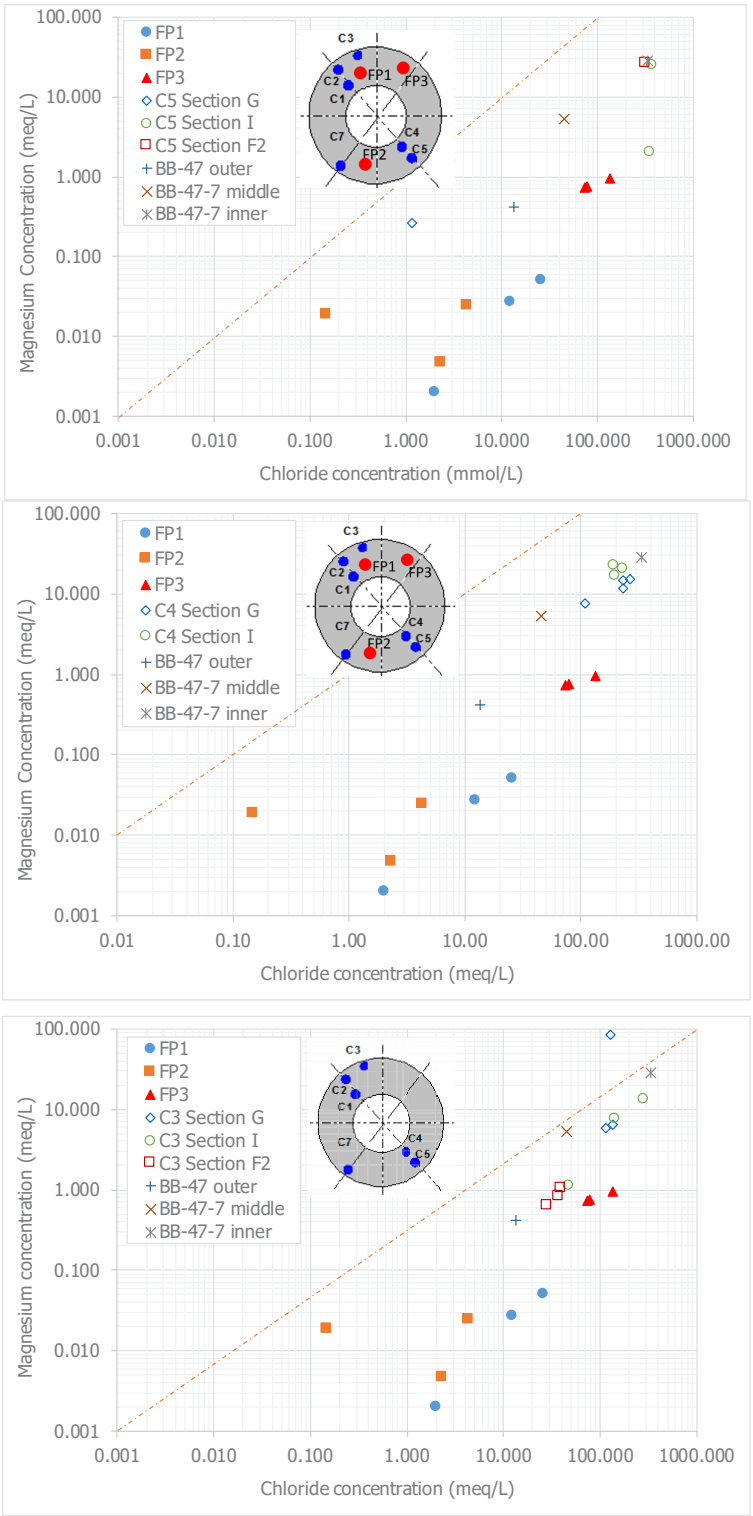

Fig. 120: Chloride versus magnesium concentration in the porewater obtained from the gas pipes (FP1, FP2 and FP3) and C5, C4 and C3 pipes

Data are compared with squeezed porewaters in Section 47 at different bentonite rings.

4.4 Redox conditions in the FEBEX *in situ* test

The behaviour of radionuclide transport in the near field is partly conditioned by the redox conditions in the EBS. These conditions strongly affect the mobility and sorption of many radionuclides, which is highly relevant in the safety assessment of an HLW repository. Knowledge of the redox conditions is, therefore, important for understanding the behaviour of radionuclides and the interpretation of the porewater chemistry evolution (Giroud, 2014).

Determination of redox conditions in a system is still no simple task and no universally accepted procedure or standardised approach exists (Christensen et al. 2000). The main problem in measuring redox potentials are:

a) the very slow chemical kinetics of redox reactions involving C, S and N species, especially in poorly mineralized systems such as granitic groundwaters

b) the common lack of internal equilibrium of redox processes

c) the presence of multiple redox couples, and d) the electrode poisoning (from organic matter, sulphide and bromide)

Actually, the only redox couple that may respond kinetically fast and have sufficient ion activity is the Fe(III)/Fe(II) redox couple, and measurements below -50 mV seem to suggest strongly reducing conditions (Christensen et al. 2000). However, the term redox can be used to characterize the dominating redox processes, and defining redox zones along a system may help to identify the major redox couples that control the redox potential (Wilson 1995, Appelo & Postma 2005, Langmuir 1997, Scott & Morgan 1990):

a) oxic (oxygen rich, O2 > 30 µM, Eh: +250 mV to +100 mV)

b) post-oxic or suboxic (iron rich, 1 µM ≤ O2 < 30 µM, Eh: +100 mV to 0 mV)

c) sulfidic (sulfide rich, O2 < 1 µM, H2S ≥ 1 µM; Eh: 0 mV to -200 mV)

d) methanic (methane rich, O2 < 1 µM; H2S < 1 µM); Eh: < -200 mV)

Electrochemical redox potentials in the FEBEX in situ test were obtained from porewaters collected from the different pipes over time (Tab. 13¸Tab. 20 to Tab. 24). The pore waters collected inside gas-tight Al-bags or in septum vials were introduced inside an anoxic glove box (< 1 ppm O_2), and the electrochemical redox potential (SHE) was measured with time, until a stable potential was obtained, which lasted more than 5 days in some samples. Simultaneously, the pH was also measured.

The results obtained from the GRS (FP-1, FP-2 and FP-3) and CIEMAT pipes (Section G, Section I, Section F2) are shown in Fig. 121. In the Second Operational Phase, most of the redox measurements values were below 0 mV (SHE). In spite of the difficulties in obtaining reliable quantitative redox potential data, values below –50 mV suggest that strongly reducing conditions prevailed in the FEBEX bentonite barrier. The Eh values are in zones belonging to different redox-sensitive species (Fig. 121). The Eh values are in zones belonging to different redox-sensitive species if the presence of organic matter is taken into account (Stumm & Morgan 1981): iron-reducing (< -50 mV), organic matter-reducing/fermentation (-200 < Eh < -150 mV), sulfate-reducing (-275 < Eh < -200 mV), and methanogenic (Eh < -250 mV).

As redox potential is difficult to measure on site, and taking into account that FEBEX in situ test was not designed for geochemical investigations and the poorly constrained redox conditions (due to it is not a gas-tight system), the redox conditions could be also derived from the gas evolution and the porewater composition. This is because a redox system may involve gases (O_2, N_2, H_2, CH_4, CO_2, ...), dissolved components (NO_3-, NH_4+, CH_2O (TOC), Fe^{2+}, Mn^{2+}, SO_4^{2-}, HS^-, H^+, ...),

as well as solids (FeOOH, MnO_2, $FeCO_3$, $MnCO_3$, ...) and components (Fe^{2+}, Mn^{2+}, NH_4^+, ...) associated with the solids by ion exchange (Christensen et al. 2000). Thus, the most important species that undergo redox reactions involve carbon, iron, sulfur and nitrogen. Therefore, the different processes that may influence the short- and long-term redox evolution in a HLW repository are:

a) metal corrosion

b) organic matter degradation

c) mineral oxidation/reduction (e.g., sulfate reduction)

d) fermentation due to microbial activity

In the FEBEX in situ test, the evolution of both gases (O_2, N_2, H_2, CH_4, CO_2, ...), and dissolved components in the porewater (Cl^-, SO_4^{2-}, NO_3^-, NH_4^+, CH_2O, Fe^{2+}, Mn^{2+}, SO_4^{2-}, H^+, ...), were measured over time from different pipes during in situ gas/water sampling campaigns. Thus, the analysis of the evolution of gases and porewater may allow us to follow the redox reactions involved in the FEBEX bentonite barrier during 18 years of heating and hydration.

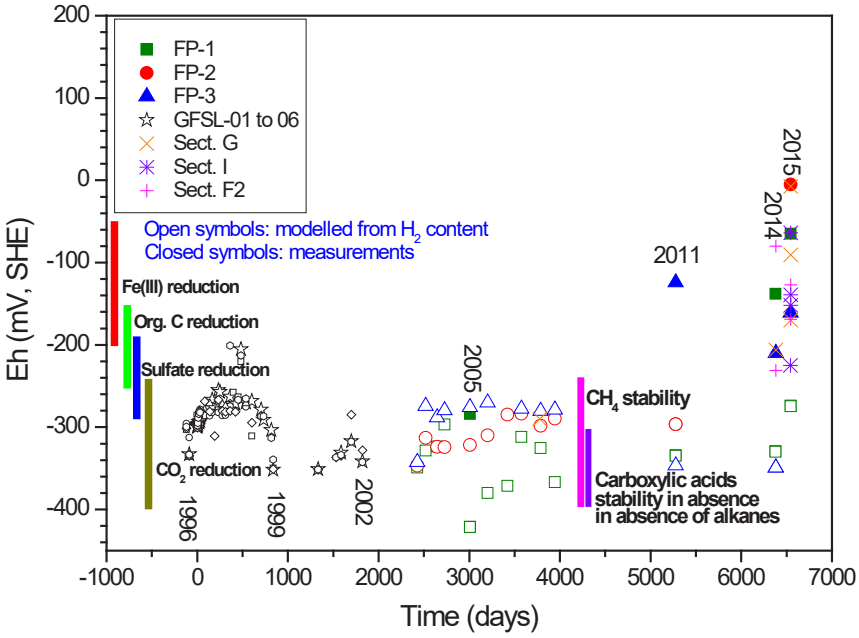

Fig. 121: Redox potential values obtained from the GRS and CIEMAT pipes located around the Heater #2

Vertical bar: theoretical redox potential at pH = 7 for different reactions. Open symbols: redox values modelled from the H_2 content

Furthermore, because the H_2(aq) concentrations constrain the redox state of the pore water, since the activity of H_2(aq) can be related directly to oxygen fugacity (fO_2) (Johnson et al. 1992):

$H_2O_{(l)} \leftrightarrow H_{2(aq)} + 0.5O_{2(g)}$ (reverse Knallgas reaction)

the measured hydrogen concentration was used for evaluating the redox potential by using the program PhreeqC (Parkhurst and Appelo, 2013), and the Thermoddem database (Blanc 2017). The solubilities of gases were described by Henry's law, which states that at constant T, the solubility of a gas in a liquid is proportional to the partial pressure of the gas: $H_2(g) = H_2(aq)$ with $H_2(aq) = P_{H2} \times K_H$ (M/bar), being K_H the Henry's constant for hydrogen ($K_H = 7.8 \times 10^{-4}$ M/bar at 25 °C and 1 atm.).

H_2 could be a general indicator of the predominant redox process and an indicator of the specific dominating TEAP (Terminal Electron Accepting Process), because anaerobic redox process can be characterised by a well-defined range of H_2 concentrations (Christensen et al. 2000, Lovley & Goodwing 1988):

e) NO_3-reduction: < 0.1 nM H_2

f) Fe-reduction: 0.2 – 0.6 nM H_2

g) sulfate-reduction: 1 – 4 nM H_2

h) CO_2 reduction: > 5 nM H_2

When the hydrogen gas content is used for modelling the Eh value of each sample, the theoretical redox zone was in the range between -221 (sulfate-reducing) to -244 mV (methanogenic), reducing conditions being attained from the beginning of the test.

From the analytical point of view, the redox measurements obtained from the porewater samples from the pipes surrounding Heater #1 were oxidized (Tab. 8), so this means that although some precautions were taken, the water samples were not anaerobic samples when analysed at CIEMAT. Indeed, at this First Operational Phase the main objective of GRS was to analyse only the gas composition inside the bentonite buffer, and not the chemical analysis of the water. However, according to redox potential obtained by geochemical modelling from the gas hydrogen content, those water samples should be at anoxic conditions.

In spite of the difficulties in obtaining reliable quantitative redox potential data, values below –50 mV suggest that strongly reducing conditions prevailed in the FEBEX bentonite barrier, at least during the Second Operational Phase. The precipitation of ferrous sulfide in some water samples is observed (Fig. 65 – Fig. 69), and the oxygen, methane and hydrogen evolution also corroborate that strongly reducing conditions existed. However, overlapping of different processes (nitrogen-, iron-, sulfate-, organic matter-reduction, and methanogenesis) could affect the global measurement. From hydrogen contents, reducing conditions were attained from the beginning of the test in some zones.

5 Lessons learned from gas/water samplings in the FEBEX *in situ* test

Although the FEBEX *in situ* test was not designed for geochemical investigations, and most of water samples were discarded, the pipes inserted inside the bentonite allowed to collect gas and water samples over time. In this section drawbacks about the methodology used and possible alternatives are discussed as possible recommendations for further gas/water sampling campaigns in other experiments.

Two different types of pipes were used for collecting gas and water samples from the compacted FEBEX bentonite barrier: ceramic filter pipes and 316L stainless steel sintered filter pipes. Although ceramic filter pipes are preferred for collecting gas and water samples because they are less reactive to chemical and mineral species from both the rock and porewater and better for redox measurements, they are not recommended in a non-saturated compacted bentonite barrier. The ceramic pipes used during the FEBEX *in situ* test during the First Operational Phase were broken, at least partially, due to the high swelling pressures generated, between 30 and 60 bar, during the hydration of bentonite. If the compacted bentonite (or an argillaceous rock formation with a lower swelling pressure) is saturated, ceramic pipes, PVC or polyethylene filter screens can be used without problems, as demonstrated for example in most of the bio-geochemical and gas-exchange experiments performed inside the Opalinus Clay at the Mont Terri Rock Laboratory (Vinsot et al. 2014, Bagnoud et al. 2016a), or inside the Callovo-Oxfordian Argillaceous Formation (Vinsot et al. 2013) at the Meause/Haute-Marne Underground Research Laboratory at Bure (France).

Porous stainless steel pipes used in the FEBEX *in situ* test, or in other experiments, such as in Opalinus Clay (Bagnoud et al. 2016b), proved efficient because they support high external pressures. However, some doubts regarding the possible corrosion, water chemistry interactions and redox state alteration may be pointed out. Nevertheless, the stainless steel sintered filters allowed following the gas and porewater evolution in the FEBEX bentonite barrier successfully. Most of the pipes did not suffer corrosion, at least no apparent corrosion after visual checks during the dismantling operations (García-Siñeriz et al. 2016: NAB 16-11, Kober & Van Meir 2015: NAB 16-68). Only one of the CIEMAT stainless steel filters, located at the bentonite Sampling Section 36, was highly corroded. But it should be taken into account that this filter was in contact with the dummy heater in a zone with a possible higher water inflow, due to its location in a lamprophyre area. Hence, galvanic corrosion at the contact with the liner could exist. Indeed, this is the zone where a higher corrosion was observed in the dummy-liner contact (Kober & Van Meir 2015: NAB 16-68, Wersin & Kober 2017).

During the FEBEX *in situ* test different collection devices were used for gas and water samples. Highly preserved septum vials were good enough for chemical analyses, but for an optimum gas and water collection and characterization, preserving the redox system, Al-foil bags or stainless steel cylinders covered with Teflon were the best option. Most of samples from the Febex *in situ* test were taken by using Al-foil bags, which gave very good results.

After gas collection, a carrier gas was used for flushing the gas/water sampling lines from the pipes (total volume ~ 3.5 L each one as average) to extract additional pore water samples. Nitrogen gas was used in most of the sampling campaigns for this issue, apart from filling the sampling circuit (total volume of ~ 0.2 L) with a pressure of 1 bar for avoiding degassing. However, helium gas was used in the last two campaigns (2014 and 2015). Nitrogen is the main gas dissolved in granitic waters and is generated and/or consumed in different bio-geochemical reactions, so using unreactive gases such as argon or helium, is recommended. Helium was used

in the FEBEX *in situ* test because reliable Ar gas data could provide valuable information on the contact of the samples with the atmosphere, which has an Ar content of 0.93 vol.-%; and because Grimsel granitic groundwater contains also Ar.

Most of the gas contents measured during the FEBEX *in situ* test were analysed from the gas phase (at equilibrium with water samples, but as a separated phase). This was because the initial purpose of GRS was only to analyse the gas phase, and most of the water samples were discarded. Therefore, the gas concentration dissolved in the water phase was missed in the FEBEX *in situ* test. In addition, not so much water could be sampled from the bentonite, especially from the pipes located at the inner sections. Because the analysis of dissolved gases is important and analytical methodologies have been improved since the construction of the FEBEX *in situ* test in 1996, these should be carried out in further experiments. Nowadays, *in situ* gas measurements are being performed in some experiments, such as in the HT-Experiment and FE-Experiments at Mont Terri, where gas monitoring of H_2, N_2, O_2, etc. is performed either with a Raman equipment installed after the sampling lines (Vinsot et al., 2014), or by different type of sensors installed inside a bentonite barrier (Vogt et al. 2015, Giroud et al. 2019, Tomonaga et al. 2019).

For a complete understanding of the processes and redox conditions involved in an engineered barrier system (EBS), a complete characterization of gas and porewater composition (including, Fe^{2+}, NH_4^+ S^{2-} and TOC) is needed; not only the main components of both phases, but also the isotopic gas and water composition, as well the characterization of organics species (pyruvate, lactate, acetate, other organic acids, etc.). This implies the installation of long sections of filters inside the bentonite for collecting a large enough water volume. In the CIEMAT pipes, the volume of water that could be extracted from the filters (5 – 10 mL) was not enough for these purposes. However, the long GRS filters, with an internal volume of ~ 3.5 L were excessively large due to the low permeability of the bentonite. It would be more interesting to install different filters of about 50-100 mL distributed along the bentonite barrier for analysing gas and water samples at different locations, discriminating processes occurring at different zones. In any case, any type of system for extracting water should take into account the conditions in the bentonite in terms of physical space, swelling pressure or suction pressure.

Finally, a microbiological analysis of water samples should be performed. This was tried in the 2015 sampling campaign from the GRS pipes, because in 2014 a lot of water could be sampled, which was slightly turbid and in addition with few black particles. However, because of the low bentonite permeability and the small time gap between the last two sampling campaigns (5 months), not enough water could be obtained for a complete analysis.

6 Summary

In different phases of the FEBEX *in situ* test (First Operational Phase: 1996 – 2002, and Second Operational Phase: 2002 – 2015), various pipes were introduced inside the bentonite buffer for analysing the gas generation/consumption and the chemical composition of the porewater. GRS introduced six ceramic filter pipes 3 m long around Heater #1 in 1996 (called GF-SL-x) and three sintered stainless steel pipes around Heater #2 in 2003 (called FP-x), with the aim of mainly analysing the evolution of gases. CIEMAT installed six stainless steel filter pipes around Heater #2 in 2003 (called Cx) for determining the chemical evolution of the pore water chemistry and recording the relative humidity and temperature.

Different gas/water sampling campaigns were performed since 1996 until 2011, before and after dismantling of Heater #1. Two additional campaigns were carried out in 2014 and 2015 prior to dismantling the Heater #2 for collecting gas and porewater samples and to establish the redox state inside the bentonite barrier.

For GRS gas studies, the total volume inside the pipes was 3.78 L during the First Operational Phase (ceramic filters), and 3.20 L during the Second Operational Phase (sintered stainless steel filters). Prior to collect the gas samples from each pipe, the interval fluid pressure was measured, and the external sampling circuit (0.2 L volume) was filled with a carrier gas at a pressure of 1 bar for avoiding degassing. N_2 was used as carrier gas in all sampling campaigns, except in 2014 and 2015 when He was used. After recirculation and homogeneization of the fluid inside each pipe, samples (a gas/water mixture) were collected mainly inside Al-bags.

The main gases detected in the FEBEX *in situ* during the 18 years of experiment were O_2, N_2, CO_2, CO, H_2, CH_4 and other saturated and unsaturated aliphatic hydrocarbons (alkanes up to C4 chain length: ethane (C_2), propane (C_3) and isobutane (iC_4); and alkenes). In the two last 2014 and 2015 sampling campaigns, n-alkanes up to C5 chains (saturated) and n-alkenes (unsaturated) hydrocarbons were also detected in all pipes.

Oxygen was consumed very rapidly (around 83 % lower than atmospheric in 1 – 2 years). However, oxygen was never depleted, showing minimum values between 3 and 0.2 vol.-%. The presence of a remaining O_2 may be due to: a) atmospheric air income, transported from the gallery access towards the barrier through the concrete plug, responding to atmospheric pressure variations; b) gas/water sampling artefacts and other monitoring activities (gas permeability measurements, water and colloid sampling from radial and parallel boreholes drilled in the granitic formation, which ended in the test interval of the FEBEX *in situ* test); and c) Excavation disturbed zone (EDZ) effects. Indeed, the FEBEX *in situ* test cannot be considered a gas-tight system. However, the presence of hydrogen, methane and other hydrocarbons indicate spatial microenvironments where anoxic/anaerobic conditions were established, as observed by the reducing redox potentials measured in some pore waters collected from the different pipes. Electrochemical Redox potential measurements indicated Eh values below – 50 mV, suggesting strongly reducing conditions in the bentonite barrier. In addition, Eh values, obtained by geochemical modelling from dissolved H_2 concentrations, pointed to theoretical redox zones in the range between -221 (sulfate-reducing) to -244 mV (methanogenic) during the First (1996 – 2002) and Second Operational phases (2002 – 2015).

The major content of gases (> 93 vol.-%, range: 93 – 99 vol.-%) was nitrogen and oxygen, the sum of remaining gases being only between 0.5 and 6.7 vol.-% on average. When oxygen decreases (or is consumed), the amount of nitrogen (plus helium in the two last campaigns) increases in vol.-% (> 92 vol.-%), indicating the low generation rate (or deficit due to migration)

of other type of gases in the test. The total gas content of these other gases (H_2, CO_2, CH_4, etc.) was higher when Heater # 2 was running, higher as a function of the heater contact, and higher depending on the nature of surrounding materials. For example, in the pipe FP-1 which was close to a corroded fissurometer, the total gas content of other gases than O_2 and N_2 was higher than in the rest of pipes (average contents of 6.7, 5.1 and 2.9 vol.-% for pipes FP-1, FP-2 and FP-3, respectively; whereas in GF-SL-x pipes the values ranged from 0.5 (external pipe GF-SL-1 close to granite) to 3 vol.-% (internal pipe GF-SL-5 close to Heater #1)).

Apart from low gas content of other gases, the increase of N_2 over time until almost a plateau value (~95 vol.-%), may be related with the drop of total pressure during O_2 consumption, enhancing the gas inflow into the barrier, and the entrance of atmospheric air from the access gallery due to no airtight conditions. However, N_2 could be also introduced inside the barrier during the saturation process of the bentonite due to Grimsel groundwater contains dissolved nitrogen (N_2 gas content of 98.5 vol.-% or $P_{N2} = 10^{-0.0065}$ atm).

Once the O_2 is practically consumed, the decrease of nitrogen in some periods of time is related with the higher generation of other gases, i.e. to different (bio-)geochemical reactions. For example, in pipe FP-1 N_2, O_2, H_2 and CH_4 contents were 59 vol.-%, 1.5 vol.-%, 0.3 vol.-% and 28 vol.-%, respectively, in 2014 (even though the He gas content was 9 vol. %); whereas they were 95 vol.-%, 1.6 vol.-%, 8.7 vol.-% and 0.9 vol.-%, respectively, in 2011.

Methane and other light hydrocarbons, such as ethane (C_2), propane (C_3) and isobutane (iC_4), were detected from the beginning of the experiment. At the beginning of both phases the sum of the concentration of light hydrocarbons (C2, C3, iC4), was higher than methane concentration. Methane increased over time at different rates, depending on the progressive consumption of O_2 and the variations in hydrogen. Hydrocarbons can result from organic degradation/oxidation processes. Apart from cellulose filters for tracers deposition placed at the bentonite-granite interface (1.371 kg as total amount), other organic material could be degraded over time, such as the initial organic matter present in the bentonite (0.096 wt.-% as organic carbon, which implies 111 kg in the total barrier), and degradable resins or plastics from cables and tubings. However, the generation of large amounts of hydrocarbons from these sources should not be expected due to their content and the temperatures (< 100 °C). The lowest values of total hydrocarbons were found in the pipes located close to the granite interface, and the highest values in pipes close to the heaters.

Hydrogen was present from prior to switching on the heaters and oxygen was consumed; and its content showed large fluctuations over time depending on oxygen contents, the location of the pipe (close to granite contact or heater contact) and the presence of corroded sensors. Hydrogen is mainly due to anoxic corrosion of metals and possibly fermentation of organic matter in its acidogenesis phase. Starting from a high H_2 content (up to 2000 vpm or ppmv), there was a large decrease of hydrogen, correlated with the decrease of oxygen and the increase of methane and CO_2. Hydrogen increased rapidly after oxygen depletion, and then its concentration was more or less maintained over time or decreasing slightly, depending on the location of the pipe and nature of the surrounding metals.

Carbon dioxide increased rapidly over time from atmospheric value to 10 vol.-%, the variations in CO_2 concentration being produced due to different water/bentonite interactions and/or organic matter degradation since CO_2 is practically absent in the granite groundwater. The higher values were observed during the First Operational Phase during the saturation process of the bentonite and decreased during the Second Operational Phase. CO content was only measured during the First Operational Phase, and it was always higher than atmospheric content increasing over time up to ~ 40 vpm.

Most of the fluid pressures measured, both in the GRS and CIEMAT pipes maintained values similar to atmospheric pressure. Any excess of gas pressure generated could be dissipated because the FEBEX *in situ* test was an open system (e.g. towards release pathway to the open tunnel), and, in addition, most of the gases generated could be consumed in different (bio-)geochemical processes. In the GRS pipes, fluid pressures ranged between 0.805 and 0.929 bar over time. Small fluctuations of pressure (~0.132 bar) are probably due to atmospheric pumping of the air inside the buffer, possibly through the cables perforating the concrete plug and the EDZ, and favoured by temperature variations. Only an increase of fluid pressures (between 2.5 and 4.5 bar) was detected in the GRS ceramic pipes located at the granite interface during the First Operational Phase, when Heater #1 was running; which was related to porewater pressures because the saturation phase of the bentonite. In CIEMAT pipes the fluid pressures measured during the Second Operational Phase correspond to water pressures, the values ranging between 0.775 and 2.320 bar.

Porewater from the FEBEX *in situ* test was collected and analysed over time from both the GRS and CIEMAT pipes. In the two last campaigns (2014 and 2015), the composition of the pore water from the GRS pipes was analysed by Hydroisotop from the gas/water mixture samples firstly collected inside Al-bags. These analyses were in good agreement with the chemical composition of waters obtained by CIEMAT from water samples taken after gas collection in a subsequent sampling of each pipe by flushing the sampling lines with He carrier gas (the lines being left under vacuum at the end of each sampling campaign).

The chemical composition of the porewaters is mainly Na-Cl type with ionic strengths ranging between 0.01 to 0.4 M. The composition of the collected waters was in the range of those found from squeezed bentonite block samples (outer, middle and inner blocks) obtained during the dismantling operations in 2002 and 2015. Chloride contents increased towards the inner parts of the bentonite barrier due to the infiltration of granite groundwater and advective transport of solutes, cations being controlled by dissolution/precipitation processes and exchange reactions, as observed in squeezing and aqueous leaching experiments (Fernández et al. 2018). However, differences in the chemical composition among all extracted porewaters with respect its location were found. In any case, the salinity of the porewaters from the CIEMAT pipes, in terms of Cl content or ionic strength, was much higher than those found in the GRS pipes.

The gases analysed in the FEBEX *in situ* test were generated and consumed by different (bio-) geochemical reactions: corrosion of different metallic components (liner, heater, fissurometer, sensors, bolts, etc.) and organic matter degradation, as visually observed from the bentonite state during dismantling operations of the compacted material around Heater #1 (in 2002) and Heater #2 (in 2015). Corrosion of metallic compounds consumes O_2, H_2O and CO_2 (by carbonate precipitation) and produces H_2 under anaerobic conditions; whereas the degradation of organic compounds, microbially mediated or by abiotic oxidation reactions, may produce H_2, CO_2, CO, CH_4 and other hydrocarbons, and consumes O_2. However, the impact of these possible reactions was not homogeneous in the whole bentonite barrier, as observed in the gas content variations in the different pipes over time (e.g., hydrogen content was higher in pipes close to corroded metals). The variations in gas content depended on the location of the pipes (close to granite interface or to heater contact) and on the surrounding materials (metals, plastics, cellulose, etc.). In any case, data interpretation of the results showed in this report is beyond the scope of the current report.

7 References

Abós, H. & Martínez, V. (AITEMIN) (2015): Sample Log Book 34 to 62 FEBEX-DP. AN 15-578 September 2015.

AITEMIN (2002): Sampling plan for dismantling of Section 1 of in situ test. Sampling book. Procedure 70-AIT-G-6-27.

AITEMIN (2014): Sensors Data Report, In Situ Experiment. Report Nº: 8 – Full Report, June 2014.

Amann-Hidenbrand, A., Kross, B.M., Harrington, J., Cuss, R., Davy, C., Skoczylas, F., Jacops, E. & Maes, N. (2015): Gas transfer through clay barriers. In: Natural and Engineered Clay Barriers. Eds. Tournassat, C., Steefel, C.I., Bourg, I.C., Bergaya, F. Developments in Clay Science 6, 227-267.

Appelo, C.A.J. & Postma, D. (2005): Geochemistry, Groundwater and Pollution**.** A.A. Balkema Publishers, Leiden, The Netherlands. 2nd Ed., 649 pp.

Bagnoud, A., de Bruijn, I., Andersson, A.F., Diomidis, N., Leupin, O.X., Schwyn, B. & Bernier-Latmani, R. (2016b): A minimalistic microbial food web in an excavated deep subsurface clay rock. FEMS Microbiology Ecology 92, 1-11.

Bagnoud, A., de Bruijn, I., Leupin, O.X., Schwyn, B. & Bernier-Latmani, R. (2016a): Rates of microbial hydrogen and sulfate reduction in Opalinus Clay rock. Applied Geochemistry 72, 42-50.

Bárcena, I., Fuentes-Cantillana, J.L. & García-Siñeriz, J.L. (2003): Dismantling of the Heater 1 at the FEBEX in situ test. Description of operations. Enresa Technical Report 9/2003.

Bárcena, I. & García-Siñeriz, J.L. (2015a): FEBEX-DP (GTS) Full Dismantling Sampling Plan. Nagra Arbeitsbericht NAB 15-14.

Bárcena, I. & García-Siñeriz, J.L. (2015b): FEBEX-DP (GTS) Full Dismantling Test Plan. Nagra Arbeitsbericht NAB 15-15.

Bengtsson, A., Blom, A., Taborowski, T., Schippers, A., Edlund, J. & Pedersen, K. (2017): FEBEX-DP: Microbial Report. Nagra Arbeitsbericht NAB 16-15.

Bernard, B.B., Brooks, J.M. & Sackett, W.M. (1977): A geochemical model for the characterization of hydrocarbon gas sources in marine sediments. Proc. Offshore Technol. Conf., 2934, 435–438.

Blanc, P. (2017): Thermoddem: update for the 2017 version. Report BRGM/RP-66811-FR, 20 pp.

Boyd, S. R., Hall, A. & Pillinger, C. T. (1993): The measurement of $\delta^{15}N$ in crustal rocks by static vacuum mass spectrometry: Application to the origin of the ammonium in the Cornubian batholith, southwest England. Geochim. Cosmochim. Acta 57, 1339–1347.

Bradbury, M. & Baeyens, B. (1998): A physicochemical characterization and geochemical modelling approach for determining porewater chemistries in argillaceous rocks. Geochimica et Cosmochimica Acta*,* 62, No. 5, 783–795.

Bradbury, M.H. (1989): Laboratory investigations in support of the migration experiments. Nagra Technical Report 88–23.

Christensen, T.H., Bjerg, P.L., Banwart, S.A., Jakobsen, R., Heron, G. & Albrechtsen, H-J. (2000): Characterization of redox conditions in groundwater contaminant plumes. Journal of Contaminant Hydrology, 45, 165–241.

Cuevas, J., Villar, M.V., Fernández, A.M., Gómez, P. & Martín, P.L. (1997): Porewaters extracted from compacted bentonite subjected to simultaneous heating and hydration. Applied Geochemistry 12, 473–481.

Daucouse, D. & Lloret, A. (2003): Results of *in situ* measurements of water content and dry density. FEBEX-II internal Report 70-UPC-L-5-012, 103 pp.

ENRESA (2000): FEBEX Project. Full-scale engineered barriers experiment for a deep geological repository for high level radioactive waste in crystalline host rock. Final Report. Technical Publication ENRESA 1/2000, 354 pp. Madrid.

Fernández A.M. (2004): Caracterización y modelización del agua intersticial en materiales arcillosos: Estudio de la bentonita de Cortijo de Archidona. Ph. D. Thesis. CIEMAT, Madrid, 505 pp.

Fernández A.M. & Villar, M.V. (2010): Geochemical behaviour of a bentonite barrier: results up to 8 years of thermo-hydraulic treatment in the laboratory. Applied Geochemistry 25, 809–824.

Fernández, A.M. & Rivas, P. (2005): Porewater chemistry of saturated Febex bentonite compacted at different densities. In: Alonso, E.E., Ledesma, A. (Eds.), Advances in understanding Engineered Clay Barriers. A.A. Balkema Publishers, Leiden, pp. 505–514.

Fernández, A. M., Sánchez-Ledesma, D. M., Tournassat, C., Melón, A., Gaucher, E. C., Astudillo, J. & Vinsot, A. (2014): Applying the Squeezing Technique to Highly Consolidated Clayrocks for Porewater Characterisation: Lessons Learned from Experiments at the Mont Terri Rock Laboratory. Applied Geochemistry, 49, 2):21.

Fernández, A.M., Baeyens, B., Bradbury, M. & Rivas, P. (2004): Analysis of the porewater chemical composition of a Spanish compacted bentonite used in an engineered barrier. Physics and Chemistry of the Earth 29, 105–118.

Fernández, A.M., Cuevas, J. & Rivas, P. (2001): Porewater chemistry of the FEBEX bentonite. In: Hart, K.P. and Lumpkin, G.R. (Eds.), Scientific Basis for Nuclear Waste Management XXIV. Mat. Res. Soc. Symp. Proc. 663, 573–588.

Fernández, A.M., Jockwer, N. & Martín P.L. (2007): Evolution of the Chemical Parameters in the FEBEX in situ experiment. NF-PRO Project (Contract Number: FI6W-CT-2003-02389). Deliverable D2.2.10, 32 pp.

Fernández, A.M., Sánchez-Ledesma, D.M., Melón, A., Robredo, L. M., Labajo, M., Clavero, M.A., Carretero, S. & González, A.E. (2018): Thermo-hydro-chemical (THC) behaviour of a Spanish bentonite after dismantling of the FEBEX *in situ* test at Grimsel Test Site. FEBEX-DP Project. Nagra Arbeitsbericht NAB 16-25.

Frick, U., Alexander, W.R., Baeyens, B., Bossart, P., Bradbury, M.H., Bühler, Ch., Eikenberg, J., Fierz, Th., Heer, W., Hoehn, E., McKinley, I.G. & Smith, P.A. (1992): The radionuclide migration experiment – Overview of investigations 1985 – 1990. Nagra Technical Report NTB 91-04.

Fuentes-Cantillana, J.L. & García-Siñeriz, J.L. (1998): FEBEX Full-scale Engineered Barriers Experiment in Crystalline Host Rock. Final Design and installation of the "in situ" Test at Grimsel". Enresa Technical Report 12/98.

Fuentes-Cantillana, J.L., García-Siñeriz, J.L., Franco, J.J., Obis, J., Pérez, A., Jullien, F., Alberdi, J., Barcala, J.M., Campos, R., Cuevas, J., Fernández, A.M., Gamero, E., García, M., Gómez, P., Hernández, A., Illera, A., Martín, P.L., Melón, A.M., Missana, T., Ortuno, F., Pardillo, J., Rivas, P., Turrero, M.J., Villar, M.V., Mingarro, M., Pelayo, M., Caballero, E., Cuadros, J., Huertas, F., Huertas, F.J., Jiménez de Cisneros, C., Linares, J., Bazargan-Sabet, B., Ghoreychi, M.; Jockwer, N., Wieczorek, K.; Kickmaier, W., Marschall, P. (Nagra); Martínez, M.A.; Carretero, P., Dai, Z., Delgado, J., Juncosa, R., Molinero, J., Ruiz, A., Samper, J., Vázquez, A. ; Alonso, E., Carrera, J., Gens, A., García-Molina, A.J., Guimera, J., Guimaraes, L.do N., Lloret, A., Martínez, L., Olivella, S., Pintado, X., Sánchez, M., Elorza, F.J., Borregón, J.L., Canamon, I., Rodriguez Pons-Esparver, R., Fariña, P., Farias, J. & Huertas, F. (2000): FEBEX full-scale engineered barriers experiment for a deep geological repository for high level radioactive waste in crystalline host rock Final Report. Enresa, Technical Report 1/2000.

Fuentes-Cantillana, J.L., García-Siñeriz, J.L., Obis, J., Pérez, A.; Alberdi, J., Barcala, J.M., Campos, R., Cuevas, J., Fernández, A.M., Gamero, E., García, M., Gómez, P., Hernández, A., Illera, A., Martín, P.L., Melón, A.M., Mingarro, M., Ortuño, F., Pardillo, J., Pelayo, M., Rivas, P., Rodriguez, V., Turrero, M.J., Villar, M.V.; Caballero, E., Jiménez de Cisneros, C., Linares, J. ; Martínez, M.A. ; Samper, J., Delgado, J., Juncosa, R., Molinero, J., Alonso, E., Carrera, J., Gens, A., García-Molina, A.J., Guimera, J., Guimaraes, L.do N., Lloret, A., Martínez, L., (UPC-DIT); Elorza, F.J., Borregón, J.L., Fariña, P., Farias, J. & Huertas, F. (1998): FEBEX full-scale engineered barriers experiment in crystalline host rock. Pre-operational Stage. Summary Report. Enresa Technical Report 01/98.

García-Gutierrez, M. (2001): Tracers in the FEBEX Project. Internal Report 70-IMA-L-0-33, 34 pp.

García-Siñeriz, J.L., Abós, H., Martínez, V., De la Rosa, C., Mäder, U. Kober, F. (2016. FEBEX DP: Dismantling of heater 2 at the FEBEX *in situ* test. Description of operations. Nagra Arbeitsbericht NAB 16-11.

Garralón, A., Gómez, P., Peña, J., Buil, B., Turrero, M.J., Torres, E. & Sánchez, L. (2017): Hydrogeochemical characterization of the groundwater in the FEBEX gallery. Nagra Arbeitsbericht NAB 16-14.

Giroud, N. (2014): FEBEX - Assessment of redox conditions in Phase 2 before dismantling. Nagra Arbeitsbericht NAB 14-55.

GRS (1996): Project FEBEX. Installation Report of Pressure Pipes and Filter Pipes for Gas sampling and Permeability Measurements. Braunschweig, December 1996.

Hoehn, E., Fierz, T.H. & Thorne, P. (1990): Hydrogeological characterization of the migration experimental area at the Grimsel Test Site. Nagra Technical Report NTB 89-15.

Holloway, J.M. & Dahlgren, R.A. (2002): Nitrogen in rock: occurrences and biogeochemical implications. Global Biogeochemical cycles 16, 1118.

Horseman, S.T., Harrington, J.F. & Sellin, P. (1999): Gas migration in clay barriers. Eng. Geol. 54, 139–149.

Huertas, F., Fariña, P., Farias, J., García-Siñeriz, J.L., Villar, A.M., Fernández, A.M., Martín, P.L., Elorza, F.J., Gens, A., Sánchez, M., Lloret, A., Samper, J. & Martínez, M.A. (2006): FEBEX Project. Full-scale engineered barriers experiment for a deep geological repository for high level radioactive waste in crystalline host rock. Updated Final Report 1994–2004. Technical Publication ENRESA 5-0/2006, 590 pp. Madrid.

Jockwer, J. & Wieczorek, K. (2003): Gas generation measurements in the FEBEX Project. In: Workshop "Clays in Natural and Engineered Barriers for Radioactive Waste Confinement. Experiments in Underground Laboratories", Reims, France, Dec. 2002. Technical report published by Agence nationale pour la gestion des déchets radioactifs, Châtenay-Malabry, France, pp. 108–117.

Jockwer, J. & Wieczorek, K. (2008): Investigations on gas generation, release, and migration in the frame of FEBEX. GRS Report 243, 79 pp.

Jockwer, N. & Wieczorek, K. (2001): First Operational Phase: Gas sampling and analysis. FEBEX-II project. Project deliverable D02, 32 pp.

Jockwer, N., Wieczorek, K. (1999): FEBEX Summary Report 1996-1999: GRS Contribution. Investigation of Gas Generation, Release and Migration. FEBEX Project internal report.

Johnson, J.W., Oelkers, E.H. & Helgeson, H.C. (1992): SUPCRT92: Software package for calculating the standard molal thermodynamic properties of minerals, gases, aqueous species and reactions among them as function of temperature and pressure. Comp. Geo. 18, 899–947.

Johnson, L.H. (2006): Gas production and transport in the near field of SF and HLW repositories in clay and crystalline rocks: Processes, uncertainties and performance assessment aspects. Deliverable Nº 5.1.6. of the NF-PRO project. EU Contract Nº F16W-CT-2007-01.

Kenward, P.A., Godstein, R.H., González, L.A. & Roberts, J.A. (2009): Precipitation of low-temperature dolomite from an anaerobic microbial consortium: the role of methanogenic Archaea. Geobiology, 7, 556–565.

Kober, F. (2015): FEBEX-DP. Summary of Daily Reports 1 to 104. Nagra Aktennotz AN 15-618.

Kober, F. & Van Meir, N. (2017): FEBEX-DP – Dismantling related supplementary documents. Nagra Arbeitsbericht NAB 16-68.

Konno, U., Kouduka, M., Komatsu, D.D., Ishii, K., Fukuda, A., Tsunogai, U., Ito, K. & Suzuki, Y. (2013): Novel microbial populations in deep granitic groundwater from Grimsel Test Site, Switzerland. Microb. Ecol. 65, 626–637.

Langmuir, D. (1997): Aqueous Environmental Geochemistry. Prentice Hall, New Yersey, 600 pp.

Lanyon G.W. & Gaus, I. (2016): Main outcomes and review of the FEBEX-In Situ Test (GTS) and Mock-Up after 15 years of operation. Nagra Arbeitsbericht NAB 15-04.

Leupin, O.X., Zeyer, J., Cloet, V., Smith, P., Bernier-Latmani, R., Marschall P., Papafotiou, A., Schwyin, B. & Stroes-Gascoyne, S. (2016): An assessment of the possible fate of gas generated in a repository for low- and intermediate-level waste. Nagra Technical Report NTB 16-05.

Lide, D.R. (1997): CRC Handbook of Chemistry and Physics. CRC Press Inc.

Lovley, D.R. & Goodwin, S. (1988): Hydrogen concentrations as an indicator of the predominant terminal electron accepting reactions in aquatic sediments, Geochim. Cosmochim. Acta., 52, 2993–3003.

Madina, V. (2016): Corrosion study of FEBEX-DP components. Nagra NAB 16-54 report, 103 pp.

Madina, V. & Azkarate, I. (2004): FEBEX Project Post-mortem Analysis: Corrosion Study. Enresa Technical Publication 08/2004, 87 pp.

Marschall, G., Horseman, S. & Gimmi, T. (2005): Characterization of gas transport properties of the Opalinus Clay, a potential host rock formation for radioactive waste disposal. Oil Gas Sci. Technol. IFP Int. Workshop Rev. IFP 60, 121–139.

Martínez, V., Abós, H. & García-Siñeriz, J.L. (2016): Final Sensor Data Report (FEBEX in situ experiment. Nagra Arbeitsbericht NAB 16-19.

Mazurek, M., Oyama T., Wersin, P. & Alt-Epping, P. (2015): Pore-water squeezing from indurated shales. Chemical Geology, Vol. 400, 106–121.

Mingarro, M. & Rodriguez, V. (1999): Estudio microbiológico de la bentonita FEBEX. FEBEX Project internal report 70-IMA-L-68, 62 pp.

Mingarro, M., García-Gutiérrez, M. & Quiñones, J. (2004): ¿Es la bóveda de un repositorio un medio viable para la actividad microbiana?. Reunión Anual de la Sociedad Nuclear Española. Alicante, pp. 18.

Missana, T., Alonso, U., García-Gutierrez, M. & López, T. (2014): *In situ* analysis of bentonite colloid formation at the FEBEX gallery of the Grimsel Test Site, Switzerland: Evaluation of the experimental data obtained from 2006 to 2014. CIEMAT/M15/Belbar/01/2014, 80 pp.

Muurinen A (2003): Chemical Conditions in the A0 Parcel of the Long-Term Test of Buffer Material in Äspö (LOT). Olkiluoto, Finland: Posiva Oy. Working Report 2003–32.

Muurinen, A. & Lehikoinen, J. (1999): Porewater chemistry in compacted bentonite. Engineering Geology 54, 207–214.

Nagra (2008): Effects of post-disposal gas generation in a repository for low- and intermediate-level waste sited in the Opalinus Clay of Northern Switzerland. Nagra Technical Report NTB 08-07.

NEA (2001): Gas Generation and Migration in Radioactive Waste Disposal Safety-relevant Issues. Workshop Proceedings Reims, France, 26-28 June 2000. OECD publication, 188 pp.

Neeft, E.A.C. (2018): Final overview of CAST. Carbon-14 Source Term (CAST Project). Deliverable D7.23, 40 pp.

Norris, S. (2010): Summary of Gas Generation and Migration. Current State of the Art. FORGE Project. Mikestibe M15, 184 pp.

Pardillo, J., Campos, R. & Guimerá, J. (1997): Caracterización geológica de la zona de ensayo FEBEX (Grimsel-Suiza). Technical Report CIEMAT-70-IMA-M-2-01.

Parkhurst, D.L. & Appelo, C.A.J. (2013): Description of input and examples for PHREEQC version 3 – A computer program for speciation, batch-reaction, one-dimensional transport, and inverse geochemical calculations: U.S. Geological Survey Techniques and Methods, book 6, chap. A43, pp. 497.

Pearson, F.J., Arcos, D., Bath, A., Boisson, J. Y., Fernández, A.M., Gäbler, H-E, Gaucher, E., Gautschi, A., Griffault, L., Hernán, P. & Waber, H.N. (2003): Geochemistry of water in the Opalinus Clay Formation at the Mont Terri Rock Laboratory. Swiss Federal Office for Water and Geology Series, Nº 5, 319 pp.

Pearson, F.J., Tournassat, C. & Gaucher, E.C. (2011): Biogeochemical processes in a clay formation in situ experiment: part E – equilibrium controls on chemistry of porewater from the Opalinus Clay, Mont Terri Underground Research Laboratory, Switzerland. Appl. Geochem. 26, 990–1008.

Poinssot, C., Toulhoat, P. & Goffe, B. (1998): The influence of thermal gradients on the long-term evolution of the near-field environment of high level nuclear wastes disposal. In: McKinley, I.G., McCombie, C. (Eds.), Scientific Basis for Nuclear Waste Management XXI. Mat. Res. Soc. Symp. Proc. 506, 431–438.

Prítrský, J., Matejovic, I., Ondra, F. & Necas, V. (2006): Assessment of gas producing radioactive waste disposal. Journal of Electrical Engineering, 57 (4), 235–237.

Rey, M., Bárcena, I. & García-Siñeriz, J.L. (2015): Full Dismantling Sampling Plan. Rev. 5. AITEMIN May 2015.

Rey, M., Sanz, F.J. & García-Siñeriz, J.L. (2016): FEBEX-DP Post-mortem analysis: Sensors. Nagra NAB 16-20 report, 118 pp.

Rodwell, W., Norris, S., Cool, W., Cuñado, M., Johnson, L., Mäntynen, M., Müller, W., Sellin, P., Snellman, M., Talandier, J. & Vieno, T. (2003): A Thematic Network on Gas issues in Safety Assessment of Deep Repositories for Radioactive Waste (GASNET). European Commission, Report EUR20620 EN, Luxemburg, 45 pp.

Rodwell, W.R., Harris, A.W., Horseman, S.T., Lalieux, P., Müller, M., Ortiz Amaya, L. & Pruess, K. (1999): Gas migration and two-phase flow through engineered and geological barriers for a deep repository for radioactive waste. EC/NEA Status Report EUR 19122 EN.

Sacchi, E., Michelot, J.L., Pitsch, H., Lalieux, P. & Aranyossy, J.F. (2001): Extraction of water and solutes from argillaceous rocks for geochemical characterization: Methods, processes, and current understanding. Journal of Hydrogeology 9, 17–33.

Schneeberger, R., Mäder, U.K. & Waber, H.N. (2017): Hydrochemical and isotopic (δ^2H, $\delta^{18}O$, δ^3H) characterization of fracture water in crystalline rock (Grimsel, Switzerland). Procedia Earth and Planetary Science 17, 738–741.

Schoell, M. (1980): The hydrogen and carbon isotopic composition of methane from natural gases of various origins. Geochim. Cosmochim. Acta 44, 649–661.

Scott, M.J. & Morgan, J.J. (1990): Energetics and conservative properties of redox systems, Chapter 29. In: Melchior, D.C., Bassett, R.L. (Eds.), Chemical Modeling of Aqueous Systems II, ACS Symposium Series, vol. 416. American Chemical Society, Washington, DC, pp. 368–378.

Shaw, R.P. (2015): Gas generation and migration in deep geological radioactive waste repositories. Geological Society. Special Publication 415, 264 pp.

Shoell, M. (1988): Multiple origins of methane in the Earth. Chemical Geology 71, 1–10.

Stumm, W. & Morgan, J.J. (1981): Aquatic Chemistry. An introduction emphasizing chemical equilibria in natural waters. John Wiley & Sons, 789 pp.

Suckling, P., Avis, J., Humphreys, P. & King, F. (2011. T2GGM Version 2: Gas Generation and Transport Code. Report NWMO DGR-TR-2011-33, 189 pp.

Swanton, S.W., Baston, G.M.N. & Smart, N.R. (2015): Rates of steel corrosion and carbon-14 release from irradiated steels – state of the art review (Deliverable D.2.1). Carbon-14 Source Term (CAST EU Project), 160 pp.

Tomonaga, Y., Giroud, N., Brennwald, M. S., Horstmann, E., Diomidis, N., Kipfer, R. & Paul, W. (2019): On-line monitoring of the gas composition in the Full-scale Emplacement experiment at Mont Terri (Switzerland). Applied Geochemistry 100 (234–243).

Tournassat, C., Steefel, C.I., Bourg, I.C. & Bergaya, F. (2015): Natural and Engineered Clay Barriers. Developments in Clay Science 6, 432 pp.

Tournassat, C., Vinsot, A., Gaucher, E.C. & Altmann, S. (2015b): Chemical conditions in Clay-Rocks. In: Natural and Engineered Clay Barriers. Tournassat, C., Steefel, C.I., Bourg, I.C., Bergaya, F. (Ed.). Developments in Clay Science 6, 71–100.

Van Lith, Y., Warthmann, R., Vasconcelos, C. & Mckenzie, J.A. (2003): Sulfate-reducing bacteria induce low-temperature Ca-dolomite and high Mg-calcite precipitation. Geobiology, 1, 71–79.

Villar, M.V., Fernández, A.M., Romero, E, Dueck, A., Cuevas, J., Plötze, M., Kaufhold, S., Dohrmann, R., Iglesias, R., Sakaki, T., Voltolini, M., Zheng, L., Kawamoto, K. & Kober, F. (2017): FEBEX-DP: Post-mortem THM/THC Report. Analysis of Results. Nagra Arbeitsbericht NAB 16-17.

Villar, M.V., Iglesias, R.J., Abós, H. Martínez, V., de la Rosa, C. & Manchón, M.A. (2016): FEBEX-DP on-site analyses report. Nagra Arbeitsbericht NAB 16-12.

Villar, M.V., Iglesias, R.J., Gutiérrez-Álvarez, C., Carbonell, B., Campos, R., Campos, G., Martín, P.L. & Castro, B. (2017b): FEBEX-DP: Thermo-hydro-mechanical postmortem analysis of bentonite performed at CIEMAT. Technical report NAB16-024. Madrid, 134 pp.

Vinsot A., Mettler S. & Wechner S. (2008): In situ characterization of the Callovo-Oxfordian porewater composition. Phys. Chem. Earth 33, S75–S86.Walch, M., Mitchell, R., 1983. The role of microorganisms in hydrogen embrittlement of metals. CORROSION/1983. Paper Nº 249, Anaheim, CA: NACE international.

Vinsot, A., Appelo, C.A.J., Lundy, M., Wechner, S., Lettry, Y., Lerouge, C., Fernandez, A.M., Labat, M., Tournassat, C., De Cannière, P., Schwyn, B., McKelvie, J., Dewonck, S., Bossart, P. & Delay, J. (2014): In situ diffusion test of hydrogen gas in the Opalinus Clay. Geological Society London Special Publications, 400.

Vinsot, A., Linard, Y., Lundy, M., Necib, S. & Wechner, S. (2013): Insights on desaturation processes based on the chemistry of seepage water from boreholes in the Callovo-Oxfordian argillaceous rock. Procedia Earth and Planetary Science 7, 871–874.

Vogt, T., Müller, H.R., Sakaki, T., Hertrich, M., Spillmann, T., Garitte, B., Giroud, N. & Vietor, T. (2015): FE Experiment: The instrumentation and monitoring concept of a 1:1-scale heater experiment at the Mont Terri URL. Proceedings of 6th International Conference on Clays in Natural and Engineered Barriers for Radioactive Waste Confinement. Brussels, pp. 728–729.

Wersin, P. & Kober, F. (2017): FEBEX-DP. Metal Corrosion and Iron-Bentonite Interaction Studies. Nagra Arbeitsbericht NAB 16-16.

Wersin, P., Leupin, O.X., Mettler, S., Gaucher, E.C., Mäder, U., De Canniere, P., Vinsot, A., Gäbler, H.E., Kunimaro, T., Kiho, K. & Eichinge, L. (2011): Biogeochemical processes in a clay formation in situ experiment: Part A – Overview, experimental design and water data of an experiment in the Opalinus Clay at the Mont Terri Underground Research Laboratory, Switzerland. Applied Geochemistry 26, 931–953.

Whiticar, M.J. (1990): A geochemical perspective of natural gases and atmospheric methane. Org. Geochem, 16, 531–547.

Whiticar, M.J. (1999): Carbon and hydrogen isotope systematics of bacterial formation and oxidation of methane. Chemical Geology 161, 291–314.

Whiticar, M.J., Faber, E. & Schoell, M. (1986): Biogenic methane formation in marine and freshwater environments: CO_2 reduction vs. acetate fermentation—isotope evidence. Geochim. Cosmochim. Acta, 50, 693–709.

Wieland, E. & Hummel, W. (2015): Formation and stability of ^{14}C-containing organic compounds in alkaline iron-water systems: preliminary assessment based on a literature survey and thermodynamic modelling. Mineralogical Magazine 79, 1275–1286.

Wieland, E., Wanner, H., Albinsson, Y., Wersin, P. & Karland, O. (1994): A surface chemical model of the bentonite-water interface and its implications for modelling the near field chemistry in a repository for spent fuel. SKB Technical Report 94–26, 64 pp.

Wilson, N. (1995): Soil Water and Ground Water Sampling. CRC Press LLC.

Wolfaardt, G.M. & Korber, D.R. (2012): Near-field microbiological considerations relevant to a deep geological repository for used nuclear fuel. State of Science Review. NWMO TR-2012-02, 86 pp.

Yu, L. & Weetjens, E. (2009): Summary of gas generation and migration. Current state of the art. European Commission FP7 FORGE: Fate of Repository Gases. SCK•CEN ER-106 Report, 29 pp.

Zhang, Y. & Dawe, R.A. (2000): Influence of Mg^{2+} on the kinetics of calcite precipitation and calcite crystal morphology. Chemical Geology, 163, 129–138.

Acknowledgements

This work had not been possible without the collaboration of the following people:

- Nagra (Dr. Irina Gaus, Dr. Florian Kober and Dr. Niels Giroud), who supported this work
- Dr. Norbert Jockwer and Dr. Klaus Wieczorek, who designed the GRS pipes and performed most of the gas samplings during FEBEX-I and FEBEX-II projects
- Dr. Pedro Luis Martín, who designed the CIEMAT pipes
- Dr. Gesine Lorenz from Hydroisotop GmbH (responsible of the determination of the gas, water and stable isotope composition on samples from the GRS pipes in the 2014 and 2015 sampling campaigns)
- Dolores María Sánchez-Ledesma (Responsible of the Spectrophotometry and Potentiometry Laboratory at CIEMAT)
- Miguel Sánchez (Responsible of the Ionic Chromatography Laboratory at CIEMAT)
- Isabel Rucandio (Responsible of the ICP-OES and Atomic Fluorescence Laboratories at CIEMAT)
- Dr. Agnès Vinsot for her essential help to find a methodology for collecting unaltered gas samples
- Dr. Nick Waber for his essential one-hour course about isotopes
- Dr. Pierre De Canniere for his essential discussions about organics
- Dr. Christophe Tournassat for the review of this report and its useful master comments about gases and redox
- Dr. Nathalie Van Meir for the review and edition of this report
- Most of the photos were taken by AITEMIN during dismantling operations

Appendix A: Hydrochemical and gas characterization of the granitic groundwater in the Grimsel Test Site

In the Grimsel Test Site granitic groundwaters circulate by advective transport through mainly brittle fracture networks and fault zones developed in the different Grimsel rocks or major lithologies (Fig. A-1, Fig. A-2, Tab. A-1): a) Grimsel Granodiorite (GrGr), b) Central Aar Granite (CAGr) and c) metabasic dykes. The Grimsel groundwater is a relatively young meteoric water which infiltrated > 65 years ago (Schneeberger et al. 2017), and has undergone as slight increase in mineralization and accumulation of nucleogenic gases (^{4}He and ^{40}Ar).

Generally, the groundwaters are relatively poorly mineralized with an ionic strength of 1 mM or less, electric conductivities less than 120 µS/cm and pH ranging from 8.5 to 10.3, the groundwaters being classified as Na-Ca-TIC-F-(SO_4^{2-}) water type (Frick et al. 1992, Schneeberger et al. 2017, Garralón et al. 2017).

The main cations of the Grimsel groundwaters are Na and Ca (99 % of total) and the main anions are TIC, F, SO_4^{2-} and Cl (TIC and F representing the 70 % of the total). This composition is typical of an igneous rock, except for F, which is probably related to the fluorite observed in many fractures. Increases in Cl are related with a greater interaction with rock matrix pore water, which is known to be more saline (Schneeberger et al. 2017). The high pH is a reflection of the bicarbonate/carbonate/silicate system and the low pCO_2. The concentration of CO_2 in the groundwater is usually below detection limit (Bradbury 1989).

The gas contents in the groundwaters do not vary so much (Tab. A-3). The main dissolved gases are N_2 and Ar, 97 vol.-% and 3 vol.-% of the total, respectively. The dissolved Ar is in equilibrium with the atmospheric isotopic composition ($^{40}Ar/^{36}Ar$ ~300). He concentrations above atmospheric probably results from the dissolution of U from minerals of the rock matrix (Hoehn et al. 1990). The concentration of O_2 is very low, which justify the negative values of Eh and indicate reducing conditions. Methane and H_2S are below the detection limit, although usually there is a perceptible smell of the later. Small amounts of H_2 (0.1 – 20 µg/L) have been detected occasionally, probably due to microbial activity present in boreholes (Frick et al. 1992). However, biological compounds utilized as electron acceptors (NO_3^- and NO_2^-) and electron donors (NH_4^+, Fe^{2+}, HS^-, lactate, formate, CH_4, C_2H_6, etc.) are below detection limits or at very low concentrations (Konno et al. 2013).

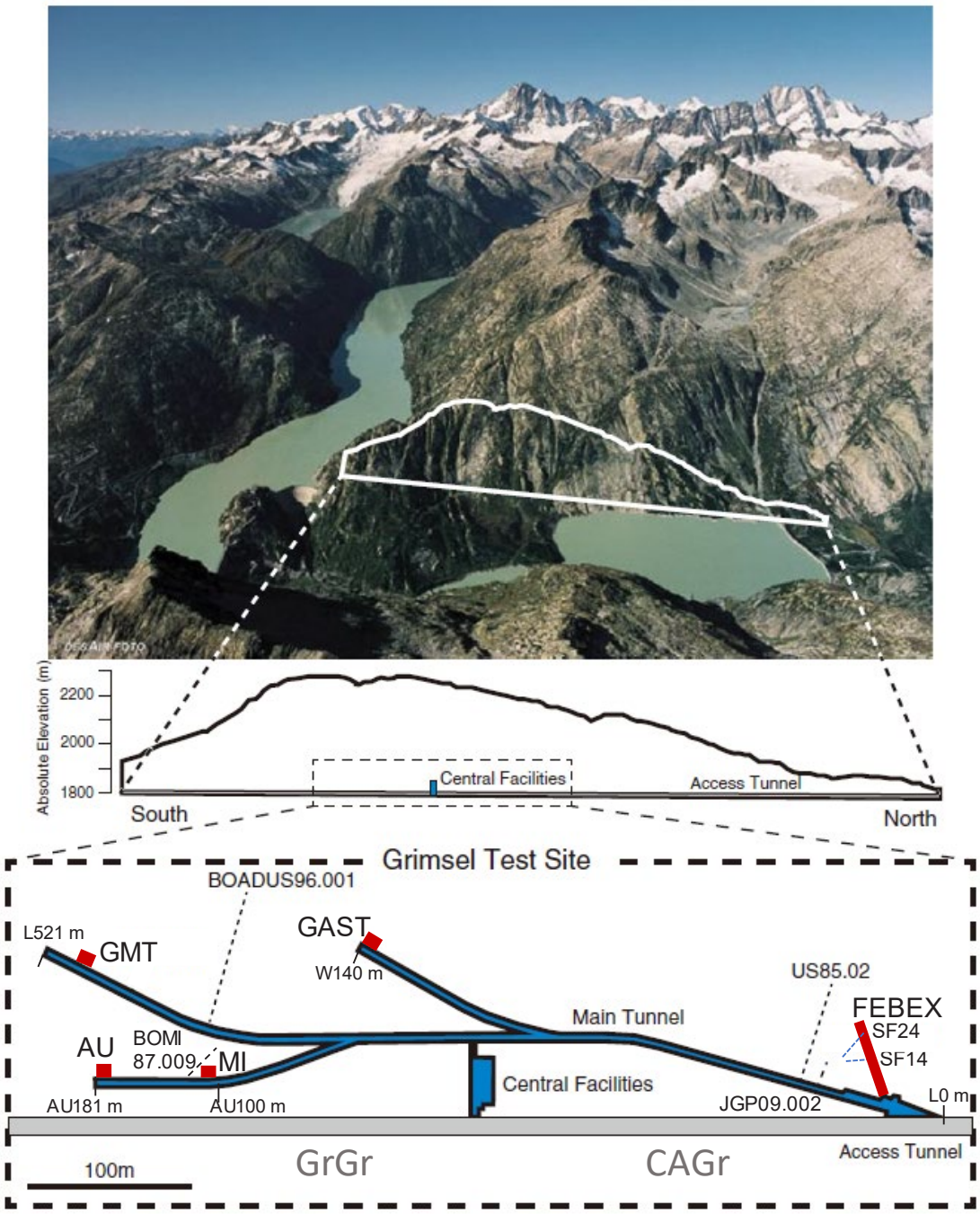

Fig. A-1: Location of different boreholes (BOADUS96.001, BOMI87.009, JGP09.002, BOUS85.02, SF14, SF24) for hydrogeochemical characterization

Experiments at Grimsel Test Site: GMT (GAS Migration), AU (Excavation effects), MI (Migration), GAST (Gas Permeable Seal Test). Lithologies: GrGr (Grimsel Granodiorite), CAGr (Central Aar Granite). After Konno et al. (2013).

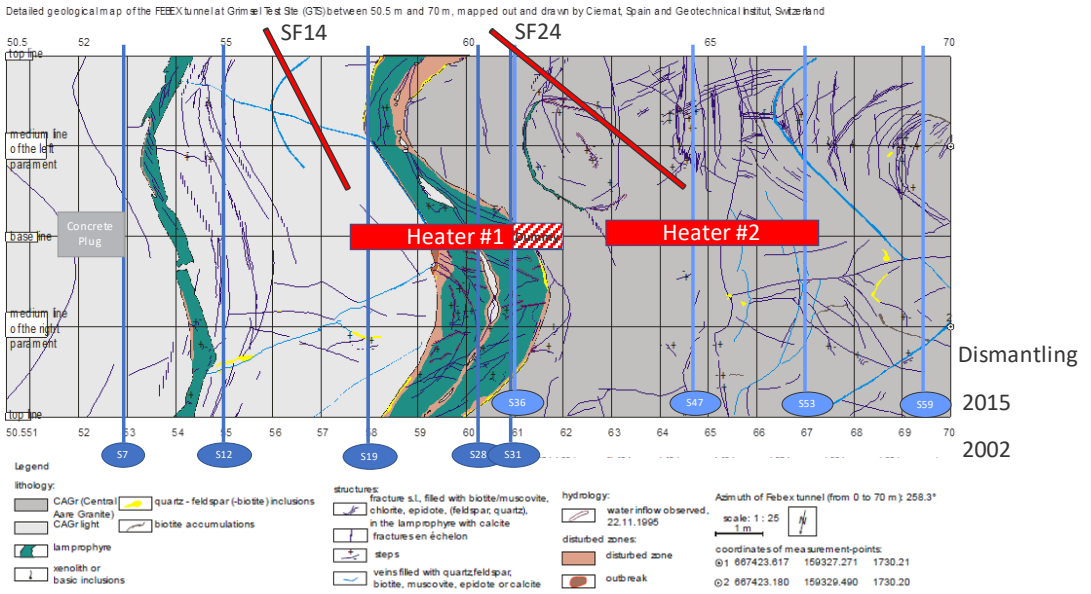

Fig. A-2: Location of the radial boreholes SF14 and SF24 and the dismantling bentonite sections analysed for THG studies after dismantling of Heater #1 and Heater #2

Tab. A-1: Differences in the groundwaters collected from the GrGr and CAGr lithologies Schneeberger et al. (2017)

Parameters	**GrGr Lithology**	**CAGr Lithology**
Location	South	North
Depth (m)	500	400
Temperature (°C)	13.7 ± 0.9	12.5 ± 0.6
pH	8.85 – 9.78	8.13 – 9.43
pCO_2 (bar)	$10^{-5.26}$	$10^{-4.91}$
Ion concentration	↑ Na, K, Li, Cl ↓ Ca, TIC	↓ Na, K, Li, Cl ↑ Ca, TIC
Circulation time of fracture water	↑	↓
Differences	Related to differences in infiltration areas, flow paths, residence time and water-rock interactions	

Tab. A-2: Chemical and microbiological characteristics of the groundwaters in the GTS

Parameter	**Unit**	**SF14 - 3**[1]	**SF24 -1**[1]	**BOUS85-02**[2]	**JGP09 002**[2]	**BOADUS 96.001**[2]	**BOMI 87.009**[3]
Water type		Lamprophyre dyke (Heater #1)	Close to Heater #2	Fracture	Fracture	Fracture	Fracture
Tunel location		North	North	North	North	South	South
Temperature	°C	17.6	14.3	12.2	12.5	14.1	12.6 ± 0.26
I ($\times 10^{-3}$)	M	1.105	1.035	-	-	-	-
Eh (mV)	mV SHE	n.d.	15.3	-100	-74	n.d.	-382 ± 17
DO	mg/L	n.d.	n.d.	0.05	0.08	0.03	-
pH	-	8.9	9.1	9.7	9.6	n.d.	9.59
Alkalinity	meq/L	0.39	0.39	0.45	0.08	0.17	0.42
Na	mg/L	8.9	8.4	9.20	13.79	13.79	16
K	mg/L	2.9	0.21	0.20	0.61	0.44	0.22
Ca	mg/L	7.13	7.17	8.37	8.14	7.63	5.6
Mg	mg/L	77.3	23.3	< 0.08	< 0.08	< 0.08	0.044
Fe^{2+}	mg/L	< 0.05	< 0.05	< 0.03	< 0.03	< 0.03	-
Sr	mg/L	0.24	0.21	n.d.	n.d.	n.d.	0.18
F^-	mg/L	4.23	3.87	4.05	3.87	4.75	6.1
Cl^-	mg/L	3.93	0.36	0.54	0.44	1.70	5.5
SO_4^{2-}	mg/L	7.37	7.37	7.66	16.98	6.39	5.5
NO_3^-	mg/L	1	< 0.1	0.01	0.02	0.01	< 0.3
NH_4^+	mg/L	< 0.1	< 0.1	< 0.21	< 0.21	< 0.21	-
NO_2^-	mg/L	< 0.1	< 0.1	< 0.01	< 0.01	< 0.01	-
Si	mg/L	9.10	9.53	n.d.	n.d.	n.d.	12
HS^-	mg/L	n.d.	n.d.	< 0.01	< 0.01	< 0.01	-
DOC	mgC/L	5.43	0.6	0.41	0.31	0.30	-
TIC	mgC/L	-	-	4.60	3.53	4.49	-
CH_4	mg/L	-	-	0.02	0.0002	0.0004	-
C_2H_6	mg/L	-	-	0.02	0.009	0.009	-
$\delta^{13}C_{TIC}$	‰VPDB	-	-	-13.0	-13.0	-11.6	-
$\delta^{13}CH_4$	‰VPDB	-	-	-79.5	-58.3	-58.6	-
$\delta^{34}S_{HS}$	‰ CDT	-	-	-0.5	-9.4	+0.8	-
$\delta^{34}SO_4$	‰ CDT	-	-	-0.4	+2.0	+2.0	-
Cell numbers	Cell/mL	-	-	$7.5 \pm 3.5 \times 10^3$	$2.9 \pm 1.4 \times 10^4$	$4.9 \pm 5.1 \times 10^3$	-

[1] Huertas et al. (2006)
[2] Konno et al. (2013)
[3] Hoehn et al. (1990)

Tab. A-3: Dissolved gases in different boreholes from the GTS

Hoehn et al. (1990)

Borehole	**Location**	**Volume** (cm^3/kg)	**O_2** (mg/kg)	**N_2** (mg/kg)	**H_2** (mg/kg)	**CO_2** (mmol/kg)	**CH_4** (mg/kg)	**He** (mg/kg)	**Ar** (mg/kg)	**H_2S**[1] (mg/kg)
BOMI 87.009	South	-	0.003	24.6	9×10^{-4}	< d.l.	< d.l.	4×10^{-4}	0.79	0.002
BOMI 87.008 outlet K	South	16.7	0.03	20.3	5×10^{-4}	$< 7 \cdot 10^{-4}$	< d.l.	6×10^{-4}	0.72	< d.l.
BOEM 85.012	South	18.1	$< 5 \times 10^{-4}$	22.0	3×10^{-4}	< d.l.	$< 5 \times 10^{-4}$	$< 5 \times 10^{-4}$	0.73	< 0.02

[1] Slight smell

< d.l.: below detection limit

Appendix B: Gas concentration in the GRS pipes from the First and Second Operational Phases

Tab. B-1: Gas concentration in the gas pipe GF-S-L-01 during the First Operational Phase

Date	**N_2** (vol.-%)	**O_2** (vol.-%)	**CO_2** (vpm)	**CO** (vpm)	**H_2** (vpm)	**CH_4** (vpm)	**C_2H_6** (vpm)	**C_3H_8** (vpm)	**i-C_4H_{10}** (vpm)	**Sum hydro-carbons** (vpm) (= ppmv)
30.10.1996	76.79	22.85	451.86	7.41	93.87	1.90	-	-	-	1.90
02.12.1996	78.63	21.41	573.44	13.10	349.41	4.42	0.77	74.39	22.40	101.97
27.02.1997	94.20	5.58	774.08	21.22	110.60	9.20	0.93	63.54	22.90	96.58
28.02.1997	81.63	21.42	749.78	11.50	84.45	8.56	0.85	59.28	18.98	87.67
06.03.1997	80.84	20.23	1'118.32	12.47	91.58	9.77	1.04	74.60	27.03	112.45
10.03.1997	79.86	19.94	1'523.57	8.69	63.65	10.21	0.93	79.05	29.46	119.64
17.03.1997	78.94	20.26	1'885.08	9.80	33.44	8.90	0.94	72.79	29.23	111.86
24.03.1997	79.47	19.99	2'225.00	8.48	-	7.44	0.80	69.04	29.41	106.68
01.04.1997	80.53	19.81	4'435.24	11.64	24.07	10.50	1.47	83.62	37.86	133.45
28.04.1997	85.11	12.88	9'509.63	12.06	34.05	13.45	1.60	87.11	40.85	143.00
20.05.1997	84.23	12.21	13'349.40	13.83	43.29	19.95	1.62	87.92	45.05	154.54
16.06.1997	78.94	19.45	6'021.74	8.72	-	6.66	0.29	23.16	21.43	51.53
14.07.1997	76.45	21.23	6'958.35	6.81	45.51	16.07	0.51	16.80	20.18	53.57
11.08.1997	85.10	11.43	13'284.40	7.82	33.03	35.44	0.72	22.66	33.62	92.44
08.09.1997	74.89	21.86	10'264.83	6.54	-	21.48	0.30	9.98	17.63	49.39
20.10.1997	71.41	22.81	552.83	6.64	33.13	11.37	-	2.51	-	13.88
02.12.1997	98.46	1.19	2'585.84	3.85	44.45	8.56	0.24	0.67	-	9.47
05.01.1998	98.92	1.01	6'592.92	5.27	42.78	25.78	0.87	1.86	-	28.51
24.02.1998	89.02	8.43	6'012.99	5.23	18.02	42.47	1.32	2.51	-	46.29
18.08.1998	96.33	2.42	7247.51	7.06	19.01	14.20	0.44	0.36	-	15.00
16.12.1998	97.40	1.20	6'730.00	-	-	37.00	-	-	-	37.00
17.06.1999	98.10	0.90	2'815.00	6.00	-	21.00	-	6.00	-	27.00

vol.-%: volume of gas in %; vpm or ppmv: parts per million by volume

Tab. B-2: Gas concentration in the gas pipe GF-SL-02 during the First Operational Phase

Date	**N_2** (vol.-%)	**O_2** (vol.-%)	**CO_2** (vpm)	**CO** (vpm)	**H_2** (vpm)	**CH_4** (vpm)	**C_2H_6** (vpm)	**C_3H_8** (vpm)	**i-C_4H_{10}** (vpm)	**Sum hydro-carbons** (vpm) (= ppmv)
30.10.1996	76.78	22.92	718.15	8.45	< d.l.	1.76	< d.l.	< d.l.	< d.l.	1.76
02.12.1996	78.58	21.15	872.36	11.00	1'840.41	4.51	0.75	75.40	24.27	104.93
02.12.1996	79.16	21.27	1'119.64	8.63	1'834.95	4.40	0.72	73.85	23.75	102.72
27.02.1997	80.70	21.01	999.77	14.94	108.07	9.18	0.95	60.55	20.39	91.07
28.02.1997	81.37	21.62	961.74	10.12	60.06	7.71	0.78	54.96	18.36	81.81
03.03.1997	80.18	19.37	1'070.43	9.62	86.45	9.15	0.95	67.18	24.33	101.62
06.03.1997	80.04	20.26	1'390.89	9.15	54.12	8.72	0.96	70.44	26.93	107.04
10.03.1997	80.07	20.48	1'839.05	7.75	47.03	9.49	0.93	73.99	27.05	111.45
17.03.1997	79.68	19.34	2'486.06	8.28	64.87	10.20	1.00	77.92	30.86	119.98
24.03.1997	79.77	19.57	2'973.12	6.09	27.89	8.57	0.91	76.30	32.27	118.05
01.04.1997	80.41	19.05	5'703.66	7.53	58.63	11.30	0.96	88.99	37.71	138.95
28.04.1997	81.69	16.38	8'165.72	7.70	< d.l.	7.69	0.71	65.32	30.85	104.57
20.05.1997	81.22	12.85	12'298.89	7.20	< d.l.	17.70	1.30	82.95	41.75	143.70
16.06.1997	84.58	10.65	15'897.32	8.23	< d.l.	21.80	1.10	50.90	34.15	107.95
14.07.1997	87.65	9.67	16'774.85	6.70	13.81	28.05	1.01	27.95	27.02	84.02
02.12.1997	100.0	1.09	5'931.37	2.60	15.17	15.75	1.09	2.22	1.04	20.10
05.01.1998	98.47	0.95	6'059.50	2.90	18.15	227.84	1.80	3.92	1.85	235.41
18.08.1998	97.87	0.89	7'454.26	3.46	13.93	365.76	0.83	0.51	< d.l.	367.09

Tab. B-3: Gas concentration in the gas pipe GF-SL-03 during the First Operational Phase

Date	**N_2** (vol.-%)	**O_2** (vol.-%)	**CO_2** (vpm)	**CO** (vpm)	**H_2** (vpm)	**CH_4** (vpm)	**C_2H_6** (vpm)	**C_3H_8** (vpm)	**i-C_4H_{10}** (vpm)	**Sum hydro-carbons** (vpm) (= ppmv)
30.10.1996	77.33	22.68	305.47	8.81	164.72	1.87	< d.l.	< d.l.	< d.l.	1.87
02.12.1996	78.81	21.37	257.44	9.33	2'105.31	4.74	0.82	80.21	30.42	116.19
19.06.1997	86.41	12.15	13'836.29	18.08	< d.l.	20.88	0.20	3.40	0.60	25.08
14.07.1997	85.52	9.23	18'840.48	7.03	< d.l.	27.76	0.32	7.65	28.24	63.97
11.08.1997	86.05	8.96	18'554.29	7.10	18.80	32.32	< d.l.	4.09	23.72	60.13
08.09.1997	78.59	13.78	13'498.22	6.28	< d.l.	21.69	< d.l.	2.23	18.62	42.53
20.10.1997	76.34	15.26	12'108.42	4.82	25.74	25.61	< d.l.	1.26	12.45	39.31
04.11.1997	83.16	9.17	12'848.44	4.90	< d.l.	44.40	< d.l.	1.96	23.42	69.78
02.12.1997	87.56	5.63	25'359.01	6.37	26.35	55.52	< d.l.	2.19	26.43	84.14
05.01.1998	85.24	12.29	18'109.26	6.66	< d.l.	35.08	< d.l.	1.44	20.03	56.56
24.02.1998	86.84	8.41	23'322.32	6.17	18.31	66.85	0.41	2.61	29.26	99.13
30.03.1998	88.93	6.17	30'945.77	4.75	4.84	69.76	0.39	2.79	28.25	101.19
24.04.1998	82.19	13.61	19'167.54	7.26	28.37	38.65	0.38	3.16	20.92	63.10
25.05.1998	89.30	6.23	30'463.23	13.98	7.52	78.01	< d.l.	3.52	29.68	111.20
24.06.1998	90.05	5.59	33'204.86	7.48	0.26	82.75	0.57	3.94	30.99	118.25
18.08.1998	90.36	4.45	38'866.81	8.51	16.28	94.40	1.16	4.37	32.92	132.85
22.10.1998	89.60	5.84	34'789.83	12.65	308.25	104.47	14.28	5.45	31.08	155.28
16.12.1998	90.50	3.80	49'015.00	10.00	-	107.00	30.00	-	35.00	172.00
11.01.1999	83.80	12.20	29'100.00	26.00	< d.l.	60.00	18.00	< d.l.	28.00	106.00
01.02.1999	89.40	4.30	47'790.00	13.00	< d.l.	111.00	33.00	< d.l.	36.00	180.00
03.03.1999	90.10	4.60	50'770.00	8.00	< d.l.	120.00	28.00	-	38.00	186.00
25.05.1999	78.90	19.70	13'212.00	20.00	-	18.00	-	57.00	15.00	90.00
17.06.1999	89.50	5.20	3'900.00	15.00	6'429.0	114.00	25.00	112.0	26.00	277.00

Tab. B-4: Gas concentration in the gas pipe GF-SL-04 during the First Operational Phase

Date	**N_2** (vol.-%)	**O_2** (vol.-%)	**CO_2** (vpm)	**CO** (vpm)	**H_2** (vpm)	**CH_4** (vpm)	**C_2H_6** (vpm)	**C_3H_8** (vpm)	**i-C_4H_{10}** (vpm)	**Sum hydro-carbons** (vpm) (= ppmv)
30.10.1996	77.29	23.03	366.76	10.39	144.66	1.85	< d.l.	< d.l.	< d.l.	1.85
02.12.1996	77.84	21.66	360.61	9.68	2020.69	4.58	0.80	76.30	25.07	106.75
27.02.1997	81.04	20.70	538.87	16.71	136.28	9.72	0.92	68.33	24.15	103.11
28.02.1997	79.94	19.48	713.92	12.39	111.76	9.39	0.89	68.63	22.88	101.78
03.03.1997	80.16	18.95	1'035.52	10.31	98.29	9.75	0.93	71.29	24.88	106.85
06.03.1997	80.95	20.39	1'420.16	10.57	82.89	10.11	0.89	77.51	28.37	116.88
10.03.1997	80.07	20.48	1'839.05	7.75	47.03	9.49	0.93	73.99	27.05	111.45
17.03.1997	79.96	19.47	1'917.86	10.27	35.40	10.25	1.03	78.36	30.93	120.57
24.03.1997	79.26	19.78	2'336.05	10.17	< dl	8.03	0.84	72.01	30.73	111.61
01.04.1997	79.85	18.84	4'752.84	18.10	29.95	11.26	1.07	87.00	37.20	136.53
28.04.1997	84.13	13.38	8'085.69	19.57	< d.l.	11.95	0.96	74.30	33.74	120.94
20.05.1997	71.85	21.58	5'109.76	10.84	11.30	5.19	0.42	37.42	21.67	64.70
16.06.1997	79.31	19.11	12'378.39	15.19	< d.l.	16.83	0.78	50.16	30.93	98.70
14.07.1997	88.37	9.68	17'156.65	16.20	30.22	28.07	0.95	40.14	33.02	102.18
08.09.1997	85.61	11.70	13'993.14	13.91	309.00	30.04	0.56	21.72	28.23	80.55
20.10.1997	74.68	22.00	856.98	9.36	9.84	1.94	0.46	< d.l.	8.54	10.94
04.11.1997	86.07	7.05	23'235.52	13.61	< d.l.	51.61	0.46	11.42	28.13	91.62
02.12.1997	90.53	5.92	24'535.97	12.44	28.61	55.67	0.48	9.35	28.54	94.04
05.01.1998	89.77	6.47	25'180.10	13.46	31.00	58.83	0.44	7.49	27.02	93.78
24.02.1998	91.66	4.58	30'107.50	13.20	28.37	73.40	0.61	6.72	30.52	111.25
30.03.1998	78.32	17.53	12'200.14	9.77	< d.l.	18.92	0.24	2.59	15.44	37.19
24.04.1998	87.41	7.64	28'884.35	15.24	30.97	67.59	0.56	4.76	25.78	98.69
25.05.1998	78.89	18.71	9'395.00	56.49	< d.l.	13.77	< d.l.	1.78	11.55	27.11
24.06.1998	78.27	19.14	9'582.97	47.49	< d.l.	12.65	< d.l.	1.65	12.82	27.12
18.08.1998	86.55	8.34	31'656.43	12.26	< d.l.	71.63	0.87	3.74	25.77	102.01
22.10.1998	91.40	3.88	42'351.89	15.60	85.93	107.68	17.34	4.66	31.43	161.11
16.12.1998	87.80	6.80	39'840.00	18.00	< d.l.	90.00	28.00	< d.l.	29.00	147.00
11.01.1999	92.10	3.80	47'060.00	22.00	< d.l.	116.00	31.00	< d.l.	31.00	178.00
01.02.1999	89.40	4.20	47'540.00	21.00	44.00	115.00	32.00	< d.l.	32.00	179.00
03.03.1999	82.80	14.90	26'930.00	28.00	< d.l.	54.00	11.00	-	23.00	88.00
25.05.1999	80.10	18.10	17'800.00	21.00	-	29.00	-	63.00	17.00	109.00
17.06.1999	89.30	3.30	51'430.00	16.00	7'044.0	132.00	38.00	137.0	29.00	336.00
24.10.2000	87.60	2.10	83'400.00	-	7'500.0	360.00	-	-	-	360.00
09.05.2001	85.90	0.30	87'980.00	30.00	2'300.0	395.00	7.00	12.00	27.00	441.00
04.07.2001	86.40	2.20	10'2540.0	33.00	1'980.0	410.00	-	13.00	29.00	452.00
24.10.2001	78.80	15.40	41'500.00	-	40.00	135.00	7.00	16.00	16.00	174.00
25.02.2002	81.80	7.50	70'460.00	26.00	1'185.0	341.00	12.00	25.00	-	378.00

Tab. B-5: Gas concentration in the gas pipe GF-SL-05 during the First Operational Phase

Date	**N_2** (vol.-%)	**O_2** (vol.-%)	**CO_2** (vpm)	**CO** (vpm)	**H_2** (vpm)	**CH_4** (vpm)	**C_2H_6** (vpm)	**C_3H_8** (vpm)	**i-C_4H_{10}** (vpm)	**Sum hydro-carbons** (vpm) (= ppmv)
30.10.1996	77.36	22.82	367.87	10.08	127.63	2.04	< d.l.	< d.l.	< d.l.	2.04
02.12.1996	78.06	21.68	425.71	9.45	1788.57	4.40	0.78	74.91	23.14	103.23
27.02.1997	80.30	22.02	574.82	13.69	39.06	7.48	0.77	58.69	20.26	87.20
28.02.1997	79.83	19.82	631.84	11.56	102.85	8.88	0.88	65.24	24.17	99.18
03.03.1997	80.57	18.98	939.92	9.24	113.86	9.76	0.96	72.39	26.22	109.34
06.03.1997	80.49	20.34	1'330.09	9.44	88.89	9.88	1.00	76.27	27.79	114.93
10.03.1997	79.97	20.29	1'548.70	8.83	53.86	9.81	0.95	75.14	27.49	113.39
17.03.1997	79.47	19.37	1'924.35	9.94	37.80	10.86	1.08	81.34	33.35	126.63
24.03.1997	80.62	18.85	2'954.49	12.00	29.99	10.77	1.07	84.88	34.10	130.82
01.04.1997	80.46	18.92	4'630.06	17.52	32.79	11.30	1.07	87.28	36.04	135.69
28.04.1997	83.91	13.56	8'638.70	18.95	< d.l.	11.79	0.94	76.92	32.96	122.61
20.05.1997	73.60	20.69	10'755.22	17.56	< d.l.	16.21	1.02	73.27	35.78	126.28
16.06.1997	78.40	20.79	11'571.30	15.75	< d.l.	20.97	0.77	57.81	35.47	115.02
14.07.1997	78.48	20.10	13'189.41	13.64	< d.l.	20.22	0.74	33.26	27.75	81.97
11.08.1997	84.37	14.49	16'332.17	13.55	< d.l.	19.91	0.61	24.86	28.54	73.92
08.09.1997	75.76	22.49	4'793.47	7.49	< d.l.	2.59	< d.l.	4.53	9.86	16.98
20.10.1997	73.53	21.66	8'767.67	9.25	< d.l.	9.63	< d.l.	2.40	5.30	17.33
04.11.1997	91.37	7.24	21'823.58	15.90	< d.l.	53.33	0.46	11.70	29.25	94.74
02.12.1997	89.99	6.51	24'873.26	13.52	< d.l.	54.07	0.44	9.11	28.07	91.68
24.02.1998	83.60	14.57	26'247.13	10.83	0.06	62.65	0.57	4.17	20.88	88.28
30.03.1998	82.41	12.14	20'737.35	12.22	< d.l.	41.68	0.39	4.01	22.05	68.13
24.04.1998	84.31	7.30	29'894.25	13.20	< d.l.	67.23	0.58	4.82	28.03	100.66
25.05.1998	89.44	5.73	30'860.21	16.84	9.82	78.27	< d.l.	4.49	26.67	109.44
24.06.1998	90.00	5.01	34'415.69	14.45	0.15	86.09	0.60	4.36	28.15	119.20
18.08.1998	90.57	4.37	37'998.94	12.80	8.85	94.83	1.05	3.97	29.57	129.41
22.10.1998	86.53	9.21	34'827.50	18.37	< d.l.	74.95	10.31	3.53	26.99	115.78
16.12.1998	90.40	3.90	45'875.00	14.00	< d.l.	108.0	31.00	< d.l.	31.00	170.00
11.01.1999	91.60	3.80	49'140.00	19.00	< d.l.	116.0	31.00	< d.l.	32.00	179.00
01.02.1999	90.50	3.60	51'360.00	19.00	46.00	118.0	33.00	< d.l.	32.00	183.00
03.03.1999	90.20	5.10	48'660.00	21.00	46.00	122.0	36.00	5.00	33.00	196.00
25.05.1999	90.40	3.40	51'430.00	18.00	367.00	133.0	30.00	139.0	31.00	333.00
17.06.1999	86.90	7.10	44'280.00	18.00	2'838.0	105.0	36.00	126.0	28.00	295.00
24.10.2000	87.50	2.20	84'410.00	-	7'200.0	334.0	-	10.00	29.00	373.00
09.05.2001	86.10	2.20	94'800.00	30.00	2'315.0	380.0	8.00	13.00	31.00	432.00
04.07.2001	86.20	1.90	106'230.0	34.00	1'860.0	400.0	-	13.00	30.00	443.00
24.10.2001	82.00	8.10	64'480.00	-	520.00	300.0	11.00	25.00	25.00	361.00
25.02.2002	83.60	1.80	89'710.00	37.00	3'600.0	476.0	6.00	16.00	31.00	529.00

Tab. B-6: Gas concentration in the gas pipe GF-SL-06 during the First Operational Phase

Date	**N_2** (vol.-%)	**O_2** (vol.-%)	**CO_2** (vpm)	**CO** (vpm)	**H_2** (vpm)	**CH_4** (vpm)	**C_2H_6** (vpm)	**C_3H_8** (vpm)	**i-C_4H_{10}** (vpm)	**Sum hydro-carbons** (vpm) (= ppmv)
30.10.1996	76.54	22.61	452.58	8.67	< d.l.	1.81	< d.l.	< d.l.	< d.l.	1.81
02.12.1996	78.11	21.74	661.64	9.47	1'723.09	4.49	0.79	76.49	24.11	105.89
27.02.1997	82.27	20.92	735.66	12.91	131.82	9.54	0.83	64.69	21.62	96.68
28.02.1997	79.50	19.72	791.04	10.92	130.35	9.58	0.94	70.26	26.05	106.82
03.03.1997	79.73	19.23	910.54	8.77	108.60	8.85	0.84	65.64	23.26	98.61
06.03.1997	80.51	20.48	1'259.53	9.50	117.83	10.00	0.95	75.43	26.80	113.18
10.03.1997	80.59	20.66	1'514.82	8.83	97.77	10.21	0.97	75.86	28.03	115.07
17.03.1997	79.83	19.41	1'785.49	9.50	80.63	9.90	0.96	79.64	32.24	122.75
24.03.1997	80.29	18.93	2'599.80	12.27	84.26	10.61	1.05	81.25	31.75	124.66
01.04.1997	80.31	18.73	4'770.44	17.95	72.22	11.86	1.20	92.14	38.07	143.27
28.04.1997	83.33	14.34	8'080.47	18.07	< d.l.	10.42	0.89	73.32	30.56	115.19
20.05.1997	81.16	13.30	10'825.27	19.25	30.15	17.24	1.12	72.71	34.28	125.35
16.06.1997	86.41	12.15	13'141.22	18.08	< d.l.	20.88	0.20	3.40	0.60	25.08
14.07.1997	84.16	10.42	13'019.48	13.77	< d.l.	25.28	0.84	36.66	30.11	92.89
11.08.1997	85.66	12.12	13'386.17	13.95	9.69	31.51	0.61	24.89	28.41	85.43
08.09.1997	86.26	7.39	19'157.74	14.39	20.77	41.61	0.60	19.55	29.13	90.89
20.10.1997	77.58	19.20	4738.36	10.85	3.97	11.05	0.12	3.01	5.46	19.64
04.11.1997	88.01	7.00	21'360.99	12.66	4.68	52.20	0.45	11.63	28.50	92.78
02.12.1997	88.79	5.72	24'286.03	11.38	< d.l.	57.70	0.43	9.69	29.48	97.30
05.01.1998	85.73	11.76	5636.26	9.74	< d.l.	7.75	0.12	2.42	22.27	32.55
24.02.1998	89.99	4.99	29'383.93	12.99	7.30	72.46	0.55	6.80	29.78	109.59
30.03.1998	88.01	6.70	28'951.62	12.58	< d.l.	69.66	0.61	5.31	27.20	102.77
24.04.1998	87.08	6.93	30'094.45	12.38	14.49	71.59	0.64	4.77	27.05	104.05
25.05.1998	76.39	21.79	13'606.65	11.70	< d.l.	15.00	< d.l.	2.00	14.20	31.20
26.06.1998	80.85	15.35	16'472.50	35.91	0.08	30.66	< d.l.	2.50	18.17	51.33
18.08.1998	91.04	3.74	41'228.03	12.88	12.85	98.24	1.09	4.50	29.94	133.77
22.10.1998	90.41	4.79	42'067.73	14.81	11.00	101.31	18.36	4.40	30.35	154.42
16.12.1998	91.40	3.10	45'670.00	14.00	< d.l.	113.00	31.00	< d.l.	31.00	175.00
11.01.1999	91.90	3.30	48'990.00	20.00	< d.l.	119.00	31.00	< d.l.	31.00	181.00
01.02.1999	88.90	5.70	45'265.00	21.00	25.00	106.00	30.00	< d.l.	30.00	166.00
03.03.1999	90.60	4.00	50'380.00	21.00	67.00	133.00	38.00	5.00	33.00	209.00
25.05.1999	88.10	7.30	43'570.00	23.00	176.00	105.00	26.00	119.0	27.00	277.00
17.06.1999	89.70	3.40	51'560.00	17.00	7'613.0	133.00	39.00	136.0	29.00	337.00
24.10.2000	87.30	2.80	8'3000	-	7050	305.00	-	9.00	27.00	341.00
04.07.2001	86.50	3.20	10'0460	29.00	1'490	360.00	-	12.00	28.00	400.00
24.10.2001	82.00	8.40	6'3550	-	500	290.00	-	11.00	25.00	326.00
25.02.2002	84.50	1.70	94'350	37.00	3'400	477.00	5	16.00	31.00	529.00

Tab. B-7: Gas composition in the GRS pipes FP1, FP2 and FP3 surrounding Heater #2 over time

Date	**O_2** (vol.-%)	**H_2** (vpm)	**CO_2** (vpm)	**CH_4** (vpm)	**C_2H_6** (vpm)	**C_3H_8** (vpm)	**i-C_4H_{10}** (vpm)	**Σ Hydro-carbons** (vpm) (= ppmv)	**He** (vol.-%)	**N_2** (vol.-%)	**Ar** (vol.-%)
FP-1											
21.10.2003	1.44	6'030	53'417 .5	172.5	18	-	252.5	443	0.0090	91.86	-
23.01.2004	1.45	1205	48'740	190	39	-	202.5	431.5	0.0085	93.50	-
28.05.2004	4.00	830	28'350	200	-	-	70	270	0.0045	93.05	-
18.08.2004	0.48	104	14'800	63.7	-	-	15	78.7	0.0016	98.02	-
24.05.2005	2.01	55'040	450	4340	-	-	70	4'410	-	92.00	-
07.12.2005	18.80	68'740	6340	13'140	-	-	121	13'261	-	72.37	-
12.07.2006	0.20	34'050	13'250	28760	-	53	88	28'901	-	92.18	-
12.12.2006	0.61	330	1'0860	275	-	-	-	275	-	98.24	-
12.07.2007	-	955	14'500	2220	-	-	-	2'220	-	98.23	-
18.12.2007	-	24'005	19'995	40'245	-	32.5	55.5	40'333	-	91.57	-
10.08.2011	1.67	8'720	15'470	8'740	< 5	< 5	17	8'757	-	95.04	-
15.08.2014*	1.50	2'600	17'000	277'000	4	57	15	277'125**	8.6	59.4	0.4
29.1.2015*	2.3	1'400	6'000	41'000	1	20	10	41'315**	45.0	46.5	0.6
FP-2											
21.10.2003	2.64	5'150	48'290	265	17	-	259.5	541.5	0.0085	91.96	-
23.01.2004	12.10	360	20'650	230	-	-	110	340	0.0040	85.77	-
28.05.2004	4.34	840	30'520	240	-	-	100	340	0.0075	92.49	-
18.08.2004	0.13	885	58'700	850	-	-	199	1'049	0.0083	93.81	-
24.05.2005	2.25	720	64'240	4350	-	-	140	4'490	-	90.81	-
07.12.2005	9.37	286	53'760	7'130	-	-	122	7'252	-	84.50	-
12.07.2006	0.20	40	63'100	13'900	-	49	125	14'074	-	92.08	-
12.12.2006	1.61	37	56'210	14'940	-	42	106	15'088	-	91.26	-
12.07.2007	-	117	49'585	19'625	-	39.5	103.5	19'768	-	93.05	-
18.12.2007	-	58.5	45'600	27'290	-	52	115.5	27'457.5	-	92.69	-
10.08.2011	0.29	80	18'520	11'700	21	66	137	11'924	-	96.66	-
18.08.2014*	0.80	$< 0.1 \times 10^{-4}$	27'000	13'500	8	155	42	13'795**	4	90.1	0.5
30.1.2015*	2.6	$< 0.1 \times 10^{-4}$	3'000	265	5	8	9	307.5**	80	16.4	0.2
FP-3											
21.10.2003	1.59	3'590	21'685	135	11.5	-	360	506.5	0.0065	95.83	-
23.01.2004	6.71	17.5	18'210	95	-	-	187.5	282.5	0.0034	91.44	-
28.05.2004	3.43	52	18'500	135	-	-	110	245	0.0053	94.69	-
18.08.2004	2.41	27	34'400	342	-	-	128	470	0.0055	94.10	-
24.05.2005	0.10	20	35'000	1'845	-	-	120	1'965	-	96.20	-
07.12.2005	6.78	13	22'450	2'800	-	-	107	2'907	-	90.68	-
12.07.2006	0.50	< d.l.	27'500	5'050	-	48	76	5'174	-	96.23	-
12.12.2006	0.20	23	29'520	7'060	-	61	92	7'213	-	96.12	-
12.07.2007	-	28.5	25'650	4'825	-	34.5	47.5	4'907	-	96.94	-
18.12.2007	-	25	25'610	6'800	-	46.5	66	6912.5	-	96.75	-

Tab. B-7: Cont.

Date	**O_2** (vol.-%)	**H_2** (vpm)	**CO_2** (vpm)	**CH_4** (vpm)	**C_2H_6** (vpm)	**C_3H_8** (vpm)	**i-C_4H_{10}** (vpm)	**Σ Hydro-carbons** (vpm) (= ppmv)	**He** (vol.-%)	**N_2** (vol.-%)	**Ar** (vol.-%)
10.08.2011	0.198	31'900	12'690	800	-	< 5	15	815	-	95.26	-
18.08.2014*	1.30	20	13'000	18'000	26	78	69	18'120**	2.1	92.00	0.5
29.01.2015*	4.5	$< 0.1 \cdot 10^{-4}$	1'700	2'070	4	8	11	2'110.3**	70.0	24.60	0.3

* The external sampling circuit (volume ~ 0.2 L) was filled with He as carrier gas at a pressure of 1 bar prior to open the pipe FPx-D/C sampling lines in 2014 and 2015, whereas N_2 was used in the rest of sampling campaigns (First and Second Operational Phases).

** During the two last sampling campaigns n-butane, i-pentane, n-pentane, ethene, propene and 1-butene were also detected (see data in Tab. 10).

vol.-%: volume of gas in %; vpm or ppmv: parts per million by volume

Appendix C: Procedure for gas/water sampling in GRS pipes

Taking into account the sampling circuit showed in Fig. C-1, the procedure for the gas/water sampling from the three GRS pipes was the following for each tubing pairs FP1-C/FP1-D, FP2-C/FP2-D, and FP3-C/FP3-D:

1. Note the pressure from the pressure gauges of the filter pipes installed in the panel.

2. Before connection of the sampling equipment to the transducer rack or valve panel (Fig. 20 or Fig. 42), connect peristaltic pump to a deionized water bottle and test and clean all collecting tubes and the pump tubes.

3. Connect the LEX-1 sensors to the closed FPx-C/FPx-D valves and close valves 6 and 7.

4. Connect "in" and out tubes of peristaltic pump to sampling equipment, connect gas bottle to valve 5, connect all tubes to sampling equipment, but not yet to vacuum pump and sampling bags.

5. Open gas bottle and valve 5, purge sampling equipment, peristaltic pump, and all tubes with He gas.

6. Close all valves and connect the vacuum pump and the sampling bags or cylinders.

7. Open valves 2, 4 and the valves of the sampling bags (3). Valves 5, 6, 7 FP-xC and FPx-D remain closed.

8. Start vacuum pump (open valve 1) and pump until vacuum is reached (pressure depending on vacuum pump: 0.1 bar absolute).

9. Close valve 1, turn off vacuum pump, open valve 5 (gas tank still connected), fill the circuit system with gas to 0.5 – 1 bar overpressure (check sampling bags, they must not be completely filled!).

10. Close valve 5.

11. Repeat steps 6 to 10 two times (three purging/evacuation cycles).

12. Perform steps 7 and 8 to obtain vacuum in the system.

13. Close valves 1 and 3.

14. Open valve 5 and fill system to 1 bar overpressure (vacuum remaining in the sampling bags).

15. Close valves 4 and 5; only valve 2 open (still 1 bar overpressure in system).

16. Start peristaltic pump (500 – 600 rpm).

17. Open valves FPx-C and FPx-D and measure the pressure in the system with the LEX 1 sensors.

18. Open valves 6 and 7 and circulate gas/water in probe/pipe for 30 min.

19. Close valve 2, open valve 3, fill sampling bags (the gas/water sampling bags or SS cylinders can be opened and closed separately. The sampling bags must not be filled with overpressure!).

20. If more gas and water sampling bags are needed, use valves 8, 9 and 10 for performing three flushing/vacuum cycles prior to open valve 3 for collecting gas/water (see Fig. 22).

21. Close valve 3, turn off peristaltic pump.

22. Pipes are needed to be left under vacuum: connect vacuum pump, close valves 2, 4 and 7 and open valve 1 (check vacuum on the LEX-1 sensor located at the circuit).

23. Close valves 6, 7, FPx-C and FPx-D.

24. Disconnect sampling system and perform complete procedure for next pair FPx-C/FPx-D.

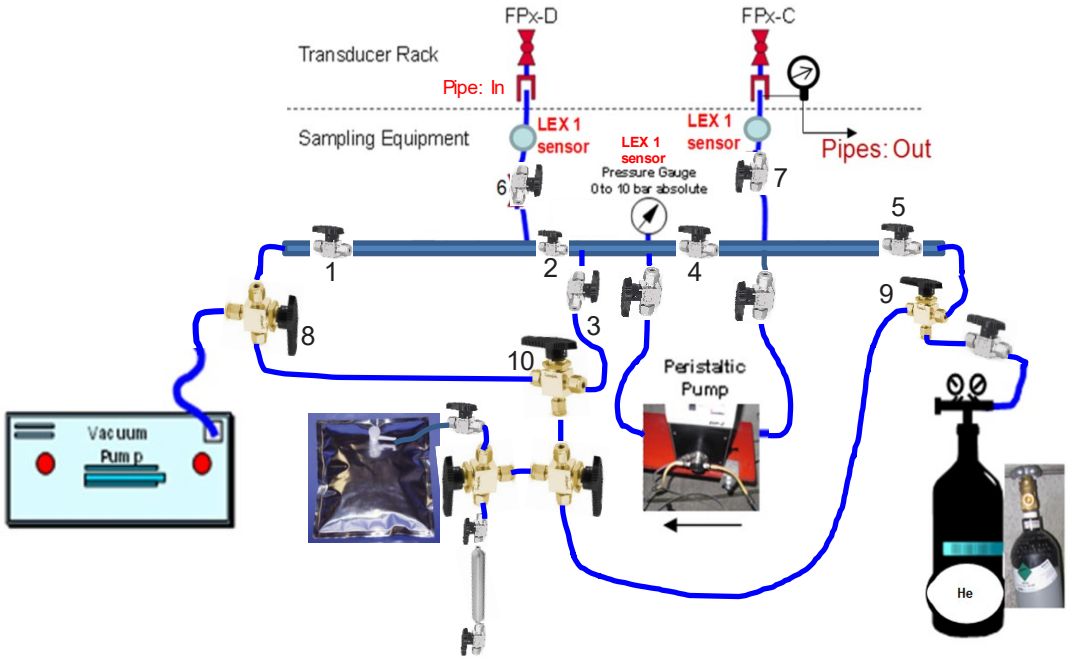

Fig. C-1: Sampling circuit for gas/water sampling used in the GRS pipes

Appendix D: Procedure for sampling CIEMAT pipes

Taking into account the sampling circuit showed in Fig. D-1, the procedure for the water sampling was the following:

1. Select the pipe to be sampled. Be sure that the two valves coming from the pipe (blue ones) are closed.

2. Prepare the sampling system with the LEX manometer for collecting water according to Fig. D-1.

3. Prepare the tubings for the connection of one of the valves of the sampling system to a gas bottle for flushing with gas the whole system.

4. Connect that valve (at closed position) with the gas bottle.

5. Prepare the tubings for the connection of one of the valves of the sampling system to the vacuum pump.

6. Connect that valve (at closed position) with the vacuum pump.

7. Connect one of the blue valves from the pipe to the gas circulation valve in the system (in-gas valve).

8. Connect the other blue valve from the pipe to the pressure/water collecting valve in the system (out-water valve).

9. Connect the sampling bag according to the Fig. D-1.

10. Open the valve of the LEX manometer, maintaining all the rest closed.

11. Open the gas valve and flush the system with gas at a low pressure (1.0 bar, 2 bar max.).

12. Close the gas valve and open the vacuum pump valve.

13. Repeat 11 and 12 at least three times (cycles of flushing/vacuum to eliminate oxygen from the sampling system).

14. Check the gas pressure and vacuum in the system with the LEX manometer for checking possible leaks in the sampling system.

15. Close all valves and check the tightness in the system.

16. Open the sampling bag valve and perform three gas flushing and vacuum cycles (step 11 and 12). Left the system at vacuum at close the sampling bag. Close all valves.

17. Once the system is oxygen-free, open pressure interval valve via the out-water blue valve. Check the pressure inside the pipe interval. Let to stabilize the pressure measurement and annotate the value.

18. Open the valve of the sampling bag for collecting water.

19. Check the water coming from the pipe through the transparent FEP tubing.

20. If no more water or no water is coming from the pipes, close the sampling bag valve. Open the gas valve and the in-gas valve and collect the water by flushing the pipe line with gas. When water is coming from the line, open the sampling bag valve. Be carefully with the gas, avoiding an overpressure in the bag.

21. When no more water is coming from the line pipe, close the in-gas, water-out valve and sampling bag valves. Close the FEP valve of the sampling bag and label the bag with the appropriate name (pipe number, date, etc.). Preserve the bag inside a plastic box.

22. Leave the pipe lines under vacuum.

23. Remove the system from the blue valves from the pipe line.

24. Clean the sampling system with deionised water three times by using the gas and the vacuum system.

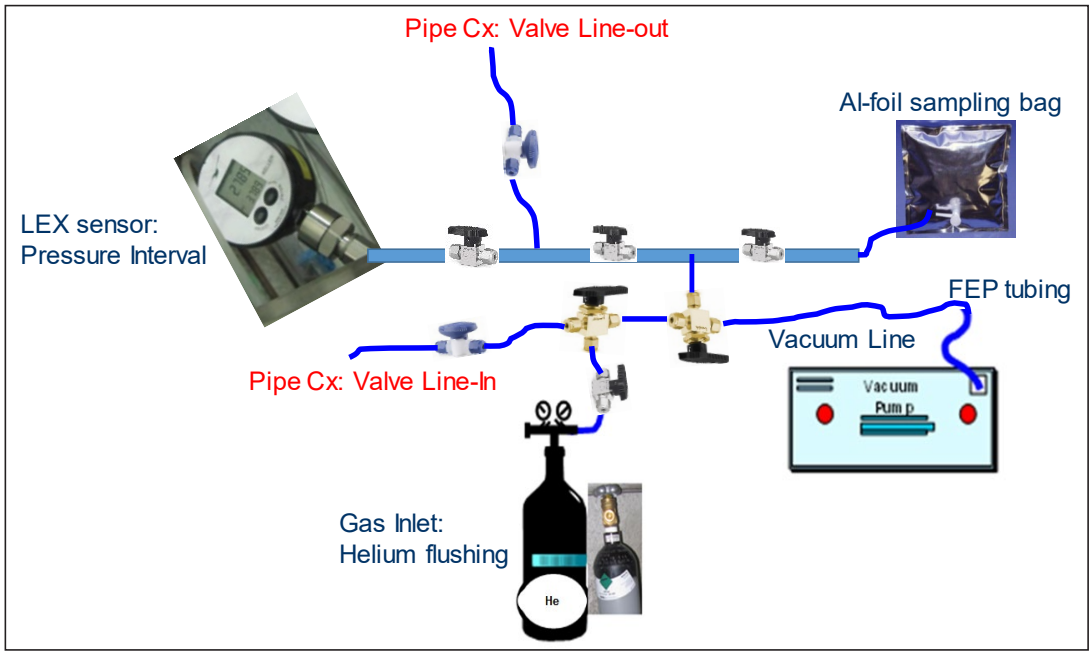

Fig. D-1: Sampling circuit designed for the CIEMAT pipes

Appendix E: Visual aspect of the pipes during dismantling

1. Visual aspect of the GRS pipes after dismantling of the Heater #1

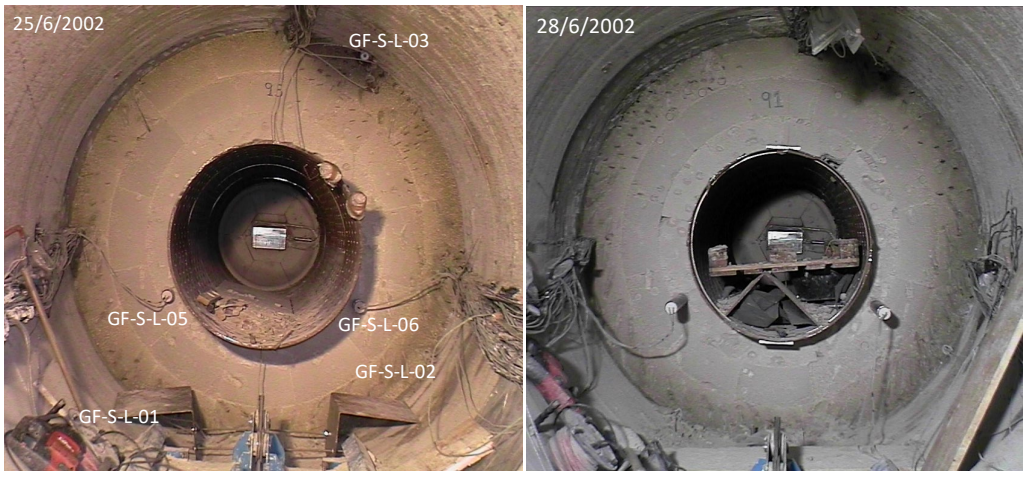

Fig. E-1: Visual aspect of the bentonite during dismantling of Heater #1 at different layers where the gas pipes were inserted for collecting gases

Fig. E-2: Visual aspect of the GF-SL-03 pipe during the dismantling of the Heater #1 from the Slice 79 (S79) or Bentonite Sampling Section 29 (BSS29) in 10 July 2002

Fig. E-3: Visual aspect of bentonite blocks from Section 20 (Slice 96, Instrumented Section L), showing a bentonite greenish halo around a broken ceramic pipe

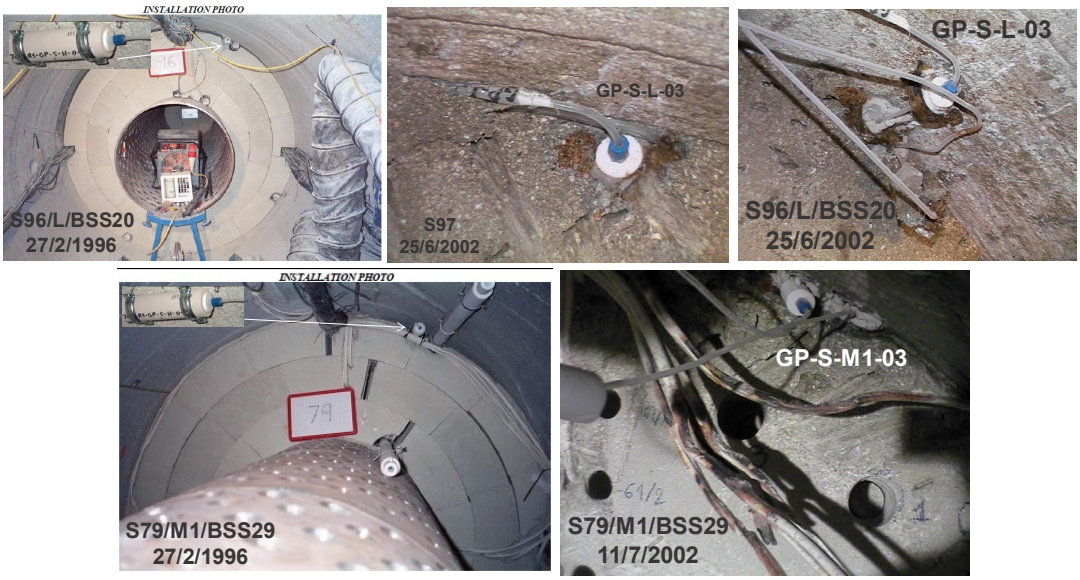

Fig. E-4: Visual aspect of the GRS pipes GP-S-L-3 and GP-S-M1-3 for pore pressure measurements prior and during the dismantling of the Heater #1 in the bentonite Sections 96 and 79 (Instrumented Sections L and M1, respectively)

Fig. E-5: Visual aspect of the GRS pipes GF-S-L-05 (left side, bentonite Section 96 (BSS20): 25 June 2002) and GF-S-L-06 (right side, bentonite Section 94 (BSS21): 26 June 2002) during dismantling operations of the Heater #1

These pipes were not broken due to they were inserted inside perforated SS tubings and could be extracted at intact conditions on June 28th 2002.

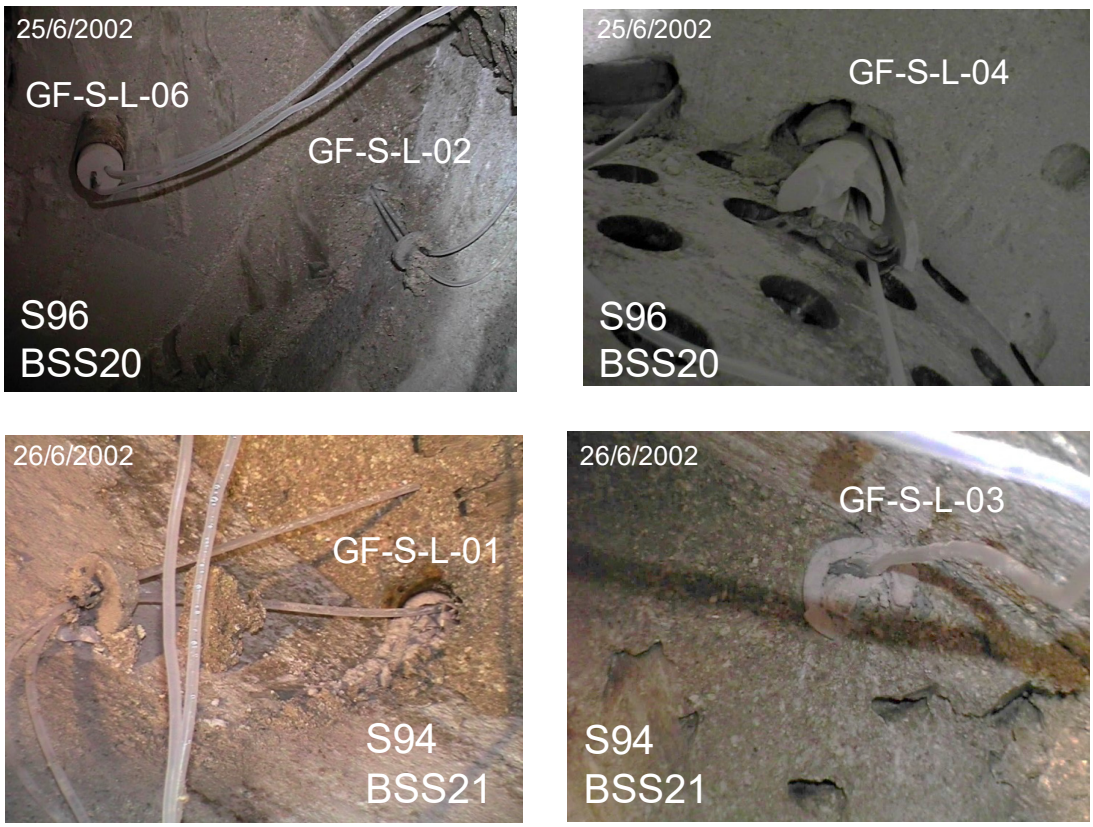

Fig. E-6: Visual aspect of the GRS pipes during the dismantling of the Heater #1: bentonite Slice 96 (BSS20, Instrumented Section L) in 25 June 2002, and Slice 94 (Bentonite Sampling Section BSS21) in 26 June 2002

The pipes GF01, GF03, GF02 and GF04 were broken due to bentonite swelling and a heterogeneous stress.

Fig. E-7: Visual aspect of the GRS pipe GP-S-H-3 for pore pressure measurements during the dismantling of the Heater #2 (29.05.2015) in the Slice 63 (BSS40, Instrumented Section H)

2. Visual aspect of the GRS pipes after dismantling of the Heater #2

As can be seen in Martínez et al. (2016) different sensors were introduced at the instrumented Sections I, M2, F2, E2 and D2, where the gas/water sampling intervals were located:

a) Instrumented Section I (Slice 59, Sampling Section 42): displacement sensors (2), temperature (13), total pressure (1).

b) Instrumented Section M2 (Slice 46): water gravimentric (10 TDRs).

c) Instrumented Section F2 (Slice 42, Sampling Section 48): water content (8), pore pressure (8), water content (8 phychrometers), temperature (4), expansion (2).

d) Instrumented Section E2 (Slice 32, Sampling Section 51): water content (10), pore pressure (8), water content (8 phychrometers), temperature (2), total pressure (2), expansion (2).

e) Instrumented Section D2 (Slice 24, Sampling Section 54): displacement sensors (3), temperature (13).

Fig. E-8: First visual position of the PP-H 100 tubings of the gas pipes taking inside the four 1/8" SS sampling tubings at the bentonite Slice 74 (Sampling Section 36, Instrumented Section P) in contact with the concrete plug (12 May 2015)

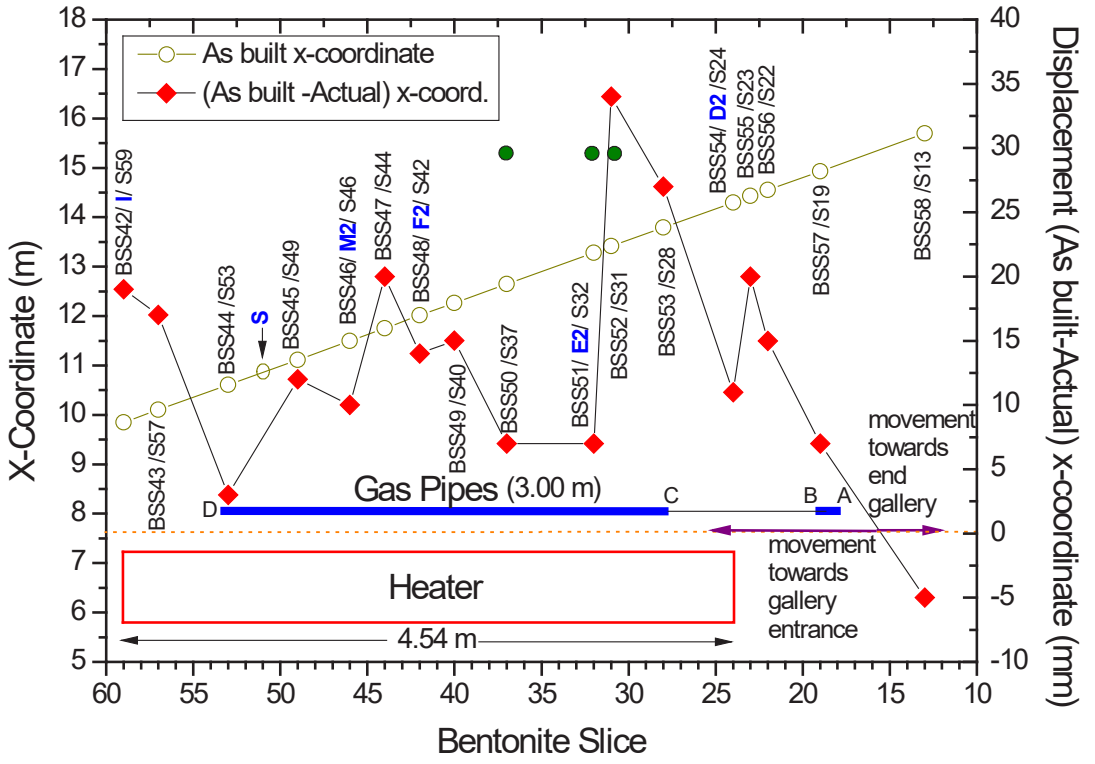

Fig. E-9: Location of the sampling intervals D-C (gas/water sampling) and B-A (permeability tests) from the gas pipes with respect to the bentonite slices and the Heater #2

The displacements of the dismantled bentonite slices with respect to the as built x-coordinate is also shown (+ values: displacements towards the gallery entry; - values: displacements towards the end of the gallery). Instrumented sections (I, S, M2, F2, E2 and D2) are shown in blue colours. Slices with cellulose filter papers with tracers are shown in green colour circles.

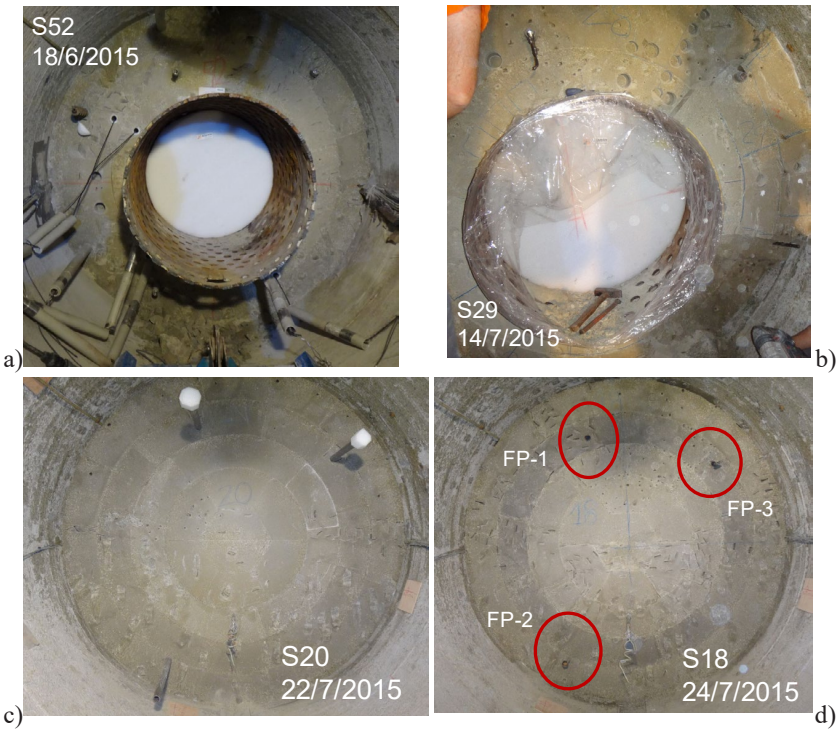

Fig. E-10: a) Bentonite Slice 52 (close to the bentonite Sampling Section BSS44) were the FPx-D sampling port is located. b) Bentonite Slice 29 (close to the bentonite Sampling Section 53) were the FPx-C sampling port is located. c) 1.4 m of non-porous stainless steel until next sampling interval (B-A). d) Bentonite Slice 18 (close to Sampling Section 57) where the FPx-A sampling port is located, 0.80 m beyond the Heater #2.

Fig. E-11: Visual aspect of the stainless steel pipes with no evidences of external corrosion

Fig. E-12: Metal coupons at Section 42 (Sampling Section BSS48/Instrumented Section F2)

a)

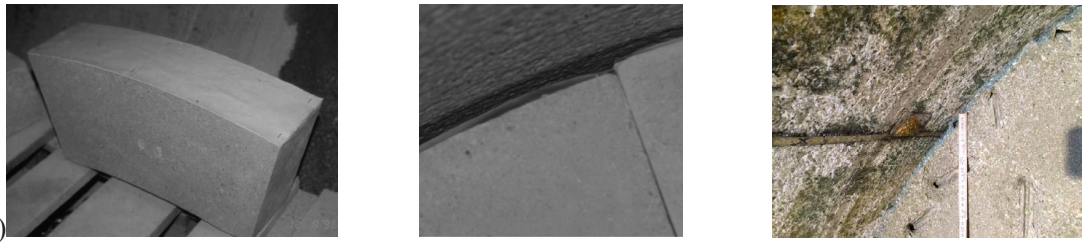

b)

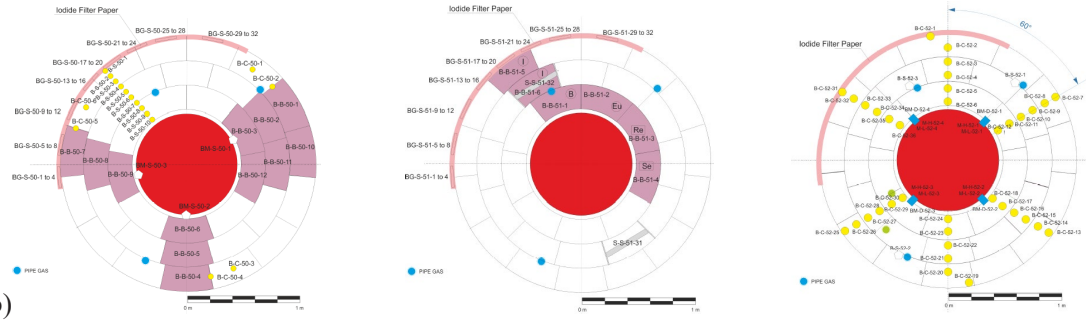

Fig. E-13: a) Filter papers of cellulose for tracers deposition located at the bentonite-granite interface at Sections S70, S74, S37, S32 and S31 (García-Gutiérrez, 2001). A greenish discoloration near a cellulose filter paper impregned with Na-iodide was observed at the bentonite-granite interface in Section 37 (BSS50). b) Cellulose papers impregned with Na-iodide at Sections S37 (BSS50), S32 (BSS51/E2) and S31(BSS52).

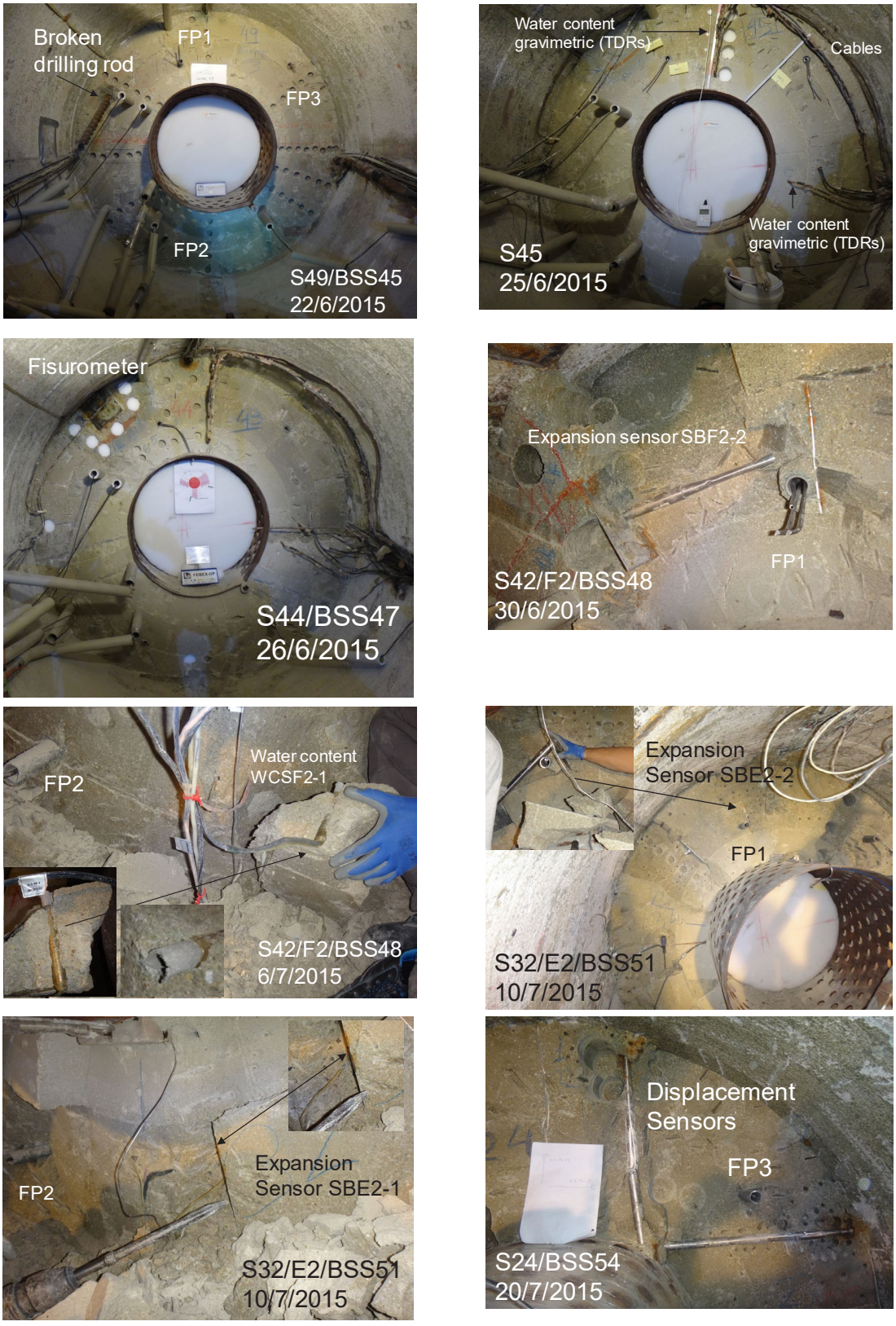

Fig. E-14: Types of materials to be potentially corroded and degraded in the bentonite barrier close to gas pipes FP-1, FP-2 and FP-3

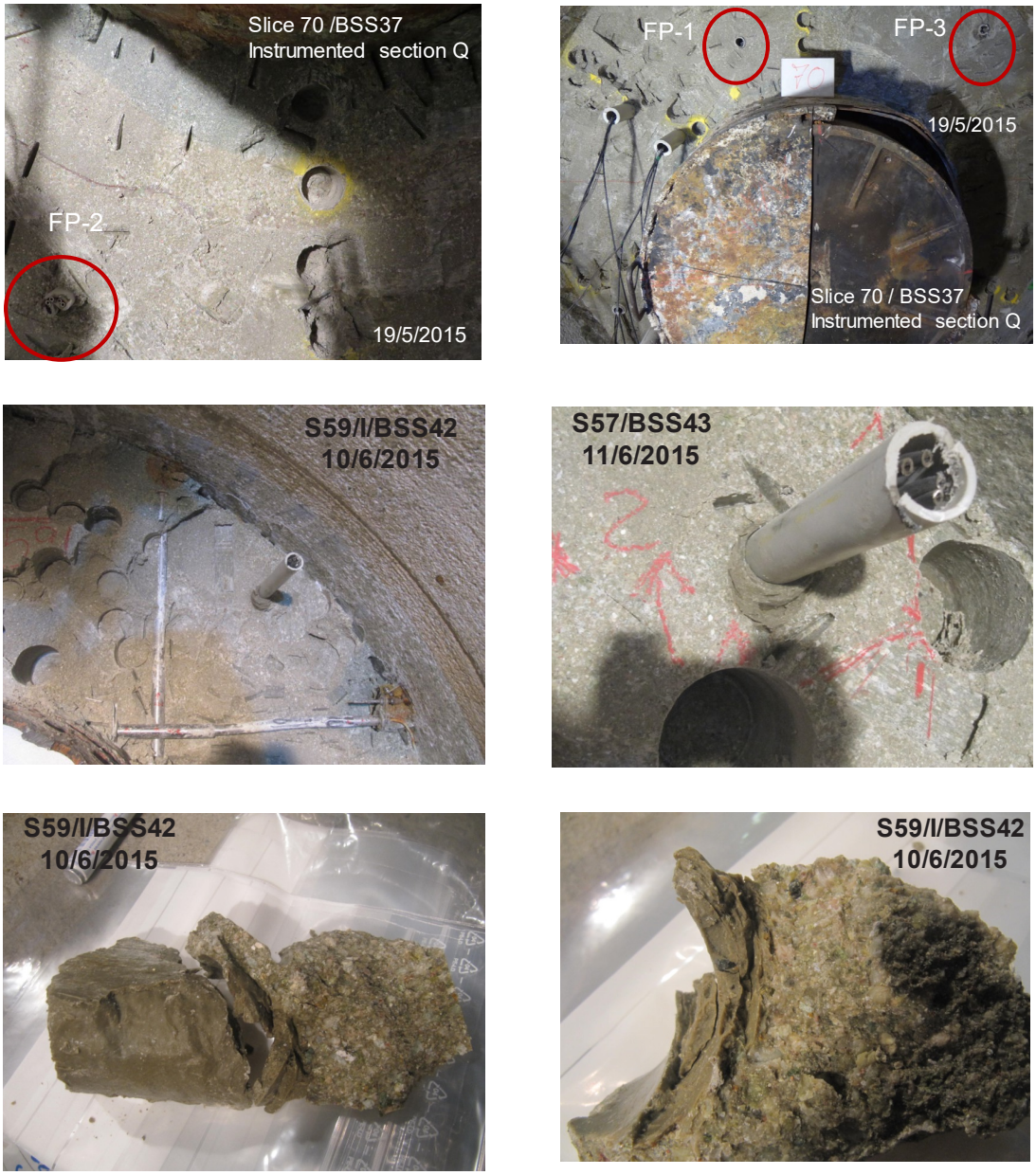

Fig. E-15: Gel of smectite generated around the pipe FP3, which was observed from the bentonite Slice 70 (BSS37, Instrumented Section Q) until the end of the tube (Section 52)

The formation of this gel was not observed in the other pipes FP1 and FP2.

3. Visual aspect of the CIEMAT's pipes after dismantling of the Heater #2

The stainless steel sintered filters for water sampling in the CIEMAT pipes were located at the Instrumented Sections G, I and F2. The type of sensors introduced at the Instrumented Sections G (S67, BSS38), I (S59, BSS42), and F2 (S42, BSS48) corresponds to: displacement sensors, total pressure, pore pressure, temperature, psychrometers, TDRs and expansion sensors. Iodide cellulose filter papers were introduced in Sections P (S74, BSS36) and Q (S70, BSS37), which were close to Section G. In the Slice 44 (Bentonite Sampling Section BSS47), close to Section F2, a fissurometer (or tri-axial crackmeter) was introduced inside the bentonite, which suffered a high degree of corrosion (see Wersin and Kober, 2016: NAB 16-16). As can be seen in Madina (2016), most of the sensors were found partially corroded.

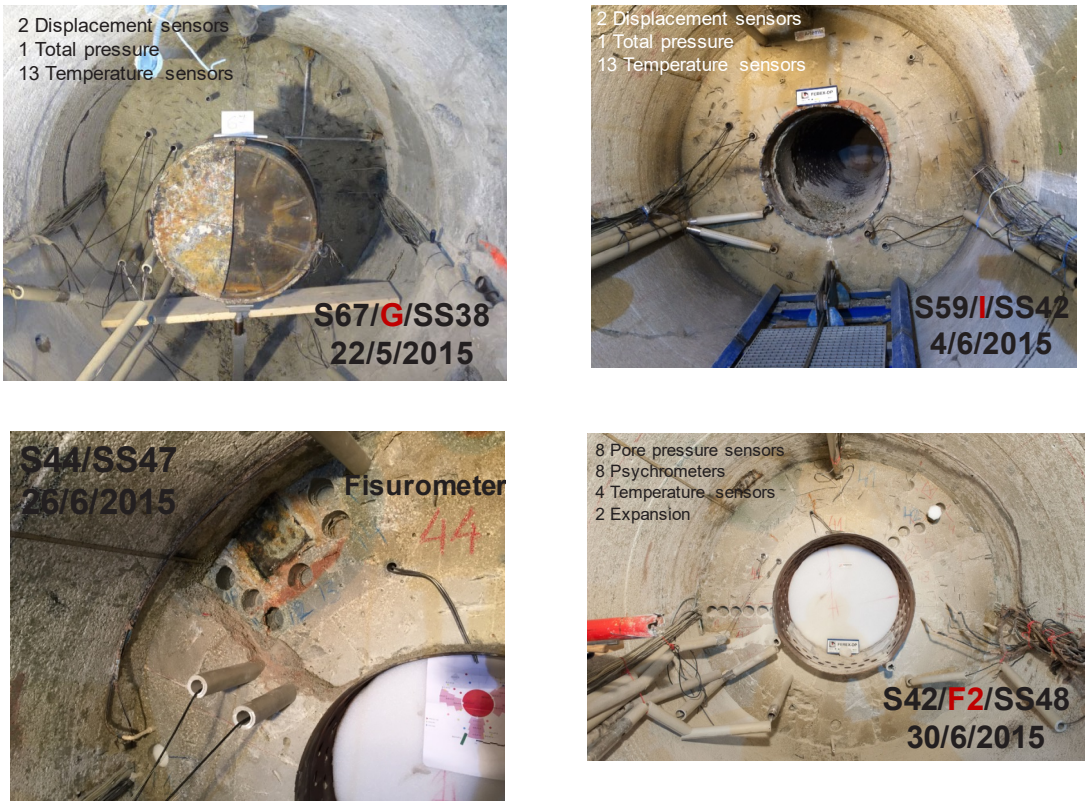

Fig. E-16: Visual aspect of the bentonite in the instrumented Sections G, I and F2 where the sintered filters for pore water sampling and RH measurements were located

Fig. E-17: Visual aspect of the heater prior and after the FEBEX *in situ* test

Detail of the gap between heater and liner prior and after test. This gap was filled by bentonite and it seems to be enlarged in the direction of the vertical diameter because a small deformation is observed. The bentonite penetrated the liner perforations at both ends but not in the centre of the liner (García-Siñeriz et al. 2016, Kober 2015b).

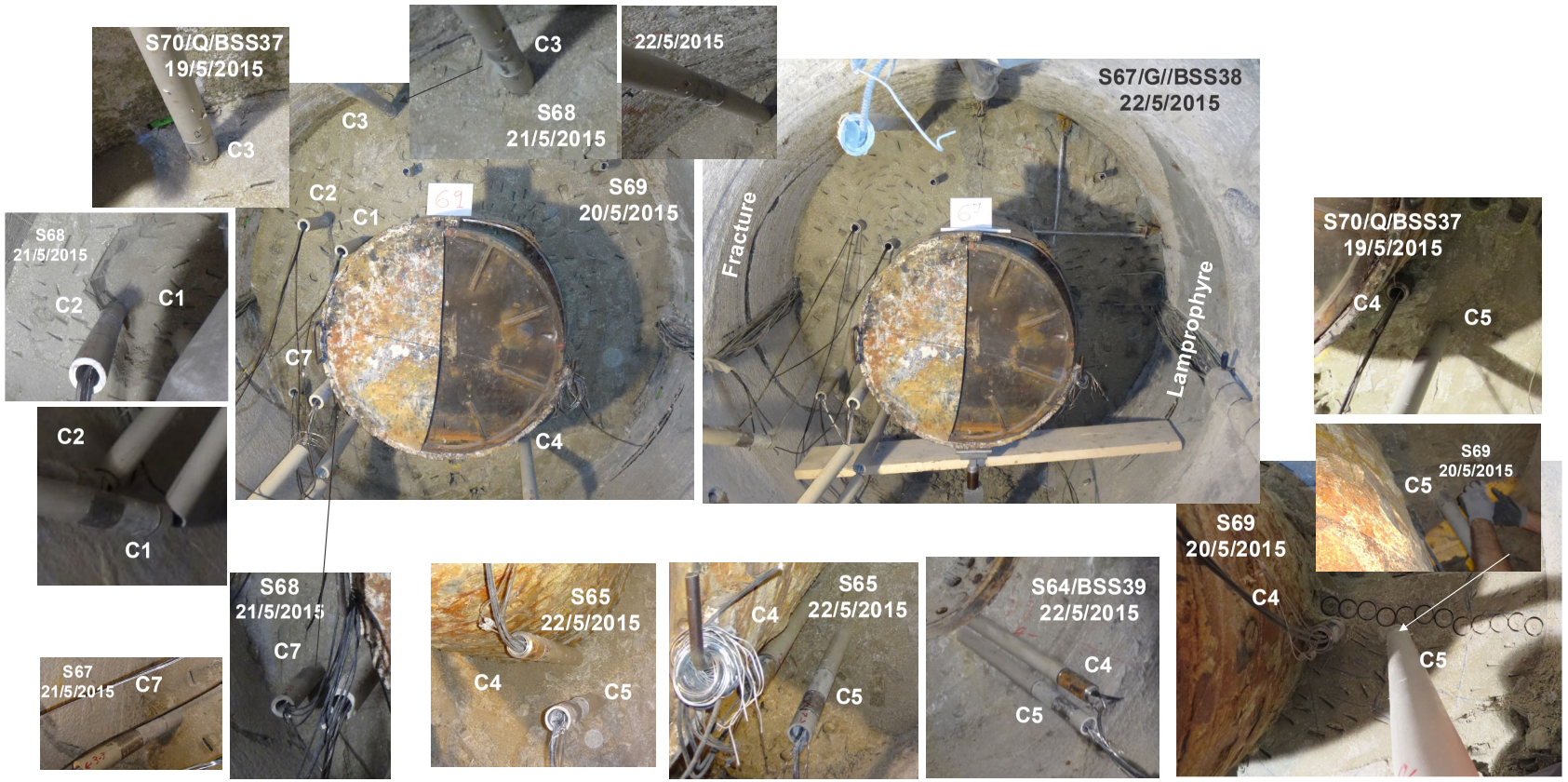

Fig. E-18: Visual aspect of the pipes at the instrumented Section G (S67, BSS38)

The filter from pipe C4 was corroded. The filters from pipes C3 and C4 were found at Section S69, whereas the rest of pipes at the Section S68; two slices before than expected. The zone is close to a lamprophyre at the right part of the gallery.

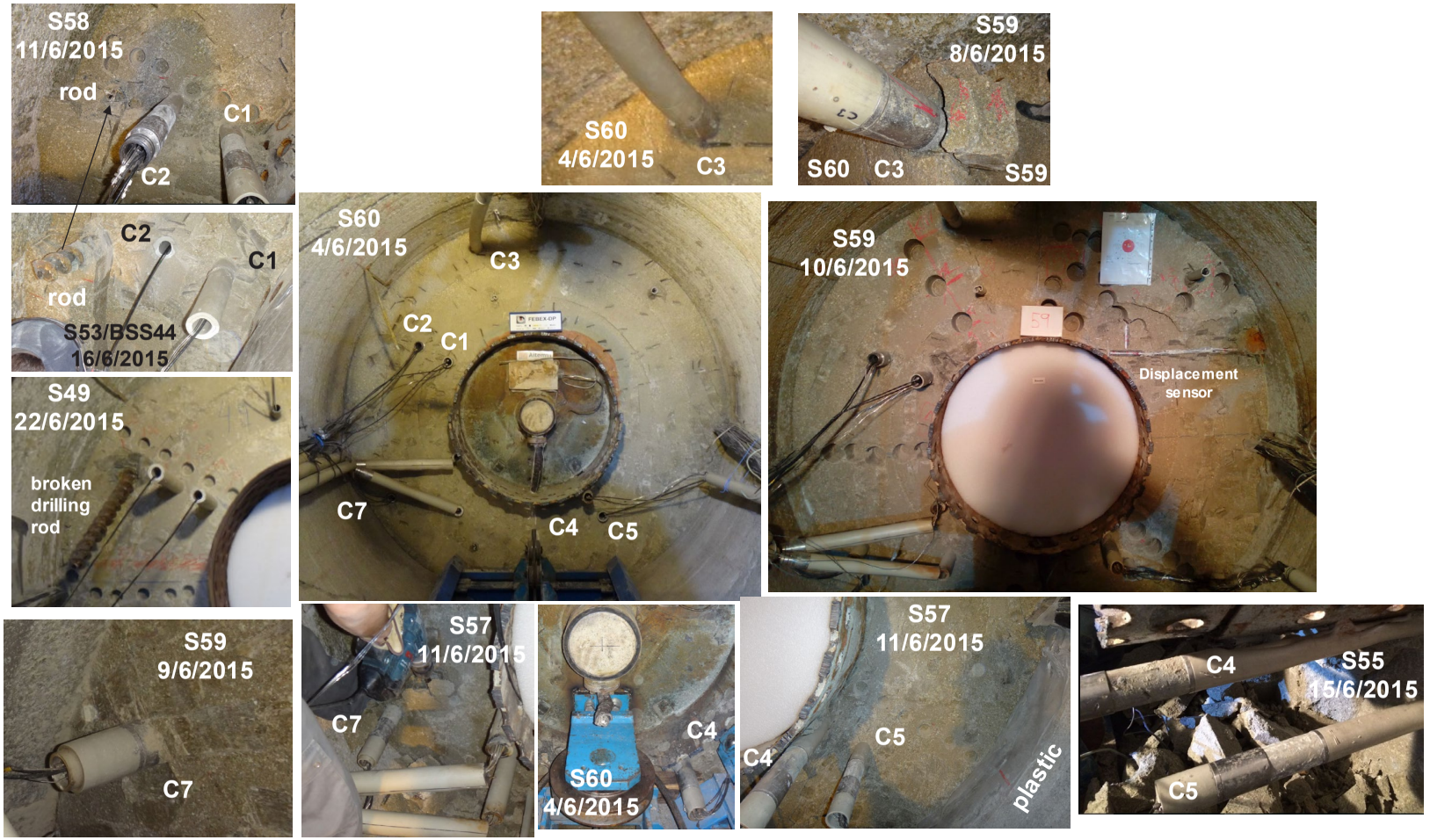

Fig. E-19: Visual aspect of the pipes at the instrumented Section I (S59, BSS42)

Details of the broken drilling rod and displacement sensor. The filters from pipes C3 and C4 were found at Section S60, whereas the rest of pipes at the intended Section S59.

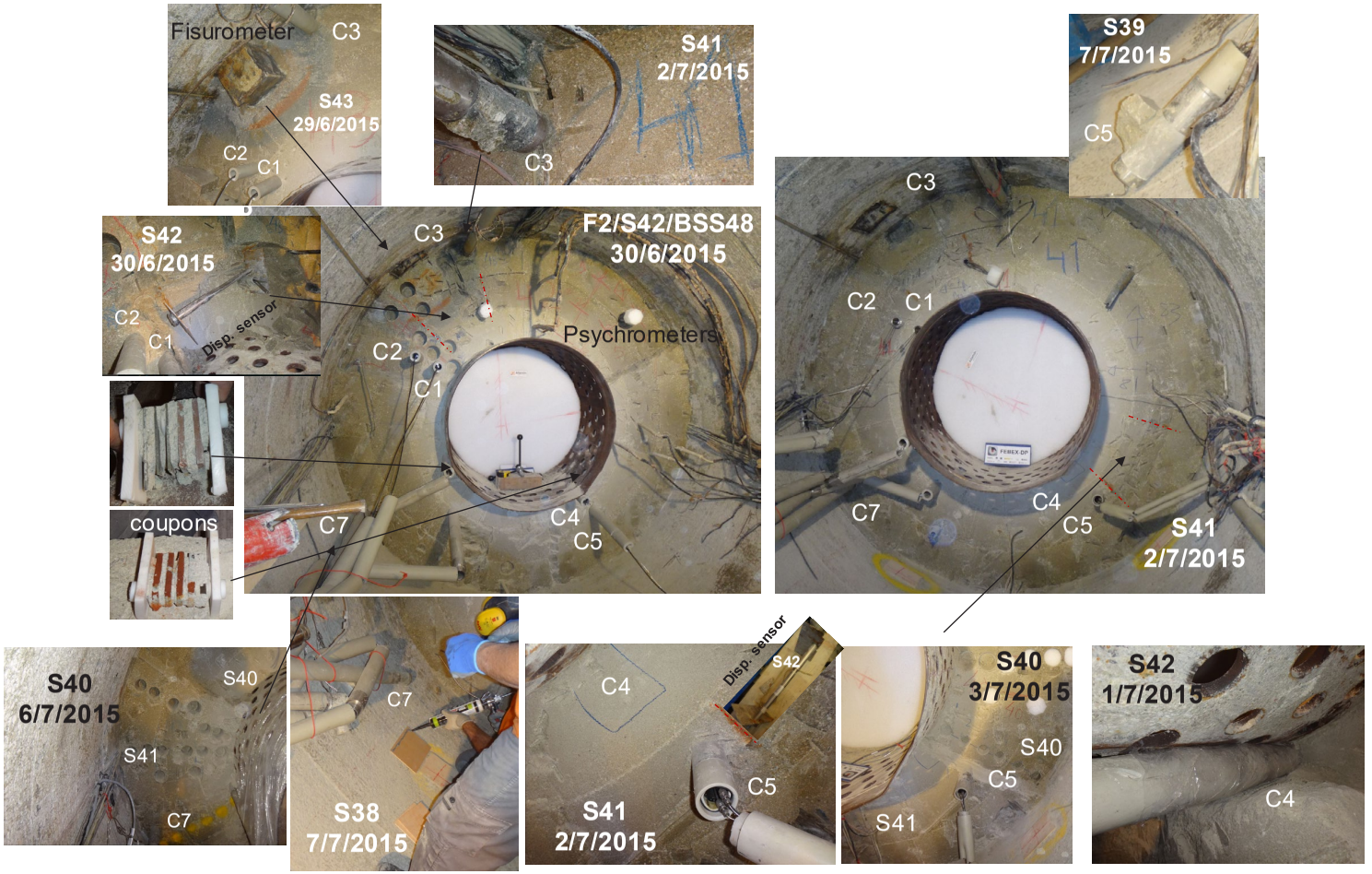

Fig. E-20: Visual aspect of the pipes at the instrumented Section F2 (S42, BSS48)

In this section the displacement sensors and a fissurometer can be observed. The filters from pipes C3 and C4 were found at intended Section S42, whereas the rest of pipes at the Section S41.

Fig. E-21: a) Gallery at ~ 3 o'clock showing interface of granite/lamprophyre and contact to bentonite further to the left (Section 37). b) Galleries' left side, detail lamprophyre under "Part B, Structure 5" (Section 39)

Kober (2015): AN 15-619

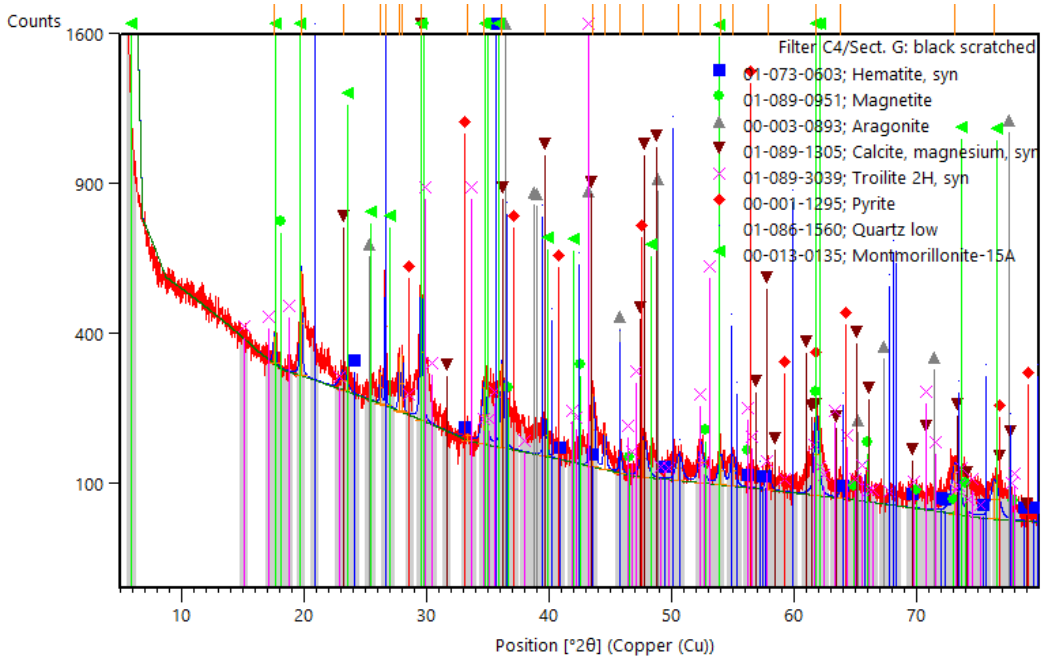

Fig. E-22: XRD patterns from the black scratched powder from the corroded C4 filter at Section G showing smectite, aragonite, calcite, quartz, feldspars, iron sulfur (pyrite, troilite), hematite, and magnetite

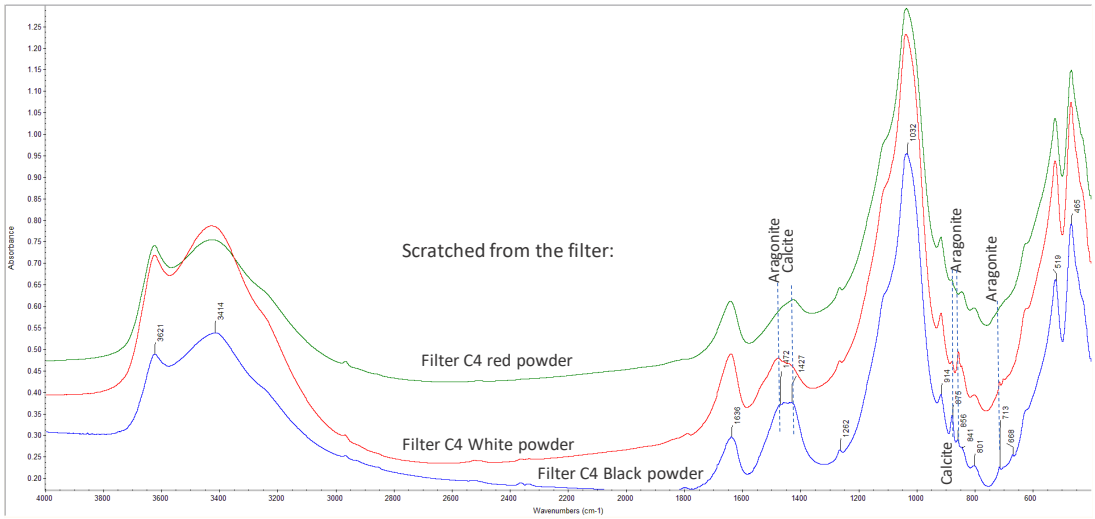

Fig. E-23: FTIR spectra from the scratched powders (red, white, black) from the corroded C4 filter at Section G showing smectite, aragonite, calcite and quartz

Fig. E-24: Visual aspect of the pipe C4 from Section 55 to Section 45 (from the frontal part to centre of the heater): deformation probably due to thermal stress by overheating